AKADEMIE DER WISSENSCHAFTEN DER DDR
Forschungsbereich Geo- und Kosmoswissenschaften
ZENTRALINSTITUT FUR PHYSIK DER ERDE

Veröffentlichungen des Zentralinstituts für Physik der Erde
Nr. 102

6th International Symposium
„Geodesy and Physics of the Earth"

GDR Potsdam, August 22–27, 1988

PROCEEDINGS

Part II
Gravity field variations

Development of precise terrestrial
and space techniques of geodetic measuring

Herausgeber: Der Direktor des Zentralinstituts für Physik der Erde

Als Manuskript gedruckt
Potsdam 1989

I

C O N T E N T S
I N H A L T S V E R Z E I C H N I S

Part II
Teil II

GRAVITY FIELD VARIATIONS

HELMERT-Commemorative Lecture

Absolute Gravimetry in its
Operational Phase - Some
Results and Problems

By Wolfgang Torge
Institut für Erdmessung
Universität Hannover (F.R.G.)

Abstract: Until the 1950s, absolute gravimetry has been governed by the pen-
dulum method, with limited progress in accuracy and economy. This finally
led to the concept of the Potsdam Gravity System, which was based on only
one absolute gravity value; global, regional and local gravimetric surveys
were connected by relative gravity measurements. Since 20 years the free-fall
method has succeeded, with transportable absolute gravimeters reaching accu-
racies which correspond to that of relative gravimeters. This situation has
changed the strategy at the establishment of gravity control networks, with
static or geodynamic objective. At the example of the JILA absolute gravi-
meter (Faller type), operated by the Institut für Erdmessung, University of
Hannover, the possibilities and problems of this new technology are demon-
strated.

Zusammenfassung: Die absolute Schweremessung war bis in die 1950er Jahre von
der Pendelmethode beherrscht, wobei der Fortschritt in Genauigkeit und Wirt-
schaftlichkeit über 300 Jahre begrenzt blieb. Das führte schließlich zur
Konzeption des Potsdamer Schweresystems, das sich auf eine absolute Schwere-
messung stützte; globale, regionale und lokale gravimetrische Aufnahmen wur-
den daran mit Hilfe relativer Gravimeter angeschlossen. Seit 20 Jahren hat
sich die Freifallmethode durchgesetzt, transportable Absolutgravimeter er-
lauben Meßgenauigkeiten, die denen der Relativgravimetrie entsprechen. Damit
ändert sich die Konzeption beim Aufbau von Schwerefestpunktfeldern statischer
und geodynamischer Zielsetzung. Die Möglichkeiten und Probleme dieser neuen
Technologie werden exemplarisch am Beispiel des JILA-Absolutgravimeters
(System Faller) des Instituts für Erdmessung, Universität Hannover, darge-
stellt.

1. Introduction

With the law of the free fall (about 1590) and the pendulum law
(about 1609), Galileo Galilei established the two basic rela-
tionships, which governed absolute gravimetry until present time.
In this context, we understand "absolute gravimetry" as the
method to determine the magnitude of gravity by measurement of
the fundamental acceleration quantities length and time. More
than 300 years of gravimetric history brought a remarkable in-
crease of accuracy   and efficiency at absolute gravity measure-
ments. This was achieved by improved length and time standards,
better understanding of error sources, and adopting new technolo-
gies as soon as possible. Since Richer 1672/73 found the latitude
dependence of gravity, an accuracy increase of five orders of
magnitude was achieved, with the pendulum method exclusively used

until the 1950s, superseded then by the free-fall method. This development was not straightforward, especially as more economic relative gravity measurements since the end of the 19th century delivered the bulk of gravity data, and absolute gravity values only had to play the role of defining the gravity standard, see Figure 1 (TORGE 1982).
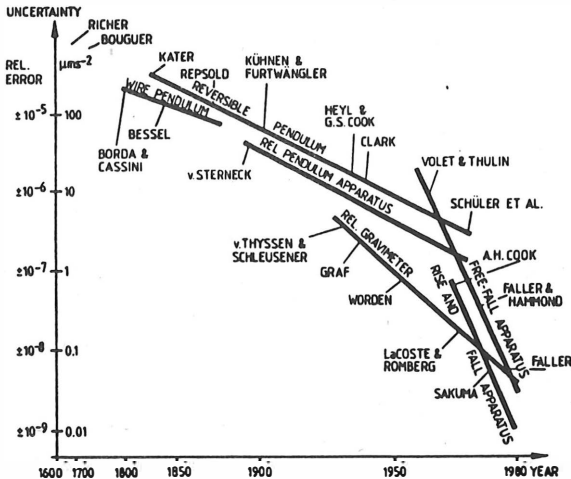
Fig. 1: Increase of accuracy in terrestrial gravimetry, after TORGE (1982)

This philosophy is partially changing now, with operational absolute gravity meters available, delivering the same accuracy as relative gravimeters within a reasonable time. Nevertheless, there are still one to two orders of magnitude difference at hardware cost and observation time per station, between absolute and relative gravimetric techniques.

In the sequel, we first outline the development of the pendulum method, and the solution which was found at the beginning of this century for surveying the gravity field of the earth. This solution was strongly influenced and promoted by the fundamental work of Helmert, Direktor of the Royal Prussian Geodetic Institute in Potsdam. We then proceed to the rapid break-through of the free-fall method, and discuss the main features of free-fall gravimeters and strategies for reducing errors. Finally, the operational stage of absolute gravimetry is demonstrated at the results obtained with the JILA-gravimeter (Faller-type) operated since 1986 by the Institut für Erdmessung (IfE), University of Hannover.

2. The pendulum as absolute gravimeter and the Potsdam Gravity System

Based on the work of GALILEI (1632), and with the pendulum-clock constructed by HUYGENS (1673), the pendulum could be used for gravity determinations, with a first result relevant to geodesy obtained by the measurements of RICHER (1679). At those early experiments, approximations to the <u>mathematical pendulum</u> have been employed.[1] We mention the precise determination performed by Borda and Cassini de Thury in 1792 in the Paris astronomic observatory, and the transportable device used by Biot in western Europe in the beginning of the 19th century. The potential of this constructive solution was exhausted by BESSEL (1828), with a wire pendulum swinging at two different pendulum lengths (difference method). The physical pendulum was made operational by KATER (1818) with the <u>reversible pendulum</u>, and successfully employed at arc measurements in western Europe and at French and English marine expeditions. Already at that time, the method of determining gravity differences with respect to a base station was prefered, using "invariable" pendulums. The accuracy of the gravity determinations performed in the first decades of the 19th century may be estimated to be at the order of 100 μms^{-2}.

Upon initiative of the "Mitteleuropäische Gradmessung", the precursor of the International Association of Geodesy (IAG), gravity measurements were more intensively taken up since 1862. Following suggestions of Bessel, J. <u>Repsold</u> built a <u>transportable reversible pendulum</u> apparatus, and instruments of this type and similar ones were used in many countries, during the next 20 to 30 years. But in spite of all efforts, the number of gravity stations increased rather slowly. So, only 122 gravity values were available to HELMERT (1880/1884) in order to calculate normal gravity and flattening of the earth's ellipsoid.

<u>Friedrich Robert Helmert</u> (1843-1917), who in 1887 became Director of the Central Bureau of the IAG (Internationale Erdmessung) hosted at the Geodetic Institute Potsdam, took up this challenge. By his position as Director of this Institute, he was already occupied with gravity measurements in Prussia, being one task of the Geodetic Institute. The problem of a more efficient determination of the earth's gravity field, in the regional and global sense, was attacked by him from the theoretical, experimental und organisational point of view. He revised thoroughly the theory of the reversible pendulum (HELMERT 1898), started investigations about the use of elastic springs for gravity measurements, and immediately recognized the chance offered by the relative pendulum apparatus developed by VON STERNECK (1887). Improvements of the Repsold apparatus, studies of the Sterneck apparatus, and relative gravity measurements between Vienna and Potsdam followed, in order to transfer the Vienna absolute gravity value to the Geodetic Institute Potsdam. The Vienna Gravity System had been introduced by a report presented by Helmert to the 13. General Conference of the IAG in Paris 1900 (HELMERT 1901). This was the first

1) More details on the historical development and the present state of gravimetry can be found in TORGE (1989).

attempt to establish a global gravity standard by few accurate
absolute gravity measurements, and relative connections between
a number of fundamental stations distributed over the earth
(TORGE 1988). In 1896, preparations for a new absolute gravity
measurement in Potsdam started, and from 1898 to 1904, an abso-
lute determination followed, performed by KÜHNEN and FURTWÄNGLER
(1906). Using five different reversible pendulums, a large number
of observation series after adjustment delivered the famous value
of 9.81274 ± 0.00003 ms^{-2}. In a report, prepared by E. BORRASS
(1911), and presented by Helmert to the 16. General Conference
of the IAG in London 1909, 2736 gravity measurements made on 2398
stations between 1808 and 1909, were collected and referred to
the Potsdam absolute value. With the formulation "... die Zahlen
entsprechen denn auch der Gesamtheit aller absoluten Bestimmungen
und werden von uns als 'Potsdamer System' bezeichnet ...".
(HELMERT 1910, p. 110/111) and the adoption of this report by the
IAG, The "Potsdam Gravity System" was established.

This was a solution, which served gravity standardization pur-
poses in metrology, geodesy, and geophysics for the first half of
the 20th century. Relative connections between Potsdam and gra-
vity fundamental stations transferred the Potsdam System to many
national gravity networks. While relative pendulum measurements
served for this transfer and for establishing gravity base net-
works, regional and local interpolation became a task of spring
gravimeters, since the 1930s. In the same time, the Potsdam gra-
vity value was called in question, which finally initiated two
new absolute determinations at the National Bureau of Standards,
Washington (1936), and the National Physical Laboratory, Tedding-
ton (1939). The accuracy of these experiments now reached few
10 μms^{-2}, and revealed the Potsdam value to be 100 to 150 μms^{-2}
too high. After 1945 geodesy and geophysics strengthened their
endeavours to establish a new global gravity reference system.
During the 1950s, it became obvious that such a system could be
based now on free-fall determinations of gravity (see below), and
that the pendulum method had reached its limits (COOK 1965).
Two experiments performed with up-to-date technology, and
thorough discussions of error sources and accuracies mark the
end of the pendulum era. The reversible pendulum method (4 pendu-
lum pairs) was applied at the Zentralinstitut für Physik der
Erde, Potsdam, and gave a standard deviation of ± 3 μms^{-2}, and
an agreement of 1 μms^2 to the present gravity standard (SCHÜLER
et al. 1971). The wire pendulum experiment (difference method)
at the Finnish Geodetic Institute resulted in a standard devia-
tion of ± 17 μms^{-2}, but a systematic bias of 59 μms^{-2} remained
(HYTÖNEN 1972). Main error sources preventing further develop-
ments of the pendulum method are elastic deformations of the
pendulum, and deformations and movements in the knife-edge-
bearing system.

3. Appearance and advance of the free-fall method

In the 1950s, time measurement technology, with short-term fre-
quency stability of 10^{-9}, made it possible, to use the free-fall
method for gravity measurements. This had already been proposed
by GUILLET (1938), and first experiments started in the Bureau
International des Poids et Mesures, Sèvres (VOLET 1952).
Improved vacuum technique was the other prerequisite for the
application of this method, as the atmospheric air pressure
effect produces errors of the order 10^{-3}g.

We may distinguish different stages of development of the free-
fall method, see also SAKUMA (1984) and FALLER and MARSON (1988):

- Stationary experiments in the 1950s and 1960s, with the length
  reference being represented either by the falling body or by
  mechanically defined measurement planes, and methods of geo-
  metric optics used for defining the position of the falling
  body. The accuracy of the results soon reached ± $10\mu ms^{-2}$,

- the introduction of optical interferometry (Michelson inter-
  ferometer principle), permitting the simultaneous measurement
  of position and time and leading soon to an accuracy increase
  of one order of magnitude (FALLER 1965, SAKUMA 1963).

Figure 2 shows the principle of this method which is employed in
all absolute gravimeters operated today. The interferometer is
represented by two corner-cube reflectors, one of them being
the falling body and the other one serving as a fixed reference.
As light source, He-Ne-gas lasers (wavelength 633 nm) are used
exclusively today. Counting the number of interference fringes,
and measuring the time at preselected numbers gives, after sca-
ling with the laser wavelength, the relations between position
and time of the falling body, needed for the calculation of gra-
vity.
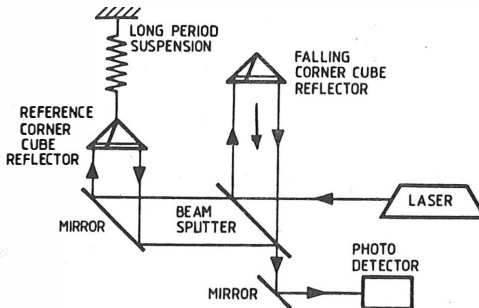
Fig. 2: Michelson interferometer system used at the
free-fall method

- the application of the <u>symmetrical rise-and-fall</u> method, which
  is less sensitive to the effects of residual air and frequency-
  dependent effects in the electronics, since the same velocity
  and fringe frequency occur twice during the flight (SAKUMA
  1963, COOK 1967),

- the development of <u>transportable</u> free-fall and rise-and-fall
  gravimeters since the 1970s with an observation time per sta-
  tion between one day and one week. The first instrument of
  this type (free-fall, ± 0.5 μms^{-2} HAMMOND and FALLER 1971) was
  successfully employed at the establishment of the <u>Internatio-
  nal Gravity Standardization Net1971</u> (I.G.S.N.71), which re-
  placed the Potsdam Gravity System (MORELLI et al. 1974),

- <u>the operational application</u> of transportable instruments since
  the middle of the 1970s, with inclusion of powerful microcom-
  puters for on-line evaluation of a large (up to 1000 or more)
  number of position/time-measurements during one experiment
  (multiposition method).

Common <u>characteristics</u> of recent transportable instruments and
measurement procedures include:

- Reduction of residual <u>air-pressure</u> effects to the 0.01 μms^{-2}
  order by evacuating the fall-chamber to 10^{-4}Pa (10^{-2}Pa at
  rise-and-fall instruments), which is now done by ion pumps
  operated also during transportation. In addition, a co-acce-
  lerated chamber is used in the Faller-type instruments, in
  order to reduce the residual air drag,

- application of <u>long-period isolation</u> devices for reducing the
  effects of vertical ground motion resulting from natural and
  artifical microseismic on the "fixed" reference corner-cube,

- performing of a <u>multitude</u> of <u>experiments</u> per station in order
  to reduce residual microseismics by randomization. With 100 to
  1000 experiments (the repetition number depending on the
  instrument's construction and the local microseismic), an
  error reduction by the factor 1/10 to 1/30 achieved.

The <u>accuracy</u> of the gravity values obtained with these instru-
ments depends on

- reproducibility (time stability) of <u>length</u> and <u>time standards,</u>
  which are about 10^{-9}/a for a stabilized He-Ne-Laser, and
  10^{-10}/a for a Rubidium frequency standard,

- the elimination or sufficient reduction of <u>non-gravitational
  forces</u> (residual gas pressure, pressure and temperature gra-
  dient effects, electrostatic and magnetic effects),

- the <u>stability</u> of the <u>reference frame</u> with respect to micro-
  seismics and man-made vibrations. A severe problem is the
  sensitivity of the interferometer to tilt. While the random
  part of tilt effects will only increase the scatter of the
  individual results, tilts produced by the measurement process
  itself may systematically falsify the results (floor recoil],

- the electronic_system counting and timing the occurence of
interference fringes. This zero-crossing-detection may con-
tain systematic errors if a frequency-dependent time delay
exists. The rise- and-fall method offers an advantage with
respect to this effect.

From error_analyses, as done for nearly all of the existing
absolute gravimeters (e.g. FALLER and MARSON 1988), one may
state that the random error part of an absolute gravity deter-
mination may be reduced to a few μms^{-2}, and that residual syste-
matic errors amount to $0.03...0.04$ μms^{-2}. In addition, the
uncertainties of gravimetric earth tides and polar motion re-
ductions, as well as the gravitational effects of air pressure
and groundwater variations, if not sufficiently reduced, enter
into the results. Finally, when comparing the gravity values
obtained with different gravimeters one has to take into
account the transfer error, between the reference height (about
1 m in most instruments) for the absolute value and the ground
mark used for comparisons. So, the overall accuracy of $\pm$ 0.1 μms^{-2}
stated for most of the more recent absolute gravity determination,
seems to be realistic. Nevertheless, comparisons of absolute re-
sults obtained with different instruments sometimes show discre-
pancies of some 0.1 μms^{-2}, which cannot be explained by the
apriori error budget. Table 1 gives such an example summarizing
the results from eight different absolute gravimeters, obtained
in the BIPM Sèvres, between 1976 and 1986 and reduced by local
gravimetric connections to the point Sèvres A.

Instrument	Epoch	Gravity at BIPM, Sèvres,A (μms^{-2})	Remarks
		9 809 250	
IMGC	May 1976	+ 9.77	rise and fall
	June 1976	9.87	
	Jan. 1977	9.81	
	March 1977	9.91	
	April 1982	9.85	
	June 1985	9.95	
BIPM (stat.)	1976	9.90	rise and fall
GABL	Sept. 1977	9.94	free fall
	Oct. 1981	9.98	
	Nov. 1981	9.96	
	June 1985	10.02	
JILAG	Nov. 1981	9.78	free fall
	June 1985	9.99	
NIM	April 1980	10.04	free fall without
	June 1985	10.16	micros.insulation
BIPM	March 1982	9.97	rise and fall
(Jaeger)	June 1985	9.76	
IGPP	June 1985	10.13	free fall
JILAG-3/IfE	June 1986	9.75	free fall

simple mean (n = 19) 9.92

Table 1: Absolute gravity measurements in BIPM, Sèvres, point A,
after TORGE (1987)

From table 1, we recognize most of the <u>institutions</u> operating
<u>transportable absolute gravimeters</u> today:

- Istituto di Metrologia "G. Colonnetti", Torino (IMGC),
  ALASIA et al. 1982,

- Institute of Automation and Electrometry, Siberian Branch,
  USSR Academy of Sciences (GABL), ARNAUTOV et al. 1983,

- Joint Institute for Laboratory Astrophysics, National Bureau
  of Standards and University of Colorado, Boulder (JILA),
  FALLER et al. 1983,

- National Institute of Metrology, Beijing (NIM), FENG et al.
  1982,

- Jaeger S.A., Division Aeronautique, transportable absolute
  gravimeter GA -60, operated by BIPM, SAKUMA 1983,

- Institute of Geophysics and Planetary Physics, University of
  California (IGPP), ZUMBERGE et al. 1986,

- JILA-Gravimeter JILAG-3, Institut für Erdmessung, University
  of Hannover, TORGE et al. (1987).

With four more instruments of the last type operated by different
institutions (U.S. National Geodetic Survey/DMA, Geological
Survey Canada, Finnish Geodetic Institute, Institut for Geophysic,
Univ. Vienna), two Japanese developments (Earthquake Research
Institute, Tokyo University, International Latitude Observatory
Mizusawa), and one Jaeger gravimeter handled by the Geophysical
Survey Institute, Japan, altogether 14 transportable devices
have been available in 1988.

Between 1976 and 1988, about 200 stations have been surveyed
world-wide with these instruments, some of them repeatedly.
The different observation campaigns served for the following
purposes:

- <u>testing</u> of new instruments and <u>comparison</u> with other gravi-
  meters (e.g. BOULANGER 1983, 1986),

- establishment of large scale <u>gravimeter calibration lines</u>
  (e.g.CANNIZZO et al. 1978),

- control of <u>I.G.S.N.71</u> and establishment of stations for the
  planned <u>global absolute gravity network</u> (e.g. ARNAUTOV et al.
  1979),

- control of existing and strengthening of new <u>national funda-
  mental gravity networks</u> (e.g. OGIER and SAKUMA 1983, XU SHAN
  et al. 1986),

- monitoring of <u>gravity variations with time,</u> related to recent
  geodynamic processes especially in earthquake regions
  (e.g. HANADA et al. 1985, ZUMBERGE et al. 1986).

4. Some results obtained with the JILAG-3 gravimeter

of IfE Hannover

Within a cooperative program between the Joint Institute for
Laboraty Astrophysics (JILA), National Bureau of Standards
and University of Colorado (Prof. Faller) and the Institut
für Erdmessung (IfE), University of Hannover, and with support
of Deutsche Forschungsgemeinschaft (DFG), Bonn, IfE obtained
one of the recent JILA free-fall gravimeters in 1986. After
laboratory investigations and software improvements, more than
80 gravity determinations on about 50 stations have been per-
formed until October 1988 (approximately 150 000 individual
free-fall experiments). We summarize some of the results and
experiences, as an example of the present state of absolute
gravimetry (TORGE et al. 1987, 1988).

The JILA gravimeter employs the direct free-fall method, using
a dropping distance of 0.2 m, see Figure 3. There are two re-
markable
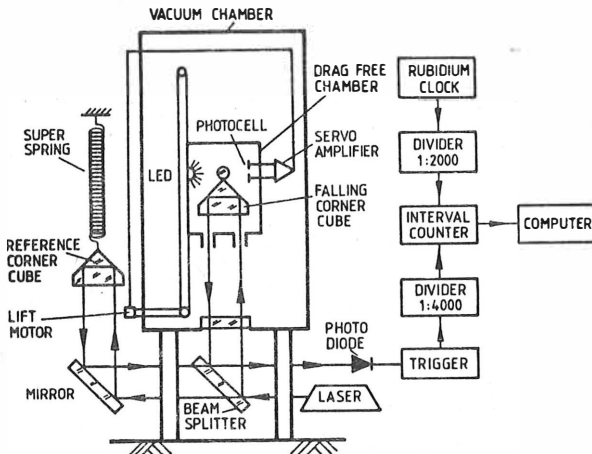
Fig.3: JILA free-fall gravimeter principle

constructive measures in this instrument, the drag-free chamber
and the super-spring. The first one reduces the effect of resi-
dual gas molecules by screening the dropped object in a servo-
controlled, motor-driven evacuated chamber which moves inside
the main vaccum system. The second one isolates the reference
corner cube against ground vibration, through a long-periodic
(T = 30 to 60 s) spring, where the oscillation period is gene-
rated electronically with a spring of 30 cm length. Thus, the
drop-to-drop dispersion is reduced by a factor of 10 to 100.

The mean wavelength of the two wavelengths frequency-stabilized
He-Ne-laser remains constant to 2 x 10^{-9}/a and is calibrated
regularly with a iodine-stabilized laser. In operation, inclu-
ding transport, the vacuum (10^{-4}Pa) is continuously maintained.
With a stable set-up in rooms at ground level with room tempe-
ratures of 15° to 25°C standard deviations of a few ± 0.01μms^{-2}
were achieved with 500 to 2000 drops, at observation times of
2 to 6 hours. Fig. 4 shows the microseismic scatter and the
histogram of the residuals, at average station conditions.
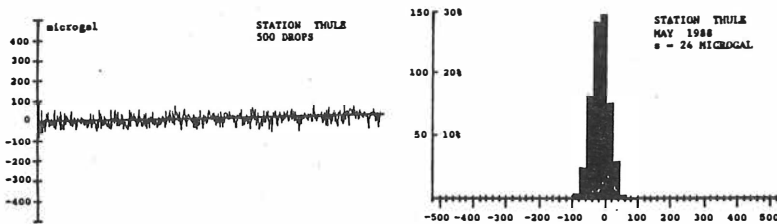
Fig. 4: Microseismic scatter and histogram of the
residuals, station Thule, Greenland

For the HP 9816 process-computer, an on-line program was deve-
loped, which performs the evaluation and all required reductions
(earth tides with ± 0.01 μms^{-2}, atmospheric pressure, polar
motion finite, velocity of light inside the interferometer).
Pulse division by 4000 leads to a time counter recording of 200
divided pulses, corresponding to observing time values at 200
equidistant positions of the dropped prism separated by about
1.25 mm (4000 times half the laser wavelength). The microcomputer
performs an on-line adjustment and stores the gravity value on
flexible disk. One drop takes about 2 s, and for data transfer
and evaluation another 8 s are necessary, thus one experiment is
performed in 10 s. 50 drops per each wavelength (red/blue) are
combined to a sub-set, 10 to 30 sub-sets or more are performed
per station. The instrument's adjustment is generally controlled
after ten sub-sets. The measurement on one station can be comple-
ted in one day, whereby the measurement process is completely
automatic (after the selection of the number of sets). The gravity
difference between the absolute gravity reference height (0.8 m)
and ground level is observed with two LaCoste-Romberg gravimeters
equipped with electronic feed-back systems, with an accuracy of
± 0.01...0.02 μms^{-2}, RÖDER et al. (1985).

From results, obtained over two years in Hannover, a repeatability
of ± 0.1 μms^{-2} has been found, see Fig. 5.
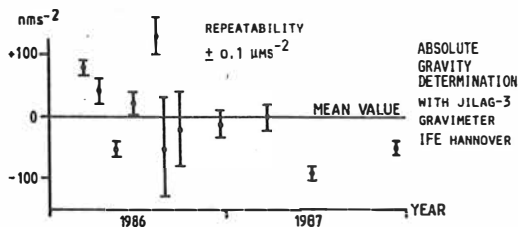
Fig.5: Gravity values observed over two years with JILAG-3
gravimeter in station 101 (mean value 9.812 633 08ms^{-2}),
IfE Hannover

In the sequel, we list the measurements performed since 1986,
and their scientific objectives:

- Absolute gravity sites, observed with other instruments, in
  order to check the accuracy of the instrument. This includes
  the BIPM, Sèvres (see Table 1), 6 station established with
  the Italian IMGC absolute gravimeter (see Table 2), and the
  station Potsdam, observed several times with the USSR GABL
  gravimeter

Station	Epoch JILAG-3	JILAG (μms^{-2})	IMGC (μms^{-2})	Diff. (μms^{-2})	Bias-red. diff. (μms^{-2})
BRAUNSCHWEIG	860327	981 252 9.14	9.23	−0.09	0.04
BRAUNSCHWEIG	870219	981 252 9.30	9.23	0.07	0.20
HAMBURG	860417	981 363 6.56	6.92	−0.36	−0.23
HAMBURG	870326	981 363 6.46	6.92	−0.46	−0.33
MUENCHEN	860420	980 723 1.11	1.28	−0.17	−0.04
WIESBADEN	860422	981 036 8.45	8.67	−0.22	−0.09
SEVRES A3	860607	980 925 9.13	9.17	−0.04	0.09
COPENHAGEN	860820	981 495 5.91	5.82	0.09	0.22
BRUXELLES A	870610	981 117 2.65	2.66	−0.01	0.12

Mean: −0.13   −0.02

RMS Difference: ±0.22   ±0.18

Table 2: Comparison of JILAG-3 observations with IMGC
          observations (IMGC observations with IfE gradients),
          after TORGE et al. (1987)

- 12 stations (including 4 IMGC sites) of the Gravity Base Net-
  work of the Federal Republic of Germany (DSGN76), and of the
  1. order gravity network of Lower Saxony, in order to control
  the accuracy of these networks, and the relative accuracy of
  the absolute gravity values,

- 9 stations (including 3 base net stations) on the <u>calibration line Cuxhaven-Hannover-Harz</u> (KANNGIESER et al. 1983), in order to control the absolute gravity level and the scale of this line,

- 7 gravity stations (including one DSGN76 station) in Southwest Germany, as calibration standard and for strengthening gravimetric control in the <u>Hohenzollern-Graben geodynamic test</u> area ,

- multiple determination in the <u>earth-tide station Brussels</u> for drift and (eventually) absolute calibration control of the superconducting gravimeter operated at the Royal Astronomical Observatory,

- 3 stations of the southernmost <u>Scandinavian gravity land uplift line</u> for absolute gravity control,

- 5 stations on the Faeroer (1), in Reykjavik, and in Greenland (3) as control and improvement of the <u>global gravity network,</u> as a basis for <u>regional networks,</u> and part of the <u>global absolute network,</u>

- 6 gravity stations in northern Iceland, for supporting the existing gravity control, maintained for monitoring <u>temporal gravity variations</u> of tectonic origin (TORGE and KANNGIESER 1985),

- 6 stations in <u>Venezuela,</u> as a support for the existing <u>geodynamic gravity control networks, regional</u> gravity control, and part of the <u>global</u> absolute network.

After nearly 3 years of experiments, hard- und software improvements, and a number of observation campaigns performed under different and partly extreme conditions, it may be stated that the JILAG gravimeter can be operated by an expert team in an almost routine manner, delivering an average station accuracy of ± 0.1 μms^{-2}. Systematic discrepancies have been found with respect to the results of other gravimeters, which may be due to instrumental effects.

5. Conclusions

The following conclusions may be drawn for absolute gravimetry:

- free-fall absolute gravimeters are <u>operational</u> today, with transportable devices delivering an average accuracy of ± 0.1 μms^{-2} within one day, under optimum conditions,

- larger errors, which are difficult to detect and identity, may occur under difficult <u>environmental</u> conditions,

- systematic discrepancies between different absolute gravimeters indicate <u>instrumental effects</u> which are not yet fully understood. Further comparisons and investigations in this direction are urgently needed.

Nevertheless, absolute gravimeters can already be employed for numerous purposes, for delivering the absolute gravity standard,

and for calibration and strengthening of networks established
with relative gravimeters. If the absolute standard is strived
for, an instrumental control by comparison with other absolute
gravimeter results should be performed. We mention the following
applications:

- Establishment of the International Absolute Gravity Basestation
  Network (IAGBN), as proposed by IAG (BOEDECKER and FRITZER 1986),

- establishment of new and improvement of existing national or
  regional fundamental gravity networks, the reasonable gravity
  difference between absolute stations now being about 1000
  μms^{-2},

- inclusion in regional and local geodynamic control networks,
  in connection with relative gravimetry, geodetic space tech-
  niques, and levelling,

- calibration of relative gravimeters (field instruments and
  recording devices),

- drift control for recording gravimeters.

References

ALASIA, F., L. CANNIZZO, G. CERUTTI, I. MARSON: Absolute
    gravity acceleration measurements: Experiences with a
    transportable gravimeter. Metrologia 18, 221-229, 1982.

ARNAUTOV, G.P., Yu. D. BOULANGER, G.D. KARNER, S.N.SCHEGLOV:
    Absolute determination of gravity in Australia and Papua
    New Guinea during 1979. Bureau of Mineral Resources
    J. of Australian Geology and Geophysics 4, 383-393, 1979.

ARNAUTOV, G.P., Yu. D. BOULANGER, E.N. KALISH, V.P. KORONKEVITCH,
    Yu.F. STUS, V.G. TARASYUK: "Gabl", an absolute free-fall
    laser gravimeter. Metrologia 19, 49-55, 1983.

BESSEL, F.W.: Untersuchungen über die Länge des einfachen Sekun-
    denpendels. Abh. Kgl.Preuß.Akad. d.Wiss. zu Berlin, math.Kl.,
    Berlin 1828.

BOEDECKER, G., B. RICHTER: Das Schweregrundnetz 1976 der Bundes-
    republik Deutschland (DSGN76), Teil II: Netzentwurf,instru-
    mentelle Vorarbeiten und Datenaufbereitung. Deutsche Geod.
    Komm., Reihe B, Nr. 271, München 1984.

BORRASS, E.: Bericht über die relativen Messungen der Schwerkraft
    mit Pendelapparaten in der Zeit von 1808 bis 1909 und ihre
    Darstellung im Potsdamer Schweresystem. Verh. d. 16. Allg.
    Conf. d.Int. Erdmessung, London 1909, III. Teil: Spezial-
    bericht über die relativen Schweremessungen, Berlin 1911.

BOULANGER, Yu.D., G.P. ARNAUTOV, S.N. SCHEGLOV: Results of compa-
    rison of absolute gravimeters, Sèvres 1981. Bull. d'Inf. Bur.
    Grav.Int. No.52, 99-124, 1983a.

BOULANGER, Yu.D., J.E. FALLER, E. GROTEN et al. (eds.): Results
    of the second international comparison of absolute gravi-
    meters in Sèvres 1985. Bull. d'Inf. Bur. Grav. Int., No.59
    89-103, 1986.

CANNIZZO, L., G. CERUTTI, I. MARSON: Absolute-gravity measurements
    in Europe. II Nuovo Cimento 1C, 39-85, 1978.

COOK, A.H.: The absolute determination of the acceleration due
    to gravity. Metrologia 1, 84-114, 1965.

COOK, A.H.: A new absolute determination of the acceleration
    due to gravity at the National Physical Laboratory, Eng-
    land. Phil. Trans. Roy. Soc., London, A 261, 211-252,1967.

FALLER, J.E.: Results of an absolute determination of the
    acceleration of gravity. J. Geophys. Res. 70, 4035-4038,
    1965.

FALLER, J.E., Y.G. GUO, J. GSCHWIND, T.M. NIEBAUER, R.L. Rinker,
    J. XUE. The JILA portable absolute gravity apparatus.
    Bull. d'Inf. Bur. Grav. Int. No.53, 87-97, 1983.

FALLER, J.E., I. MARSON: Ballistic methods of measuring g- the
    direct free-fall and symmetrical rise-and-fall methods
    compared. Metrologia 25, 49-55, 1988.

FENG, Y., G. ZHANG, D. LI, X.QUI, J. ZHOU, J. GAO, D. HUANG,
    CH. HUANG, Y. GUO: A transportable absolute gravimeter
    for determining the acceleration due to the earth's
    gravity. Metrologia 18, 139-143, 1982.

GALILEI, Galileo: Dialogo di Galileo Galilei Linceo soprai due
    massimi sistemi del mondo Tolemaico e Copernicano Florenz
    1632.

GUILLET, A.: Mesure precise de l'acceleration g de la chute des
    corps dans le vide. Comptes Rendus Acad. Sci. Paris 207,
    614-616, 1938.

HAMMOND, J.A., J.E. FALLER: Results of absolute gravity deter-
    minations at a number of different sites. J. Geophys. Res.
    76, 7850-7854, 1971.

HANADA, H., T. TSUBOKAWA, M. OOE: Results of absolute gravity
    surveys in Tohoku district, Japan. Bull. d'Inf. Bur. Grav.
    Int. No.57, 97-112, 1985.

HELMERT, F.R.: Die mathematischen und physikalischen Theorien
    der höheren Geodäsie. Teubner, Leipzig 1880/1884.
    (Nachdruck Minerva GmbH, Frankfurt a.M. 1962).

HELMERT, F.R.: Beiträge zur Theorie des Reversionspendels.
    Veröff. Kgl.Preuß.Geod.Inst. und Centralbur. Int.Erdmessung,
    Berlin 1898.

HELMERT, F.R.: Bericht über die relativen Messungen der Schwerkraft mit Pendelapparaten. Verh. d. 13. Allgem. Conf. d. Int. Erdmessung, Paris 1900, II. Teil: Spezialberichte u. Wiss. Mitt., 139-377, Berlin 1901.

HELMERT, F.R.: Bericht über die Schwerebestimmungen. Verh. d. 16. Allg. Conf. d. Int. Erdmessung, London 1909, I. Teil: Sitzungsberichte und Landesberichte über die Arbeiten in den einzelnen Staaten, Berlin 1910.

HUYGENS, Christiani: Horologium oszillatorium sive de motu pendulorum ad horologia aptato. Paris 1673.

HYTÖNEN, E.: Absolute gravity measurement with long wire pendulum. Publ. Finn.Geod.Inst., No.75, Helsinki 1972.

KANNGIESER, E., K. KUMMER, W. TORGE, H.-G. WENTEL: Das Gravimeter-Eichsystem Hannover. Wiss. Arb. Univ. Hannover Nr.120, 1983.

KATER, H.: An account of experiments for determining the length of the pendulum vibrating seconds in the latitude of London. Phil. Trans. Roy. Soc., London, A 108, 33-102, 1818.

KÜHNEN, F., Ph. FURTWÄNGLER: Bestimmung der absoluten Größe der Schwerkraft zu Potsdam mit Reversionspendeln. Veröff. Kgl. Preuß. Geod. Inst. Potsdam, N.F. Nr.27, Berlin 1906.

MORELLI, C., C. GANTAR, T. HONKASALO, R.K. McCONNELL, J.G. TANNER, B. SZABO, U. UOTILA, C.T. WHALEN: The International Standardization Net 1971 (ISGN71). I.U.G.G.-I.A.G.-Publ. Spec. No.4, Paris 1974.

OGIER, M., A. SAKUMA: Mesures absolues de pesanteur en France. Bull. d'Inf. Bur.Grav. Int. No.53, 98-113, 1983.

RICHER, J.: Observations astronomiques et physiques faites en l'isle de Caienne. Paris 1679.

RÖDER, R.H., M. SCHNÜLL, H.-G. WENZEL: Gravimetry with an electrostatic feedback system. Bull. d'Inf. Bur. Grav.Int. No.57, 72-81, 1985.

SAKUMA, A.: Etat actuel de la nouvelle dètermination absolue de la pesanteur au Bureau International des Poids et Mésures, Sèvres. Bull.Géod. No.69, 249-260, 1963.

SAKUMA, A.: An industrialized absolute gravimeter: Type GA 60. Bull. d'Inf. Bur. Grav.Int. No.53, 114-118, 1983.

SAKUMA, A.: Gravitational acceleration, mass, and electrical quantities. In: B.N. Taylor, W.D. Phillips (eds.), Precision Measurement and Fundamental Constants II, Nat. Bur. Stand. (U.S.) Spec. Publ. 617, 397-404, 1984.

SCHÜLER, R., G. HANISCH, H. FISCHER, R. FREY: Absolute Schwere-
        messungen mit Reversionspendeln in Potsdam 1968-1969.
        Veröff. Zentralinst. f. Phys. d.Erde Nr.10, Potsdam 1971.

STERNECK, R. von: Der neue Pendelapparat des k.u.k. Militär-
        Geographischen Institutes. Mitt. d. K.K. Milit.Geogr.Inst.,
        VII, Wien 1887.

  TORGE, W.: The present state of relative gravimetry. In: Proceed.
        Gen. Meeting of the I.A.G., 319-324, Tokyo 1982.

  TORGE, W.: Absolute Schweremessung mit transportablen Gravi-
        metern - ein Umbruch in der Gravimetrie. Z.f.Verm.wesen
        112, 224-234, 1987.

  TORGE, W.: Zum Aufbau von Schwerebezugssystemen. In: Fest-
        schrift Rudolf Sigl zum 60. Geburtstag. Deutsche Geod.
        Komm., Reihe B, Nr. 287, 207-217, München 1988.

  TORGE, W.: Gravimetry. W. de Gruyter, Berlin-New York 1989.

  TORGE, W., E. KANNGIESER: Regional and local vertical crustal
        movements in northern Iceland, 1965-1980. J. Geophys.Res.
        90, 10173-10177, 1985.

  TORGE, W., R.H. RÖDER, M. SCHNÜLL, H.-G. WENZEL, J.E. FALLER:
        First results with the transportable gravity meter
        JILAG-3. Bull. Géod.61, 161-176, 1987.

  TORGE, W., R.H. RÖDER, M. SCHNÜLL, H.-G. WENZEL, J.E. FALLER:
        Laboratory and field tests of JILAG-3 absolute gravi-
        meter. Bull. d'Inf. Bur.Grav.Int. No.62, 36-40, 1988.

  VOLET, CH.: Mesure de l`accélération due à la pesanteur, au
        Pavillon de Breteüil. Comptes Rendus Acad.Sci. Paris 235,
        442-444, 1952.

  XU SHAN, QUI QIXIAN, JIAN ZHIHENG, F. ALASIA, G. CERUTTI,
        S. DESOGUS, I. MARSON: Sino-Italian joint absolute gra-
        vity measurements in China. Bull d'Inf. Bur.Grav. Int.
        No. 59, 149-159, 1986.

  ZUMBERGE, M.A., G. SASAGAWA, M. KAPPUS: Absolute gravity
        measurements in California. J.Geophys. Res. 91,
        9135-9144, 1986.

THE CONTRIBUTION OF DETERMINATIONS OF GRAVITY FIELD VARIATIONS TO GEODYNAMICS .
A COMPARISON WITH OTHER TECHNIQUES

by E. Groten and M. Becker

Institut für Physikalische Geodäsie
Technische Hochschule Darmstadt
Petersenstraße 13
D-6100 Darmstadt
Fed. Rep. of Germany

Abstract

Present high-precision (± 1 cm and better) techniques such as VLBI, SLR, LLR
etc., yield deformations of the earth's surface related to more or less
arbitrary geodetic datums. Moreover, these basically relative and geometrical
methods give uplift and subsidence with respect to an arbitrary ellipsoid which
has no fundamental physical meaning. Precise relationship with respect to the
gravity field in terms of level surfaces etc. implies very precise gravity
control in terms of repeated gravimetry or similar techniques. From a variety of
such experiences we meanwhile know accuracies, perturbations, unresolved
problems and special requirements of such measurements. Typical examples are:
(1) the Paris micronet measurements, (2) the international D-meter campaign
(locally), (3) the Turkey-testnet (regional), (4) the A-B-C-profile and
Fennoscandia (large scale) and (5) the Norway experiment (man-made effects). A
variety of perturbing effects such as load-tide still needs further
investigation in order to achieve accuracies of a few microgal in these cases.
Further projects such as (a) Northern India and (b) the African experiment are
described. The necessities of combining relative gravimetry with absolute
gravity observations, geometrical measurements and local observations such as
tilt- or tube measurements in order to eliminate local perturbations are
discussed. A critical review and a detailed outlook on the contribution of
gravimetry to monitoring tectonic plate motion and similar geodynamic aspects is
given.

1. Introduction

Repeated relative gravity has meanwhile achieved an accuracy which makes it
compatible with modern space techniques such as VLBI, SLR etc. Whenever tidal
loading effects are available so that associated reductions can be made with
sufficient accuracy and scaling by relating relative gravimetry to a few
absolute gravity stations is feasible we can obtain, by using simultaneously 10
or so gravimeters, resolution of the order of ± 10 microgal even under
unfavorable conditions, which corresponds to about ± 1 cm or so in vertical
displacement. Over shorter distances and in more favorable conditions it can be
much better: Thus we may summarize our results as follows: (1) in the BIPM
(Paris) indoor a micronet resolution of about ± 1 microgal was achieved and
corroborated by repeated observations, (2) in the International D-meter campaign
over distances of 100 km about ± 2 microgal was obtained; (3) in a local network
in Anatolia for geodynamic purposes over 30 km about ± 4 microgal were found in

several repetitions; (4) in the Fennoscandian uplift experiment over two decades resolution of similar type was reached over much longer distances; (5) under quite unfavorable conditions in Southern Norway resolution of about ± 5 to ± 6 microgal is achieved; (6) under extremely unfavorable conditions in the high Andes accuracy of ± 5 (by train) and ± 10 to 12 microgal (by car and aircraft) were found for long distances. By applying a 3 sigma rule 30 microgal would be available as an accuracy limit today. In all north-south or mountain experiments calibration can pose a problem unless zero-network-techniques are applied. For verification in the norwegian experiment tilt measurements using vertical pendulums around the project area are used; level measurements by using tubes can mainly be used in a similar fashion (averaging out local perturbations) in underground experiments.

By repeating gravity observations we obtain gravity variations with time besides relative gravity values themselves. As VLBI, SLR, GPS etc. yield ellipsoidal height variations the tranformation into orthometric height variations has to be done using gravity data. Thus gravimetry serves a double purpose.

2. The present state of relative gravity networks

The instrumental error sources of the LaCoste gravimeters used in high precision gravity work are well known and are analyzed in numerous papers, see (Groten, 1983) or (Becker, 1984) for a review. From these investigations the following figure describing the effects of the instrumental errors can be deduced.
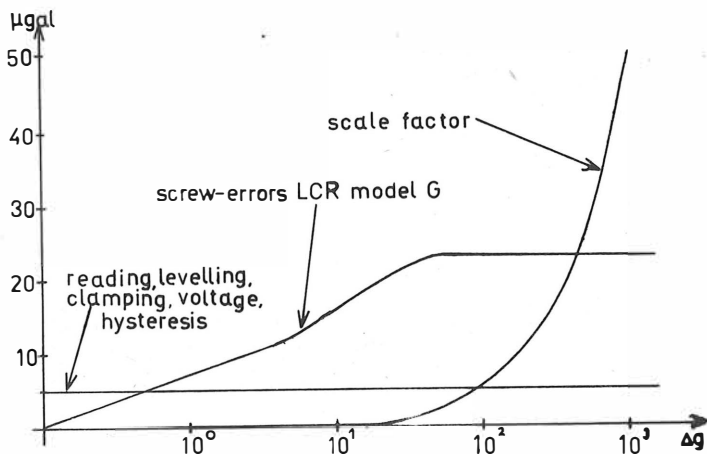
Fig. 1 INSTRUMENTAL ERRORS OF LACOSTE GRAVIMETERS VERSUS GRAVITY DIFFERENCE

However, in the analysis of data gathered in field surveys of various networks
often a clear association of the residuals with a certain error source is hard
to find. In spite of rather sophisticated modeling the different effects are
obscured and the adjustment results in an error estimate which is depending on
the effectiveness of certain error source-types in the network under
consideration. Based on the experiences at the Institut of Physical Geodesy we
would like to demonstrate the potential of gravity measurements in a number of
quite different applications and, what is also important, using different
instruments.

The BIPM micronet for connecting the sites of absolute gravity measurements is
an example of an almost ideal situation where the utmost precision should be
obtainable. The sites are indoor in one house, the temperature is rather stable,
gravity differences are below 1 mgal and the only remaining unknown error surce
are possible magnetic effects for different gravimeters used. Detailed analysis
are published in (Becker, 1983, 1985), (Boulanger, Faller, Groten, 1986). In
general the accuracy of the adjusted gravity differences in both the 1981 and
the 1985 campaigns was about 0.8 μgal for a combined adjustment of 6 to 14
instruments and about 1.4 μgal for single instruments in the average, see Tab.
1. However, the averaging of several gravimeters is a must because systematic
discrepancies between instruments of up to 10 μgal for an adjusted gravity
difference may occur.

year	1981	1985
free net gravity value accuracy [μgal]	± 0.9	± 0.4[*]
number of observations	274	667
number of sites	5	6
vertikal. gradient accuracy [μgal]	± 1.3	± 0.8
number of observations	190	706
number of sites	4	6
number of gravimeters	6	14

[*] For single instruments between 0.3 to 3.3, 1.5 μgal in the average

Tab. 1 BIPM micronet accuracies

With the broader use of electrostatic feedback systems, see (Harrison and Sato,
1984), (Vaillant et al., 1986), for field measurements with LaCoste G- and D-
meters the situation is not changed dramatically. As the results published in
(Röder and Wenzel, 1986) show, the accuracy of feedback-instruments is slightly
better whereas the internal precision should obviously be the same as for
properly operated standard gravimeters. However, there still are systematic
discrepancies of 4 to 8 μgal between single instruments.

An other outcome of these campaigns of BIPM was the fact, that great care has to
be taken in choosing the observation sites and identifying the exact locations.

Mass distributions of pillars and walls can cause horizontal gradients of 10 μgal/m and variations just as big in the vertical gradient.

At the occasion of the IAG D-meter campaign in 1983, where 12 LaCoste Model D-gravity meters were used, it was demonstrated that accuracies of one to two μgal for the adjusted gravity differences can in principle be obtained also under field conditions with longer transportation times and larger gravity differences. As shown in the detailed analysis (Becker, 1984) several gravimeters reached the same precision in indoor calibrations and on the 200 mgal calibration line Hannover-Harz. This however is a special case where extraordinary efforts in design of measurements, site selection, transportation, number of observations and modeling were undertaken.

In general and especially with Model G gravity meters, which have to be used in case of larger gravity differences, the results in networks for monitoring gravity changes were found to be less accurate than calibration measurements. In the sequel we will compare the results of three different projects of this type, namely the monitoring net across the North Anatolian Transform Fault (NATF), the net at the Blasjo-artificial lake and the Southamerica Geodynamics Profiles.

The plate motion situation in Turkey is discussed in detail in (Jackson and McKenzie, 1988). Although the main movements along the NATF are horizontal displacements, see e.g. (Jackson and McKenzie, 1988), there is evidence from geomorphology for considerable height changes. The gravity net extends across the fault and since its installation in 1982 four main repetitive observations took place. Due to the North-South extension and mountain ranges the "zero-network type", where all gravity differences are smaller than 1 mgal and so minimizing the calibration errors, could not be used. Tab. 2 gives the accuracies obtained in the various campaigns using 2 gravity meters.

year	1982	1984	1985	1986
free net gravity value accuracy [μgal]	± 2	± 3	± 3	± 4
number of observations	204	162	142	90
number of stations	9	10	10	14

Tab. 2   Accuracies of Turkey network

In the analysis of gravity variations, see (Aksoy et al., 1988), the variations of 0-10 μgal turned out to be insignificant and not caused by a systematic height or gravity change. This result is corresponding to other geodetic studies indicating a phase of inactivity for this region of the NATF. Here repeated gravity measurements were successful in verifying that no significant changes occured till now. The network is considered to be a densification of the WEGENER/MEDLAS-project as soon as the GPS determination of coordinate variations associated with gravity changes are carried out.

Whereas the net mentioned above is designed to monitor changes by geophysical processes man can not affect, the situation at the Blasjo lake is different. Here the gravity and height changes associated to the filling of Nothern Europe's biggest reservoir shall be monitored. As, e.g., the investigations of
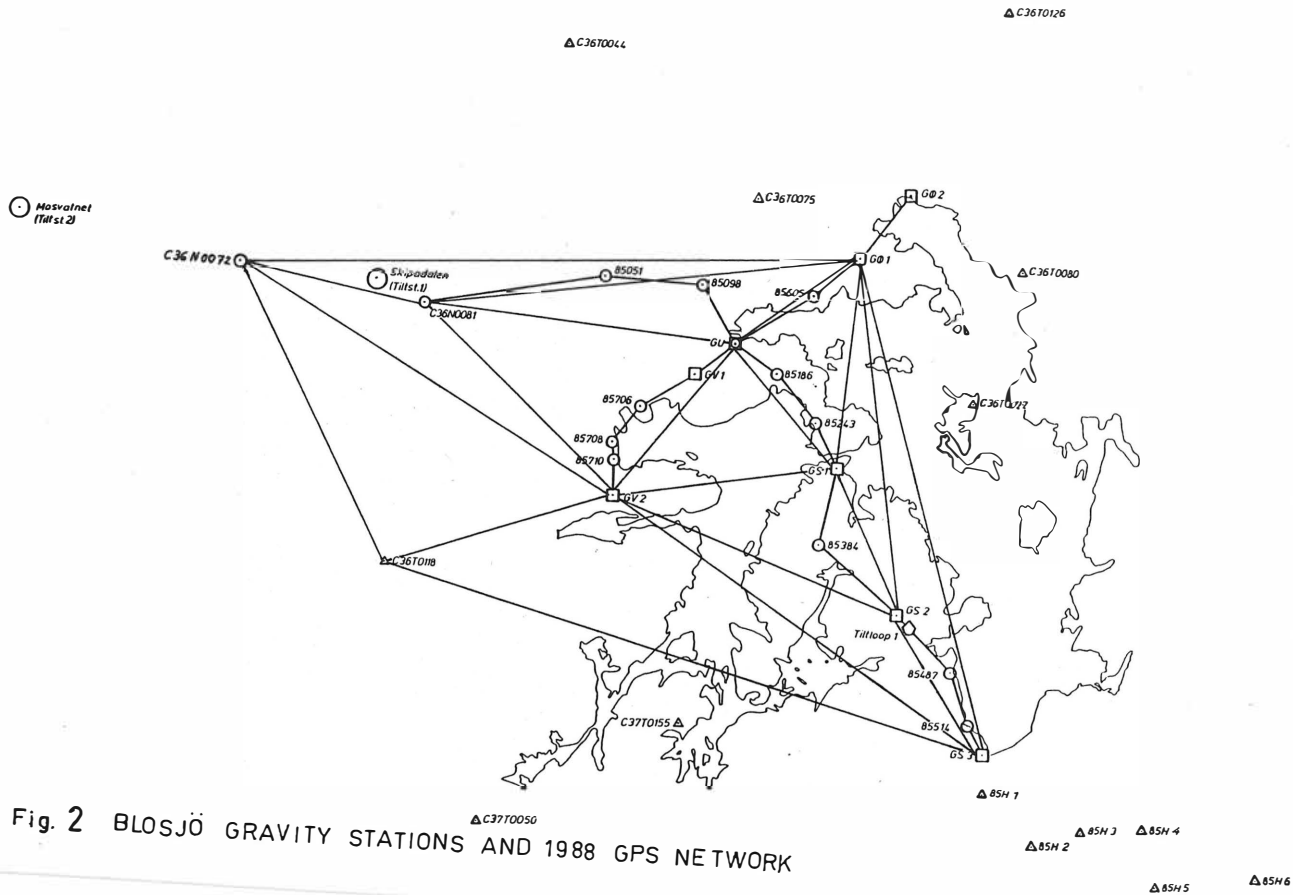
Fig. 2 BLOSJÖ GRAVITY STATIONS AND 1988 GPS NETWORK

21

Lambert et al.(1986) show, rather complicated phenomena, like uplift together
with increasing gravity are occuring in connection with those artificial man
made changes. Therefore Blasjo is a rather universal object also for studies of
seismicity, tilt-changes and loading effects. In addition to the gravity network
shown in Fig. 2 precise levelling was performed in parallel to the gravimeter
measurements and on the same sites, see (Becker et al., 1988) for details and
first results. Moreover in the 1988 campaign a GPS-network was added for the
first time in order to check the geometrical deformation independently. Statens
Kartverk, the Norwegian Mapping Authority, observed the net with two Ti4100 and
two Trimble receivers. As we want to focus on the potential of gravity
measurements here, Tab. 3 gives the accuracies obtained in the different
campaigns. In spite of the fact that the net in view of gravity differences and
distances is very similar to the NATF net in Turkey the accuracy is somewhat
lower.

year	1985	1986	1987
free net gravity value accuracy [μgal]	± 4.5	± 6.5	± 4.5
number of observations	457	539	300
number of sites	28	30	16
number of gravimeters	6	5	4

Tab. 3 Blasjo gravity-monitoring network accuracies

This is probably due to severe environmental disturbances from heavy wind and
hard rain prevailing in this area during most of the observation days in all
campaigns. Another reason may be helicopter transport to the external reference
stations where the elimination of vibrations was not perfect. Comparison of the
gravity values of different epochs revealed significant changes in some
stations, however, part of these changes is due to the direct attraction affect
of the changing water mass which until now we could not yet compute. Gravity
variations due to subsidence or uplift will be determined after application of
these corrections and using lake-levels with maximum difference.

The third example to be presented is conceptually different. In order to monitor
the uplift associated with the subduction process at the active continental
margin in Western Southamerica the "ABC-Profiles" connecting stations in
Argentina, Bolivia and Chile are extending over distances of more than 1000 km,
over height changes of more than 4500 m and gravity differences of up to 2 gal,
see Fig. 3 and (Becker, Groten, Gao, 1985) for details. The figures mentioned
above already indicate that the measurements are affected by quite a number of
disturbances. There are among others rapid pressure and temperature changes due
to aircraft transportation and height variation, vibrational effects in
aircrafts and on roads without pavement, no daily drift control on the longer
profiles etc. In contrary to the small networks cited above, where relative
short transportation times and a proper observation scheme can minimize errors
due to imperfect tidal corrections, in this large network tidal parameters and
ocean tidal loading have to be considered carefully.

The ABC profiles were observed first in 1984 and in 1987 and 1988 the first
repetition was completed using 4 to 8 gravity meters in parallel.

A B C – PROFILES
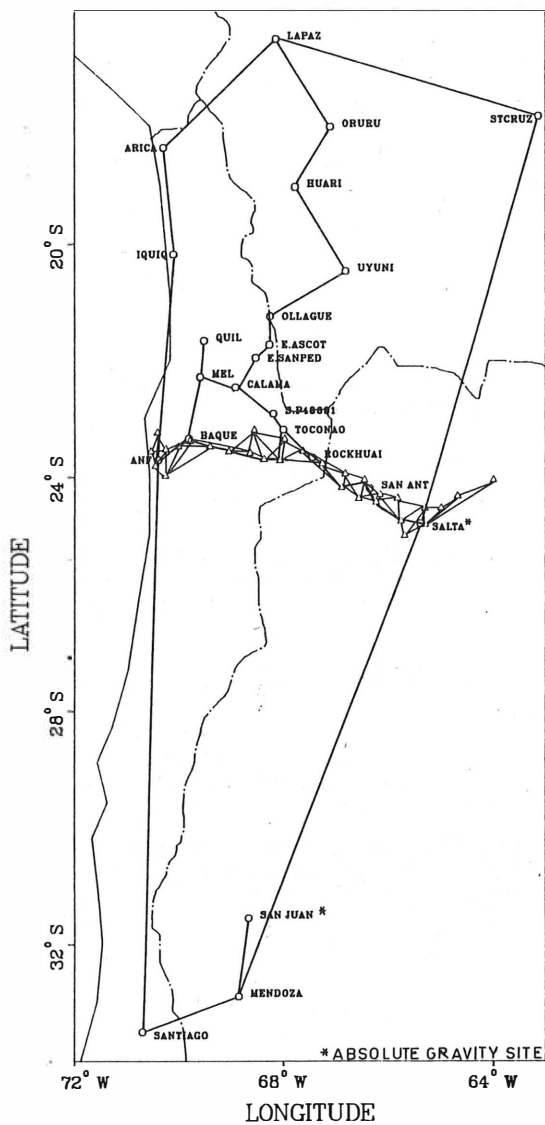
Fig. 3 Gravity stations and GPS-traverse of the South-America profiles

Further gravity monitoring projects in geophysically interesting areas are planned for the northwestern Himalayas, where the convergence of the Indian and Eurasian plates produces motion rates of about 2-4 cm/year horizontally and 1 cm vertically. Combined GPS and gravimetric traverses across the main faults are designed to determine the actual deformation in the area described in view of the gravity field in (Verma and Prasad, 1987).

A project in Sudan and Nigeria with high precision gravity measurements is under consideration in view of the completely different geophysical structure prevailing in these african countries; this area is at the southern and of the WEGENER-MEDLAS-project.

Summarizing the experiences in the various applications Fig. 4 it may be deduced in order to demonstrate the potential of gravimetric observations for geodynamical purposes and for combination with other techniques.
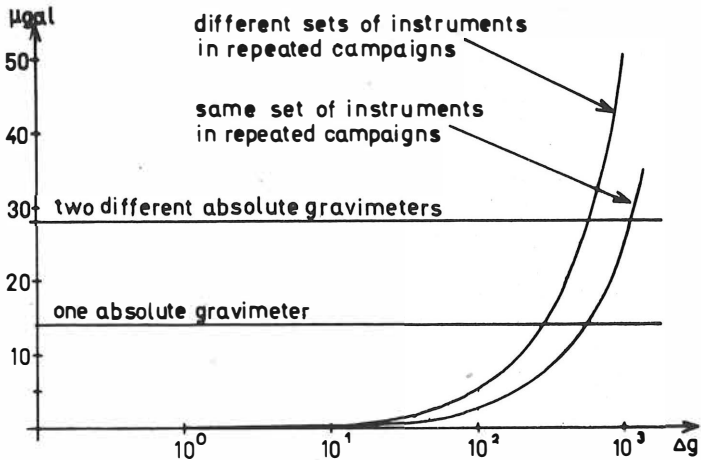
Fig. 4   ACCURACY OF GRAVITY DIFFERENCES
FROM COMBINED ADJUSTMENT WITH
SEVERAL GRAVIMETERS

3. A comparison of station location with the gravity field

It is well known that relative maxima and minima of the Bouguer field are considered in geophysics as indicators of local subsidence and uplift, respectively. In that case, of course, long-range trends have to be removed. This is quite important in high-mountain areas such as the high Andes. In order to demonstrate the last mentioned fact we undertook a low-pass filtering of Rapp's (1981) global spherical harmonics expension of degree n≤180 using the Stokes kernel in spherical harmonics form as a low pass filter $(n-1)^{-1}$. The result is formally called a geoid for the area under consideration; the first degree and a conventional normal gravity field were subtracted. Fig. 5 shows the result. By subtracting, in addition, the global topography in spherical harmonics up to the same degree we obtained what is called analogously a "Bouguer geoid" for the area under consideration. It is consequently based on a spherical Bouguer correction which differs significantly from the flat Bouguer anomaly which will be applied for regional purposes below; this is shown in Fig. 6 and clearly reveals the mass deficit of the isostatic "roots". The trend corresponding to these "roots" is formally eliminated by applying an isostatic correction of Airy-Heiskanen type with a depth of compensation T=50 km which is justified lateron; see Fig. 7 for the associated "Isostatic geoid".
The comparison of the trends inherent in these figures justifies the use of isostatic and trend-removed Bouguer maps. As we aimed at a somewhat shorter wavelength of about 50 to 40 km we used for the detailed comparison the expansion of degree n≤360 by Rapp et al. (1986), Model E; it is here called OSU 86. Its deviation from (Rapp, 1981) is significant only in some parts of the area under investigation. This is demonstrated for free-air, spherical Bouguer and isostatic "geoids" (low-pass-filtered gravity fields as described before). Figs. 8 to 14 contain, together with the main stations of our geodynamic network, the free-air (81 and 86), Bouguer (flat plate (81 and 86), flat refined ["ref."] and spherical (81)); and isostatic (81) "geoids". The free-air and Bouguer data reveal relatively small deviations from each other.

In order to illustrate the trends we took the recent GEM Tl low-degree expansion and plotted the free air gravity field and the associated geoid; see Fig. 15 and 16. This effect should have been subtracted from the local representation but it is seen that it is quite regular in the area under consideration and therefore, does not affect the aforementioned comparison sensibly or significantly.

We used the "geoids" here instead of the gravity maps which better reveal the local part because in the graphical representation its illustration and visualization is easier to understand in the low-pass filtered form. For the detailed comparison, of course, the gravity field itself is of interest. Fig. 17 to 22 show, for a basically qualitative comparison the area under consideration together with the main stations, the free air (81 and 86), Bouguer (flat, flat refined ["ref."] and spherical ["SPH"]) for 81 and the isostatic (81) gravity fields. All our isostatic data are related to compensation depth 50 km.

We may conclude from this comparison that we succeeded only to a certain extent to locate our geodynamic stations at local Bouguer minima and maxima. The reason is, to some degree, to be seen in logistic, topographic and other practical difficulties.

Local comparison:

For the Northern part of Chile, Argentina and Southern Bolivia where a densified gravity network together with GPS-observations was established we had for a similar, but more intensified, study a recent gravity survey made by Goetze

(1986) at our disposal. As these data did not enter Rapp's combination solution
they enable an independent check with each other which gives interesting insight
into the accuracy of Rapp's results. Figs. 23 to 25 show Goetze's free air,
Bouguer (flat plate) and isostatic (compensation depth of 40 km, Airy-Heiskanen
model) gravity fields for this local part. Even though a detailed trend analysis
of the field reveals that a trend-removed Bouguer field significantly deviates
from the isostatic field it seems to be justified to base our considerations on
the isostatic field.

For reasons of accuracy interpretation we show in Figs. 26 to 28 (for the same
local area) the same gravity fields (free air, Bouguer, flat plate and
isostatic) where the isostatic compensation depth was, however, 50 km. By
comparing both fields the similarity of principal parts of the field are obvious
but significant deviations do exist between Goetze's and Rapp's 86-solutions. In
this case the errors inherent in Goetze's solution should be negligible in spite
of distortions in elevation, absolute gravity references etc. In order to
compare the influence of the selected depth of compensation in the isostatic
field we plotted in Figs. 29 to 32 the gravity field for four different depths
T=0,30,50 and 80 km corresponding to Rapp's 81-solution. The direct comparison
corroborates, to some extent, the compensation depths 40 to 50 km chosen by
Goetze and us, respectively. An analogous comparison with the Rapp-86E-solution
yields basically the same result.

It is surprising to see, on inspecting the data, that the free air gravity field
is not as strongly correlated with the terrain as is expected. The actual
gravity deviates obviously in a significant way from the isostatic model, as was
already outlined in connection with Fig. 6. But isostatic compensation appears
to be overwhelming, in principle.

In Figs. 33 and 34 we chose an even more detailed representation with all GPS-
gravity sites (where GPS- and gravity-data where measured) and compared it with
isostatic (T=50 km) and Bouguer fields based on Rapp's 86-data.

It is noteworthy that the vertical gravity gradient varies in the area under
consideration by up to five percent or even more around the normal value. With
elevations of up to 5000 m associated differences between conventional geoidal
and modern surface anomalies differs by more than 50 mgals.

4. **Conclusions**

Microgravimetry is hampered by non-uniqueness problems. With new fast and
efficient high-precision space techniques such as GPS, VLBI etc. the non-
uniqueness problem can be solved and gravity plus geometry is able to attack
four-dimensional boundary value problems by fully exploiting the substantially
increased accuracy and reliability even under unfavorable conditions, of modern
gravimetry.

Geophysical interpretations of gravity fields for detecting areas of uplift and
subsidence is, to some extent also hampered by, slightly different, non-
uniqueness problems. Insofar it is non a full alternative to the geodetic
approach of repeated observations, as far as vertical motion is concerned.

We tried to focus here particularly on the question, to what extent presently
available global gravity models of high resolution (degree of harmonics n≤360
etc.) are reliable enough, in areas where the combination solutions are
particularly poor, for such an interpretation. Our very comprehensive and
detailed comparison based on eventually <u>independent</u> data (this is in contrast to

most present similar studies) shows that in an area which also Rapp and other
experts consider as an area of a poorly determined gravity field (Northern
Argentina) such models cannot yet replace terrestrial surveys dedicated to these
purposes.

As far as time-dependent boundary value problems (BVP) are concerned (Groten and
Hausch, 1986) we have to clearly distinguish between the deformations of the
earth's surface and the associated deformations of level surfaces where the
latter are usually only about ten percent of the first ones; as long as the
accuracy of observations of the surface deformations are not much better than
ten percent of the deformations themselves there is often little meaning in
solving the BVP for the level surfaces.
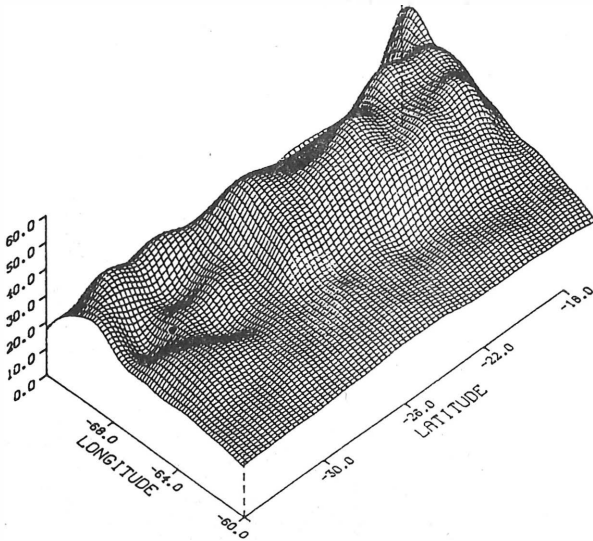
Fig. 5 Free-air-geoid, computed by spherical harmonics of degree 180 (RAPP81)
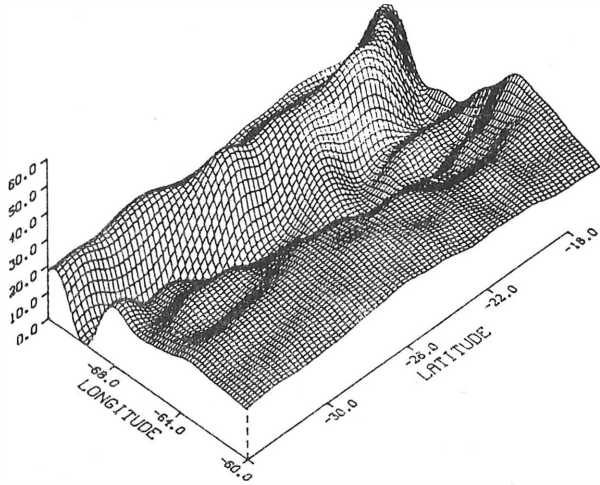
Fig. 6 Bouguer-geoid, computed by spherical harmonics of degree 180 (RAPP81)
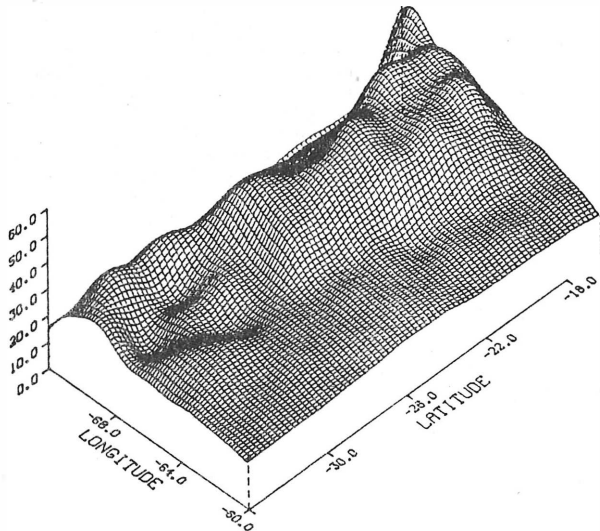
Fig. 7 Isostatic-geoid, computed by spherical harmonics of degree 180 (RAPP81)
level of compensation −50 km

Fig. 8 Free-air-geoid, computed by spherical harmonics of degree 180 (RAPP81)
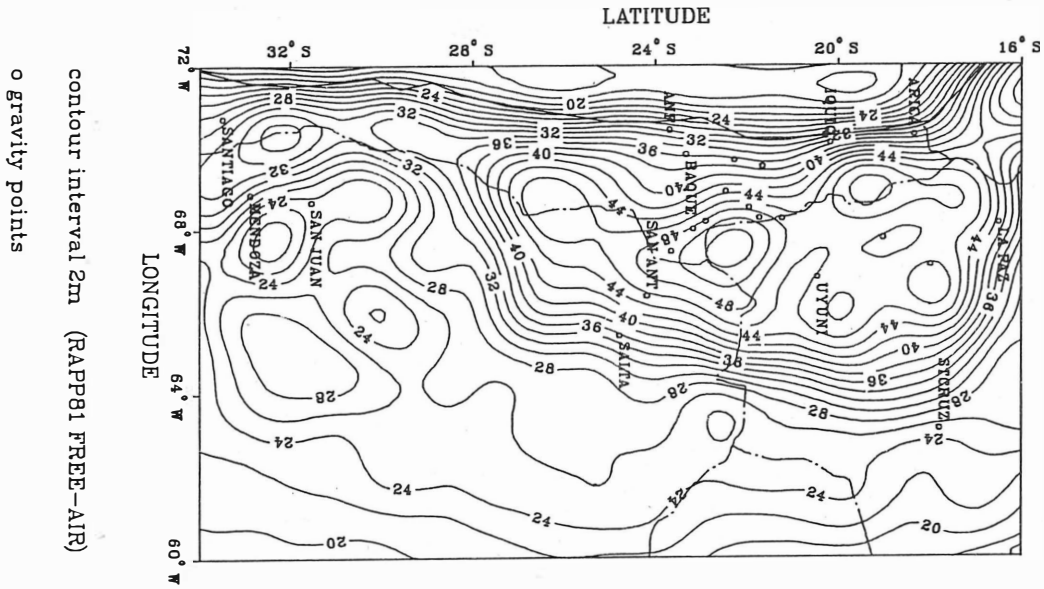
o gravity points

contour interval 2m (RAPP81 FREE-AIR)
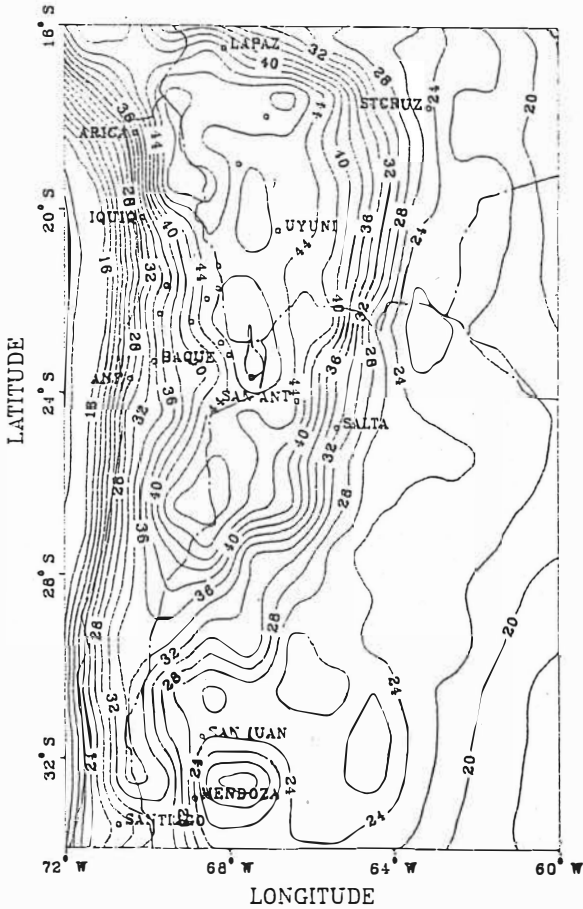
contour interval 2m (OSU86E FREE–AIR)

o gravity points

Fig. 9 Free-air-geoid, computed by spherical harmonics of degree 360 (OSU86E)
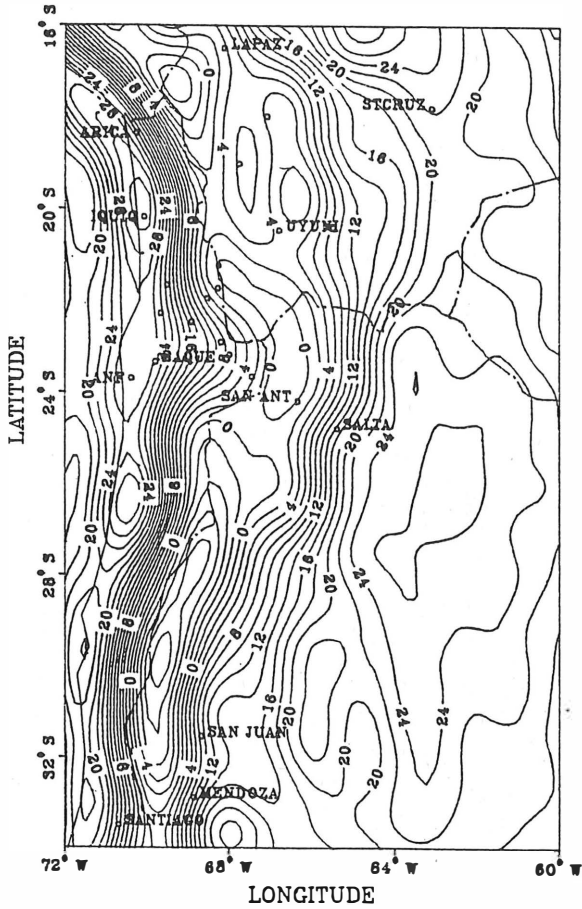
contour interval 2m   (RAPP81 BOUGUER)

o gravity points

Fig. 10   Bouguer-geoid, computed by spherical harmonics of degree 180 (RAPP81)
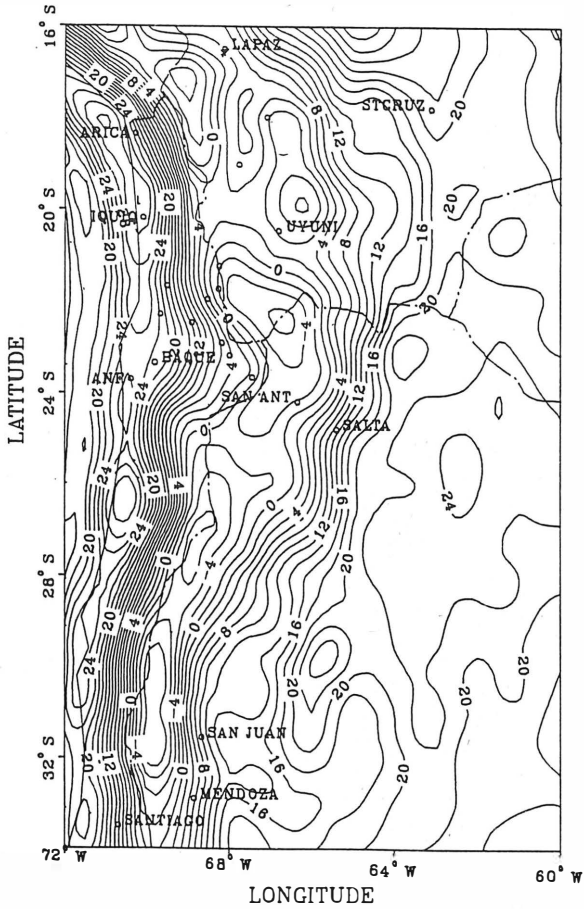
contour interval 2m   (OSU86E BOUGUER)

o gravity points

Fig. 11 Bouguer-geoid, computed by spherical harmonics of degree 360 (OSU86E)
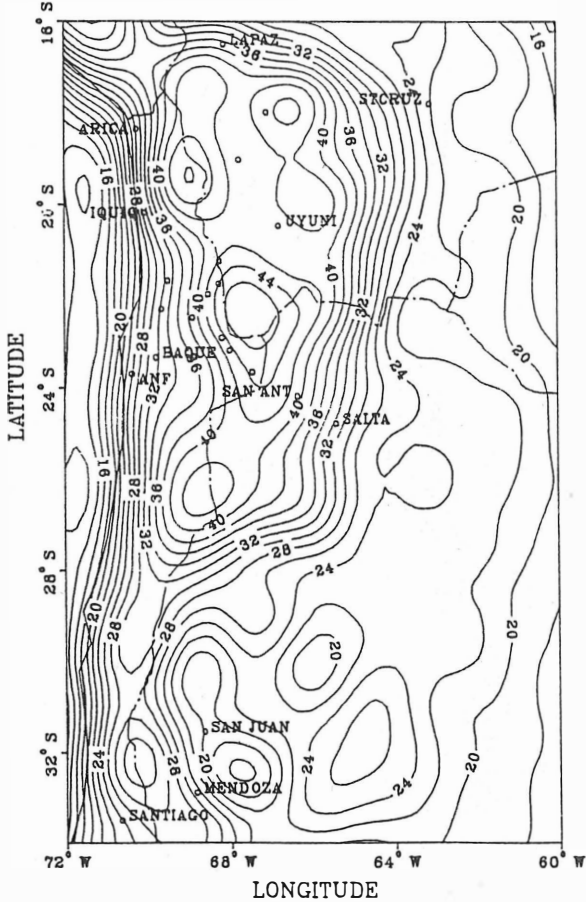
contour interval 2m (RAPP81 BOUGUER REF)

o gravity points

Fig. 12 Refined-Bouguer-geoid, computed by spherical harmonics of degree 180
(RAPP81)
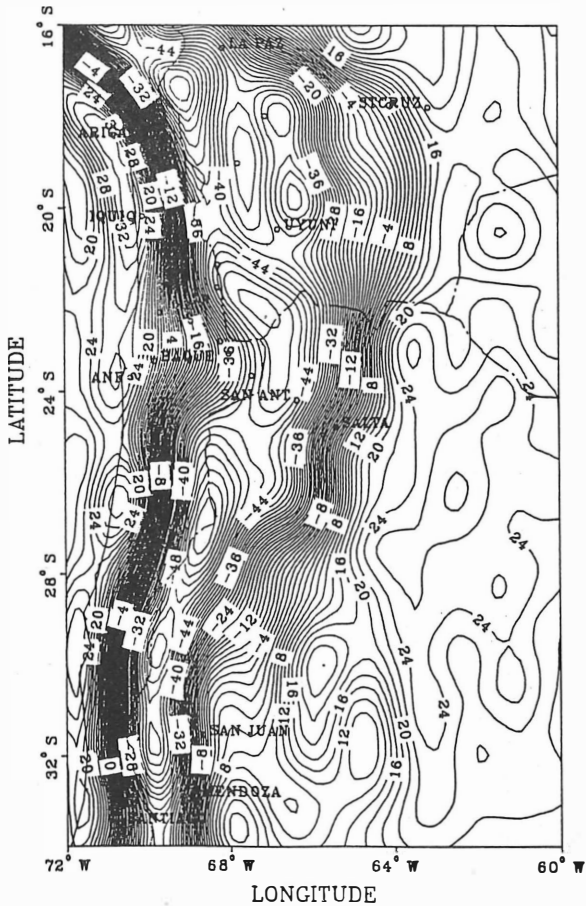
contour interval 2m (RAPP81 BOUGUER)

o gravity points   SPH

Fig. 13 Spherical-Bouguer-geoid, computed by spherical harmonics of degree 180
(RAPP81)
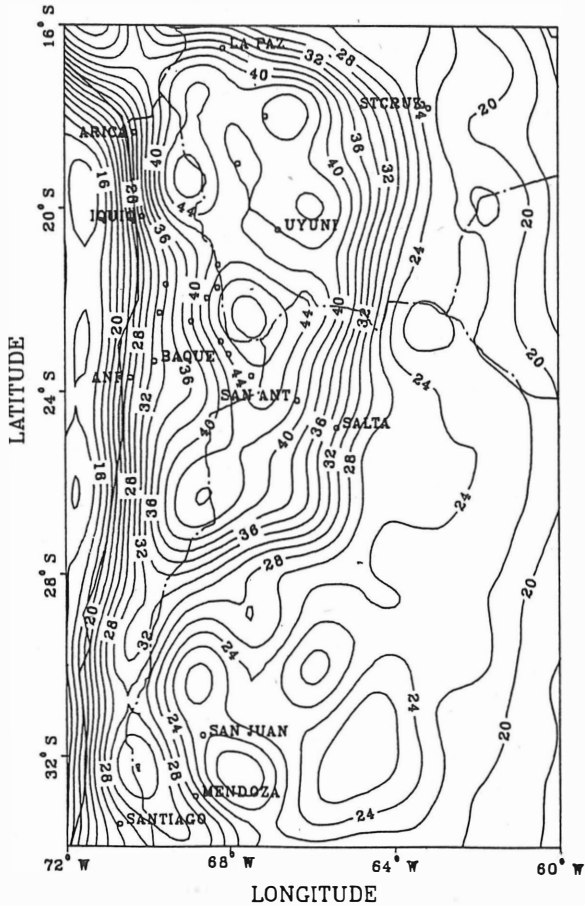
contour inteval 2m (RAPP81 ISOSTASY)

o gravity points

Fig. 14 Isostatic-geoid, computed by spherical harmonics of degree 180 (RAPP81)
level of compensation 0 km

Gravity anomalies South–America
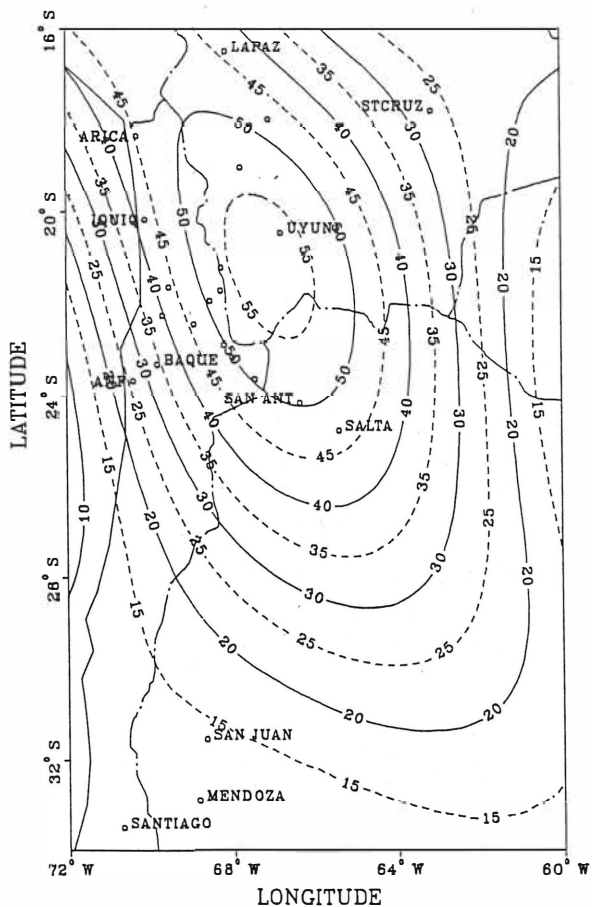
contour interval 5mgal   (GEM–T1 FREE–AIR)

o gravity points

Fig. 15   Free-air-anomalies, computed by spherical harmonics of degree 36
(GEM-T1)

Geoid heights South—America
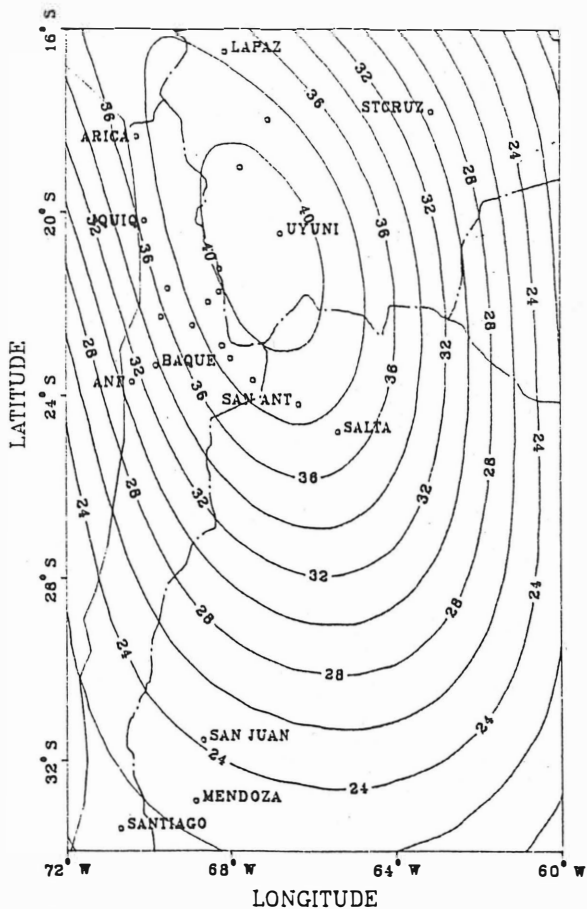
contour interval 2m   (GEM—T1 FREE—AIR)

o gravity points

Fig. 16   Free-air-geoid, computed by spherical harmonics of degree 36 (GEM-T1)

Gravity anomalies South–America
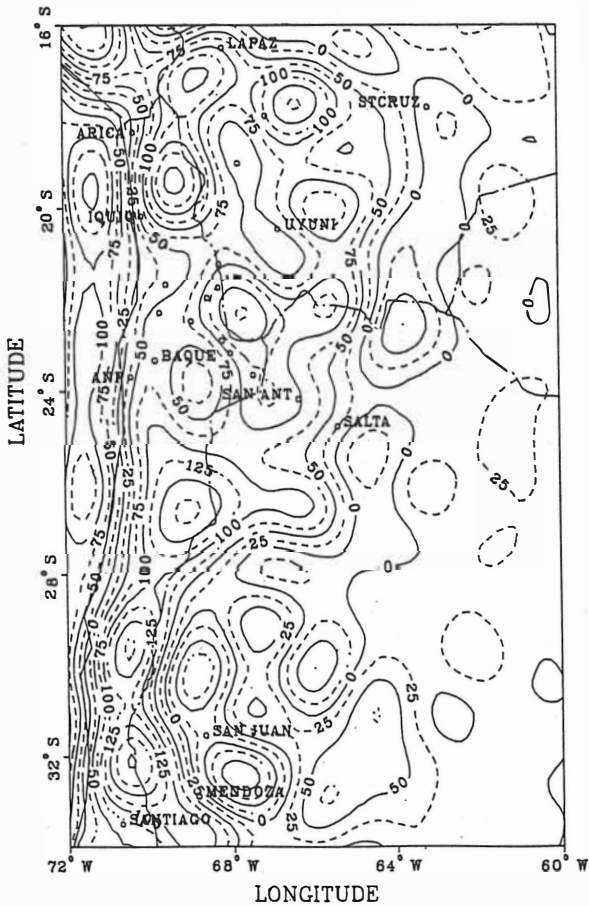
contour interval 25mgal   (RAPP81 FREE–AIR)

o gravity points

Fig. 17 Free-air-anomalies, computed by spherical harmonics of degree 180
(RAPP81)

Gravity anomalies South–America
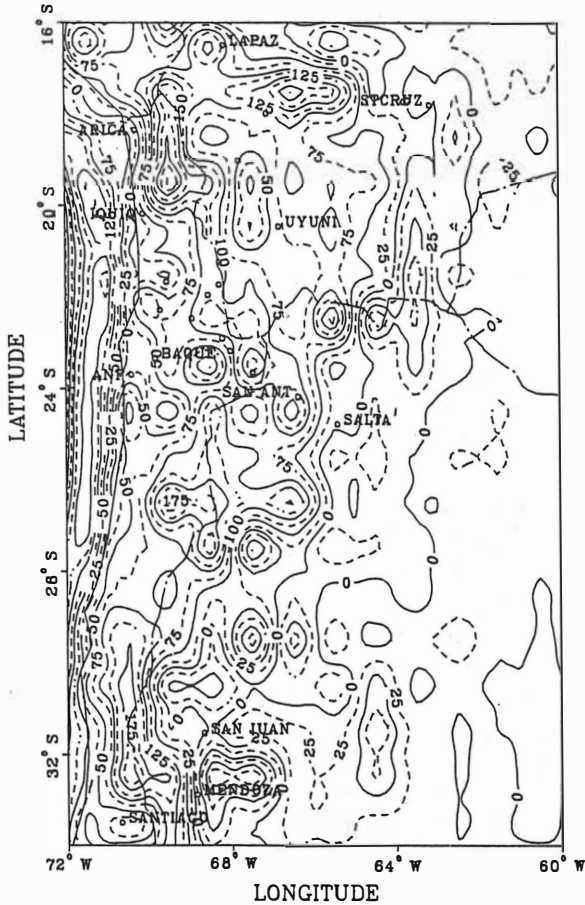
contour interval 25mgal   (OSU86E FREE–AIR)

o gravity points

Fig. 18   Free-air-anomalies, computed by spherical harmonics of degree 360
(OSU86E)

Fig. 19 Bouguer anomalies, computed by spherical harmonics of degree 180 (RAPP81)
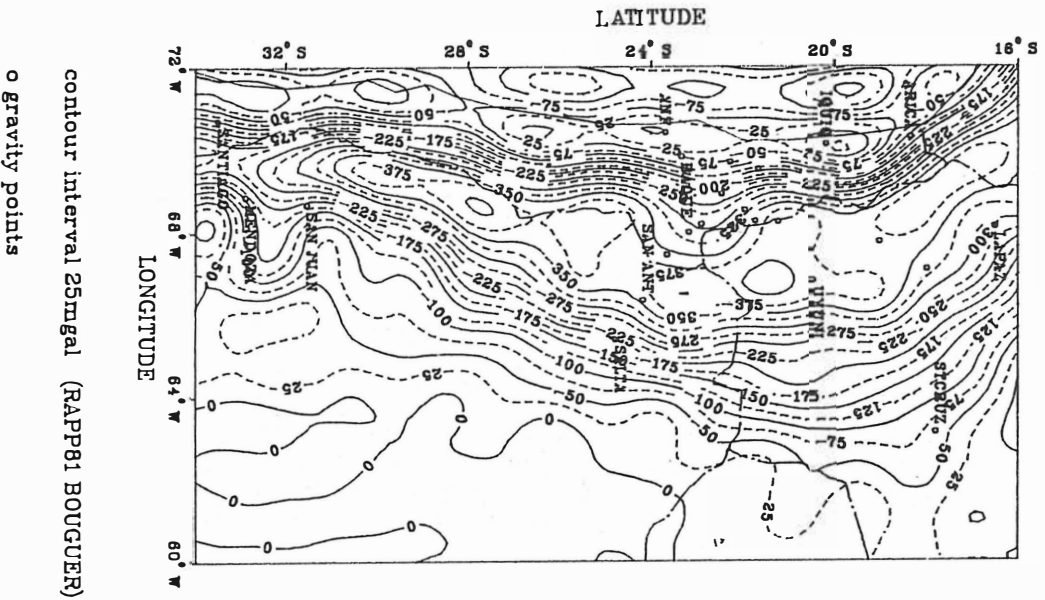
o gravity points

contour interval 25mgal (RAPP81 BOUGUER)

Gravity anomalies South—America
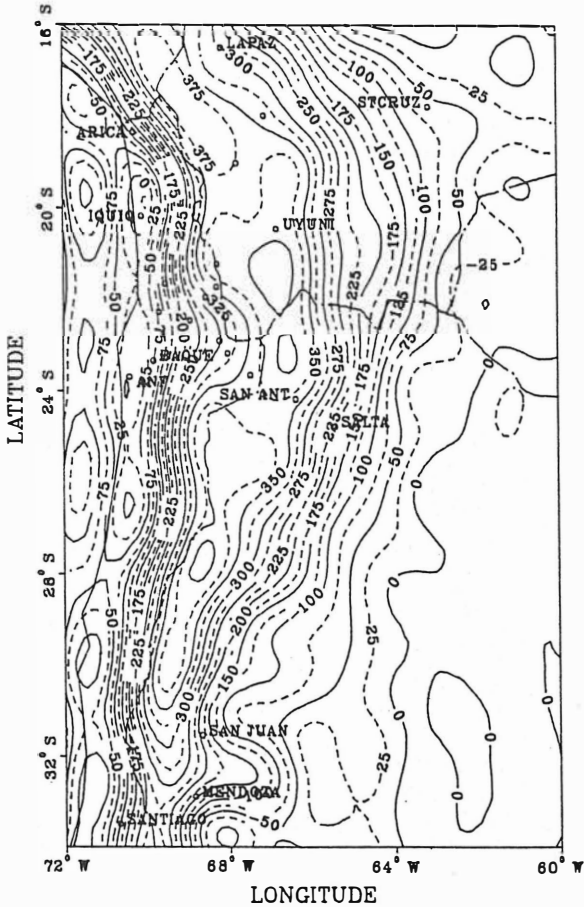
contour interval 25mgal (RAPP81 BOUGUER REF)

o gravity points

Fig. 20 Refined-Bouguer-anomalies, computed by spherical harmonics of degree
180 (RAPP81)

Gravity anomalies South–America
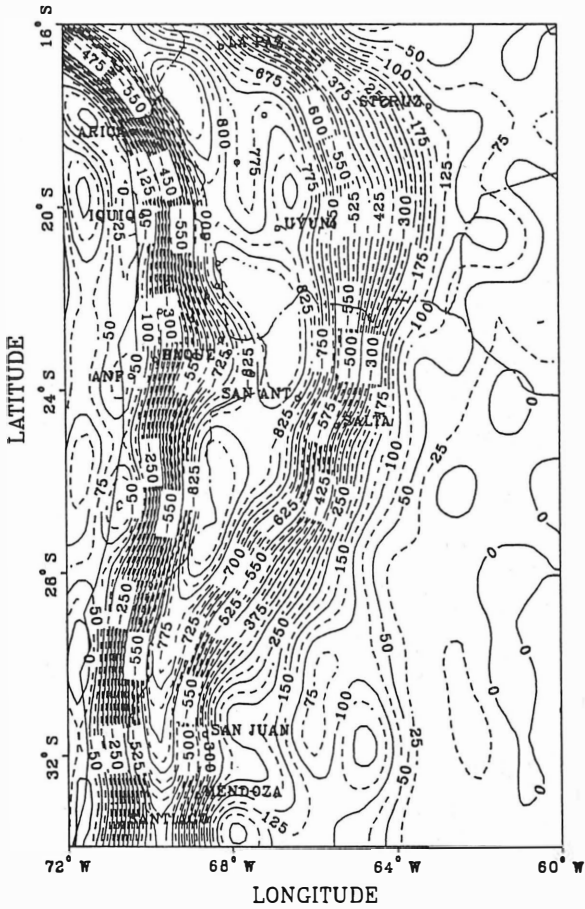
contour interval 25mgal   (RAPP81 BOUGUER)

o gravity points   SPH

Fig. 21 Spherical-Bouguer-anomalies, computed by spherical harmonics of degree
180 (RAPP81)

Gravity anomalies South—America
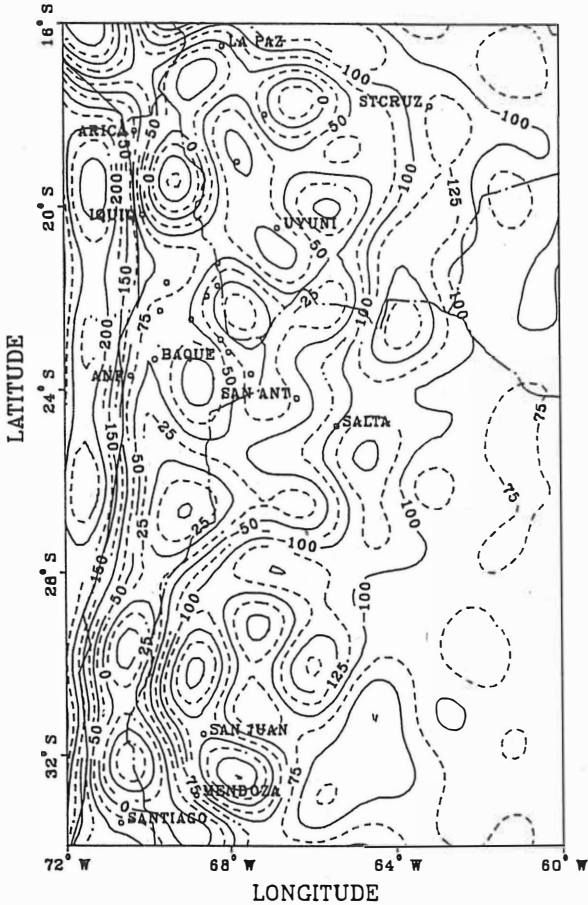
contour interval 25mgal (RAPP81 ISOSTASY)

o gravity points

Fig. 22 Isostatic-anomalies, computed by spherical harmonics of degree 180
(RAPP81), level of compensation 0 km

Fig. 23 Free-air-anomalies, contour interval 10 mgal

Fig. 24 Bouguer-anomalies, contour interval 10 mgal

BOUGUER-ANOMALIE

1 : 2.500.000

ISOLINIENABSTAND: 10 MGAL
REDUKTIONSDICHTE 2.67 G/CCM

ARBEITSGRUPPE GRAVIMETRIE
GEOLOGISCHES INSTITUT
UNIVERSITAET BONN

46
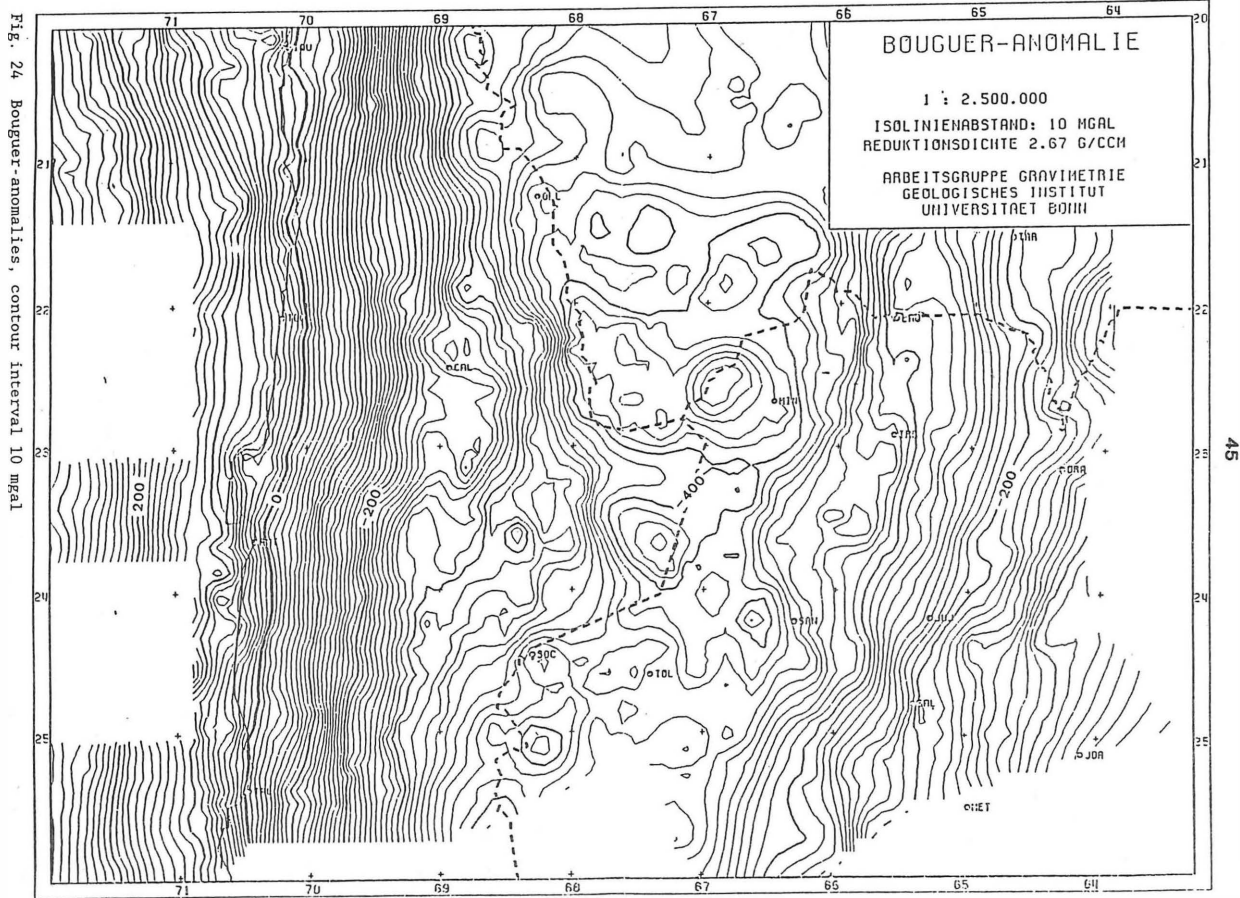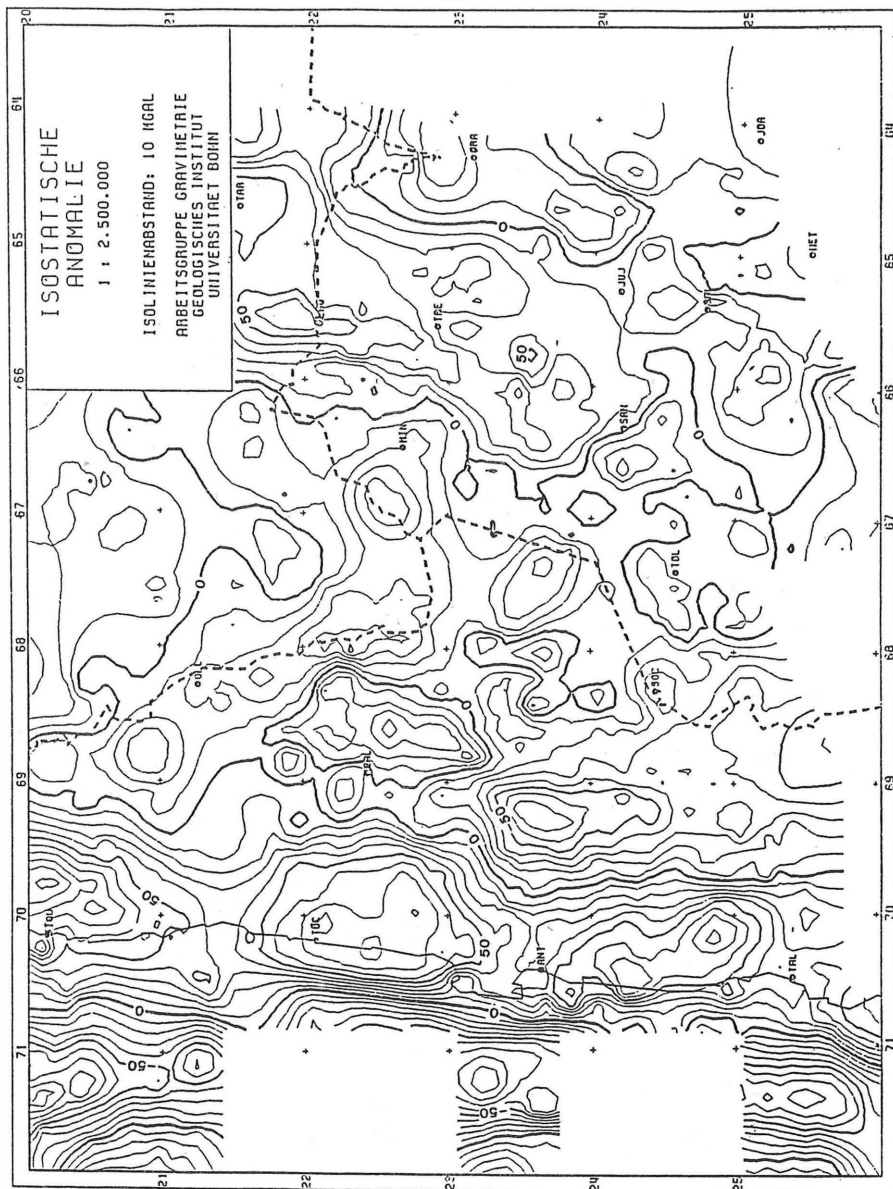
Fig. 25   Isostatic-anomalies, contour interval 10 mgal

Gravity anomalies South–America
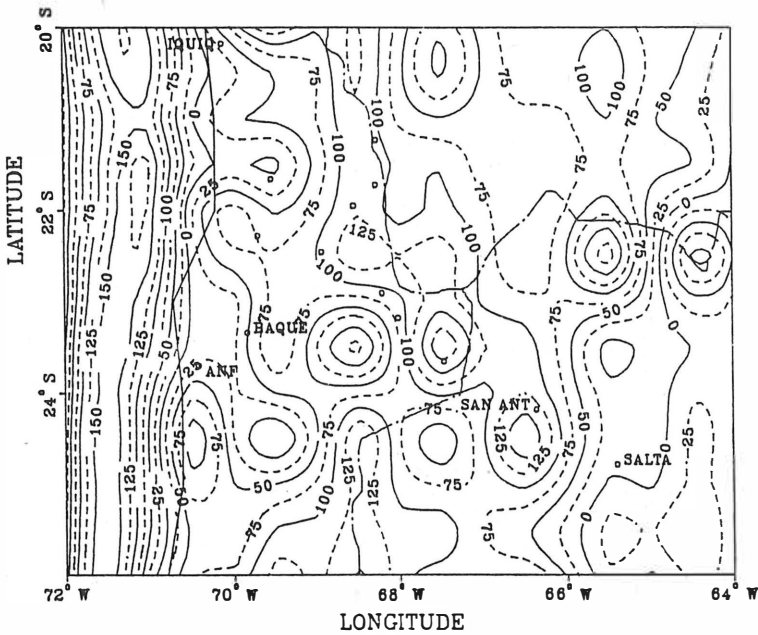
contour interval 25mgal   (OSU86E FREE–AIR)

o gravity points

Fig. 26   Free-air-anomalies, computed by spherical harmonics of degree 360
(OSU86E)

Gravity anomalies South–America
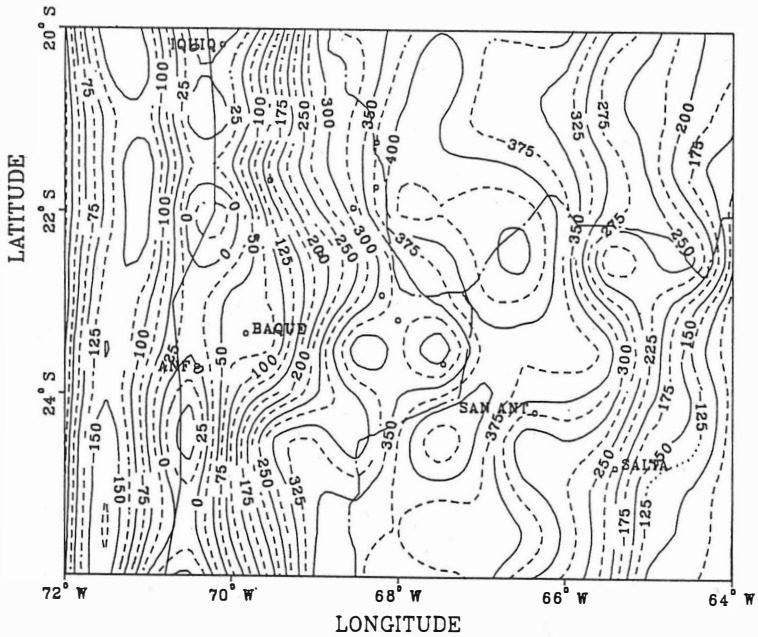
contour interval 25mgal (OSU86E BOUGUER)

o gravity points

Fig. 27   Bouguer-anomalies, computed by spherical harmonics of degree 360
(OSU86E)

Gravity anomalies South–America
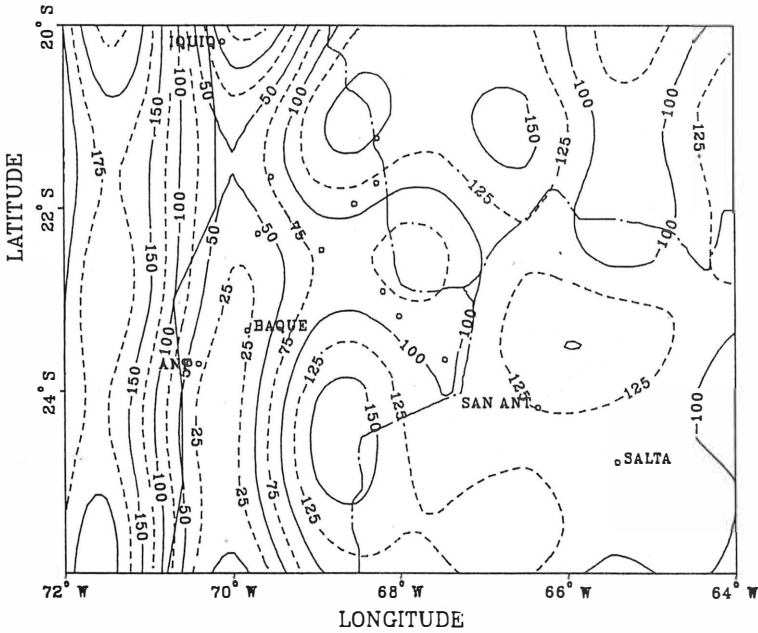
contour interval 25mgal (RAPP81 ISOSTASY)

o gravity points   level of compensation −50km

Fig. 28   Isostatic-anomalies, computed by spherical harmonics of degree 180
         (RAPP81)

Gravity anomalies South–America
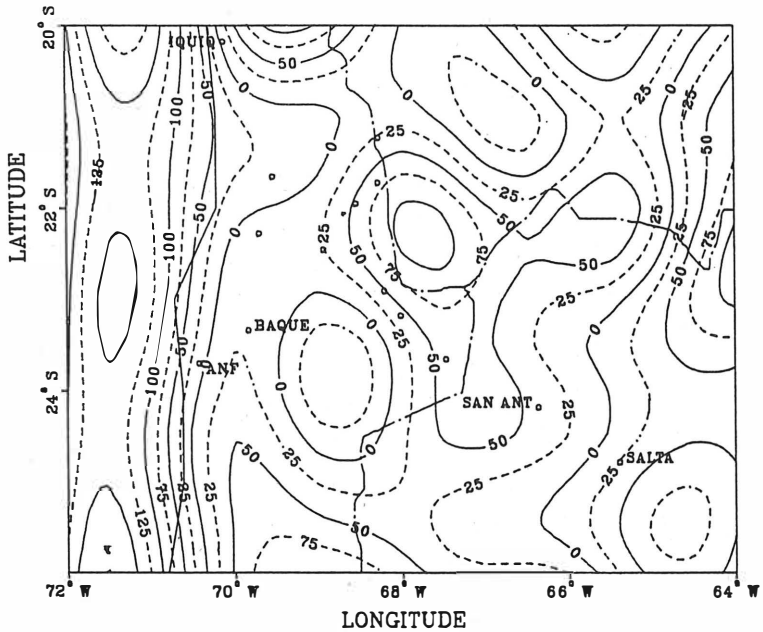
contour interval 25mgal   (RAPP81 ISOSTASY)

o gravity points   level of compensation 0km

Fig. 29   Isostatic-anomalies, computed by spherical harmonics of degree 180
(RAPP81), beginning with n = 2

Gravity anomalies South–America
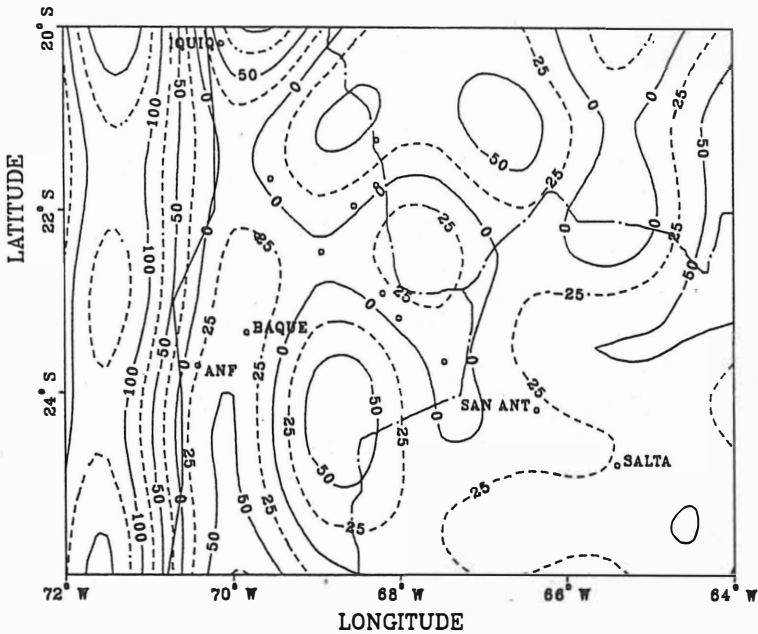
contour interval 25mgal   (RAPP81 ISOSTASY)

o gravity points   level of compensation −30km

Fig. 30   Isostatic-anomalies, computed by spherical harmonics of degree 180
(RAPP81), beginning with n = 2

Gravity anomalies South—America
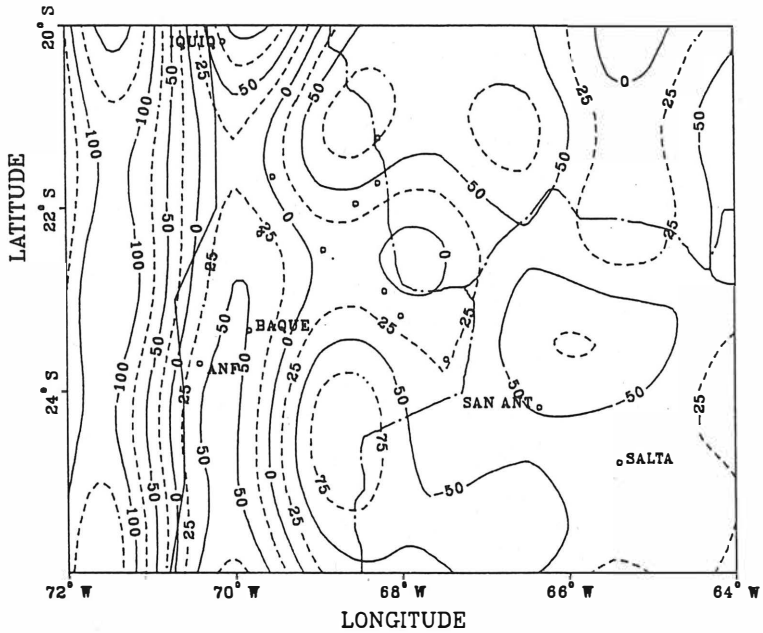
contour interval 25mgal   (RAPP81 ISOSTASY)

o gravity points   level of compensation −50km

Fig. 31   Isostatic-anomalies, computed by spherical harmonics of degree 180
(RAPP81), beginning with n − 2

Gravity anomalies South—America
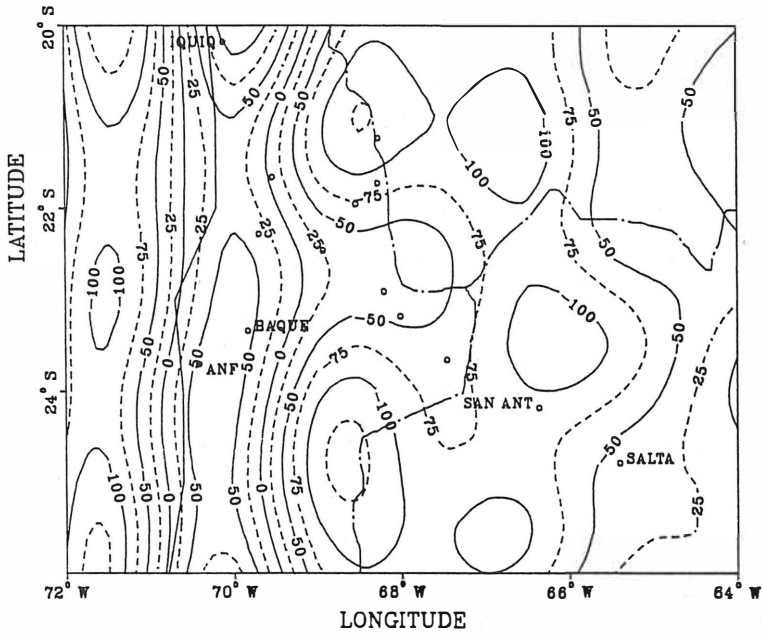
contour interval 25mgal   (RAPP81 ISOSTASY)

o gravity points   level of compensation −80km

Fig. 32   Isostatic-anomalies, computed by spherical harmonics of degree 180
(Rapp81), beginning with n − 2

Gravity anomalies South-America
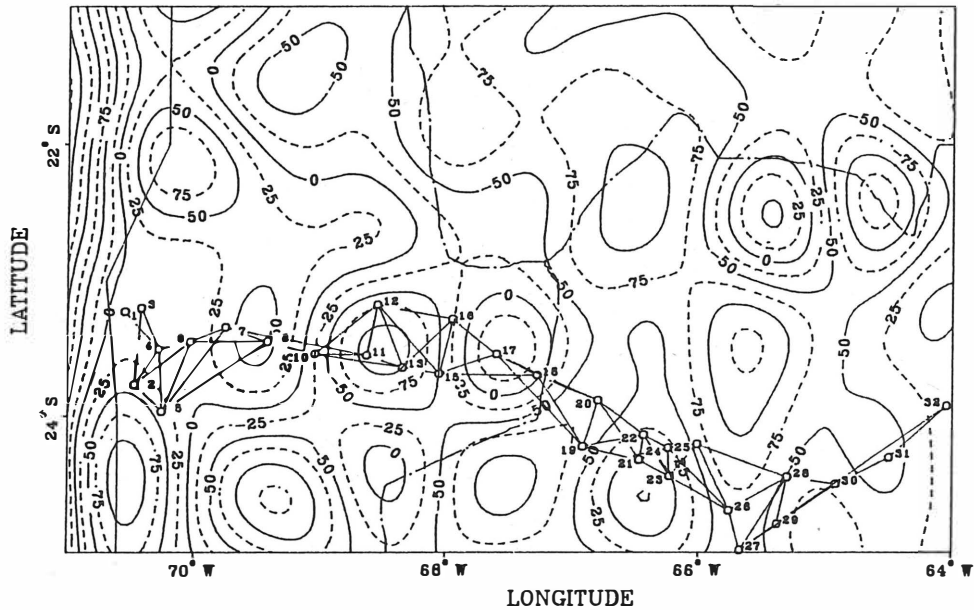
contour interval 25mgal (OSU86E ISOSTASY)   o GPS-stations

Fig. 33   Isostatic-anomalies, computed by spherical harmonics of degree 360
          (OSU86E),
          level of compensation −50 km

Gravity anomalies South–America
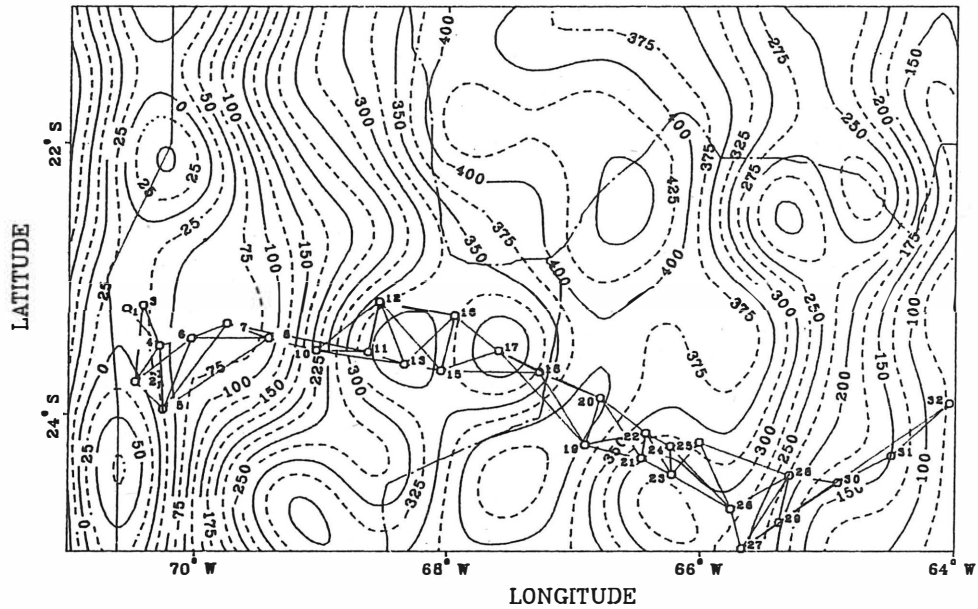
contour interval 25mgal (OSU86E BOUGUER)   o GPS–stations

Fig. 34 Bouguer-anomalies, computed by spherical harmonics of degree 360
         (OSU86E).

References

Aksoy, A., M. Becker, H. Demirel, E. Groten and W. Hönig,
Präzisionsschweremessungen zur Überwachung von Vertikalbewegungen in der
Nordanatolischen Verwerfung, Festschrift Rudolf Sigl zum 60. Geburtstag,
DGK, Reihe B, Nr. 287, 1-7, München 1988

Becker, M. and E. Groten, Relative gravimeter measurements at the 1981 absolute
gravimeter campaign in Paris, Sèvres, Bull. D'Inf., 52, 86-96, BGI
Toulouse 1983

Becker, M., A. Aksoy, H. Demirel and E. Groten, High precision gravity
measuements across the North Anatolien transform fault, Bull. D'Inf., 57,
31-45, BGI Toulouse 1985

Becker, M., Analyse von hochpräzisen Schweremessungen, DGK, Reihe C, Nr. 294,
München 1984

Becker, M., E. Groten and X.M. Gao, First results of precise gravity
measurements on the A-B-C Profile; Symp. Int. Movimientos Recientes de la
Corteza Terrestre, Tectonophysics 130, 33-47, Amsterdam 1985

Becker, M., S. Bakkelid, E. Groten, B.G. Harsson and A. Midsundstadt,
Investigation of crustal deformation induced by loading of an artificial
lake - The Blasjö project, Bull. D'Inf. 62, 111-117, BGI Toulouse 1987

Boulanger, Yu., J. Faller, E. Groten (ed), 1986, Results of the Second Intern.
Comparison of absolute Gravimeters in Sèvres 1985, Bull. D'Inf., 52,
89-103, Toulouse 1986

Groten, E. (ed.), Report on high precision gravimetry, Vol. II, Nachrichten aus
dem Karten- und Vermessungswesen, Reihe II, Nr. 41, Frankfurt 1983

Groten, E. and W. Hausch, The treatment of time-dependent phenomena in geodetic
observations, in 1st Hotine-Marussi-Symp. on Mathematical Geodesy, Roma,
June 1985, F. Sanso (ed), 39-68, vol. I, Inst. Top. Fotog. e. Geofisica
Politecn., Milano 1986

Groten, E., Airborne and satellite borne gravimetric studies, pp. at the COSPAR
XXVII Plenary Meeting and Associated Activities, 18-29 Juli, Helsinki
1988

Goetze, H.J., Schweremessungen und deren Interpretation im mittleren und
östlichen Teil der Anden-Geotraverse, DFG-Abschlußbericht Go 380/1, Bonn
1986

Harrison, J.C. and T. Sato, Implementation of electro-static feedback with a
LaCoste Romberg gravity meter, JGR 89, 7957-7961, 1984

Jackson, J. and Don McKenzie, The relationship between plate motions and
seismic moment tensors and the rates of active deformation in the
Mediterranean and Middle East, Geophys. J. 93, 45-73, 1988

Lambert, A., I.O. Liard and A. Mainville, Vertical movements and gravity
changes near the LaGrande-2reservoir, Quebec, JGR 91, B9, 9150-9160, 1986

Marsh, J.G. and F.J. Lerch, Orbit determination for altimeter missions: the
impact of new NASA/Goddard Space Flight Center gravitational models, pp.
at the XXVII COSPAR, Espoo, Finland, July 1988

Marsh, J.G. , Ch. J. Koblinsky and F. J. Lerch, Direct use of satellite
altimeter data for orbit determination, gravitational modeling
improvements, and recovery of dynamic topography, pp. at the XXVII
COSPAR, Espoo, Finland, July 1988

Rapp, R.H., The earth's gravity field to degree and order 180 using SEASAT
altimeter data, terrestrial gravity data, and other data, Dept. of Geod.
Sci. and Surv., Ohio State Univ., Columbus, Rep. No. 322, 1981

Rapp, R.H. and J.Y. Cruz, Spherical harmonic expansions of the earth's
gravitational potential to degree 360 using 30' mean anomalies, Dept. of
Geod. Sci. and Surv., The Ohio State Univ. Columbus, Rep. No. 376, 1986

Rapp, R.H., Development of a potential field to degree 360, Fourth Int. Summer
School in the Mountains, Admont, Austria, 1986

Röder, R.H. and H.-G. Wenzel, Relative gravity observations at BIPM, Sèvres
in 1985 and 1986, Bull. D'Inf. 59, 177-189, BGI Toulouse 1986

Röder, R.H., M. Schnüll and H.-G. Wenzel, SRW feedback for LaCoste Romberg
    Gravimeters with extent range, Bull. D'Inf. 62, 46-50, BGI Toulouse, 1988
Torge, W., Zum Aufbau von Schwerebezugssystemen, Festschrift Rudolf Sigl zum
    60. Geburtstag, DGK, Reihe B, Nr. 287, 207-217, München 1988
Vaillant, H.D., C. Gagnon and J.F. Halfpenny, An inherently linear
    electrostatic feedback method for gravity meters, JGR 91, 6202-6228, 1986
Verma, R.K. and K.A.V.L. Prasad, Analysis of gravity fields in the northwestern
    Himalayas and Kohistan region using deep seismic sounding data, Geophys.
    J. RAS 91, 869-889, 1987

EQUILIBRIUM FIGURES IN GEODESY AND GEOPHYSICS

Helmut Moritz

Technical University, Graz, Austria

Abstract: Already around 1960, geodetic satellite observations have shown that the earth cannot be in exact hydrostatic equilibrium. Nevertheless, hydrostatic earth models are useful reference figures for geophysics.

There is an enormous literature on geodetic equilibrium figures, but the various works have not always been interrelated, also for linguistic reasons (English, French, German, Italian, Russian). The author attemps to systematize the various approaches and to use the standard second-order theory for a study of the deviation of the actual earth and of the equipotential reference ellipsoid from an equilibrium figure.

Zusammenfassung: Bereits um 1960 zeigten die Ergebnisse geodätischer Satellitenbeobachtungen, daß die Erde nicht in exaktem hydrostatischen Gleichgewicht sein kann. Nichtsdestoweniger sind hydrostatische Erdmodelle natürliche Bezugsfiguren für die Geophysik.

Es gibt eine außerordentlich umfangreiche Literatur über geodätische Gleichgewichtsfiguren, aber die verschiedenen Arbeiten sind oft ohne gegenseitigen Zusammenhang, auch aus sprachlichen Gründen (Deutsch, Englisch, Französisch, Italienisch, Russisch). Der Verfasser versucht, die verschiedenen Verfahren vereinfachend zu systematisieren und die Standardtheorie 2. Ordnung auf die Untersuchung der Abweichungen der tatsächlichen Erde und des Niveauellipsoids von einer Gleichgewichtsfigur anzuwenden.

1. Introduction

At present, interest in terrestrial equilibrium figures is very low indeed. The last major textbook in physical geodesy that extensively considered equilibrium figures was (Ledersteger, 1969), whereas (Moritz, 1980) does not even mention them.

The reason is that one of the first results of satellite geodesy, already around 1960, was a value of the earth's flattening $f(\doteq 1/298.25)$ which was incompatible with the hydrostatic value of $1/297.34$ (Bullard, 1948); cf. also (Heiskanen and Moritz, 1967, pp. 340-341). This discrepancy shows that the earth cannot be in hydrostatic equilibrium.

The equipotential ellipsoid which underlies the modern definition of a Geodetic Reference System, from the International Gravity Formula 1930 to the Geodetic Reference System 1980 (Moritz, 1984), is not an equilibrium figure either.

On the other hand, a hydrostatic earth model continues to be the reference for the geophysical theory of a rotating and oscillating elastic earth; cf. (Melchior, 1983, sec. 6.2; Moritz and Mueller, 1987, sec. 4.2).

Here we have three unrelated facts: earth not in hydrostatic equilibrium, nonhydrostatic geodetic reference, hydrostatic geophysical reference, which call for interrelation; and the basis for this continues to be a precise theory of a hydrostatic earth.

Since the time when Clairaut published his fundamental equation in 1743 to about twenty years ago, the problem of terrestrial hydrostatic equilibrium figures has fascinated the attention of mathematicians, geophysicists, astronomers and geodesists alike, producing theoretically highly interesting and practically very useful results. There remains the curious fact that these works have not always been interrelated. The practically oriented literature in English has frequently taken little notice of great theoretical advances published in French, German, Italian or Russian.

The present paper attempts a review of various approaches. It does not pretend anything like completeness and should be regarded as a first approximation only.

2. Clairaut's Equation

The theory of spheroidal figures of equilibrium is governed
by the famous differential equation of Clairaut, published in
1743:

$$\frac{d^2f}{dr^2} + \frac{6}{r}\frac{\rho}{D}\frac{df}{dr} + \frac{6}{r^2}\left(\frac{\rho}{D} - 1\right)f = 0 \ . \tag{1}$$

Here the earth is considered a rotationally symmetric body;
the surfaces of constant density ρ (which are at the same
time surfaces of constant gravity potential W , see below),
are slightly flattened spheroids which at a first approximation
might be identified with ellipsoids, of semimajor axis a ,
semiminor axis b and mean radius r , so that

$$f = \frac{a-b}{a} = f(r) \tag{2}$$

represents the flattening. The mean radius r , so to speak,
labels the internal equipotential surfaces, so that also

$$\rho = \rho(r) \tag{3}$$

holds. Finally,

$$D = \frac{3}{r^3}\int_0^r \rho(r')r'^2 dr' = D(r) \tag{4}$$

denotes the mean density inside the surface $\rho = \rho(r)$, which
for the present purpose may even be regarded as a sphere. As
an integration variable, r is denoted by r' , a distinction
which we shall later drop, using r also as integration variable
when no confusion is likely.

Clairaut's equation is an approximation linear in f ;
terms of order f^2 are neglected. For contemporary accuracy,
second-order terms must be retained, leading to the second-order
theory to be discussed in sec. 6.

The standard derivation of (1) is the one given, e.g. in (Jeffreys, 1970, sec. 4.03). It will also be used in sec. 6, so that here we can limit ourselves to a brief sketch.

The fundamental equation of hydrostatic equilibrium is

$$dp = \rho dW \ , \tag{5}$$

p denoting the pressure, ρ the density and W the gravity potential already introduced. An immediate consequence of (5) is that

$$W = W(\rho) \ , \tag{6}$$

the potential is a function of density only, so that the surfaces of constant density, ρ = const., are also equipotential surfaces W = const. In the sequel, we shall simply speak of <u>equisurfaces.</u>

Now the internal gravity potential is brought into a form

$$W(r,\theta) = W_0(r) + W_2(r) P_2(\cos \theta) \ , \tag{7}$$

where θ denotes the spherical colatitude (spherical polar distance); because of rotational symmetry there is no dependence on longitude λ . Note that r denotes the <u>mean</u> radius as above.

Since $\rho = \rho(r)$, it follows from (6) that also W must only depend on r, so that

$$W_2(r) = 0 \ ; \tag{8}$$

$P_2(\cos \theta)$ denotes the usual Legendre polynomial of second degree. The condition (8) leads to

$$- \frac{f(r)}{r} \int_0^r \rho r^2 dr + \frac{1}{5r^3} \int_0^r \rho \frac{d(fr^5)}{dr} dr +$$

$$+ \frac{1}{5} r^2 \int_r^R \rho \frac{df}{dr} dr + \frac{\omega^2 r^2}{8 \pi G} = 0 \ . \tag{9}$$

Here "r" behind the integral always indicates the integration variable; it should have been correctly denoted by r' as in (4). The symbol R stands for the mean radius of the earth, R = 6371 km, ω denotes the earth's rotational velocity and G the gravitational constant as usual.

By skilful manipulation of (9) both integrals can be removed by differentiation, resulting in (1).

The further treatment of (1) by Radau's classical transformation leads to the famous result

$$J_2 = \frac{2}{3}\left(1 - \frac{2}{5}\sqrt{\frac{5m}{2f} - 1}\right)H ,$$ (10)

which, supplemented by second-order terms, permits the computation of the second-degree zonal coefficient

$$J_2 = \frac{C-A}{Ma^2}$$ (11)

from the quantity

$$H = \frac{C-A}{C}$$ (12)

very precisely known from astronomical precession. The notations are standard: C and A are the earth's principal moments of inertia (polar and equatorial), M denotes the earth's mass and a its mean equatorial radius.

Now, J_2 is directly related to the flattening by

$$f = \frac{3}{2}J_2 + \frac{1}{2}m + O(f^2) ,$$ (13)

$O(f^2)$ denoting terms on the order of f^2 or higher and

$$m = \frac{\omega^2 a}{\gamma_e} ,$$ (14)

the very small ratio of centrifugal force at the equator to normal gravity at the equator, γ_e .

Before the advent of artificial satellites, the flattening
f was computed by combining eqs. (10) and (13), since J_2 could
only be computed indirectly from H by (10), presupposing
hydrostatic equilibrium.

The artificial satellites made J_2 directly observable,
which lead to the discrepancy mentioned in sec. 1, and to the
consequent waning of the geodesists' interest in equilibrium
figures, in spite of papers such as (Khan, 1968, 1969;
Nakiboglu, 1979; Denis and Ibrahim, 1981).

3. The Method of Integral Equations

The mathematically rigorous treatment of equilibrium
figures goes back to the French mathematician Poincaré (1885)
and to his contemporary, the Russian mathematician Liapunov.
Whereas Poincaré concentrated his research on homogeneous
equilibrium figures (density ρ = const.), Liapunov (1904)
studied heterogeneous figures as well,thus providing a rigorous
justification of Clairaut's theory.

Lichtenstein (1933) continued Liapunov's work and tried
to simplify it, but his attempt to achieve perfect mathematical
rigor still makes his book extremely difficult to read, so that
his work, also because it is written in German, has shared the
fate of Liapunov's researches of being largely ignored by the
geodetic and geophysical community.

Their result may be described as follows: Consider a
nonrotating heterogeneous mass in hydrostatic equilibrium of
arbitrary density distribution in the absence of external forces.
The density is subject only to the natural condition of being
positive and non-decreasing towards the interior. In this case
it can be proved that the configuration must be spherically
symmetric: $\rho = \rho(r)$ is an arbitrary (in the above sense) function
of the radius r of the spherical equisurfaces.

If this configuration is subjected to a "sufficiently slow"
rotation, then a spheroidal equilibrium figure exists which is
"close" to the original spherical configuration and possesses
the same density law $\rho(r)$, r now denoting the mean radius

of the equisurfaces. In other words, Liapunov and Lichtenstein
proved the existence and uniqueness of an equilibrium figure
"in the neighborhood" of a given spherical mass configuration.
To be sure, "smallness" of the angular velocity ω is to be
considered in the mathematical sense, without implying that
the earth's actual rotational velocity is "sufficiently small"
in this sense. The author does not know whether the required
extremely laborious estimates for this purposes have ever been
performed numerically.

In a sense, Liapunov and Lichtenstein achieved for Clairaut's
problem essentially what Hörmander in 1976 did for Molodensky's
gravimetric boundary value problem (cf. Moritz, 1980, sec. 51):
a proof of existence and uniqueness under certain mathematical
restrictions.

It would be presumptuous in this paper to even give a
mathematical description of the proof, so the reader is referred
to Lichtenstein's book.

The basis of the proof, however, is a linear integral
equation, which has a certain analogy with Molodensky's famous
integral equation and may, therefore, interest the geodetic
reader. Hence we shall attempt to sketch a simple geometric
derivation of Lichtenstein's fundamental integral equation.

Consider a nonrotating spherically symmetric mass Σ ,
and submit it to a rotation with angular velocity ω which
deforms it into the spheroid S . Denote by $\zeta = QP$ the
distance of a "new" equisurface from the corresponding "old"
one. The deviation ζ satisfies an integral equation which
can be found as follows (Fig. 1).

Denote the "normal" gravity potential of the spherical
configuration by U and that of the actual spheroidal
configuration by W . The potential U is purely gravitational
(nonrotating!), whereas W includes the centrifugal force.

The effect of the configuration change, spherical to
spheroidal, consists of three parts:

(1) The volume element dv , containing the density
$\rho' = \rho(r')$, is moved from Q' to P' . Thus ρ' is now at
P , whereas the new density at Q' is
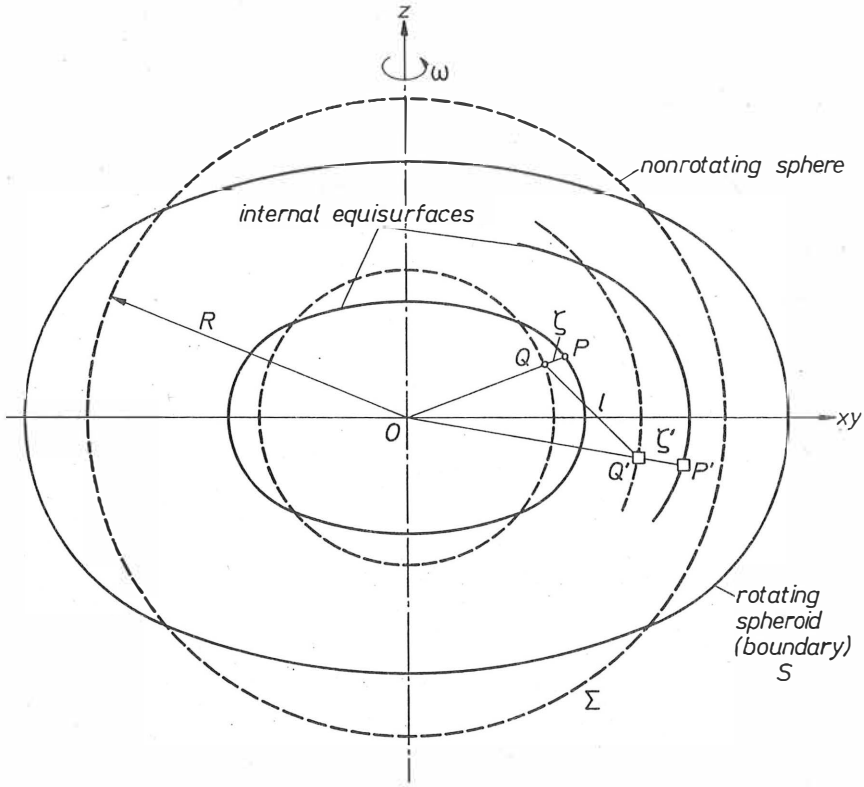
Figure 1. Rotation deforms a sphere into a spheroid

$$\rho' - \frac{\partial \rho'}{\partial r'} \zeta' \ .$$

Thus the total effect of the change at the potential at point Q is

$$- G \iiint\limits_{V} \zeta' \frac{\partial \rho'}{\partial r'} \frac{1}{\ell} \, dv \ . \tag{15}$$

The meaning of ℓ , r' and ζ' is seen from Fig. 1, G denoting the gravitational constant and v the volume of Σ .

(2) The effect of the "bulge" (positive if S is above Σ ,

negative otherwise) can be considered as a surface layer on the sphere Σ , with surface density $\rho'\zeta'$ (the integration variable is denoted by a prime even if the integration point is on Σ). This gives the contribution

$$G \iint_{\Sigma} \zeta'\rho'\frac{1}{\ell}\,d\Sigma \ . \tag{16}$$

(3) The centrifugal potential

$$\frac{1}{2}\omega^2(x^2 + y^2) \ . \tag{17}$$

Adding (15), (16), and (17) to the normal potential $U(Q)$ gives $W(Q)$:

$$W(Q) = U(Q) - G \iiint_{V} \zeta' \frac{d\rho'}{dr'} \frac{1}{\ell}\,dv$$

$$+ G \iint_{\Sigma} \zeta'\rho'\frac{1}{\ell}\,d\Sigma + \frac{1}{2}\omega^2(x^2 + y^2) \ . \tag{18}$$

Now we perform the transition $Q \to P$, getting

$$W(P) = W(Q) + \frac{\partial W}{\partial \zeta}\zeta = W(Q) - g\zeta \ . \tag{19}$$

By the very definition of the equisurfaces, $W(P)$ and $U(Q)$ are functions of r , the radius vector of the sphere passing through Q , which is identical to the mean radius vector of the equisurface passing through P . Thus

$$W(P) - U(Q) = v(r) \tag{20}$$

is a small function of r only, of which we can dispose suitably.

Combining all these equations we get

$$- g\zeta - G \iiint_V \zeta' \frac{\partial \rho'}{\partial r'} \frac{1}{\ell} dv + G \iint_\Sigma \zeta' \rho' \frac{1}{\ell} d\Sigma +$$

$$+ \frac{1}{2} \omega^2 (x^2 + y^2) - v(r) = 0 . \tag{21}$$

This fundamental integral equation for ζ has been derived rigorously in (Lichtenstein, 1933, pp. 97-101). Note that it is extended over the original spherically symmetric configuration.

Lichtenstein (1933, p. 22) has also shown that equilibrium figures must be symmetric with respect to the equatorial plane (the xy plane in Fig. 1). If, in addition, we assume rotational symmetry (this is not necessary but natural), ζ must have the form

$$\zeta = \sum_0^\infty \zeta_{2n}(r) P_{2n}(\cos \theta) , \tag{22}$$

containing only _even_ zonal harmonics. (The existence of _odd_ zonal harmonics in the geopotential is another indication of the earth's deviation from hydrostatic equilibrium!)

Limiting ourselves to the first approximation, we thus have

$$\zeta = \zeta_0(r) + \zeta_2(r) P_2(\cos \theta) .$$

This is substituted into (21). Now the integrations can be performed, taking the orthogonality of spherical harmonics into account. We then find that $\zeta_0(r)$ can be made zero by selecting

$$\zeta_0(r) = \frac{1}{3} \omega^2 r^2 , \tag{23}$$

whereas for ζ_2 we obtain the integral equation

$$4\pi G \frac{\zeta_2(r)}{r^2} \int_0^r \rho(r') r'^2 dr' - \frac{4\pi G}{5} \left\{ \frac{1}{r^3} \int_0^r \rho(r') d\left[r'^4 \zeta_2(r')\right] \right.$$

$$\left. + r^2 \int_r^R \rho(r') d\left[\frac{\zeta_2(r')}{r'}\right] \right\} + \frac{1}{3} \omega^2 r^2 = 0 , \tag{24}$$

which is easily seen to be basically identical to (9). This
provides another method for deriving Clairaut's equation.

4. The Geometry of Equilibrium Surfaces

Clairaut's equation (1) for the basic geometric quantity,
the flattening f , is a homogeneous differential equation.

Homogeneous differential equations (with right-hand side
zero) with independent variable t , time, correspond to free
motion, as opposed to forced motion. In the present case, the
independent variable is the radius r rather than time, but
the argument may indicate that the geometry of the equisurfaces
for equilibrium figures seems to have a considerable autonomy.

This idea was thoroughly investigated in the fundamental
book (Wavre, 1932). Since it is little known in the English-
speaking scientific community, we shall briefly outline Wavre's
theory of stratification of equilibrium figures.

4.1. Stratification of Equisurfaces

Let S(t) denote the set of equisurfaces (surfaces of
constant density and of constant potential), as a function of
a parameter t (there is no danger of confusing it with time!).
The parameter t thus "labels" the individual equisurfaces
and could, in principle, be selected in many ways. Formerly,
we have labeled the equisurfaces by its mean radius r , but
in Wavre's theory it is more convenient instead to take the
parameter t as the seminor axis of the spheroidal equisurface
under consideration. (This is well known since the ellipsoidal
coordinate u also has this character, cf. (Heiskanen and
Moritz, 1967, p.40)). For the limiting ("free") surface S we
take t = 1 , so that S = S(1) .

We again assume rotational symmetry about the z-axis,
knowing already that the stratification must also be symmetric
with respect to the equatorial plane (invariance for z → − z) .
Thus we have no dependence on longitude λ ; as latitudinal
coordinate we take a parameter θ that labels the plumblines

as indicated in Fig. 2.
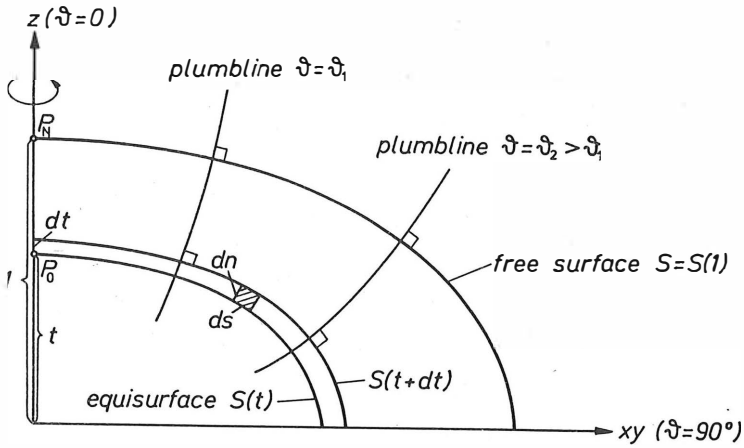
Figure 2. The geometry of stratification

Since the equisurfaces t = const. are not parallel, their
infinitesimal distance dn differs, in general, from dt . We
put

$$\frac{dn}{dt} = N(t,\theta) \ , \tag{25}$$

where the function N is unknown a priori. Note that N is
always positive (from geometry), dimensionless (by our choice
of units) and equals 1 on the axis $\theta = 0$.

Since, by definition, the potential W depends on t only,
we have for gravity

$$g = -\frac{\partial W}{\partial n} = -\frac{dW}{dt}\frac{dt}{dn} = -\frac{1}{N}\frac{dW}{dt} \ . \tag{26}$$

Hence

$$\frac{dW}{dt} = -gN = W'(t) \tag{27}$$

is a function only of t , although g and N depend also on
θ . In other terms,

$$(gN)_{\theta_1} = (gN)_{\theta_2} ;$$
(28)

the product gN is independent of θ along an equisurface S(t).

Since (28) is an identity in t , it can be differentiated:

$$\left(\frac{\partial g}{\partial t} N + g \frac{\partial N}{\partial t}\right)_{\theta_1} = \left(\frac{\partial g}{\partial t} N + g \frac{\partial N}{\partial t}\right)_{\theta_2} .$$
(29)

Now by (25),

$$\frac{\partial g}{\partial t} = \frac{\partial g}{\partial n} \frac{dn}{dt} = N \frac{\partial g}{\partial n} ,$$
(30)

and Bruns' formula (Heiskanen and Moritz, 1967, p. 53) gives

$$\frac{\partial g}{\partial n} = -2Jg + 4\pi G\rho - 2\omega^2 = -2Jg - f ,$$
(31)

calling with Wavre

$$f = -4\pi G\rho + 2\omega^2 \quad (\equiv \Delta W!)$$
(32)

the "transformed density"; it is nothing else than the result
of applying the Laplace operator Δ to the gravity potential
W , and the reader will recognize Poisson's equation. In (31),
J denotes the mean curvature of the equisurfaces.

Substituting (31) into (30), and the result into (29), we
obtain after some elementary computations, also using (26), Wavre's
fundamental formula

$$\frac{f(t)}{W'(t)} = \frac{(2JN - \partial \ln N/\partial t)_{\theta_2} - (2JN - \partial \ln N/\partial t)_{\theta_1}}{(N^2)_{\theta_2} - (N^2)_{\theta_1}} .$$
(33)

This equation is remarkable in that it provides a neat separation
of the geometry and the physics of equilibrium surfaces: the

left-hand side, containing physical quantities such as density
ρ and potential W , depends only on t , whereas the right-hand
side depends only on the geometry of stratification (J,N) and
is independent of the density distribution!

4.2. Wavre's Theorem

Put for the left-hand side of (33)

$$\Psi(t) = \frac{f(t)}{W'(t)} \ . \tag{34}$$

Then (30), using (26), (31) and (34), can be brought into the
form

$$\frac{1}{g} \frac{\partial g}{\partial t} = -2JN + \Psi N^2 \ , \tag{35}$$

which again is a function of the geometrical stratification only
and does not depend on the density! This is a direct consequence
of the definition (34) and of the remarkable properties of (33)
just pointed out.

Eq. (35) holds for any θ , and in particular for $\theta = 0$,
on the rotation axis. Thus we may integrate it along this axis
from P_N to P_0 (Fig. 2):

$$\int_{P_N}^{P_0} \frac{1}{g} \frac{\partial g}{\partial t} \ dt = \int_1^t (-2JN + \Psi N^2) dt = \ln g_0 - \ln g_N \ , \tag{36}$$

so that

$$g_0 = g_N \exp \left[\int_1^t (-2JN + \Psi N^2) dt \right] = g(t,0) \ , \tag{37}$$

where $g_N = g(1,0)$ denotes gravity at the pole.

Now (28), with $\theta_1 = 0$ and $\theta_2 = \theta$, together with (37),
gives

$$g(t,\theta) = \frac{1}{N(t,\theta)} \; g(t,0) = \frac{g_N}{N(t,\theta)} \exp\left[\int_1^t (-2JN + \Psi N^2)\,dt\right], \quad (38)$$

noting that $N(t,0) = 1$ as we have already remarked. Finally (34) and (27) give

$$f(t) = -\Psi(t)N(t,\theta)g(t,\theta) , \tag{39}$$

and hence the density $\rho(t)$ by (32).

Note the truly remarkable logical structure of these formulas: the physics, especially the density distribution $\rho(t)$, is uniquely determined by the geometrical stratification. In fact, given the geometry (J,N) , we can compute $\Psi(t)$ by (33) and (34). Then gravity $g(t,\theta)$ is obtained by (38), and finally the density ρ by (39) and (32). The only constants that must be given in addition to the set of surfaces $S(t)$, are the angular velocity ω and polar gravity g_N , which, however, are uniquely determined by ω and the total mass M ("Stokes elements"), using the theory of the external gravity field. Thus we have

Wavre's Theorem

> The physics of equilibrium figures (density ρ , gravity g) is completely determined by the geometrical stratification, i.e., the set of equisurfaces $S(t)$ $(0 \le t \le 1)$, together with the total mass M and the angular velocity ω .

4.3. Spherical Stratification as an Exception

For spherical stratification, Wavre's theorem does not apply since the right-hand side of (33) becomes $0/0$ here, so that $\Psi(t)$ is not defined.

In fact, we have seen that a nonrotating spherical equilibrium configuration admits arbitrary density laws

(ρ positive and nondecreasing towards the center). The actual
earth is close to a spherical stratification, so that Wavre's
theorem, although theoretically applicable, is not "stable":
a large change of the density law may go along with an
unmeasurably small variation of the geometrical configuration.

Thus, of course, the density distribution of the earth can
only be determined empirically : from seismology, free oscillations,
etc.

4.4. Impossibility of a Purely Ellipsoidal Stratification

Wavre (1932, p. 60) also provides a very elegant version
of Pizzetti's (1913, p. 193) proof that a family of strictly
ellipsoidal equisurfaces S(t) is impossible, provided the
density distribution is heterogeneous (this goes back to Hamy
in 1887). Homogeneous ellipsoidal equilibrium figures --
ellipsoids of MacLaurin and Jacobi -- do, of course, exist, but
they are without geodetic relevance.

In sec. 6 we shall see that even the equipotential ellipsoid
(Heiskanen and Moritz, 1967, sec. 2-7) cannot be an equilibrium
figure. This was pointed out, to the author's dismay, by
Karl Ledersteger. In fact, it should be noticed here that
Ledersteger was the last great geodesist who seriously and
deeply occupied himself with Wavre's theory; this should be
recognized even if one is not prepared to follow him all the
way.

4.5. Another Derivation of Clairaut's Equation

Although **rigorously,** the spheroidal equisurfaces are not
ellipsoids, they are so **in linear approximation** (in f). Thus
Wavre's equation (33) can be used for a very elegant derivation
of Clairaut's equation. We put $\theta_1 = 0$, $\theta_2 = 90°$, and write,
noting $N(t,0) = 1$,

$$g(t,0) = g_p(t) , \qquad\qquad N(t,90°) = N_E(t) ,$$

$$J(t,0) = J_p(t) , \qquad\qquad J(t,90°) = J_E(t) . \tag{40}$$

The equisurfaces are (approximately!) ellipsoids of semiaxes $a(t)$ and $b(t) = t$, so that

$$a(t) = \frac{1}{1-f} \doteq 1 + f(t) . \tag{41}$$

We further have

$$N_E(t) = \frac{da}{dt} = a'(t) \doteq f'(t) \tag{42}$$

and conventional ellipsoidal formulas give for the mean curvatures, to linear approximation

$$J_p = \frac{1}{t} (1 - 2f) , \qquad\qquad J_E = \frac{1}{t} , \tag{43}$$

so that (33), with (32), easily becomes

$$\frac{4\pi G\rho - 2\omega^2}{g_p(t)} = \frac{-t^2 f'' + 6f}{2t^2 f' + 2tf}$$

or

$$(2t^2 f' + 2tf)(4\pi G\rho - 2\omega^2) = (-t^2 f'' + 6f) g_p(t) . \tag{44}$$

Corresponding to our approximation, we neglect the product $f\omega^2$ (this removes ω^2 from our further considerations) and take $g_p(t)$ spherical:

$$g_p(t) = \frac{4\pi}{3} G t D(t) , \tag{45}$$

a well-known formula, equal to $Gm(t)/t^2$, where $m(t)$ denotes the mass inside a sphere of radius t ; $D(t)$ is the mean density (4). Thus (44) reduces to

$$3\rho(2t^2f' + 2tf) = tD(-t^2f'' + 6f) \tag{46}$$

from which Clairaut's formula (1) follows immediately (with
$t \doteq r$ in our approximation).

4.6. Concluding Remarks

Eq. (33) holds for arbitrary θ_1 and θ_2. If we replace
θ_2 by θ_3, we get the purely geometrical relation

$$\frac{(2JN - \partial\ln N/\partial t)_{\theta_3} - (2JN - \partial\ln N/\partial t)_{\theta_1}}{(N^2)_{\theta_3} - (N^2)_{\theta_1}} =$$

$$= \frac{(2JN - \partial\ln N/\partial t)_{\theta_2} - (2JN - \partial\ln N/\partial t)_{\theta_1}}{(N^2)_{\theta_2} - (N^2)_{\theta_1}} \tag{47}$$

which is a necessary condition for all stratifications of
equilibrium figures.

Is this condition also sufficient? If it were so, then we
could remove the layer above any internal equisurface $S(t)$,
cf. Fig. 2. For the remaining "reduced" figure bounded by $S(t)$,
eq. (47) continues to hold for any of its internal equisurfaces,
and the reduced figure would also be a possible figure of
equilibrium.

This is Ledersteger's (1969, p.536) "Prinzip der
Entblätterung" (principle of removing layers bounded by two
equisurfaces). For homogeneous equilibrium figures (MacLaurin
ellipsoids), this principle indeed holds since in this case,
such layers are bounded by geometrically similar ellipsoids,
and it is well known that such an "ellipsoidal homeoid" exerts
no attraction in its interior; cf. (Kellogg, 1929, p.22) or
(Chandrasekhar, 1969, p. 39).

For heterogeneous figures, this principle does not, however,
hold (Voss, 1965). This shows that (47) is only necessary but
not sufficient. Hence, before applying Wavre's procedure
described by (38) and (39), we must first make sure that the

<u>given stratification really corresponds to a possible figure</u>
<u>of equilibrium,</u> which is by no means a trivial matter.

The deeper reason why Wavre's theory is "incomplete" in
this sense seems to be the fact that he uses only the "local"
Poisson equation (32) but not the "global" condition that the
corresponding gravitational potential V (gravity potential W
minus centrifugal potential) must be harmonic everywhere outside
the boundary surface and go to zero as GM/r for r → ∞ . Thus
Wavre's theory continues to hold if S were surrounded by a
rotationally symmetric mass configuration (such as an equatorial
ring of Saturn type). Then, however, we do not any longer speak
of free equilibrium figures. (In fact, the layer between S(t)
and S(1) is such an external rotationally symmetric mass
configuration for the figure bounded by S(t)!)

A final word on the relationship between Wavre's approach
and the approach by Clairaut-Liapunov-Lichtenstein described
in sec. 3. In a sense, the two approaches are "dialectical
opposites". Wavre starts from a given stratification (the geometry)
and determines the corresponding density distribution (the
physics), whereas Lichtenstein starts from a given density
distribution (which is initially spherical) and determines the
configuration or stratification which results from a "small"
rotation ω . Hence Wavre determines the physics of the problem
from its geometry, whereas Lichtenstein determines the geometry
from the physics. Also, for Lichtenstein, the spherical
configuration is the starting point, whereas for Wavre it is
a singularity (0/0) !

Wavre's approach is also described in the books (Baeschlin,
1948) and (Ledersteger, 1969), whereas the basic book in English,
(Jardetzky, 1958), does not present it, although he outlines
an approximation method also due to Wavre ("procedé uniforme")
which intends, by an ingenious but complicated trick, to
circumvent the convergence problem of certain series of spherical
harmonics. We shall not treat this here because the author believes
that this problem can be tackled in a much simpler way as we
shall see in sec. 6.

5. Stationary Potential Energy

In various domains of physics, equilibrium is associated with a stationary (maximum or minimum, depending on the sign) value of potential energy. Liapunov and Poincaré have treated homogeneous equilibrium figures from this point of view; a modern treatment is found in the book (Macke, 1967, p. 543). Macke's approach has been generalized to heterogeneous (terrestrial) equilibrium figures (Macke et al., 1964; Voss, 1965, 1966). This approach is interesting because it reflects the typical thinking and mathematical methods of modern theoretical physics.

5.1. Potential Energy

The gravitational energy of a material particle of mass m in a field of potential V is mV , and that of a system of particles thus

$$E = \sum m_i V_i ; \tag{48}$$

the sign (+ or -) is conventional.

Thus holds for an external potential field V . If the field is produced by the mutual gravitational attraction of the particles themselves:

$$V_i = G \sum_j \frac{m_j}{\ell_{ij}} \qquad (j \neq i) , \tag{49}$$

then (48) gives

$$G \sum_{i,j} \frac{m_i m_j}{\ell_{ij}} .$$

Each term occurs twice, however (interchange i and j), so that we must devide by 2, obtaining

$$E_V = \frac{1}{2} G \sum_i \sum_j \frac{m_i m_j}{\ell_{ij}} \qquad (j \neq i) \; ; \qquad (50)$$

cf. also (Kellogg, 1929, pp. 79-81) or (Poincaré, 1903, pp. 7-8).
The continuous analog of (50) is

$$E_V = \frac{1}{2} G \iiint_V \iiint_V \frac{\rho(\underline{x}) \rho(\underline{x}')}{|\underline{x} - \underline{x}'|} \, dv \, dv' \qquad (51)$$

with obvious notations: $\underline{x}$, $\underline{x}'$ position vectors; dv , dv' volume
elements, and $\ell = |\underline{x} - \underline{x}'|$. Another form of (51) is

$$E_V = \frac{1}{2} \iiint_V V \rho \, dv \; , \qquad (52)$$

where V is the usual gravitational potential. Comparing with
(48) note the factor 1/2 reflecting the fact that E_V is
produced by an internal field created by the mass elements
dm = ρ dv themselves.

For the centrifugal part we have

$$E_\Phi = \sum m_i \Phi_i = \iiint_V \Phi \rho \, dv \; , \qquad (53)$$

in agreement with (48), since the centrifugal potential Φ acts
as an external field.

The potential energy of the gravity potential W = V + Φ
thus is the sum of (52) and (53):

$$E_W = \int (\frac{1}{2} V + \Phi) \rho \, dv \; , \qquad (54)$$

using only a simple integral sign for notational convenience.

5.2. Dirac's and Heaviside's Functions

We recall the basic definition of Dirac's delta function:

$$\delta(x) = 0 \qquad \text{except for} \quad x = 0 \ ,$$

$$\delta(0) = \infty \qquad \text{in such a way that} \qquad (55)$$

$$\int_{-\infty}^{\infty} \delta(x)\,dx = 1 \ . \qquad (56)$$

It is a somewhat strange "function" but is extremely useful and popular in physics.

Its integral is Heaviside's step function:

$$\theta(x) = \int_{-\infty}^{x} \delta(x')\,dx' \ . \qquad (57)$$

From (55) and (56) it immediately follows that

$$\theta(x) = \begin{cases} 0 \text{ for } x < 0 \ , \\ 1 \text{ for } x > 0 \ . \end{cases} \qquad (58)$$

For $\theta(0)$ we may take the value $1/2$.

From (57) there follows the basic relation

$$\delta(x) = \frac{d\theta(x)}{dx} = \theta'(x) \ . \qquad (59)$$

5.3. A Remarkable Expression for the Density

Assume the body to consist of n layers bounded by surfaces S_k and S_{k+1} (Fig. 3). The density within each layer is constant, denoted in our case by ρ_{k+1} .

Let the surface S_k have the equation

$$f_k(\underline{x}) = 0 \ , \qquad (60)$$

and let f_k be monotonic with

$$f_k(\underline{x}) > 0 \qquad \text{inside} \quad S_k \qquad (61)$$

(otherwise change the sign of f_k !).

Then the density everywhere within the stratified body can be described by the single expression

$$\rho(\underline{x}) = \sum_{k=1}^{n} (\rho_k - \rho_{k+1}) \theta [f_k(\underline{x})] \cdot . \tag{62}$$

The reader is invited to verify this on the basis of (58) and (61). Eq. (62) holds with the understanding that $\rho_{n+1} = 0$ since the density is zero outside the boundary surface $S = S_n$.
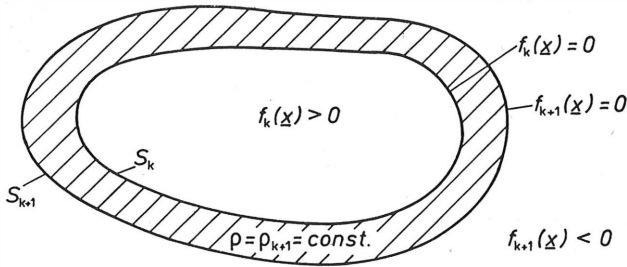
Figure 3. A layer of constant density

5.4. Variation of the Potential Energy

Let us find the extremum of the potential energy $E = E_w$ as given by (54):

$$E = \int (\frac{1}{2} V + \Phi) \rho \, dv \tag{63}$$

where ρ is expressed by (62). The side condition is that the volume enclosed by any surface S_k (Fig. 3) remains unchanged:

$$v_k = \int_{S_k} dv = const. \tag{64}$$

This equation remains constant when multiplied by $\rho_k - \rho_{k+1}$, which gives

$$M_k = \int_{S_k} (\rho_k - \rho_{k+1}) \, dv = \int (\rho_k - \rho_{k+1}) \theta [f_k(\underline{x})] \, dv = \text{const.} \qquad (65)$$

This expression has the dimension of a mass, but no very direct physical meaning. Note, however, that the factor $\theta[f_k(\underline{x})]$ has allowed us to extend the volume integral formally over the whole space because the integrand vanishes outside S_k since $f_k(\underline{x}) < 0$ there.

Introducing Lagrangian multipliers λ_k , we thus must minimize (or maximize)

$$E - \sum_{k=1}^{n} \lambda_k M_k \ .$$

This leads to the variational condition

$$\delta \left[E - \sum_{k=1}^{n} \lambda_k M_k \right] = 0 \qquad (66)$$

or

$$\int (V + \Phi) \delta\rho \, dv - \sum_k \lambda_k \delta M_k = 0 \ . \qquad (67)$$

Note that we are varying the density ρ by $\delta\rho$ and that, as compared to (63) the factor 1/2 seems to be missing. However, by (51), E_V is a quadratic functional of ρ , which introduces the usual factor of 2 on differentiation, which combines with 1/2 to 1. With the gravity potential $W = V + \Phi$ this reduces to

$$\int W \delta\rho \, dv - \sum_{k=1}^{n} \lambda_k \delta M_k = 0 \ . \qquad (68)$$

Now we must express the density variations $\delta\rho$ by $\delta f_k(\underline{x})$ since $\delta\rho$ is caused by a change in the boundary surfaces only. Now our expression (62) comes in handy: we have

$$\delta \theta [f_k(\underline{x})] = \theta' [f_k(\underline{x})] \delta f_k(\underline{x}) \ , \qquad (69)$$

where $\theta'(x) = \delta(x)$ is the delta function by (59); we prefer
the notation θ' to avoid confusion with the variation δ .
   With (69) everything is straightforward: (62) gives $\delta\rho$,
and (65) gives δM_k . Thus (68) becomes

$$\int dv \left\{ \sum_{k=1}^{n} (\rho_k - \rho_{k+1})(W(\underline{x}) - \lambda_k)\theta'[f_k(\underline{x})] \right\} \delta f_k(\underline{x}) = 0 . \tag{70}$$

The small deformations $\delta f_k(\underline{x})$ being arbitrary, the integrand
between brackets { } must vanish:

$$\sum_{k=1}^{n} (\rho_k - \rho_{k+1})(W(\underline{x}) - \lambda_k)\delta[f_k(\underline{x})] = 0 . \tag{71}$$

Now there is no more danger of confusion, so that we could use
the standard symbol δ instead of θ' for the Dirac delta
function.
   By the definition (55), $\delta[f_k(x)]$ vanishes everywhere except
on the surface S_k , where it is different from zero (that it
is even infinite there gives mathematicians a shudder but leaves
physicists entirely cold). Thus since $\delta[f_k(x)] \neq 0$ on S_k ,
we must have

$$W(\underline{x}) = \lambda_k = \text{constant on } S_k , \tag{72}$$

which means that the boundary surfaces S_k of regions of constant
density <u>must be equipotential surfaces.</u>
   In the limit $n \to \infty$ of a continuous density we thus have
recovered the basic fact that <u>the surfaces of constant density</u>
<u>must be surfaces of constant potential.</u> This is our well-known
condition for equilibrium figures.
   What is new? Formerly, in sec. 2 we have derived this
condition from (5) by means of the <u>pressure</u> p , a quantity which
we have not used afterwards any more. For some peoples' taste,
it is not very elegant to introduce an auxiliary concept which
plays the role of a <u>deus ex machina</u> and disappears again. Here
we have derived our basic condition $\rho = \text{const.} \Leftrightarrow W = \text{const.}$
from the principle of stationary energy, which is logically more

satisfactory for many people, especially in view of the fact
that maximum or minimum principles play a fundamental role in
physics.

Another beautiful fact: the Lagrange multiplyer λ_k admits
a natural physical interpretation; it is nothing else than the
constant value of the potential W on S_k , cf. (72).

5.5. A General Integral Equation

Now we are also in a position to give an explicit
representation for the functions $f_k(\underline{x})$ which characterize the
equisurface S_k : we may simply put

$$f_k(\underline{x}) = W(\underline{x}) - \lambda_k . \tag{73}$$

In fact, on S_k we have $f_k(\underline{x}) = 0$ by (72), and inside S_k
there is $f_k(\underline{x}) > 0$ since W increases monotonically towards
the center. Thus (60) and (61) are satisfied.

Now, in

$$W(\underline{x}) = G \int \frac{\rho}{\ell} \, dv + \frac{1}{2} \omega^2 (x^2 + y^2) \qquad (= V + \Phi) \tag{74}$$

we may substitute (62) together with (73), obtaining

$$W(\underline{x}) = G \int \frac{dv}{\ell} \sum_{k=1}^{n} (\rho_k - \rho_{k+1}) \, \theta \left[W(\underline{x}') - \lambda_k \right] + \frac{1}{2} \omega^2 (x^2 + y^2) \tag{75}$$

with $\ell = |\underline{x} - \underline{x}'|$. This is a nonlinear integral equation for
$W(\underline{x})$; the Lagrangian parameters λ_k are determined by the
condition of constant volume (64):

$$v_k = \int \theta \left[W(\underline{x}) - \lambda_k \right] dv , \qquad k = 1, 2, \ldots, n . \tag{76}$$

It is straightforward to let $n \to \infty$ and perform the
transition to a continuous (or piecewise continuous) mass
distribution; then the index k becomes a continuous variable
u :

$$W(\underline{x}) = -G \int \frac{dv}{\ell} \int_{u=0}^{\infty} d\rho(u) \; \theta\left[W(\underline{x}') - \lambda(u)\right] + \frac{1}{2}\omega^2(x^2+y^2) \; , \qquad (77)$$

$$v(u) = \int \theta\left[W(\underline{x}) - \lambda(u)\right] dv \; . \qquad (78)$$

Doubtlessly, this formulation for hydrostatic equilibrium figures is extremely elegant and general. Voss (1965, 1966) has tried to solve this equation by a series expression in terms of f , f^2 , etc. (f is the flattening as usual). The linear terms again give Clairaut's theory, essentially the linear integral equation (21). Voss has also computed second-order terms, but the details are very complicated and these terms can be calculated much more directly as we shall see in the next section. Another application of the potential energy approach is found in (Chandrasekhar and Roberts, 1963).

Thus the main importance of the method described in the present section is theoretical and conceptual, but it is great indeed.

6. Second-Order Theory

It is relatively straightforward to improve Clairaut's theory by second-order terms, that is, of order f^2 , f denoting the flattening. This has been done by many authors; we mention only (Darwin, 1899), Wavre (1932), Kopal (1960), and (Lanzano, 1982, ch. 2, to third order), forerunners being Airy in 1826 and Callandreau in 1889. The formulas given, without derivation, by de Sitter (1924), with corrections by Jeffreys (1953), are now considered standard, cf. (Jones, 1954), and will be used also here.

A theoretical difficulty lies in the use of the Legendre series for $1/\ell$, see eqs. (81) and (91) below, which may not be convergent. This has lead Wavre (1932) to devise an ingenious method (procedé uniforme, already mentioned above) that works with convergent series only. This complicated procedure is not really necessary, as we shall see below. Our approach, based on recent progress in understanding analytical continuation

(Moritz, 1980, secs. 6 and 7) is extremely simple and may be new.

6.1. Interior Potential

The gravitational potential at a point P in the interior of the body bounded by the surface S (Fig. 4) is

$$V(P) = \iiint G \frac{\rho}{\ell} dv = \iiint_{I_P} + \iiint_{E_P} = V_i(P) + V_e(P) \qquad (79)$$

where I_P denotes the interior of the surface S_P of constant density (not necessarily of constant potential!) passing through P, and E_P denotes its exterior, that is, the layer between S_P and S.

Consider first only

$$V_i(P) = G \iiint_{I_P} \frac{\rho}{\ell} dv . \qquad (80)$$

Then we have the well-known Legendre series, cf. (Heiskanen and Moritz, 1967, p. 33)
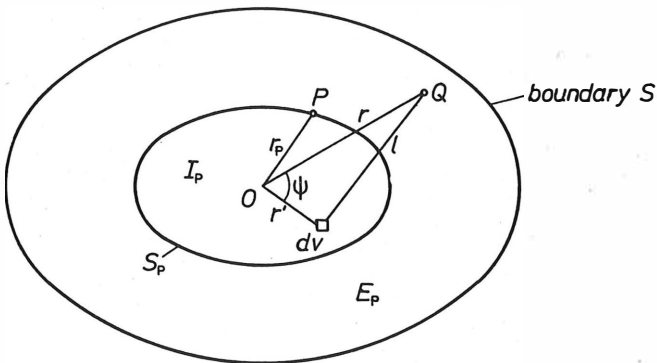
Figure 4. Illustrating the computation of $V(P)$

$$\frac{1}{\ell} = \sum_{n=0}^{\infty} \frac{r'^n}{r^{n+1}} P_n (\cos \psi) \quad , \tag{81}$$

which converges if $r' < r$. The problem is that for $r = r_p$ (Fig. 4), this convergence condition may be violated: r' may be greater than r .

The trick is to leave I_p and E_p but to calculate V first at a point Q outside S_p for which $r' < r$ is certainly always satisfied. Thus we calculate

$$V_i(Q) = G \iiint_{I_p} \frac{\rho}{\ell} \, dv = \sum_{n=0}^{\infty} \frac{1}{r^{n+1}} \cdot G \iiint_{I_p} \rho r'^n P_n (\cos \psi) \, dv$$

$$= \sum_{n=0}^{\infty} \frac{K_n}{r^{n+1}} P_n (\cos \theta) = \frac{K_0}{r} + \frac{K_2}{r^3} P_2 (\cos \theta) + \frac{K_4}{r^5} P_4 (\cos \theta) \quad , \tag{82}$$

neglecting higher-order terms. Here r, θ, λ denote the usual spherical coordinates (radius vector, polar distance, and longitude) of the point Q . Because of rotational symmetry, there is no explicit dependence on longitude λ .

The surface S_p can be written in the form

$$r = q(1 + \sum_{n=1}^{\infty} \epsilon_n P_n (\cos \theta)) = r(q,\theta)$$

$$= q(1 + \epsilon_2 P_2 (\cos \theta) + \epsilon_4 P_4 (\cos \theta)) \quad , \tag{83}$$

again neglecting higher-order terms and considering equatorial symmetry. Since the integral of all P_n over the sphere is zero, q is nothing else than the mean radius of the surface S_p , which by definition is a surface of constant density (but in general not of constant potential!). In the first-order theory of sec. 2, we were able to use r also for the mean radius, but here a notational distinction becomes indispensable.

Similarly, q' denotes the mean radius of the surface of constant density through dv , which has spherical coordinates r', θ' , λ' (Fig. 4). Thus we may introduce q', θ', λ' as new integration variables. This has the advantage that

$$\iiint_{I_P} = \iint_\sigma \int_{r'=0}^{r} = \iint_\sigma \int_{q'=0}^{q} , \tag{84}$$

where q , corresponding to S_p by (83), is now <u>constant</u>; σ denoting the unit sphere as usual.

For the volume element we have

$$dv = r'^2 \sin\theta' \, dr' d\theta' d\lambda' = r'^2 dr' d\sigma , \tag{85}$$

on introducing the element $d\sigma$ of the unit sphere as indicated. We have

$$dr' d\theta' d\lambda' = J \, dq' d\theta' d\lambda' = \frac{\partial r'}{\partial q'} \, dq' d\theta' d\lambda' , \tag{86}$$

on evaluating the Jacobian determinant J , using the form (83) also for the relation

$$r' = r(q',\theta') . \tag{87}$$

Thus, by (84) and (86),

$$G \iiint_{I_P} \rho r'^n P_n(\cos\psi) dv = G \int_{q'=0}^{q} dq' \, \rho(q') \iint_\sigma r'^n P_n(\cos\psi) \frac{\partial r'}{\partial q'} d\sigma . \tag{88}$$

The density ρ , by definition of q , depends only on q (or q').

We now develop r'^n into a series of form (83) (this is possible because powers of the Legendre polynomials P_n can always be expressed as linear combinations of P_n , cf. (102)) and use the orthogonality relations of P_n . The result is (82), where

$$K_n = K_n(q) \tag{89}$$

are functions only of q , the mean radius of S_p .

The logical trick that made (82) rigorously possible was to calculate V at an "external" point Q (Fig. 4). The trick then goes on by noting that $V(Q)$ is an analytical (harmonic) function everywhere outside and on S_p . Thus the expression (82)

continues to hold if we perform the transition from Q to P .
Thus also

$$V_i(P) = \frac{K_0(q)}{r} + \frac{K_2(q)}{r^3} P_2(\cos \theta) + \frac{K_4(q)}{r^5} P_4(\cos \theta) , \qquad (90)$$

if now $r = r_p$, $\theta = \theta_p$.

This argument thus is based on the analytical continuation
of a spherical-harmonic series, cf. (Moritz, 1980, pp. 54-55).
The convergence problem does not arise since we are working with
a truncated series only. If the reader insists, we may recur
to Runge's theorem (ibid., pp. 64-65); at any rate, regarding
convergence we are now sitting in the same boat as Wavre (1932)
with his considerably more complicated "procedé uniforme".

Now we apply the same trick with $V_e(P)$ in (79): we first
evaluate $V_e(Q)$, the gravitational potential of the shell between
S_p and S (Fig. 4) at a point Q well in the interior of the
shell, so that always $r' > r$ and the series corresponding to
(81),

$$\frac{1}{\ell} = \sum_{n=0}^{\infty} \frac{r^n}{r'^{n+1}} P_n(\cos \psi) , \qquad (91)$$

always converges. Then we perform the analytical continuation
$Q \to P$ with the result

$$V_e(P) = L_0(q) + r^2 L_2(q) P_2(\cos \theta) + r^4 L_4(q) P_4(\cos \theta) , \qquad (92)$$

analogous to (90).

The total gravitational potential V at an inner point
P with coordinates r, θ is the sum of (90) and (92), and the
gravity potential W is found by adding the centrifugal potential.
The result, in de Sitter's (1924) standard notation, may be
written

$$W = \frac{4\pi}{3} q^3 G \rho_m \left[D\left(\frac{1}{r} + \frac{1}{2}\mu\frac{r^2}{q^3}\sin^2\theta\right) - \right.$$

$$- \frac{2}{5}\left(S\frac{q^2}{r^3} + T\frac{r^2}{q^3}\right)P_2(\cos\theta) + \tag{93}$$

$$\left. + \frac{12}{35}\left(P\frac{q^4}{r^5} + \frac{8}{9}Q\frac{r^4}{q^5}\right)P_4(\cos\theta)\right]$$

where

$$\mu = \frac{\omega^2 R^3}{GMD} \tag{94}$$

is a dimensionless parameter and ρ_m denotes the earth's mean density. The functions $D = D(q)$, $S = S(q)$, ..., $Q = Q(q)$ will be considered later.

6.2. Ellipsoid and Spheroid

It is an elementary exercise to derive the following equation, accurate to f^2 , for an ellipsoid:

$$r = a(1 - f\cos^2\theta - \frac{3}{8}f^2\sin^2 2\theta) , \tag{95}$$

a and f denoting its semimajor axis and its flattening, respectively. For a general spheroid of revolution we may write

$$r = a\left[1 - f\cos^2\theta - (\frac{3}{8}f^2 + \kappa)\sin^2 2\theta\right] , \tag{96}$$

so that $a\kappa$ denotes the maximum deviation (at $\theta = 45°$) of the spheroid from the ellipsoid that has the same axes a and b .

Going from a to the mean radius β , we get from (96) after some algebra

$$r = q\left[1 - \frac{2}{3}(f + \frac{23}{42}f^2 + \frac{4}{7}\kappa)P_2(\cos\theta) + \frac{4}{35}(3f^2 + 8\kappa)P_4(\cos\theta)\right] , \tag{97}$$

which thus represents (83) expressed in terms of the flattening

f , and the parameter κ characterizing the deviation of the spheroid from its equiaxial ellipsoid. With de Sitter we find it convenient to introduce the "reduced flattening"

$$f^* = f - \frac{5}{42} f^2 + \frac{4}{7} \kappa \quad , \tag{98}$$

which deviates from f only by second-order terms so that we may put $f^{*2} = f^2$. Then we have the desired expressions

$$D = \beta^{-3} \int_0^\beta \delta \frac{d}{d\beta} \left[(1 + \frac{4}{15} f^2) \beta^3 \right] d\beta \quad ,$$

$$S = \beta^{-5} \int_0^\beta \delta \frac{d}{d\beta} \left[(f^* + \frac{2}{7} f^2) \beta^5 \right] d\beta \quad ,$$

$$T = \int_\beta^1 \delta \frac{d}{d\beta} \left[f^* + \frac{16}{21} f^2 \right] d\beta \quad , \tag{99}$$

$$P = \beta^{-7} \int_0^\beta \delta \frac{d}{d\beta} \left[(f^2 + \frac{8}{9} \kappa) \beta^7 \right] d\beta \quad ,$$

$$Q = \beta^2 \int_\beta^1 \delta \frac{d}{d\beta} \left[\kappa \beta^{-2} \right] d\beta \quad .$$

Here

$$\delta = \frac{\rho}{\rho_m} = \frac{\text{density}}{\text{mean density of the earth}} \tag{100}$$

and

$$\beta = \frac{q}{R} = \frac{\text{mean radius of } S_P}{\text{mean radius of earth}} \tag{101}$$

are dimensionless quantities; in other terms, we have expressed the mean radius β using the mean radius R of the earth as unit. Denoting the integration variable β' also by β simplifies the notation without danger of confusion.

Using the binomial theorem, we may in (93) express the

various powers of r by (97), using the well-known formula
(verify!)

$$\left[P_2 (\cos\,\theta) \right]^2 = \frac{1}{5} + \frac{2}{7} P_2 (\cos\,\theta) + \frac{18}{35} P_4 (\cos\,\theta) \ . \tag{102}$$

Then (93) becomes (with R as unit)

$$W = \frac{4\pi}{3} \beta^2 G \rho_m \left[A_0 (\beta) + A_2 (\beta) P_2 (\cos\,\theta) + A_4 (\beta) P_4 (\cos\,\theta) \right] \ , \tag{103}$$

where

$$A_0 (\beta) = D(1 + \frac{1}{3}\mu + \frac{4}{45} f^2 + \frac{4}{45} f\mu) - \frac{4}{25} fS + \frac{8}{75} fT \ ,$$

$$A_2 (\beta) = -\frac{2}{3} \left[-D(f* + \frac{6}{7} f^2) + \frac{3}{5} S(1 + \frac{4}{7} f) + \right.$$

$$\tag{104}$$

$$\left. + \frac{3}{5} T(1 - \frac{8}{21} f) + \frac{1}{2} D\mu(1 + \frac{20}{21} f) \right] \ ,$$

$$A_4 (\beta) = \frac{8}{35} \left[(-\frac{1}{2} f^2 - 4\kappa)D - \frac{9}{5} fS + \frac{6}{5} fT + \frac{3}{2} P + \frac{4}{3} Q + f\mu D \right] \ .$$

Eq. (103), together with (104), expresses the potential on a
surface of constant density, β = const., as a function of its
mean radius β and of the polar distance θ .
    For future reference, we also calculate

$$A_4 + \frac{24}{35} f A_2 = \frac{8}{35} \left[(\frac{3}{2} f^2 - 4\kappa)D - 3fS + \frac{3}{2} P + \frac{4}{3} Q \right] \ . \tag{105}$$

6.3. Hydrostatic Equilibrium

As we have pointed out several times, the preceding
developments do not presuppose that the surfaces of constant
density ρ, β = const., must also be surfaces of constant
potential W , i.e., hydrostatic equilibrium is not presupposed.
The only assumption is rotationally and equatorially symmetric
stratification of the surfaces β = const., which deviates little

from an ellipsoidal stratification (the deviation parameter κ is assumed to be of order f^2).

Now, finally, we introduce the condition of hydrostatic equilibrium. Then W must be constant on the surfaces β = const., which implies that in (103), $A_2(\beta)$ and $A_4(\beta)$ must identically vanish since they are multiplied by a function of θ : W must be independent of θ . This gives

$$A_2^H = 0 \tag{106}$$

and

$$A_4^H = 0 . \tag{107}$$

A_2^H and A_4^H denote A_2 and A_4 as given by (104) for the case of hydrostatic equilibrium.

Eq. (106) is essentially the same as (8) or (9), but supplemented by second-order terms. It is treated in the same way, arriving at a second-order differential equation for f (or more precisely, f*), which is nothing else than Clairaut's equation (1) supplemented by second-order corrections.

Eq. (107) is a new feature. Treating it, or better (105), as we treated (106), we arrive at a second-order differential equation for the deviation κ . This is <u>Darwin's equation</u> which, following (Jones, 1954, p. 12) may be written

$$\beta^2 \frac{d^2\kappa}{d\beta^2} + 6\frac{\delta}{D}\frac{d\kappa}{d\beta} - (20 - 6\frac{\delta}{D})\kappa = f^2 \left[3(1 - \frac{\delta}{D}) + \right.$$
$$\left. + (1 - \frac{9}{2}\frac{\delta}{D})\eta - \frac{1}{4}(1 + 9\frac{\delta}{D})\eta^2 \right] . \tag{108}$$

Here D is the dimensionless quantity defined by (99), which is the mean density inside the equisurface β = const. (denoted by D in (4)) devided by the earth's mean density ρ_m , and

$$\eta = \frac{\beta}{f}\frac{df}{d\beta} \tag{109}$$

is the famous Radau variable used to obtain (10) from (1).

Now (108), as opposed to (1), is an inhomogeneous differential equation if $\rho \neq$ const., so that the solution $\kappa \equiv 0$ is impossible. This confirms the impossibility of a purely ellipsoidal stratification (sec. 4.4).

It can also be shown (Wavre, 1932, p. 109), that κ (equivalent to Wavre's E) cannot be zero at the free surface: otherwise it would have to be identically zero in its interior, which we have just seen to be impossible. Thus the equipotential reference ellipsoid cannot be an equilibrium figure.

For a terrestrial equilibrium figure, κ must be positive and decreasing towards the center. At the earth's surface we have Bullard's (1948) value

$$\kappa = \kappa^H \doteq 0.000\ 000\ 68 \ ; \tag{110}$$

see also (Jones, 1954, p. 13). This means that the equilibrium spheroid lies below the ellipsoid at a distance which reaches its maximum $a\kappa \doteq 4.3$ m at latitude 45°. This effect is extremely small but nevertheless essential!

7. Real Earth and Reference Ellipsoid

Neither the earth nor the reference ellipsoid (considered an equipotential or level ellipsoid) are in hydrostatic equilibrium. Nevertheless, the second-order equations (103) and (104) hold also in this cases, since they have been derived without presupposing hydrostatic equilibrium.

However, it is possible to find two corresponding mass distributions, one for equilibrium and the other for the level ellipsoid, for which the $f*$ values are equal for each β :

$$f* = f*^H \ . \tag{111}$$

In other terms, the coefficients of P_2 in (97), with (98),

$$-\frac{2}{3}\,(f^* + \frac{2}{3}\,f^2) \;\overset{\scriptscriptstyle\bullet}{=}\; -\frac{2}{3}\,(f^* + \frac{2}{3}\,f^{*2}) \;,$$

are equal.

This follows at once from the fact that A_2 according to (104) is identical for the hydrostatic and the ellipsoidal case since D, S, T, and μ depend only on the density ρ as a function of β and since in the second-order terms, f may be put equal to f^*, so that κ does not occur (Moritz, 1973).

It should be noted, however, that since

$$\kappa \neq \kappa^H \;, \tag{112}$$

also

$$f \neq f^H \;, \tag{113}$$

except that in second order terms f may be set equal to f^H.

Thus we have the

Theorem

To each mass distribution in hydrostatic equilibrium there corresponds a mass distribution for the equipotential ellipsoid in such a way that the density ρ is the same function of β and that the values of the reduced flattening f^* are the same for any two surfaces corresponding to the same value β.

In the sequel we shall always assume that f^* is selected in this way. We then obtain an ellipsoidal mass configuration which deviates very little from an equilibrium configuration.

On this assumption, (103) reduces to

$$W = W_0(\beta) + W_4(\beta)\,P_4(\cos\theta) \tag{114}$$

since we have been able to take $A_2 = A_2^H = 0$.

Expressions for $W_0(\beta)$ and $W_4(\beta)$ are readily found on comparing (114) with (103) and using (104). For W_4 we get a

particularly simple expression on subtracting the hydrostatic
value W^H , which is found by putting $\kappa = \kappa^H$ in (104) and which
is zero by (107):

$$W_4(\beta) = \frac{4}{3} \pi G \beta^2 \rho_m \frac{32}{105} \left[-3(\kappa - \kappa^H) D + \frac{9}{8}(P - P^H) + (Q - Q^H) \right], \quad (115)$$

where, by (99)

$$\frac{9}{8}(P - P^H) = \beta^{-7} \int_0^\beta \delta \frac{d}{d\beta} \left[(\kappa - \kappa^H) \beta^7 \right] d\beta ,$$

$$\hspace{11cm} (116)$$

$$Q - Q^H = \beta^2 \int_\beta^1 \delta \frac{d}{d\beta} \left[(\kappa - \kappa^H) \beta^{-2} \right] d\beta .$$

For the deviation ζ of any surface of constant potential
from the corresponding surface of constant density we then
easily find (Bruns' theorem!)

$$\zeta = \frac{1}{g} W_4(\beta) P_4(\cos \theta) , \hspace{6cm} (117)$$

where g denotes gravity at the internal point under consideration.
For the ellipsoid we have $\kappa = 0$ at the surface. For the
real earth, satellite observations of J_4 give the surface value

$$\kappa = -0.000\ 000\ 84 \hspace{6cm} (118)$$

(Moritz, 1973, p. 48), which is even further off from the
hydrostatic value (110): note the difference in sign! Otherwise,
the preceding formulas also hold for this case, using (118).
The problem is that κ decreases monotonically towards
the center only in the hydrostatic case (110). For both $\kappa = 0$
and (118) it first increases in absolute value before decreasing,
which is not very satisfactory from an esthetic point of view.
More details can be found in (Moritz, 1973). The problem
of ellipsoidal density models in their relation to hydrostatic
equilibrium figures is particularly addressed in the short note
(Marussi et al., 1974).

An open problem is to find an "optimal" distribution of κ for the level ellipsoid, e.g. by a condition of stationary potential energy such as discussed in sec. 5.

REFERENCES

Baeschlin, C.F. (1948): Lehrbuch der Geodäsie, Orell Füssli Verlag, Zürich.

Bullard, E.C. (1948): The figure of the earth, Monthly Not. Roy. Astr. Soc., Suppl., 5, 186-192.

Chandrasekhar, S. (1969): Ellipsoidal Figures of Equilibrium, Yale Univ. Press, New Haven.

Chandrasekhar, S., and Roberts, P.H. (1963): The ellipticity of a slowly rotating configuration, Astrophys. J., 138, 801-808.

Darwin, G.H. (1899): The theory of the figure of the earth carried to the second order of small quantities, Monthly Not. Roy. Astr. Soc., 60, 82-124.

Denis, C., and Ibrahim, A. (1981): On a self-consistent represen-tation of earth models, with an application to the computing of internal flattening, Bull. Géod., 55, 179-195.

de Sitter, W. (1924): On the flattening and the constitution of the earth, Bull. Astron. Inst. Netherlands, II (55), 97-108.

Heiskanen, W.A., and Moritz, H. (1967): Physical Geodesy, Freeman, San Francisco (reprint by Section of Physical Geodesy, Techn. Univ., Steyrergasse 17, A-8010 Graz).

Jardetzky, W.S. (1958): Theories of Figures of Celestial Bodies, Interscience Publ., New York.

Jeffreys, H. (1953): The figures of rotating planets, Monthly Not. Roy. Astr. Soc., Geophys. Suppl., 113, 97-105.

Jeffreys, H. (1970): The Earth, 5th ed., Cambridge Univ. Press.

Jones, H. Spencer (1954): Dimensions and rotation, in: The Earth as a Planet (G.P. Kuiper, ed.), 1-41, Univ. of Chicago Press.

Kellogg, O.D. (1929): Foundations of Potential Theory, Springer, Berlin (reprinted 1967).

Khan, M.A. (1968): A re-evaluation of the theory for the hydrostatic figure of the earth, J. Geophys. Res., 73, 5335-5342.

Khan, M.A. (1969): General solution of the problem of hydrostatic equilibrium of the earth, Geophys. J. Roy. Astr. Soc., 18, 177-188.

Kopal, Z. (1960): Figures of Equilibrium of Celestial Bodies, Univ. of Wisconsin Press, Madison.

Lanzano, P. (1982): Deformations of an Elastic Earth, Academic Press, New York.

Ledersteger, K. (1969): Astronomische und physikalische Geodäsie (Erdmessung), v. V of Jordan/Eggert/Kneissl, Handbuch der Vermessungskunde, J.B. Metzler, Stuttgart.

Liapounoff, A. (1904): Sur l'équation de Clairaut et les équations plus générales de la théorie de la figure des planètes, Mém. de l'Acad. des Sciences de Pétersbourg, ser. 8, 15 (10), 1-66.

Lichtenstein, L. (1933): Gleichgewichtsfiguren rotierender Flüssigkeiten, Springer, Berlin.

Macke, W. (1967): Mechanik der Teilchen, Systeme und Kontinua, Geest & Portig, Leipzig.

Macke, W., Rennert, P., Rieger, F., and Voss, K. (1964): Über die Gestalt und das Schwerefeld der Erde, Z. Geophys., 30, 21-28.

Marussi, A., Moritz, H., Rapp, R.H., and Vicente, R.O. (1974): Ellipsoidal density models and hydrostatic equilibrium: interim report, Physics of the Earth and Planetary Interiors, 9, 4-6.

Melchior, P. (1983): The Tides of the Planet Earth, 2nd. ed., Pergamon Press, Oxford

Moritz, H. (1973): Computation of ellipsoidal mass distributions, Report 206, Dept. of Geodet. Sci., Ohio State Univ., Columbus.

Moritz, H. (1980): Advanced Physical Geodesy, Herbert Wichmann, Karlsruhe, and Abacus Press, Tunbridge Wells, Kent.

Moritz, H. (1984): The Geodetic Reference System 1980, Bull. géod. 58(3) ("The Geodesist's Handbook 1984"), 388-398.

Moritz, H. and Mueller, I.I. (1987): Earth Rotation: Theory and Observation, Ungar, New York.

Nakiboglu, S.M. (1979): Hydrostatic figure and related properties of the earth, Geophys. J. Roy. Astr. Soc., 57, 639-648.

Pizzetti, P. (1913): Principii della Teoria Meccanica della Figura dei Pianeti, Enrico Spoerri, Pisa.

Poincaré, H. (1885): Sur l'équilibre d'une masse fluide animée d'un mouvement de rotation, Acta Math., 7, 259-380 (reprinted in vol. VII of his Oeuvres).

Poincaré, H. (1903): Figures d'Equilibre d'une Masse Fluide, Gauthiers-Villars, Paris.

Voss, K. (1965): Über die Gestalt und das Schwerefeld der Erde II, Z. Geophys., 31, 313-326.

Voss, K. (1966): Über die Gestalt und das Schwerefeld der Erde III, Z. Geophys., 32, 216-231.

Wavre, R. (1932): Figures Planétaires et Géodésie, Gauthier-Villars, Paris.

The collected works of Liapunov are:

А.М. Ляпунов (1954-1965): Собрание Сочинений в 6-ти томах, Издательство Академий Наук СССР, Москва.

The review monograph

Итоги науки и техники, Астрономия, Том 10: Равновесие и устойчивость гравитирующих систем, ред. И.С. Шербина-Самойлова, Всесоюзний институт научной и технической информации АН СССР, Москва 1975.

gives many references in Russian.

The author is indebted to Prof. K. Bretterbauer, Prof. E. Grafarend, Dr. M.S. Petrovskaya and Prof. L. Stange for help with the references. Mr. K. Rautz has carefully checked the formulas and the text, and also drawn the figures.

After finishing this paper, the report

Denis, C.(1985): The hydrostatic figure of the earth, Geophys. Rep.Publ. No. 85/002, Department of Astronomy and Astrophysics, University of Liège

came to my attention. It is almost exactly complementary to the present paper, containing detailed numerical studies, geophysical discussions, and additional references.

I also was delighted to see the recent paper

Молоденский, М.С. (1988): Зависимость гравитационного поля Земли от изменения скорости ее вращения, Геодезия и Картография, No. 5, 11-13,

in which M.S. Molodensky occupies himself with the integral equation of Lichtenstein!

GRAVITY FIELD INTERPRETATION OVER THE MAIN ETHIOPIAN RIFT

Abera Alemu

The Royal Institute of Technology
Department of Geodesy
S-100 44 Stockholm
Sweden

Abstract

This paper presents the analysis of gravity data for about
1000 stations observed in the Main Ethiopian Rift (MER) system
since 1970.
Analysis of the gravity data has shown that the long wave
length negative Bouguer anomaly, which is characteristic of the
gravity field beneath the East African Rift system (Girdler et.al
1969), is disturbed by a positive anomaly under the entire width
of the Main Ethiopian Rift. On this broad positive anomaly over
the rift floor are superimposed other short wave length positive
anomalies which seem to be situated along the displacement lines
of the Wonji Fault Belt - axial zones of recent faulting,
volcanism, and geothermal and seismic activity.
Due to both, denser spacings of gravity stations and quality
of data, it is believed that the present gravity map of the
Central Part of the Main Ethiopian Rift (CPMER) defines the
locations of these observed gravity anomalies (the negative and
the positive anomalies) fairly accurately.
Crustal models that produce the observed gravity anomalies
matching the main geological and tectonic features of the Main
Ethiopian Rift are generated along a selected profile.
Interpretations of the models interms of mantle derived
intrusions as represting lithospheric thinning beneath the Main
Ethiopian Rift and a comparison of similar interpretation made
for the Kenyan Rift(Searle,1970) and the Afar Depression of
Ethiopia (Makris et.al, 1975) are presented.

Introduction

The Main Ethiopian Rift (MER) forms a part of the East African
Rift (EAR) System (Fig.1) which has long been recognized as a
continental extension of the World Rift System (Ewing and Heezen,
1956). Regional gravity field investigations across the rift
zone in East Africa have showen long wave length (broad) negative
Bouger anomalies with superimposed short wave length (narrow)

positive anomalies over the rift axis. The regional negative
anomalies are interpreted by Girdler et al. (1969),Girdler and
Sowerbutts (1970), and Baker and Wohlenberg (1971) interms of an
upward thinning of the lithosphere and replacement by lower
density astenosphere beneath the East African uplift regions. The
axial short wave length positive anomalies are interpreted by
Searle,(1970) as being due to intrusive zones in continuity with
the lower density astenosphere (i.e extreme thinning of the
lithosphere beneath the rift floor in East Africa).
    Regional gravity field investigations made in the MER so far
(Gouin and Mohr,1964;Gouin,1970;Searle and Gouin,1972;Abera,1983)
show that:

1.The western and eastern highlands of Ethiopia bordering the
rift are associated with broad negative Bouger anomalies.

2.Relatively broad positive Bouguer anomalies, which cover most
of the rift,are superimposed on the regional negative gravity
coinciding with the uplifted regions.

3.On the relatively broad positive Bouguer anomlies, which cover
most the rift floor,much narrower relative positive anomalies
are superimposed locally.

    Being based on similar concepts used to interpret the
nature of the gravity field across the rift zone in East Africa
by various investigators:

-The broad negative anomalies corresponding to the uplifted
regions of Ethiopia are interpreted as evidence of upward
propagation on a large scale of the low density astenospheric
material found in East Africa to higher levels and replacing the
upper mantle part of the lithosphere.

-The broad positive anomalies within the MER are interpreted
as being due to the further upward expansion of the low
density astenospheric material into higher levels of the crust
(i.e forming high density intrusion zones reaching to within a
few kilometers of the surface).

-The locally superimposed much narrower positive anomalies are
interpreted as being caused by intrusions associated with
lines of the Wonji Fault Belt (WFB) - axial zones of recent
faulting,volcanism,and geothermal and seismic activity.
    This paper describes the results of about 1000 gravity
observations made on the floor and shoulders of the MER between
latitudes 7^0 N and 8.5^0 N. The survey was undertaken with the
following objectives:

1.To present reliable gravity data which will form a sound
basis for further investigation of the rift system.
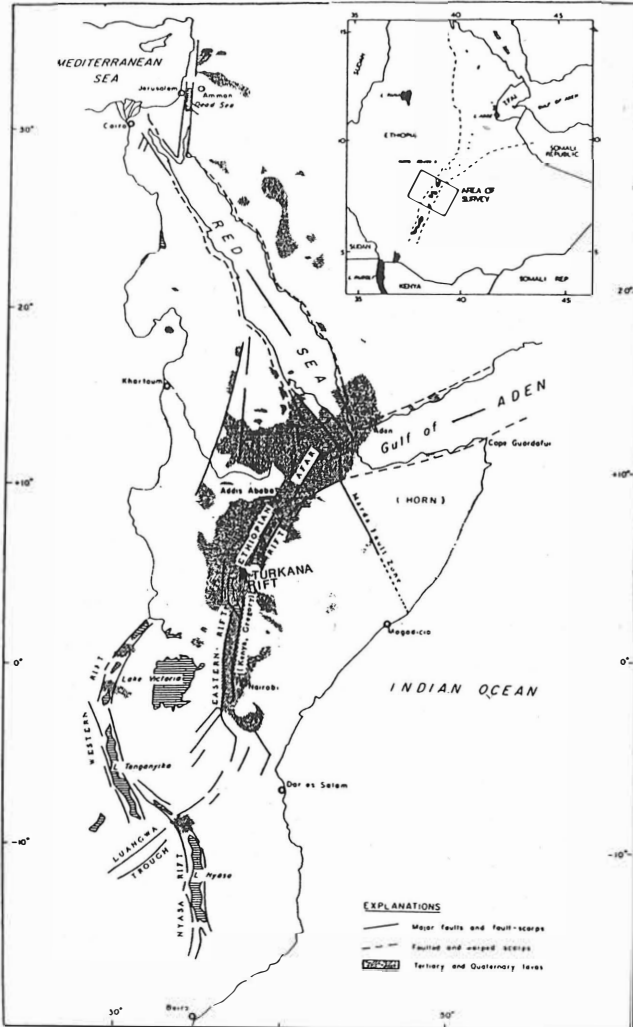
Fig. 1. The Rift System in East Africa, showing major faults.
The rift lakes are hatched. Inset: Location of survey area.

2.To define the locations of the observed positive and
negative Bouguer anomalies.

3.To generate preliminary models that produce the gravity
anomalies matching the major geological and tectonic features
of the region.

Geology of the Main Ethiopian Rift

Since the initial work of Mohr (1960),geological knowledge
of the Central Part of the Main Ethiopian Rift (CPMER) has been
enlarged as a result of prospecting work by the Ethiopian
Institute of Geological Survey (EIGS) in the " Detailed
Investigation Phase of Geothermal Resources for Power
Development". The result is that the geology in the CPMER is
fairly known.

Geological Setting

Along its approximately 400 Km length,the MER has a gently
curvillinear plan,convex to the west (Fig.1) and widens out at
its northern end to become identified with south western Afar. At
its southern end,crustal extensions are transposed west into the
seismically and tectoniclly active region of the middle Omo-Basin
The MER maintains a width of 80 ±15 Km along most of its 400 Km
length and 65 ±10 Km in its central part. A major watershed
crosses the rift floor at latitude 9^0 N and separates the Awash
Valley and Afar to the north from the CPMER to the south. The
CPMER contains five large lakes - Ziway,Langano,Abiyata,Shalla,
and Awasa (Fig.2).
The MER is offset at its southern end,west into the Turkana
Rift (Fig.1) from which there is a southward continuation into
the Gregory Rift in Kenya (Mohr & Wood,1976).

Structure

The MER commenced to form during late tertiary period
(Lloyd,1977). The rift is esentially a graben formed by the
drifting apart of the western Ethiopian highlands to the west and
the eastern highlands to the east through tensional normal
faulting.
During tertiary time there was a series of regional uplifts and
by the pleistocene the protorift was a topographically shallow
trough (Baker et.al,1976) with deep infilling of silicic
volcanics erupted from volcanic centers close to the rift
marigins. Mohr (1966b) suggests that the marginal faults are
pleistocene in age and that the separation of the western
highlands to the west and the eastern highlands to the east
occured at this time.
Fragmentation of the rift floor formed the youngest structural
deformation,largely concentrated within a narrow, 5-12 Km wide

Fig.2 Geological Map of the Lakes District

belt of normal faults,known as the Wonji Fault Belt (Mohr et.al,
1980; LIoyd,1977). The Wonji Fault Belt (WFB) maintains a NNE
orientation along the entire length of the MER and has been
forced into en-echelon offsets in order to remain within the rift
margin envelope.In the CPMER,the Wonji Fault Belt runs close or
adjacent to the eastern margin and tends to be axial between the
rift margins along the whole length of the MER. Within the lakes
district between latitudes 7^0 N and 8^0 N,the WFB is divided into
three segments,named from south to north,Corbetti-Shalla,Shalla-
Ziway,and East Ziway,by two en-echelon offsets (Lloyd,1977).

Volcanism and rocks flooring the rift

A notable feature of the MER is the occurence of young
volcanic centers along all except its most southern
part.Volcanism in the MER is of pleistocene and holocene age
(Mohr 1960,1966a,1966b ; Lloyd 1977). Rhyolite volcanism on the
rift floor of the CPMER is concentrated in four centers,Corbetti
volcanic center,Shalla Caldera,Gademota Caldera,and Aluto
volcanic center (Fig.2).
The rift floor is partially infilled with lacustrine sediments
derived from quaternary volcanic rocks of pleistocene and
holocene age. Contemporaneous with the volcanism the infill
consists of intercalations of silt stone,clay stone,pumices,etc.
Ephemeral lakes have also occupied the CPMER since the earliest
stages of its development and these lakes contributed sediment
to the rift floor. The tops of the rift scarps are covered
extensively by trap basalts of the pliocene to lower miocene age.
These trap basalts are supposed to underlie rhyolites,trachytes,
ignimbrites,agglomerates,and basalts of the upper miocene to
pleistocene age in the rift floor.

The Survey

The gravity measurements were made with the Canadian Sharp
Gravimeter No.128 belonging to the Geophysical Observatory of
Addis Ababa University. Measurements were made at 1 to 6 Km
intervals (i.e at 1 to 2 Km intervals for the Langano-Aluto area
and at 2 to 6 Km intervals for the rest). Some stations had
already been established in this area by Searle and Gouin (1971 ,
1972) along extant roads,tracks,and shorelines of lakes. Most of
their profiles were reoccupied except those along the shorelines
to establish a comparison between our survey and theirs. All the
stations occupied in the study area were tied to the Shashemene
USAF gravity base station (977536.42 mgal) and the Geophysical
Observatory USAF gravity base (977467.07 mgal).
In the Langano-Aluto area station positions and absolute
altitudes were determined by tacheometry. For stations outside of
Langano-Aluto area elevations were determined using a single
Paulin Surveying Microaltimeter. Trigonometric points and bench
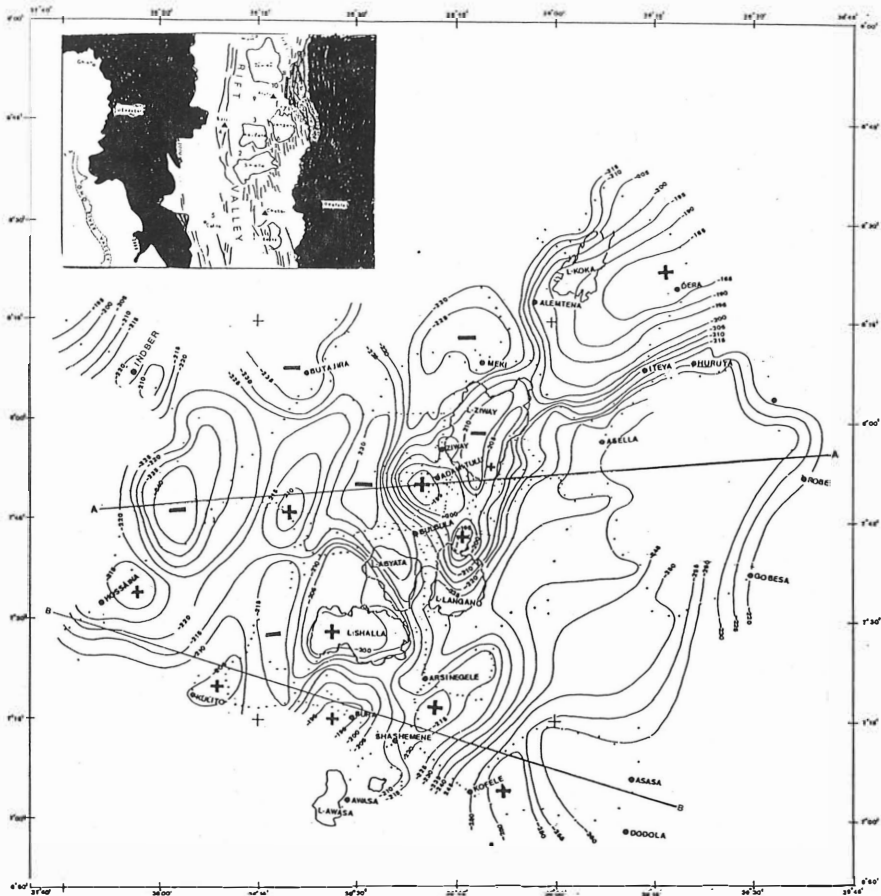
Fig. 3. Simple Bouguer anomaly map of the Central part of the Main Ethiopian Rift.
Contour intervals 5 mGals. Density 2.67 g cm⁻3. Dots represent stations occupied.
Inset: Physiographic features for the area of the gravity map.

marks established by the Ethiopian Mapping Agency (EMA) in the
study area were used for elevation control. An accuracy of ±1m
for the tacheometric observations and ±4m for the altimetric
observations may be guaranteed. The geographic coordinates of the
stations were scaled from sheets of topographic maps supplied by
the EMA at a scale of 1:50000 with an estimated accuracy of
±200m (0.1 minutes of arc).

Simple Bouguer anomalies were computed for the conventional
density 2.67 g cm^{-3}. Theoretical gravity was calculated using the
1930 international gravity formula. Terrain corrections were
determined out to 15 Km for all stations and varied between 0.1
and 9 mgals.The over all accuracy of the Bouguer anomaly values
(assuming the correct density has been chosen) is therefore
expected to be around ±2 mgals.

Figure 3 shows a contour map of the Bouguer anomalies of
the study area contoured at 5 mgals intervals.

Description of the Bouguer anomalies

As can be seen from the Bouguer anomaly map (Fig.3), there
exist positive anomalies which are central to the rift floor and
the axis of these anomalies generally coincides with the rift
axis. A typical W-E Bouguer anomaly profile (Profile AA) north
of 7.75^0 N across the rift shows that the central positive
anomalies are flanked by relatively two narrow negative anomalies
and two subsidiary positive anomalies on either side of the rift.
All the central positive anomalies and the flanking negative and
positive anomalies situated on the rift floor are flanked by
broad negative anomalies on the rift shoulders. The distribution
of the Bouguer anomalies in the MER in this fashion is considered
as a superposition of narrow positive anomalies on a broader
negative one. This phenomenon is typical of the general
characteristics of the gravity field across the rift zone in East
Africa. The two W-E Buoguer anomaly profiles marked in Fig.3
(Profiles AA ,BB shown in Fig.4) demonstrate this fact,which is
their essential similarity.

The broad negative anomalies are explained as being caused
by the low density astenosphere associated with the EAR system
and underlying the Ethiopian highlands. The relatively narrow
negative anomalies on the rift floor are explained by the fact
that the stations producing these anomalies are situated either
over large thickness of lake sediments and rift volcanics or are
affected laterally by the low density astenosphere which
underlies the rift shoulders.

Location of the positive Bouguer anomalies

As can be seen from the Bouguer anomaly map (Fig.3) the
positive anomalies beneath the central zone of the rift floor
generally seem to be situated along the displacement lines of the
WFB . In the MER between latitudes 7^0 N and 8.5^0 N the central
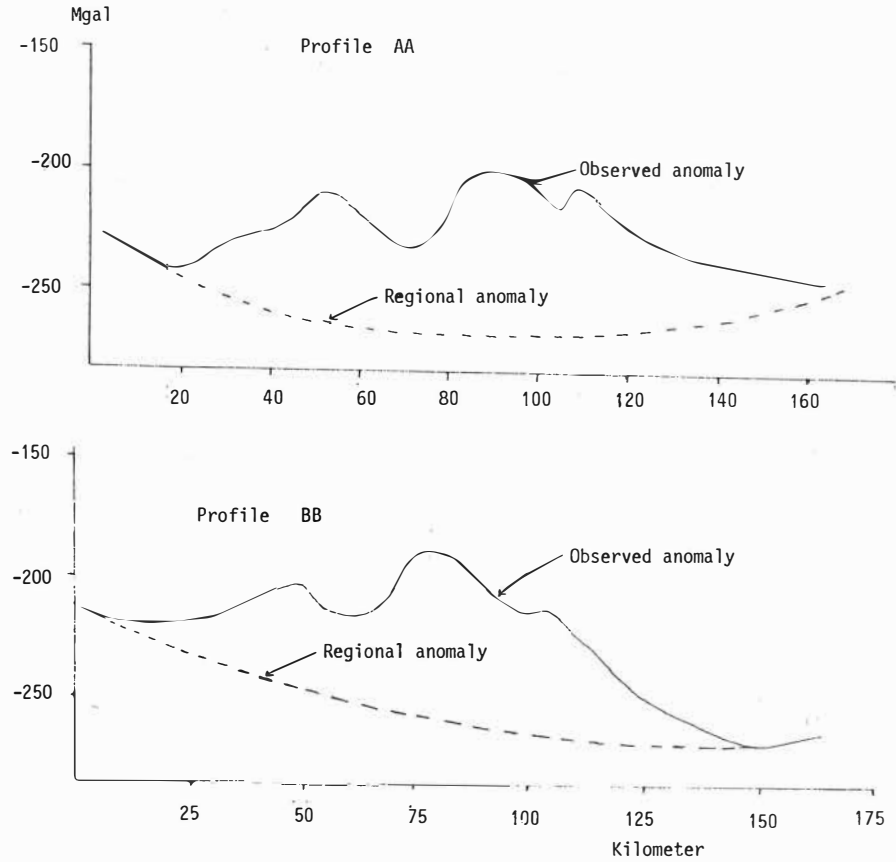
Fig.4 Profiles of Bouguer anomaly showing the observed anomalies and the Regional field.

positive anomalies culminate in six major positive anomalies.
These are situated north of Corbetti Caldera near Bura, on Shalla
caldera, south of Aluto volcanic center, east of Gademota Caldera
near Admitulu, east of Lake Ziway and north of Gedemsa Caldera
near Dera (Fig.2 & Fig.3)

Separation of the regional and local anomalies

The regional anomaly was separated using the method
(graphical method) described by Searle (1970a). The following
constraints were put on the choice of the regional anomaly.

1. The negative anomaly over the rift has a considerabely greater
width (> 100 Km).

2. The regional anomaly over the rift varies relatively smoothly

3. The resultant residual anomaly due to the outcroping rocks is
zero.

The regional field along the two W-E profiles (Profiles
AA, BB) is shown in Fig.4.

Interpretation of the positive anomaly

The central positive anomaly along profile AA is considered
to be produced by a zone of intrusives which could occur
predominantly (a) within a shallow basement (b) deeper in the
sialic crust (i.e existence of mass excess in the lower part of
the crust beneath the rift floor).

Models

For the calculation of the gravity anomalies generated by
the models to be described hereafter, a computer method based on
two-dimensional mass distribution (Hubbert, 1948 ; Talwani et.al
1959) was employed. Because of the axial tendency of the Wonji
Fault Belt within the rift margin envelope and the linear trend
of the positive anomalies along the axis of the WFB, the two-
dimensional representation assumed may be justified here.
The model calculations that will be considered below are
made for the same profile AA. The observed residual anomalies
used to calculate the models were obtained by _ subtracting the
regional field along the profile.
In Figures 5 & 6 are two preliminary models (Models A & B)
corresponding to two possibilities in which the central positive
anomaly beneath the rift is entirely caused by a zone of high
density intrusions.
In model A the excess mass is assumed to be contained as
intermediate intrusions (density 2.77 g cm^{-3}) within the basement
(i.e at less than or equal to 7 Km depth) while the lake
sediments and rift volcanics are assigned a density of 2.5 gcm^{-3}.
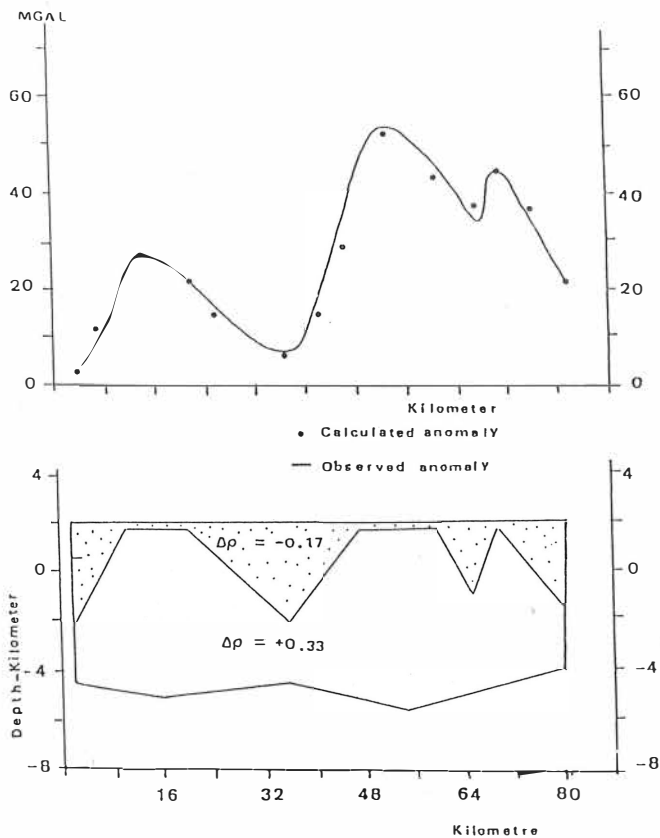
Fig.5. Model A: Residual Bouguer Anomalies with an intrusive model computed assuming a mass excess confined with in a shallow basement. -0.17 g cm^{-3} is the density contrast of lake sediments and rift volcanics. $+0.33$ g cm^{-3} is the density contrast of the intrusive body confined with in a shallow basement.
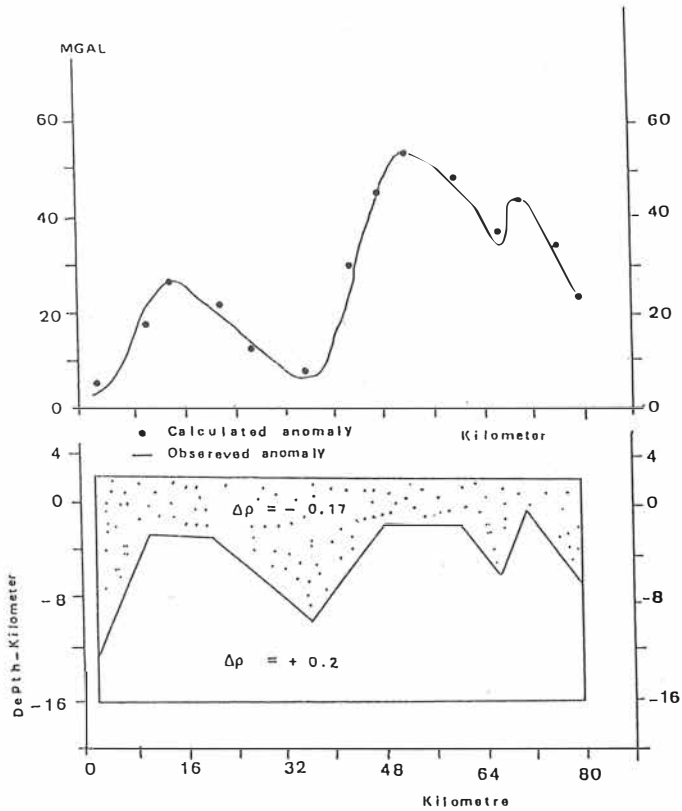
Fig.6. Model B: Residual Bouguer Anomalies with an
intrusive model computed assuming a mass excess
confined in the sialic crust. A density contrast of
-0.17. g cm^{-3} for the lake sediments plus rift volcanics
and +0.2 g cm^{-3} for the intrusive body with respect to the
crustal density was used.

In Model B the base of the intrusive body is put at 16 Km depth and assumed to be dense (density 2.87 g cm^{-3}) while the density of the lake sediments and rift volcanics is taken to be 2.5 gcm^{-3}

Shallow Model (Model A)

With the assumptions made above, model A was computed. The model showed that the density contrast 0.1 g cm^{-3} (2.77-2.67) for the intrusive body doesn't give a Bouguer anomaly which fits the observed profile. If the computed anomalies were to fit the observed profile, the the density contrast of the intrusive body should be greater than or equal to 0.33 g cm^{-3} and its upper surface coincident with the land surface at places (Fig.5). From a consideration of the available bore hole data and surface geology, it is unlikely that material in the rift floor can have such a high density contrast. This value, 0.33 g cm^{-3}, therefore represents an upper limit for the density contrast of the intrusive body. Hence it is concluded that it is impossible to account for all of the positive anomaly by means of high density intrusions confined within a shallow basement beneath the rift floor. Therefore model A is not considered to be a plausible one.

Deep Model (Model B)

If the observed Bouguer anomaly is not the result of dense intrusives confined within a shallow basement beneath the rift floor, then the only reasonable alternative seems to be deep-reaching and high standing crustal intrusions of astenospheric material or other igneous rocks derived from the astenosphere
Model B (Fig.6) has been computed on the assumption that the lake sediments plus rift volcanics have a density contrast of -0.17 g cm^{-3} (2.5-2.67) while a density contrast of + 0.20 g cm^{-3} (2.87-2.67) is assigned to the intrusive body. The depth to the base of the intrusive body is taken at 16 Km . The computed anomalies corresponding to Model B fit the observed ones to within ±2 mgals everywhere, with the intrusive body reaching to within 2-3 Km of the surface at places . The model also indicates that there are three zones of intrusions, a central zone along the rift axis and two subsidiary zones along the margins of the rift. A similar feature occures in the Kenyan Rift, although the magnitude varies (Searle, 1970).

Comparison with adjacent areas

Makris et.al (1969,1970) have published a paper on crustal and upper mantle models from gravity measurements across the Ethiopian Rift between latitudes of 8^0 N and 9^0 N. These models show a thinning of the crustal layers and an intrusion of upper mantle material beneath the rift.
There is a fair agreement with the concept that, north to south, in Ethiopia, we proceed from the oceanic crust of the central Red Sea Graben to the major crustal thinning with some
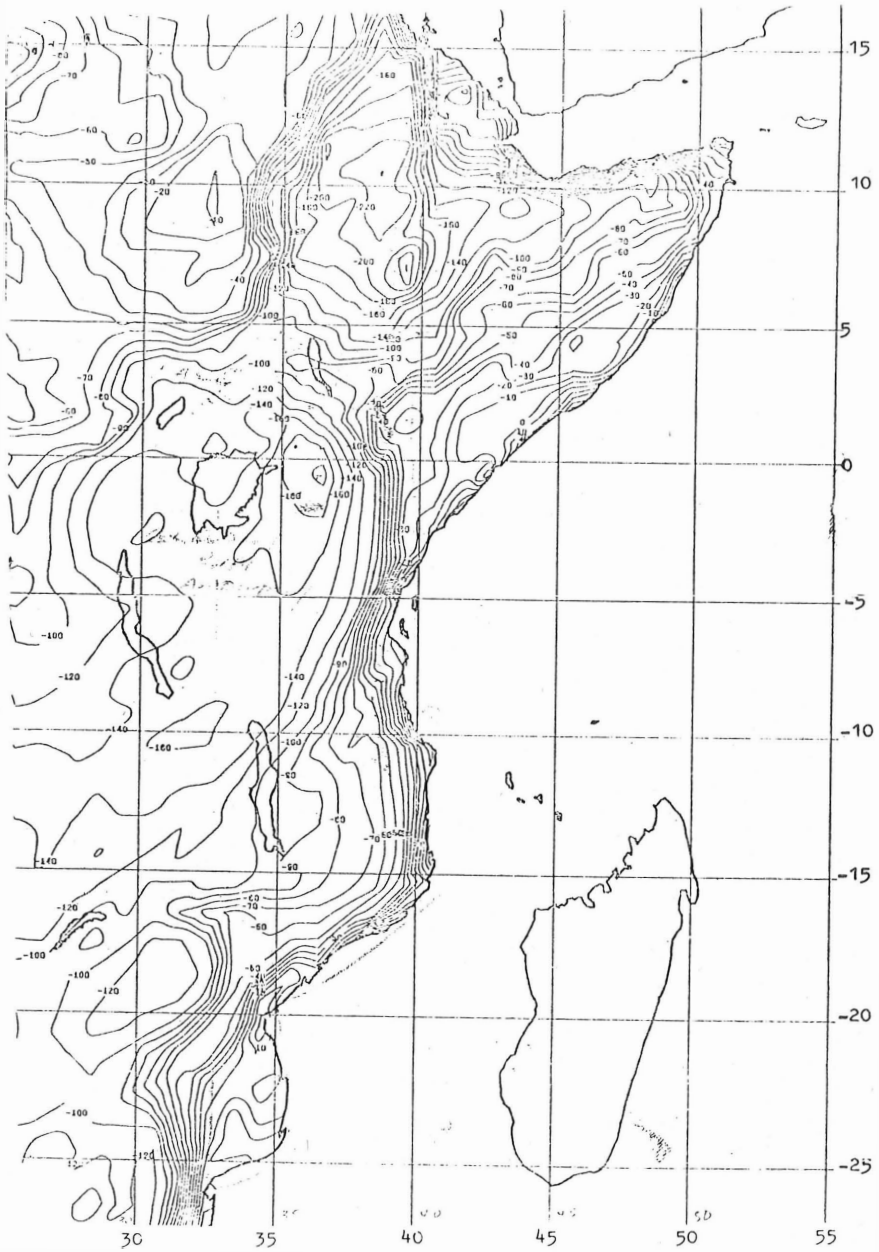
Fig. 7   N/SA Gravity Map of Africa

oceanic crust at Erte Ale in the Afar (Makris,1972) and to the
WFB - the axis of the Main Ethiopian Rift. The gravity anomalies
associated with these featuers decrease from the Red Sea through
Afar to the CPMER (Fig.7). The development of the positive
gravity anomalies seem to be depedent on the extent to which the
axial intrusives have developed. Over the Gulf of Aden and Red
Sea,the positive anomaly is much more pronounced and here the
intrusion zones are correspondingly larger.

    Further south,in Ethiopia,the axis of the MER system is
transfered to the Turkana Rift and finally to the Gregory Rift.
The Turkana Rift has a major positive anomaly with values
comparable to the Afar area. In contrast to the Turkana positive
anomaly the Gregory Rift has a broad negative anomaly with a
superimposed minor axial positive anomaly indicative of mafic
intrusions (Searle, 1970 ; Daracott et.al, 1972).

    On the basis of the axial gravity anomaly positiveness as
indicating the development and amount of intrusive activity(i.e
progression towards new crust), the CPMER might be considered as
an intermediate to the Turkana Rift and the Afar Depression. This
fact suggests that the gravity data could be viewed as indicating
a more advanced rift stage in the Turkana Rift and the Afar
Depression relative to the Main Ethiopian Gregory Rifts.

Conclusion

    The Bouguer anomalies of the CPMER have been interpreted
interms of varying geological conditions. Profile A has been
taken as representative of other profiles crossing the rift and
two models (Figs. 5 & 6) which could fit this profile have been
discussed. The main features of the results obtained in this work
may be summerized as follows:

1.Within the rift floor, a central zone of positive anomaly is
flanked,over most of the studied area, by narrow negative
anomalies. These negative anomalies could be ascribed to maximum
depths of lake sediments and rift volcanics confined to two
relatively narrow troughs.

2. The crust is thinner beneath the central zone than under the
flanking basements and this would correspond to zones of high
density intrusives. In the CPMER the centers of these intrusives
seem to be situated at Bura,Shalla,Northern Langano,Adamitulu,
Southeastern Ziway, and Dera (Fig.3).

3. The central positive anomalies are found to be associated with
the axial zones of recent faulting (WFB),volcanism,and geothermal
and seismic activity.
4. The models generated show that the positive gravity anomalies
are controlled by high density intrusives and the contributions
of the lake sediments plus rift volcanics flooring the rift is
relatively negligible.

Without doubt further refinements of the observations,and consequently of the interpretations,can be made.

Additional geophysical work such as seismic ,together with more detailed studies of the gravity field will provide better data for quantitative interpretations.

Further geological work will also be necessary to provide an improved version of the present work. In addition much density information is needed for the whole area.

ACKNOWLEDGEMENTS

Reference

Abera, A., 1983. Crustal Modelling from Gravity Data in the Ethiopian Rift. M.Sc. Thesis. Addis Ababa University.

Baker , B.H. and Wohlenberg, J.,1971. Structure and Evolution of the Kenya Rift Valley. Nature, 229: 538-542

Baker, B.H. and Mitchell, J.G.,1976. Volcanic stratigraphy and Geochronology and the Kedong-Olorgesaile Area & the Evolution of the South Kenya Rift Valley. J. Geol. Soc. London 132: 467-484.

Ewing, W.M.and Heezen ,B.C.,1956. Some Problems of Antarctic Submarine Geology, Monogr.AGU, 1: 75-81

Girdler, R.W.,1958. The Relationship of the Red Sea to the East African Rift System. Q.J.Geol.Soc. Lond.,114: 79-105.

Girdler,R.W., et.al, 1969. The Evolution of Rifting in Africa, Nature , 224: 1178-1182.

Girdler, et.al, 1970. Some Recent Geophysical Studies of the Rift System in East Africa, J.Geomagn. Geoelectr., 22: 153-163.

Gouin, P.,& Mohr, P.A., 1964. Gravity Traverses in Ethiopia (intrim report) Bull. Geophys. Obs. Addis Ababa, 7: 185-239.

Hubbert, M.K.,1948. A Line-Integeral Method of computing the
     gravimetric effects of Two-Dimensional Masses. Geophysics
     13: 215-225.
Lloyd, E.F.,1977. Geological Factors Influencing Geothermal
     Exploration in the Langano Region, Ethiopia. Privately
     circulated report, 73pp.
Makris,J., et.al, 1969. Crustal and Upper Mantle Structure of the
     Ethiopian Rift Derived from Seismic and Gravity Data. Z.
     Geophys. 36: 387-391.
Makris, J.,et al, 1970. Crustal Investigation from Gravity
     Measurements at the Scarp of the Ethiopian Plateau. Z.
     Geophys., 36: 299-311.
Mohr, P.A., 1960. Report on Geological Exercursion through
     Southern Ethiopia. Bull. Geophys. Obs. Addis Ababa. 3: 9-20.
----, 1962. The Ethiopian Rift System, Bull. Geophys. Obs. Addis
     Ababa, 5: 33-62.
----, 1966a. Chabbi Volcano (Ethiopia) Bull. Volcanol. 29:797-816
----, 1966b. Geological report on the Lake Langano and adjacent
     Plateau regions. Bull.Geophys. Obs., Addis Ababa, 9: 59-75.
----,1967. The Ethiopian Rift System. Bull. Geophys. Obs., Addis
     Ababa, 11: 1-65.
Searle, R.C., Gouin, P., 1970. Evidence of Gravity Anomalies for
     the Thinning of the Lithosphere Beneath the Rift Valley in
     Kenya. Geophys. Journal Roy. Astron. Society. 21: 13-30.
-----,1972. A Gravity Survey of the Central Part of the Ethiopian
     Rift Valley. Tectonophysics. 15: 41-52.
Talwani, M.,et.al, 1959. Rapid Gravity Computations for Two-
     Dimensional Bodies with an Application to the Mendacino
     Submarine Fracture zone. J. G.R., 64: 49-59.

ON THE INTERPRETATION OF NATURE

Gottfried Anger

Martin Luther University Halle-Wittenberg
Department of Mathematics
DDR - 4010 Halle (Saale)

Most problems in science, technology and medicine are inverse problems.
Studying such problems is the only complete way of analyzing experimen-
tal results. Often these problems concern the determination of prop-
erties of some inaccessible regions from observations on the boundary
of that region, like in geophysics and medicine. Further, the automa-
tization of physical processes leads necessarily to inverse problems,
which absolutely must be solved. The practical importance of inverse
and improperly posed problems is such that they may be considered
among the pressing problems of current mathematical research. In a
certain sense the paper gives final remarks concerning inverse prob-
lems. For inverse problems we have the following principles: only in
exceptional cases can an inverse problem be decided in a purely mathe-
matical way. In such cases, the solution often depends discontinu-
ously on the measured values. In case of ambiguity, only the set of
all solutions can be introduced and studied as a first step. One can
try to choose a solution relevant for the give use on the basis of
laboratory experiments. This result has important consequences for
scientific work. Success may be achieved only through an interdis-
ciplinary approach. For the complex systems of nature, the scientist
largely depends on practical experience. One can find all results in
the author's book on inverse problems.

For practical applications, the interpretation of experimental findings is of fundamental importance. Many physical parameters f do not lend themselves to direct measurement and the effect g which they induce is then the only known criterion; that is, often g is the only measurable value. Between f and g there exist relations based on physical laws which may be formally expressed as equations of the first kind: Af = g, with f to be determined by calculation. In doing so, an essential step consists in modelling the process resulting in a symbolic description of A. The basic equations of mathematical physics are derived by assuming the knowledge of the material parameters f at each point of the system considered. Such parameters are known, for instance, for the atmosphere, for interplanetary space and for materials for which experiments of high level exist, while in geophysics the earth's parameters are to be determined by measurements on the surface of the earth.

The calculation of Af with given f is called a direct problem. Typically, this does not offer any major difficulties, as it is possible to use the constructive methods of mathematics. The determination of f from the relation Af = g, with given g, is called an inverse problem. The solution of inverse problems is the only way to completely investigate experimental findings. Equations of the first kind are basically different from the more commonly occuring equations of the second kind: Af + f = g arising, e. g.,

in spectral theory. Equations of the first kind often have a great number of solutions f with Af = g. Each equation of the first kind describes a particular physical process and a uniform theory for such equations cannot be expected.

The first inverse problem leading to an integral equation of the first kind was solved by N. H. Abel in 1823. Suppose we slide a particle up a frictionless hill with initial energy E and measure the time T(E) required for it to return. If we vary E and measure T(E), can we determine the shape of the hill? If s is the arc length of the hill and h(s) with h(0) = 0 is its height, then both the arc length s and the energy V are coordinates suitable to describe the process as $V(s) = mg_0 h(s)$. If V is used as an independent variable, and V $\mapsto$ s(V) is a strictly increasing function, the given problem can be uniquely solved by applying the laws of point mechanics. If, however, the hill has maxima and minima, the problem cannot be solved uniquely (J. B. Keller (1976)). In this case it even has non-denumerably many solutions due to the many-valued mapping V $\mapsto$ s(V) (G. Anger (1987)). Similar conditions apply to the determination of the shape of a mountain by means of light (electromagnetic waves). The back of a mountain cannot be identified from an observation point. Further, it is not possible to look into the interior of an obstacle by means of electromagnetic waves. These examples raise the question of the information content of a physical process or of the relevant mathematical model: which values f do lend themselves to unique and stable determination using the mapping A from Af = g?

Inverse problems occurring in optics can comparatively easy be understood and formulated. In this field the direct problem consists in the calculation of the emission, the scattering and the propagation of radiation on the basis of known parameters, both of sources and of diffusers. On the other hand, the inverse problem consists in the determination of the parameters of sources, diffusers, or propagation media by means of the radiation received by a detector. We are well aware of the intuitive solution of the inverse problem: we derive the size, the shape, the surface finish and the structure of an object from the scattering and absorption of light perceived by the eye. In doing so, we have to take into consideration that the human eye has an extremely complex structure. The brain is able to synthesize information in the form of visible light to identify objects, but if optic information beyond the visual impression, or the analysis of optic information by means of electrooptic automatic instruments are required, intuition has to be replaced by mathematical reconstruction, that means by the solution of inverse problems (H. P. Baltes (1980)). This is true for practically any physical and biological process. The highest level of development has been reached with regard to inverse spectral problems as they are closely related to equations of the second kind. A first theorem of uniqueness has been proved by V. Ambarzumian (1929). In the present book, only a few results along these lines are briefly outlined, as a number of monographs exist which deal with this issue.

Another inverse problem that has been under investigation for
more than 100 years is the inverse source problem in gravimetry.
It consists in the determination of the earth's density $\varrho(x)$,
$x \in R^3$, by measuring the gravity g = grad u on the earth's sur-
face, with the gravitational field u satisfying the Laplace
equation $-\Delta u = \varrho(x)$. From the knowledge of u for the whole
space follows the uniqueness of ϱ. In this inverse problem,
u and grad u are known just with regard to the earth's sur-
face, while away from the surface of the earth the solution of
the Dirichlet problem or of the problem of the oblique deriva-
tive has to be used to determine them. The lack of information
on u inside the earth results in ambiguity with regard to the
inverse source problem. This fact was already known to G. G.
Stokes (1867), G. V. Schiaparelli (1875), C. Neumann (1906),
P. Pizetti and G. Lauricella (1907 - 1911), as well as to
G. Herglotz (1914). The first uniqueness results (for special
mass distributions) were obtained by G. Herglotz (1914), P. S.
Novikov (1938), and I. M. Rappoport (1940). As far as the in-
formation content is concerned, one can as a first step just
introduce and study the set of all mass distributions producing
the same potential on the earth. The integrals of these mass
distributions are equal for harmonic functions (G. Lauricella
(1911). It has been modern potential theory, one of the most
efficient theories in mathematics (O. Perron (1923), R. Remak
(1924), N. Wiener (1924), M. Brelot (1903 - 1987), J. L. Doob,
G. Choquet, H. Bauer, G. Anger) which, since about the year 1960
has made it possible to consider the characterization of the set
of all mass distributions having the same potential (G. Anger

(1973 - 1976)) from a systematic point of view. Additional infor-
mation is needed to uniquely choose an element out of this set in
order to arrive at a solution. This may be the information that
the density ϱ is constant but such assumptions are not true for
geophysics or for medicine. It is more essential to consider
various coupled fields. In geophysics coupling of gravitational
and seismic fields (A. S. Alekseev and B. A. Bubnov (1981, 1984)),
as well as coupling of gravitational and magnetic fields (D. Zidarov
(1968 - 1984), M. S. Zhdanov (1981, 1988)) are of particular inter-
est. In addition, satellites introduce the possibility of meas-
uring various kinds of radiation.

We are now observing just the beginning of such investigations.
The results outlined in this book ought to be extended in the di-
rection indicated, i.e., in modelling more consideration should be
given to the complexity of physical processes. Owing to the present
lack of information, we are now unable to determine the mass dis-
tributions which produce the earth's potential. The above con-
siderations apply also to sources of electrostatic fields. Never-
theless, profound structural investigations may classify the sources
(measures), which, outside a body, produce the same potential. The
set of these sources is convex and weakly compact. Thus, results
of functional analysis are available for concrete issues in physics.
The attempt may then be made in a laboratory to find, out of the set
of solutions, a solution relevant for a given use. This aspect is
gaining increasing importance in applied mathematics. Owing to the
existing lack of information, only partial processes can be solved
in complex systems by means of mathematics.

In a sense, the results outlined above apply also to inverse source problems for other differential equations, as well as to most identification problems. With regard to the latter, certain coefficients of a differential equation are to be determined on the basis of additional information. If, however, the information content of individual coefficients or of the right-hand side of a differential equation is not too large, these values can be uniquely calculated on the basis of additional information /4/. This is true for the diffusion coefficient $k(u)$ in equation $\partial_t u - \text{div}(k(u)\text{grad } u) = 0$, for the density ς in the system $\varsigma(|\nabla u|)\partial_{x_1} u_1 = \partial_{x_2} u_2$, $\varsigma(|\nabla u|)\partial_{x_2} u_1 = -\partial_{x_1} u_2$, for the right-hand side $f(u)$ in the equation $\partial_t u - \Delta u = f(u)$ and for one-dimensional inverse problems, i.e., the coefficients depend only on one variable. These special problems are a small part of the set of all identification problems.

The difficulties arising in inverse problems with regard to differential equations can be characterized in a comparatively simple way. To do so, we consider the simplest differential equations

$$u' = f, \quad u(a) = 0 .$$

The solution u depends on the integral of f. Different f may have the same value $u(b) = g$, $a < b$. If f is linear the relation between f and g is one-to-one. The function f is uniquely determined, provided u is known for the whole interval. However, this information is not available in practice.

As another example we consider the differential equation

$$u' - (q(x) + \varphi(x))u = 0, \quad u(a) = u , \quad \varphi(x) = 0 \text{ for } x \notin [\alpha, \beta] \subset [a, b],$$

with the integral of φ being zero. The function φ does not influence the solution u for $x \notin [\alpha, \beta]$. These so-called "non-radiating" physical parameters are of principal importance for the solution of equations of the first kind $Af = g$, as they do not lead to a unique solution f. They cause particular difficulties in problems arising in geophysics and in medicine where a unique solution has to be found. If $\varphi = 0$ and $q = q_0 = const.$, then q_0 can be determined upon one measurement of $u(x^0)$. The relation between $u(x^0)$ and q_0 is strictly non-linear, which is another difficulty in inverse problems.

In both physics and biology, microstructures are gaining increasing importance. At present, supercomputers render possible the precalculation of systems comprising no more than 1000 particles (Dupuis (1986)). But one cubic centimetre of a solid body contains 10^{23} atoms, so, modelling of the properties of microstructures still presents great difficulties. Therefore, one has to continue to use models based on the continuum, in particular models formulated as differential equations. It is not possible to calculate the density $\varrho(x)$ in each point of a body from finitely many measurements performed outside the body. In the case of the earth one needs non-denumerably many values for this purpose. The same situation occurs in the coefficients $a_\alpha(x)$ of a differential equation, if the information content is too large. For this reason the information content has to be reduced with regard to ϱ or a_α, respectively. This can be done by integration (averaging) of certain subsets. As has been said earlier, different ϱ or a_α may have the same average value.

124

The present state of inverse theory may be evaluated as follows:
each particular physical or biological problem is of a complex
nature; the models used in mathematics comprise only a small
number of material parameters. When faced with a multiplicity
of inverse problems, one tries to determine just one parameter
by measurement outside an open set. This approach leads to a
limitation of the problem, which in general can be dealt with
in laboratories only. In laboratories most parameters can be
kept constant, and different experiments can be controlled
(G. Duvaut and J. L. Lions (1976)). Every inverse problem re-
quires a particular approach. In designing instruments one
finds certain additional degrees of freedom as far as geomet-
rical dimensions and materials are concerned. The great success
in design engineering is due to this fact. Design perception
corresponds to deductive perception in mathematics. On the other
hand, interpretive sciences such as geophysics, soil mechanics,
meteorology, space research, biology, medicine, etc., are facing
particular difficulties. There, one tries to determine a great
number of inner parameters from a small number of measurements.
Lack of information often results in ambiguity, so different inner
parameters produce the same measured values. This ambiguity can
only be eliminated by means of additional information to be ob-
tained from experiment. For inverse problems we have the following
principles: only in exceptional cases can an inverse problem be
decided in a purely mathematical way. In such cases, the solution
often depends discontinuously on measured values (A. N. Tikhonov
(1943, 1963), V. K. Ivanov (1956, 1962), M. M. Lavrent'ev (1962)).

In case of ambiguity, only the set of all solutions can be introduced and studied as a first step (information content of an inverse problem). One can try to choose a solution relevant for the given use on the basis of laboratory experiments. This result has important consequences for scientific work. Success may be achieved only through an interdisciplinary approach (J. Polking (1987)). For the complex systems of nature, the scientist largely depends on practical experience. In the future, intense fundamental research on inverse problems will be imperative. The determination of the information content of mathematical models, that is the possibility of unique and stable determination of inner parameters, will be most important. The solution of the direct problem is the presupposition of a successful approach to the inverse problem.

We have repeatedly pointed out that an equation of the first kind $Af = g$ may have non-denumerably many solutions f with the same image g. Here Cantor's Continuum Hypothesis plays a role. More than a hundred years ago, G. Cantor of the University Halle-Wittenberg, tried to prove that any infinite set of real numbers may be mapped one-to-one either on the set N of natural numbers, or on the set R of real numbers. K. Gödel (1931) and P. Cohen (1963) pointed out that the existing mathematical axioms are not sufficient to prove or to refute this statement. Similar assertions are valid for any inverse problem. Such problems do not lend themselves to decision without substantial additional suppositions gained from experiments. It has repeatedly been outlined that with regard to such non-decidable problems profound structural investigations may be needed, and these may be of primary importance for the future.

It may be that results in inverse theory are most important for simulation. By means of these results, simulation can use the information content of the special model considered more effectively.

One can find all facts in the author's book /4/.

References

/1/ Anger, G.: On inverse problems in differential equations: a critical analysis. Veröffentl. Zentralinstitut Physik der Erde 81 (1985), no. 1, 38 - 44.

/2/ Anger, G.: Unsolved problems in the theory of inverse problems. In: Partial Differential Equations, Conference held on the occasion of the 75th birthday of Academician S. L. Sobolev, Novosibirsk, October 10 - 14, 1983, pp. 17 - 31. Novosibirsk: Nauka, 1986 (Russian). English original: Preprint 04/84. Institute of Mechanics, Academy of Sciences of the GDR, Karl-Marx-Stadt, 1984.

/3/ Anger, G.: Inverse problems: examples, counterexamples, consequences for the applications. In: Mathematical methods of solution of inverse problems of geophysical fields (M. Škorvanek ed.), pp. 7 - 20. Bratislava: Slovak Academy of Sciences, Geophysical Institute, 1987.

/4/ Anger, G.: Inverse problems in differential equations. Berlin: Akademie-Verlag, 1989.

/5/ Engl, H. W., Kunisch, K. and Neubauer, A.: Tikhonov regularization for the solution of nonlinear ill-posed problems I. Inverse Problems (to appear).

On the mathematical representation of the gravitational potential and its time variation.

K. Arnold, Potsdam

The consideration of the spherical harmonics series development for the gravitational potential W of the Earth begins usually with the mass integral

(1) $\quad W = W(r,\varphi,\lambda) = f \iiint\limits_V \frac{1}{e} \, dM$,

with

(2) $\quad \frac{1}{e} = \frac{1}{r} \sum\limits_{n=o}^{\infty} (\frac{r'}{r})^n P_n(\cos \psi), \quad r' < r$.

r is the radius of the test point P, r' that of the mass element dM. The introduction of (2) into (1) leads to the well-known harmonics series for W, convergent in the exterior of the Brillouin sphere, $r = R_{B,a}$. But, the condition for the convergence of the development for 1/e, being

(3) $\quad r' < r$,

is no more valid for the series obtained if (2) is introduced into (1). The deeper reason for the fact that (3) is lost comes from the mathematical property of (1) to have an infinity of mass distributions which generate the same potential W,

(4) $\quad W = f \iiint\limits_V \frac{1}{e} \, dM_1 = f \iiint\limits_V \frac{1}{e} \, dM_2 = f \iiint\limits_V \frac{1}{e} \, dM_3 = \dots$

This relation representing the potential W in terms of the masses has not a unique inverse. For instance, the masses within the Bjerhammar sphere give rise to a series development convergent in the exterior of the body of the Earth, $\Re$.

(5) $\quad W = \sum_{n=0}^{\infty} (\frac{1}{r})^{n+1} w_n Y_n (\varphi,\lambda) , \quad \text{in } \Omega .$

Further on, integrating over the masses, it is necessary to introduce also the condition that only continuous functions for the potential W have to come out. This condition paralyses generally the way via the mass integral, (53).

The shortest and most evident proof of the convergence of (5) is that given by the author in 1978 by downwards continuation. If W_B is the truncation of the series for W neglecting the harmonics of degree greater than B, we have

(6) $\quad W \approx W_B + V_B ,$

(6a) $\quad W = \sum_{n=0}^{B} (\frac{1}{r})^{n+1} w_n Y_n (\varphi,\lambda) + V_B .$

In the exterior of the Brillouin sphere, $r \geq R_{B,a}$, follows

(7) $\quad V_B \rightarrow 0 , \quad \text{if } B \rightarrow \infty ; \quad r \geq R_{B,a} .$

(8) $\quad \Delta V_B \approx 0 , \quad \text{in } \Omega .$

(8) yields from

(9) $\quad \Delta W = \Delta W_B = 0 , \quad \text{in } \Omega .$
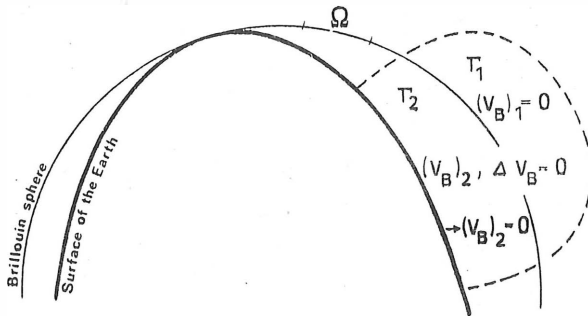
Figure 1.

The sentence about the harmonic continuation, valid for con-
tinuous potentials only, is: If V_B is harmonic in $T_1 + T_2$,
and if $(V_B)_1 = 0$ is right in T_1 , in this case, $(V_B)_1$ has
a unique harmonic continuation into T_2 . This continuation
is $(V_B)_2 = 0$.

Hence, if the residual potential V_B does go to zero for
$r \geq R_{B,a}$, V_B does go to zero simultaneously also in the
domain between the surface of the Earth and the Brillouin
sphere. Thus,

(9a) $V_B \longrightarrow 0$, if $B \longrightarrow \infty$, (in Ω).

(9a) proves the convergence of the discussed series for whole
the exterior space Ω .

The convergence of this series can be proved also by a conside-
ration of the completeness of a system of base functions. At
the beginning, the potential W was developed in terms of these
base functions, (5),

(10) $(\frac{1}{r})^{n+1} Y_n (\varphi, \lambda)$, $(n = 0,1,2,\ldots)$.

If

(11) $t = t (\varphi, \lambda)$

is the geocentric radius of the Earth's surface, we find the
following base functions $\alpha_n(\varphi, \lambda)$ valid along the Earth's
surface,

(12) $\alpha_n(\varphi, \lambda) = (\frac{1}{t(\varphi, \lambda)})^{n+1} Y_n(\varphi, \lambda)$, $(n = 0,1,2,\ldots)$.

These functions α_n are known to be linear independent,

(13) $\sum_{i=0}^{C} l_i \, \alpha_i(\varphi,\lambda) = 0$ only if $l_i = 0$,

(13a) for $i = 0,1,2,\ldots, C$.

The α_n system is complete in the space of the continuous functions, if the relations (14)

(14) $\iint_{\sigma} w(\varphi,\lambda) \; \alpha_n(\varphi,\lambda) \; d\sigma = 0$,

(14a) $(n = 0,1,2,\ldots)$,

lead necessarily to

(15) $w(\varphi,\lambda) = 0$.

$w(\varphi,\lambda)$ is an arbitrarily chosen continuous function. σ is the unit sphere. In our applications, $w(\varphi,\lambda)$ are the boundary values of the potential W. In order to prove the completeness, the potential K of a surface distribution ν along the Earth's surface S is introduced.

(16) $K = \iint_{S} \frac{\nu}{e} \, dS$.

Within the interior Brillouin sphere, $r \leq R_{B.i}$, being completely envelopped by the surface S, 1/e has the expression,

(17) $\frac{1}{e} = \frac{1}{t} \sum_{n=0}^{\infty} (\frac{r}{t})^n P_n(\cos\psi)$, $r \leq R_{B.i}$, $r \leq t$.

This series for 1/e is introduced into the potential K, then, the Legendre functions are substituted by $Y_n(\varphi,\lambda)$, $Y_n(\bar\varphi,\bar\lambda)$. Hence,

(18) $K(\bar P) = \sum_{n=0}^{\infty} \frac{1}{2n+1} (\bar r)^n Y_n(\bar\varphi,\bar\lambda) \iint_{S} \nu(\frac{1}{t})^{n+1} Y_n(\varphi,\lambda) \, dS$,

or

(19) $K = \sum_{n=0}^{\infty} \frac{1}{2n+1} (\bar r)^n Y_n (\bar\varphi,\bar\lambda) \iint_{S} \nu \alpha_n(\varphi,\lambda) \, dS$.
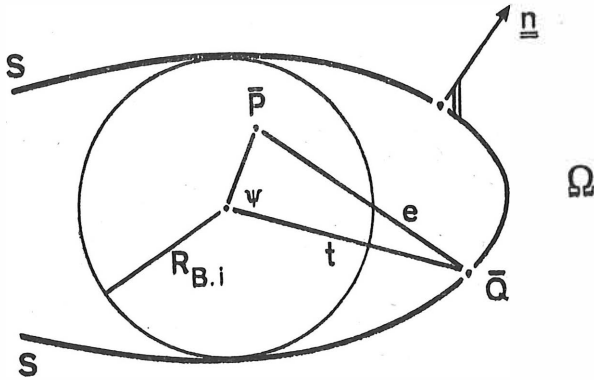
Figure 2.

With

(20) $\nu \, dS = w(\varphi, \lambda) \, d\sigma$

follows

(21) $K = \sum_{n=0}^{\infty} \frac{1}{2n+1} (\bar{r})^n Y_n(\bar{\varphi}, \bar{\lambda}) \iint\limits_{\sigma} w(\varphi, \lambda) \, \alpha_n(\varphi, \lambda) \, d\sigma$;

(22) $\bar{r} = r(\bar{P}) < R_{B.i}$.

The completeness works with the relation

(23) $\iint\limits_{\sigma} w(\varphi, \lambda) \, \alpha_n(\varphi, \lambda) \, d\sigma = 0$,

(23a) $(n = 0, 1, 2, \ldots)$.

Thus,

(24) $K = 0$,   for $\bar{r} < R_{B.i}$.

Because

(25) $\Delta K = 0$, $0 \leq r \leq \infty$,

the application of the theorem of the harmonic continuation on
the potential K gives

(26) $K = 0$, $0 \leq r \leq \infty$.

The jump relation for the normal derivative of K at the Earth's
surface yields

(27) $(\frac{\partial K}{\partial n})_{i,S} - (\frac{\partial K}{\partial n})_{a,S} = 4\pi \nu$,

and with (26)

(28) $\nu = 0$.

Hence,

(29) $w (\varphi,\lambda) = \nu \cdot \frac{dS}{d\sigma} = 0$.

Thus, the system of the base functions α_n is complete.

These α_n functions, linear independent, can be replaced by
orthonormal base functions β_n (Schmidt orthonormalization
process).

(30) $w(\varphi,\lambda) = \sum_{i=0}^{\infty} w_i \alpha_i(\varphi,\lambda) = \sum_{i=0}^{\infty} w_i^{*} \beta_i(\varphi,\lambda)$,

(30a) $\iint_{\sigma} \beta_i^2 \, d\sigma = 4\pi$.

Thus, the Parseval completeness relation,

(31) $\iint_{\sigma} w^2 \, d\sigma = \| w \|^2 = 4\pi \sum_{i=0}^{\infty} (w_i^{*})^2$.

After the completeness of the α_i system is proved, the comple-
teness of the β_i system is secured also. Consequently, (31) is
right. (31) implies the property of (30) to be convergent in
the mean,

(31a) $\iint_{\sigma} v_B^2 (t,\varphi,\lambda) \, d\sigma \longrightarrow 0$, if B $\longrightarrow \infty$, (on S).

Because, further on, w is a continuous function, the convergence

in the mean leads necessarily to the uniform convergence of
(30). The uniform convergence on S means

(32) V_B (t,φ,λ) $\longrightarrow$ 0, if B $\longrightarrow$ ∞ , (on S) .

Therefore,

(33) $W = \sum_{n=0}^{\infty} (\frac{1}{r})^{n+1} w_n Y_n (\varphi,\lambda) = W_B + V_B$

is uniform convergent on the Earth's surface S.

The maximum principle of the potential theory signifies that
the maximum of V_B lies on the Earth's surface.

(34) $|V_B (r,\varphi,\lambda)|$ $\leq$ $|V_B (t,\varphi,\lambda)|_{max.}$

(33) and (34) lead to

(35) $V_B (r,\varphi,\lambda)$ $\longrightarrow$ 0 , if B $\longrightarrow$ ∞ , (in Ω) .

Hence, the uniform convergence is valid for the whole exterior
space of the body of the Earth.

The maximum principle proves also the stability of (33): A
small alteration of the boundary values of W,

(36) $W (r=t,\varphi,\lambda) = (W)_S = w (\varphi,\lambda)$

by

(37) $\delta w = \delta w (\varphi,\lambda)$

has an impact δW on the spatial W values in the exterior space,
with

(38) $|\delta W (r,\varphi,\lambda)|$ $\leq$ $|\delta w (\varphi,\lambda)|_{max.}$.

As to the time variation of the potential W, if $W_{\bar{t}_1}$ is the W
potential at the time $\bar{t}_1$,

(39) $W_{\bar{t}_1}$, $\bar{t}_1$

and

(40) $W_{\bar{t}_2}$, $\bar{t}_2$

at the time $\bar{t}_2$, than the time variation is

(41) $W_{\bar{t}_1} - W_{\bar{t}_2} = \sum_{n=0}^{\infty} (\frac{1}{r})^{n+1} \big/ (w_n)_{\bar{t}_1} - (w_n)_{\bar{t}_2} \big/ Y_n (\varphi, \lambda)$.

Or

(42) $W(r, \varphi, \lambda; \bar{t}) = \sum_{n=0}^{\infty} (\frac{1}{r})^{n+1} w_n(\bar{t}) Y_n(\varphi, \lambda)$.

The range of validity of the convergence can be extended also
to the fourth dimeneion, the time $\bar{t}$.

A ehort description of the procedure for the computation of the
Stokes constante w_n , (5), in terme of the gravitating maeses
should be added. If the gravitating maesee M within the surface
S of the Earth are given, these masees lead to the potential
at the Earth's eurface by

(43) $W(S) = W(r = t, \varphi, \lambda) = w(\varphi, \lambda) = f \iiint_{V} \frac{1}{e} dM.$

V is the volume of the Earth, e is the straight distance
between the surface point and the mass element   dM in the
interior. The series (2) is not needed for the computation of
the integral of (43). The surface S has a star-shaped form,
S is a regular eurface shaped by the topography. The distribu-
tion of the maeses in the interior has no strict constraint,
but the masses have to yield a continuous function $w(\varphi, \lambda)$ for
the surface potential.

The calculations to get the Stokes constants w_n happen along
the following line. The functions $\alpha_n(\varphi, \lambda)$ are computed for
the given eurface S which is shaped by the topographical heights,
(12). The Schmidt orthonormalization procedure gives the ortho-
normal functtone $\beta_n(\varphi, \lambda)$ in terms of the $\alpha_i(\varphi, \lambda)$ functions, (30),

(44) $\quad \beta_0(\varphi, \lambda) = c_{0,0} \; \alpha_0(\varphi, \lambda)$,

(45) $\quad \beta_1(\varphi, \lambda) = c_{1,0} \; \alpha_0(\varphi, \lambda) + c_{1,1} \; \alpha_1(\varphi, \lambda)$,

(46) $\quad \beta_2(\varphi, \lambda) = c_{2,0} \; \alpha_0(\varphi, \lambda) + c_{2,1} \; \alpha_1(\varphi, \lambda) + c_{2,2} \; \alpha_2(\varphi, \lambda)$,

...   ...

From (43), the function $w(\varphi, \lambda)$ is known. From (44), (45), (46),
the system of the base functions $\beta_n(\varphi, \lambda)$, (n = 0,1,2,...), is
known. $w(\varphi, \lambda)$ and $\beta_n(\varphi, \lambda)$ allow the computation of the co-
efficients w_n^* , (n = 0,1,2,...), (30). w_n^* is reached by

(47) $\quad w_n^* = \frac{1}{4\pi} \iint\limits_{G} w(\varphi, \lambda) \; \beta_n(\varphi, \lambda) \; d\sigma$,

(48) $\quad$ n = 0, 1, 2, ...

Thus, the development (49) is known,

(49) $\quad w(\varphi, \lambda) = \sum\limits_{n=0} w_n^* \; \beta_n(\varphi, \lambda)$.

In (49), the functions $\beta_n(\varphi, \lambda)$ get to be replaced by the
$\alpha_n(\varphi, \lambda)$ functions. The functions (44), (45), (46) are intro-
duced into (49). (49) turns to

(50) $\quad w(\varphi, \lambda) = \sum\limits_{n=0} w_n \; \alpha_n(\varphi, \lambda)$,

with

(51) $\quad w_k = \sum\limits_{i=0} w_i^* \; c_{i,k}$,

(52) $\quad$ (i, k = 0, 1, 2,...) .

This are the required values for the coefficients w_n of the
uniform convergent series development (5).

Applying the series (2) on the integrand of (1), the Stokes
constants are obtained by the integrals of this type,

$$(53) \qquad \iiint_V (r')^n \, Y_n(\varphi,\lambda) \, dm \; .$$

This is the traditional procedure. It leads to discontinuities,
divergences. It leads to potentials of a shape not possible in
natural science.

According to the here developed procedure, (51), the representa-
tion of the potential (5) is in harmony with the prerequisites
of natural ecience. It is continuous, convergent, unique, and
stable.

References

ARNOLD, K.: The Spherical-Harmonics Expansion of the Gravitatio-
nal Potential of the Earth in the External Space and its
Convergence. Gerlands Beitr. Geophysik 87(1978) 81-90.

ARNOLD, K.: Picone's Theorem and the Convergence of the Expansion
in Spherical Harmonics of the Gravitational Potential of the
Earth in the External Space. Boll. Geof. Teor. ed Appl., Vol.
XXII, N. 86, Giugno 1980.

ARNOLD, K.: Nochmals zur Konvergenz der Kugelfunktionsentwicklung
für das Gravitationspotential der Erde. Vermessungstechnik 31
(1983) 274-276.

ARNOLD, K.: Beweis der Konvergenz der Kugelfunktionsentwicklung
für das Geopotential durch harmonische Fortsetzung. Gerlands
Beitr. Geophysik 96(1987) 509-516.

ARNOLD, K.: Geodetic boundary value problems I. Veröff. Zentral-
inst. f. Physik d. Erde, Nr. 84, Potsdam 1986.

ARNOLD, K.: Geodetic boundary value problems II. Veröff. Zentral-
inst. f. Physik d. Erde, Nr. 89, Potsdam 1988.

Marcin Barlik
Jerzy B.Rogowski

Warsaw University of Technology
Institute of Higher Geodesy
and Geodetical Astronomy

STUDY OF THE LOCAL GRAVITY VARIATIONS
ON THE MERIDIAN BASE-LINES AND TEST-FIELDS

Summary

In the paper the authors present an attempt undertaken
to answer the question if the local hydrogeological pheno-
mena and variations in ground humidity may cause variations
in differences of gravity at the gravimetric stations and
time variations of gravity. Measurements of Δg and studies
of water relations indicate that there occur variations
in acceleration differences that are bigger than the
observational mean errors and caused by variations in the
water relations on the meridian base-line points.
Formulae have been worked out for the proper reductions
of gravity to the ground dry matter for the proper
preservation of acceleration.

DIE UNTERSUCHUNG DER ÄNDERUNGEN DER GRAVITATIONSKRAFT AUF MERIDIONALEN GRAVIMETRISCHEN BASIS UND AUF TESTFELDEN

Zusammenfassung

Die Verfasser probieren im Referat eine Antwort auf die Frage geben, ob die Ursachen der Änderungen der Unterschiede der Erdbeschleunigung auf gravimetrischen Basis und der Änderungen der Gravitation in der Zeit die hydrogeologische Lokalerscheinungen und die Änderungen der Bodenfeuchte, können sein. Die Messungen Δg und Untersuchungen der Wasserverhältnisse seit mehrere Jahre zeigen auf grössere, als die Mittelfehler der Beobachtungen, die Änderungen der Unterschiede der Erdbeschleunigungen, die durch Variationen der Wasserverhältnisse auf den meridionalen Punkten der Linie hervorgerufen sind. Es wurden Gleichungen zur Berechnung entsprechenden Reduktionen der Gravitation auf die trockens Masse des Bodens ermittelt, um die richtige Wartung der Erdbeschleunigung zu bekommen.

The development of the absolute methods of gravity measurements
which has been observed for the last few years as well as increase
in the accuracy of gravimetric measurements which took place in the
last two decades make in necessary for us to answer the question
if the results obtained from the measurements of gravity accelerat-
ions and their differences are constant in time.

A negative answer to the above question forces us to formulate
next ones: how far can the gravity acceleration or its differences
vary and what causes the occurance of this phenomenon. The authors
try to answer these questions basing on the results of the investi-
gations that have been carried out for many years on two meridian
gravimetric base-lines of two observatories: Astronomical-Geodetic
Observatory of Warsaw University of Technology at Józefosław
and Space Research Center of the Polish Academy of Sciences
- Astronomical Latitude Station of CBK PAN Borowiec.

Gravimetric observations carried out on these lines are aimed
at studying stability of the plumb-line direction of these observa-
tories and their results have been recently presented at VII
Lohrman Colloqium (M.Barlik, J.Rogowski, 1988).
Both the gravimetric base-lines consist of six points that are
distributed symmetrically in relation to the observatory.

The approximate distances between the points and differences in gravity have been presented in Table 1.

Table 1.

No of the P.	Distance [kms]	Δ g [mGls]
N 13		
	7	
N 6		
	6	
N 3		
	3	
Observ.		19.0 8.5 4.9
	3	
S 3		
	6	
S 6		
	7	
S 13		

Measurements of differences in gravity acceleration have been carried out since 1976, four times a year, on the average.Astatized quartz gravity meters - Worden, Scintrex /once LaCoste-Romberg/ have been used in the measurements. Before each measuring cycle the gravimeters are checked, adjusted and tested at our laboratory.The value of the actual coefficient of the instrument is determined.

The gravimetr's constatnt has been determined by means of the tilt method (M.Barlik,K.Czarnecki,1971) with an accuracy to no less than $2 \cdot 10^{-4}$.

Observations of differences in gravity acceleration were freed from the influence of the tidal forces: the drift of the instruments is determined basing on the measurements repeated on all base-line stations.Indications of the gravimeters have been also corrected due to the difference in height the reference marks.

An example of variantions in the gravity differences Δ g between symmetrically distributed points of the base-line in relation to Józefosław N 13 - S 13, N 6 - S 6, N 3 - S 3, observed in the period from 1983 to 1988, has been presented in Fig.1.

As can be seen, variations in the gravity acceleration differences reach up to 250 µGl = 0.25 µm·s^{-2} when the errors of observations, on average, reach 20 µmGl = 0.02 µm·s^{-2}, i.e. smaller by one order. Variations of the same order have been obtained at the base of the Observatory at Borowiec and in the investigations which have

been carried out for the last ten years in the geodynamical test -
field of Czorsztyn - Pieniny Mts (Z.Ząbek and others,1980) .

In 1981 studies were undertaken on assesing the influence of hy-
drological factors on the observed gravity variations. The distri-
bution of aquiferous layers in the surrondings of each of the base
points has been determined using the method of a geoelectric probing.
Piezometers have been installed on these stands where variations of
the ground water level may significantly effect the measurements of
the values of gravity accelerations.Since that moment, apart from
the gravimetric measurements, observations of the ground water level
depth have been carried out on these points. Basing on the determi-
ned ground porosity, formulae have been worked out which are to help
us introduce corrections to the measured values of gravity accele-
ration (M.Barlik,J.B.Rogowski,1983) .Diagrams of such corrections
for the part of the base S 3 - S 6 of the Observatory at Józefos-
ław for the period 1983-1988 have been presented in Fig.2.

The correction made due to the variations in the ground water
level does not exceed 30 μmGl = 0.03 μm·s^{-2}, and thus is if the order
of the mean error of the gravimetric measurements.

Another factor which may have a local, systematical also, influ-
ence on the determined values of the differences in gravity between
the points of the gravimetric stations are the variations in the
ground humidity.

An attempt has been undertaken to determine these quantities.Ba-
sing on the field investigations and theoretical analyses, formulae
have been developed to let us calculate these corrections in the fun-
ction of the ground humidity variations in the selected places sur-
rounding the gravimetric points.

In order to determine humidity, samples of an untouched structu-
re are taken at the depth of 1 m. Then humidity and water content
in a given sample are determined at the laboratory.

Variations in the ground humidity and water content in the ground
for the points of the base that are placed symmetrically in relation
to Józefosław have been presented in Fig.3.

Since 1983 a correction has been introduced to the gravimetric
measurements which is aimed at eliminating the influence of varia-
tions in the water content in the outer ground layer through the in-
troduction of e correction reducing the value of gravity accelera-
tion to such a state in which we will eliminate water from the outer
ground layer (reduction to the ground dry matter) .

The correction introduced due to the above is much bigger than the one caused by variations in the ground water level. Its values for the sections N 13 - S 13, N 6 - S 6 and N 3 - S 3 for the base at the observatory of Józefosław have been presented in Fig.4. The greatest values of the variations of the correction resulting from the ground humidity variations have been obtained for the shortest section of the base N 3 - S 3, for which it exceeds 100 µmGl.

A statistical analysis of the gravity differences before and after introducing the two above mentioned corrections let us state that in 62% there occured a decrease in the time variations of gravity, in 28% it did not remarkably influence on the results and in 10% it caused increase in the amplitude of variations.

For the section N 3 - S 3, in the period from July 1983 to September 1985, there occuried' a complete compensation of the gravity variations and in the other period, variations in the gravity acceleration differences were similar in character as the influence of variations in water relations in the ground surrounding the gravimetric stations.

Summing up the results of the works carried out so far, we should state that hydrogeological effects and ground humidity variations should be taken into account while, for instance, using the gravimetric stations in the calibration of gravimeters. The results obtained from gravimetric observations, when used in geodynamical analyses, should be freed from the influence of these local geophysical factors before their regional and global interpretation (crustal movements, the Earth's pole movements, plumb-line variations).

R e f e r e n c e s

1. Barlik,M.,Czarnecki,K.,1971,Cechowanie grawimetrów typu GAK 7T i Sharpe CG-2 metodą nachylania w laboratorium grawimetrycznym PW, Geod.iKart.,PAN,t.XX,z.3,Warszawa
2. Barlik,M.,Rogowski,J.,B.,1983,On Some Geophysical Effects in Latitude Variations at Józefosław,VI Int.Koll.Geod.Astromet.,Wiss.Z. TU Dresden,H.6/1984
3. Ząbek,Z.,and others,1980,Investigations in the Czorsztyn - Geodynamical Test Field,Prace Nauk.PW,z.23,Geodezja,Warszawa.
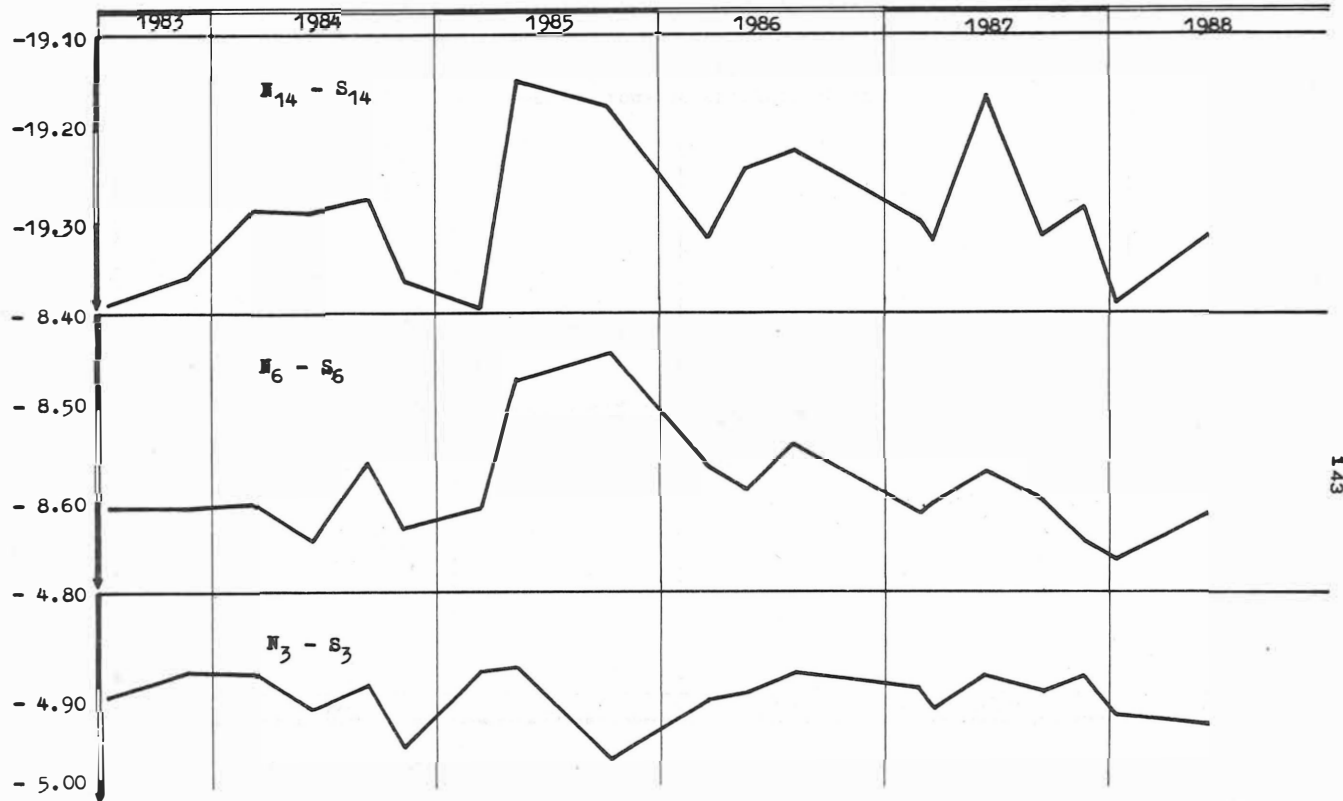
Fig.1. Time variations of the gravity
differences on the meridian base-line
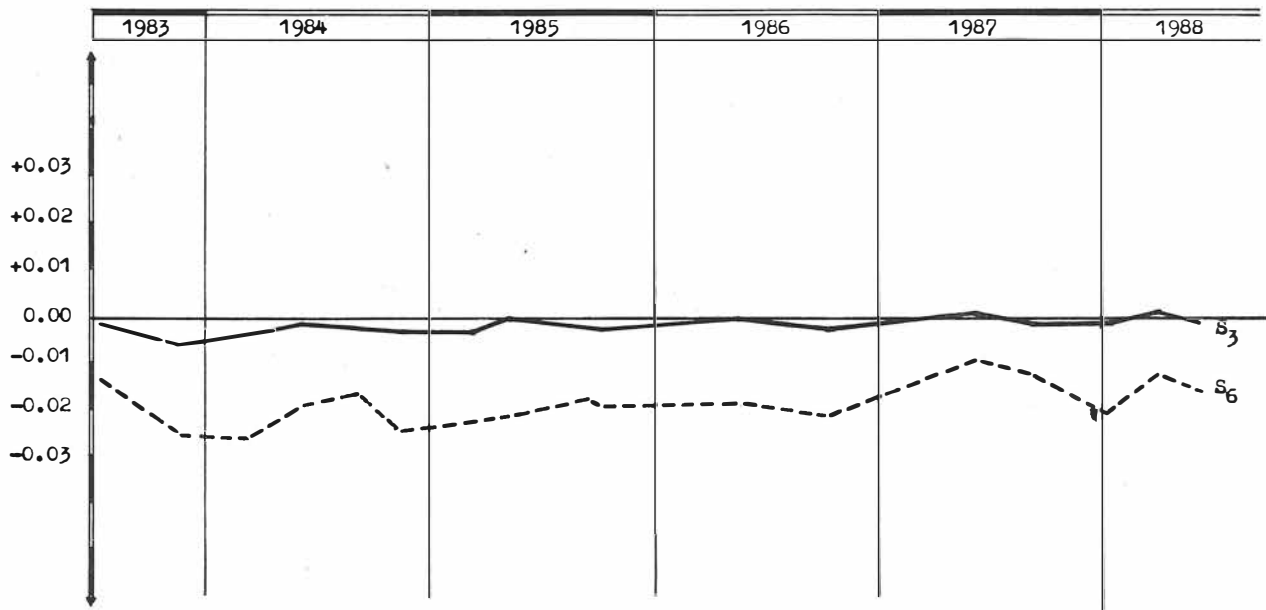
Fig 2. Corrections to the gravity from
ground water level variations
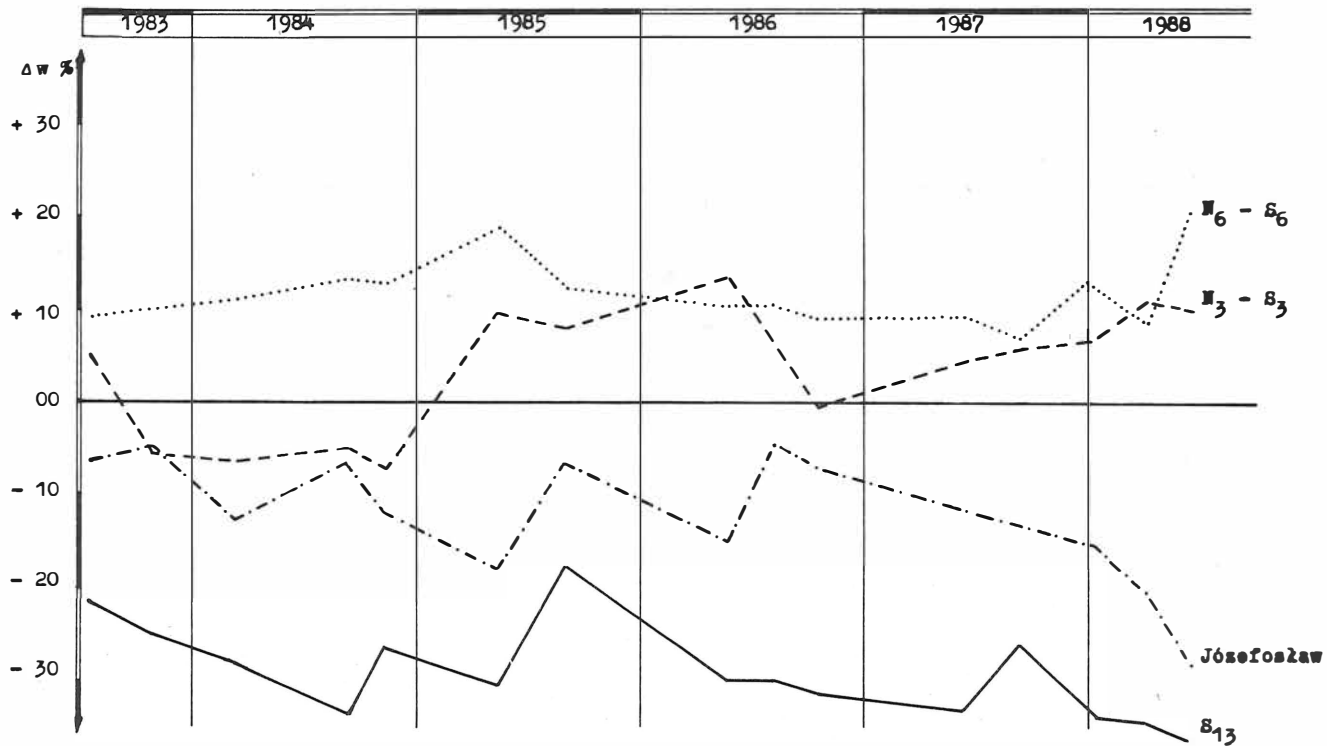
Fig.3. Humidity of a soil in the vicinity
of the gravity stations
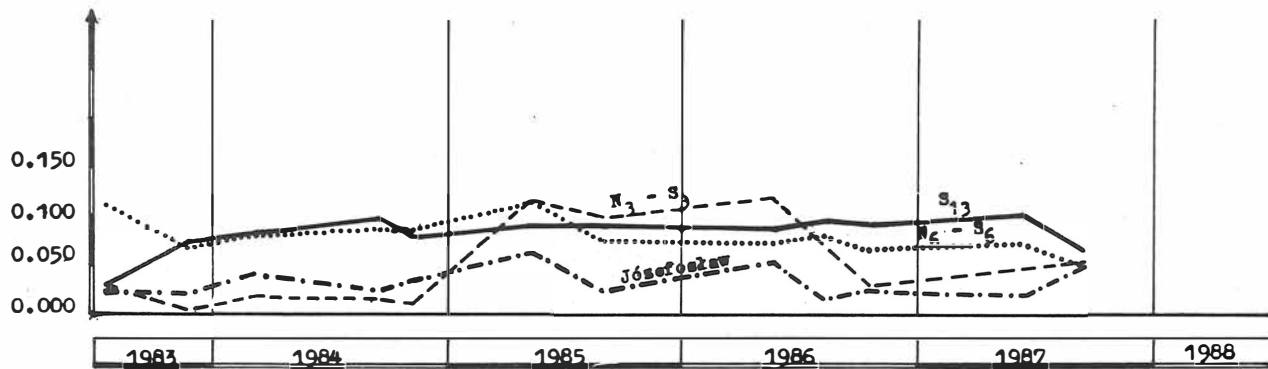
Fig.4. Corrections to the gravity from
the humidity variations

COMPLEX TREATMENT OF 2D GEODATA

Bartha,G.[x], Bányai,L.[x], Czompó,J.[x], Papp,G.[x]

SUMMARY

For the security of a big industrial object, controlling geodetic network should be used to monitor the motion of the surrounding area. The controlling network should be allocated on the tectonical possible active parts of the territory.

In the paper a concept of a method for the allocation and its demonstration are given. The method is based on the assumption of the common signal caused by tectonical disturbances. The common signal is supposed to be present in the geofunctions of the territory like topography, gravity anomaly, magnetic anomaly etc., and the harmonic analysis is used to find this common signal.

The process is demonstrated by a practical example, and it is tested by seismic investigations.

[x]Geodetic and Geophysical Research Institute of the Hungarian Academy of Sciences, H-9401 Sopron, POB 5, Hungary

INTRODUCTION

The security of the big industrial objects requires the
geodetic and the geophysical monitoring of the surrounding
area - what can be called as microscaled (10-100 km^2) moni-
toring. In the microscaled monitoring the problems are:
1) what signals are to be monitored; 2) where to do it;
3) how to do it.

The answer for the first term of the what-where-how triad
is rather obvious from the aspect of the geodesy: to monitor
the horizontal and vertical movement of a controlling network
by repeated measurement.

The answer for the second question seems to be also
obvious. The controlling network should be allocated to cover
the active, possible dangerous part of the surrounding area.
How to allocate the active zone(s)? Is there any "standard
process" of the allocation?

These questions are investigated in the present paper and
a "standarzible process" is given which is based on the complex
treatment of 2D geodata like the topography, gravity, magnetics.
The process is demonstrated by a real investigation of the sur-
rounding area around an atomic power station.

CONCEPT OF COMPLEX TREATMENT

The physical principle of the complex treatment is: a
common signal $f(x,y)$ is supposed in the 2D geofunctions of the
area (like the topography $z(x,y)$, the gravity anomaly $g(x,y)$,
the magnetic anomaly $m(x,y)$ etc.) which is caused by an active
disturbance (fault). The reality of this supposition is sup-
ported by some earlier work [i.e Syberg, 1972; Kanasewich-
-Agarwal, 1970; LeRoy M. Dorman-Brian T. Lewis, 1970] .

The mathematical principle of the complex treatment is the 2D harmonic analysis which provides an unified data management in the processing of the different dataset.

According to the supposition of the physical principle, the mentioned geofunctions are written as:

$$z = f + n_1$$
$$g = f + n_2 \qquad (1)$$
$$m = f + n_3$$

where the functions n_1, n_2, n_3 are the "noise" functions. It is also supposed that the noise functions are uncorrelated with the signal function f, further with each other:

$$c(f,n_i) = c(n_i,n_j) = 0 \qquad i \neq j \qquad (2)$$

Then the cross correlation functions of the geofunctions are equal to the autocovariance function of f:

$$c(f,f) = c(m,z) = c(z,g) = c(f,f) \qquad (3)$$

The autocovariance function $c(f,f)$ is the Fourier pair (Fourier transform) of the power density function of f [Bäth, 1974] that is:

$$c(f,f) \xrightarrow{\text{Fourier pair}} E(\omega_x \omega_y) = F(\omega_x \omega_y)^2 \qquad (4)$$

where F is the Fourier transform of f. For 2D functions the next relations hold in digital form Oppenheim-Schafer, 1975 :

$$F(n,m) = \frac{1}{NM} \sum_{1=1}^{N} \sum_{k=1}^{M} f(x_1 y_k) \, e^{-i(2\pi n/N)x_1} \, e^{-i(2\pi m/M)y_1}$$

$$f(x_1 y_k) = a_0 + \sum_{n=1}^{N/2} \sum_{m=1}^{M/2} a_{nm} \cos\ (2\pi n/N)x_1 + (2\pi m/M)y_k\ +$$

$$+ \sum_{n=1}^{N/2} \sum_{m=1}^{M/2} b_{nm} \sin\ (2\pi n/N)x_1 + (2\pi m/M)y_k$$

$$a_0 = \frac{1}{NM} \sum_{l=1}^{N} \sum_{k=1}^{M} f(x_1 y_k)$$

$$a_{nm} = \frac{4}{NM} \sum_{l=1}^{N} \sum_{k=1}^{M} f(x_1 y_k) \cos\ (2\pi n/N)x_1 + (2\pi m/M)y_k$$

$$b_{nm} = \frac{4}{NM} \sum_{l=1}^{N} \sum_{k=1}^{M} f(x_1 y_k) \sin\ (2\pi n/N)x_1 + (2\pi m/M)y_k \tag{5}$$

Computing from the digitalized geofunctions the auto-covariance $c(f,f)$ one can determine the <u>dominant frequencies</u> ω_x^i, ω_y^j of function f which are the local extreme of F (peaks of the spectrum).

If the spectrum F has I and J peaks, then the function f is given as:

$$z(x_1 y_k) = a_0 + \sum_{i=1}^{I} \sum_{j=1}^{J} a_{ij} \cos\left(\omega_x^i x_1 + \omega_y^j y_k\right) +$$

$$+ b_{ij} \sin\left(\omega_x^i x_1 + \omega_y^j y_k\right) \tag{6}$$

where a_0, a_{ij}, b_{ij} are given by Eq. 5 but $f(x_1,y_k)$ $2\pi n/N$ and $2\pi m/M$ are replaced by $z(x_1 y_k)$, ω_x^i and ω_y^j, respectively. The function z can be considered as a "filtered" version of the topography function z which should show (if it exists!) the common disturbing signal of the geofunctions.

DEMONSTRATION OF THE METHOD

The geofunctions z(x,y), g(x,y), m(x,y) around the in-
dustrial object (signed x on Fig. 1) were given in digital form
an equispaced grid (100 x 100 m). The total area was
6000 x 6000 m^2. The functions are given by Fig. 1.

The process given by Eqs 4-6, has been accomplished and
the "filtered' surface is given on Fig. 2. The disturbance
(signed by → ←) can be easily identified.

In the area an seismic coss section was prepared to
cross the area located by the previous method, therefore a
chance has been given to test the method.

The cross sections of the geofunctions (the filtered
surface z(x,y), the topography z(x,y), the gravity anomaly
g(x,y), the vertical magnetic anomaly m(x,y)) were prepared
in the line of the seismic cross section (given by Fig. 3)
and they are shown together on Fig. 4. It can be seen that
the "appointed disturbance" is located above the broken part
(fault) of the basin (depth of the basin ∼ 800 m).

DISCUSSION

In the previous paragraphs a cenception and its demonstra-
tion of a method for the allocation of the tectonical active
area was given. The method is based on the assumption of the
common signal of the tectonical disturbances in the geofunc-
tions like topography, gravity, magnetics. The digitalized
geofunctions are processed by 2D harmonical analysis - provid-
ing a unified process for data management. In the demonstration
the identification of the active area was strenghtened by the
seismic cross section.

Since the method is rather simple and not so expensive
(usually the mentioned geodata can be collected without extra
field work) that can be proposed as a preinvestigation to
allocate the monitoring network of an industrial object.

REFERENCES

Bäth,M.: Spectral Analysis in Geophysics. Elsevier Co.,
  New York, 1975

Kanasewich,E.R. - Agarwal,R.G.: Analysis of Combined Gravity
  and Magnetic Fields. JGR Vol. 75, p. 5702, 1970

LeRoy M. Dorman - Brian T.R. Lewis: Experimental Isostasy.
  JGR Vol. 75, p. 3357, 1970

Oppenheim,A. - Schafer,R.: Digital Signal Processing. Prentice
  Hall, New Yersey, 1975

Syberg,F.: A Fourier Method for the Regional Residual Problem
  of Potential Fields. Geoph. Prospecting, Vol. XX, p. 47, 1972

magnetic anomaly

gravity anomaly

topography

Fig. 1.

filtered surface

topography

Fig. 2.

Fig. 3.

seismic line

magnetic dZ anomaly

gravity anomaly

surface

filtered surface

seismic section

Fig. 4.

156
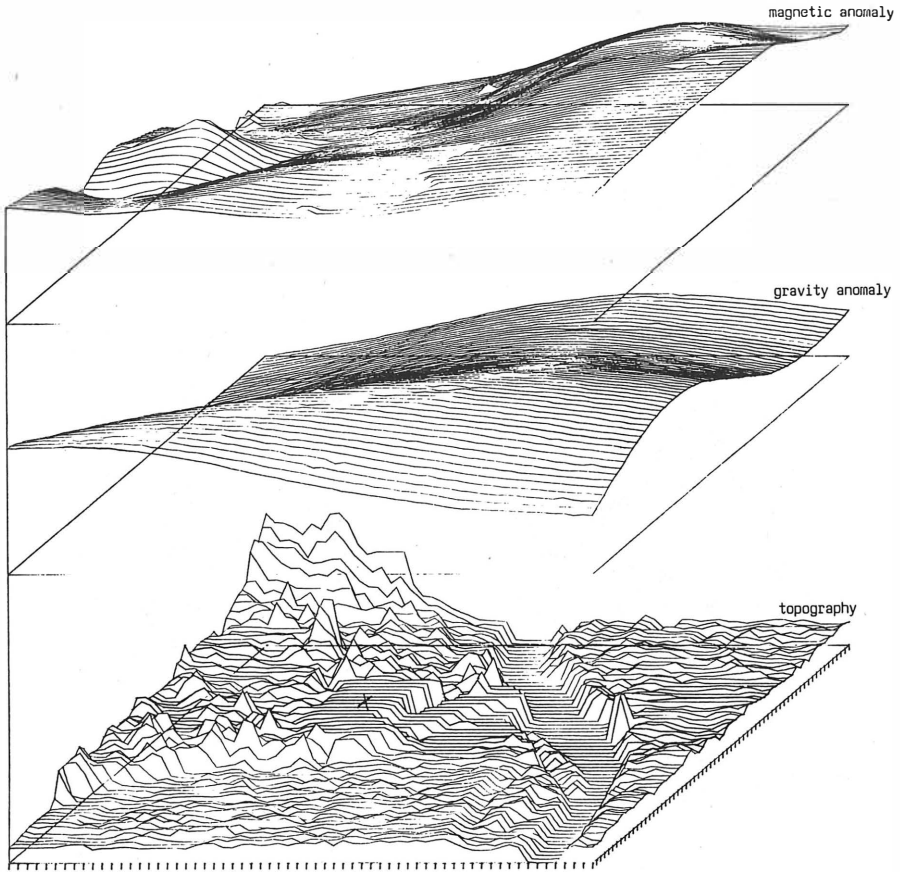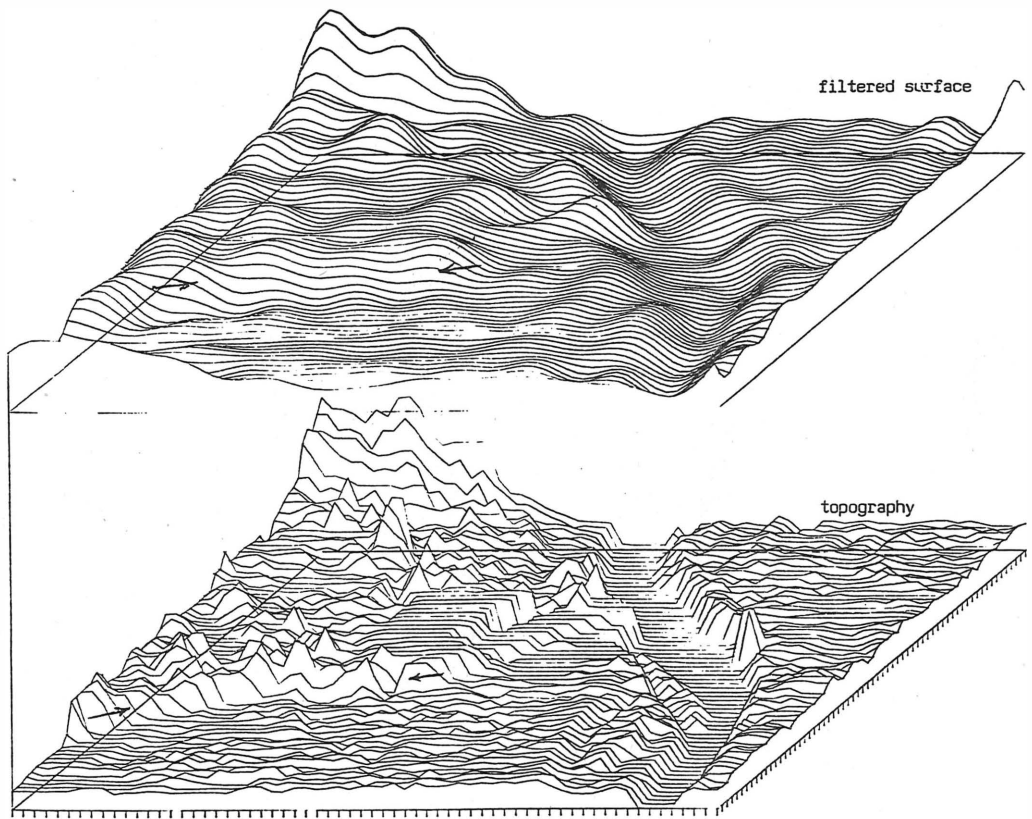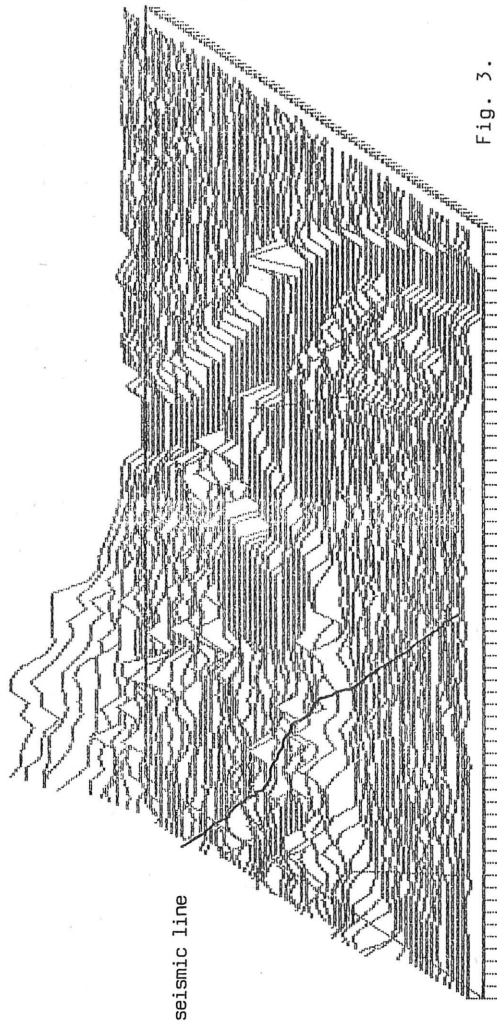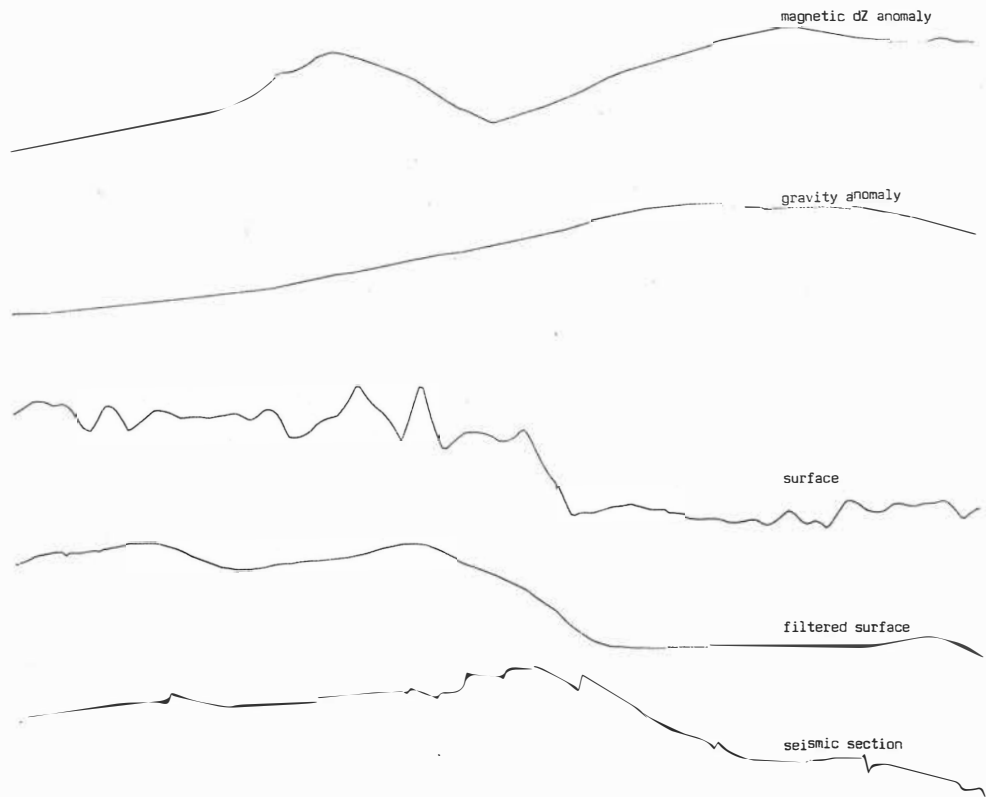
LOCAL GRAVITY FIELD APPROXIMATION
BY POINT MASSES WITH OPTIMIZED POSITIONS

F. Barthelmes

Academy of Sciences of the GDR
Central Institute for Physics of the Earth
Potsdam, 1561, GDR

Summary: The approximation of gravity anomalies in local or
regional areas by point masses with optimized positions is
performed. First results of practical computations using gravity
anomalies from the White Sands test area, New Mexico, USA, are
presented.

1. Introduction

The problem of gravity field approximation (globally as well as
locally) became more and more important during the recent years.
Above all, this was caused by the large increase of available
observations since the advent of various new, very precise
measurement techniques, and naturally by the demand to use these
measurements for geodetical, navigational and geophysical
purposes without loss of information.
The activities of IAG made allowance for this situation at
present and in the past and the investigations, first results of
which are presented in the following, have been induced by the
SSG 3.90 "Evaluation of Local Gravity Field Determination
Methods" (1983 - 1987; President: C.C. Tscherning) which partly
continued the work of SSG 4.70 "Gravity Field Approximation
Techniques" (1979 - 1983; President: K.P. Schwarz). The work of
these two SSG mainly based upon data from the White Sands test
area, New Mexico, USA (see: SCHWARZ 1983; KEARSLEY et.al. 1985),
and the work of SSG 3.90 was directed on the evaluation of
available gravity field determination methods, their efficiency,

stability, range of applicability and their inherent limitations
(see.: TSCHERNING 1987). In this connection the investigation of
point mass techniques was planned too, but could not be realized
up to now.

2. The approximation method

Starting point for elaborating the method was the algorithm which
has been described in detail, including mathematical foundation
and numerical tests, in (BARTHELMES 1986). Nevertheless it is
based on data in form of gravity disturbance vectors equally
distributed over the whole surface of the earth. The basic idea
of this method is to construct a point mass model step by step
approximating the observations not only by optimizing the
parameters (masses), but by selecting the base functions too
(adjusting the positions of the masses, or in other words, the
positions of the knots of the kernel functions), which results in
a non-linear optimization problem.
On principle the algorithm can be formulated (verbally) as
follows:

Assumption: N-1 point masses have already been determined

N-th step:

1. Subtraction of the field produced by the N-1 point masses from
   the measurements $\longrightarrow$ residuals

2. Selection of the position P_{max} of the maximum absolute value
   among the residuals

3. a) Determination of the approximate value for the N-th point
      mass position by putting it below the point P_{max} at a
      starting depth D_o
   b) Iterative improvement of the point mass position by
      non-linear optimization

4. Selection of those point masses among the N-1 previous masses
   up to a fixed number N_ϵ which have the smallest distance to
   the new N-th point mass

5. Common iterative improvement of masses and positions of the
   new N-th point mass and the selected neighbouring masses by
   non-linear optimization

In dependence on the datatype the basic equations of the
optimization problem have to be specified. For gravity anomalies
the corresponding relations can be written as follows (see
fig. 1):

The gravity anomaly according to Molodensky is defined as

(1) $\Delta g(P) = g(P) - \gamma(Q)$,

where g denotes gravity and γ normal gravity.
Using the anomalous potential

(2) $T = W - U$,

the gravity anomaly can be expressed by:

(3) $\Delta g(P) = |\text{grad } T(P) + \vec{\gamma}(P)| - \gamma(Q)$

Because of $|\text{grad } T(P)| \ll \gamma(P)$,

(4) $\Delta g(P) = \left(\frac{\vec{\gamma}}{\gamma} \cdot \text{grad } T(P) \right) + \gamma(P) - \gamma(Q)$

holds with sufficient accuracy.

With

(5) $\gamma(P) - \gamma(Q) = \frac{\partial \gamma}{\partial h} \bigg|_Q \cdot \zeta$

and

(6) $\zeta = \frac{T(P)}{\gamma(Q)}$

we obtain

(7) $\Delta g(P) = \left(\frac{\vec{\gamma}}{\gamma} \cdot \text{grad } T(P) \right) + \frac{1}{\gamma(Q)} \cdot \frac{\partial \gamma}{\partial h} \bigg|_Q \cdot T(P)$

If the anomalous potential and its gradient are represented by N point masses with masses $\{m_i\}$ (containing the gravitational constant) and positions $\{q_i\}$:

$$(8) \quad T(P) = \sum_{i=1}^{N} m_i \frac{1}{I(P,q_i)}$$

and

$$(9) \quad \text{grad } T(P) = \sum_{i=1}^{N} m_i \frac{\vec{I}(P,q_i)}{l^3(P,q_i)}$$

then (7) gives the gravity anomaly in depence on point masses. After this the derivatives $\partial(\Delta g)/\partial q_i$, needed for the non-linear iterative optimization of the point mass positions q_i, are also derivable without any difficulties. For solving this optimization problem the Levenberg-Marquardt method – Marquardt's strategy (SCALES 1985, pp.115) has proved successful.
The optimization of masses and positions was divided into alternate improvements of radii and masses on the one hand and longitudes and latitudes on the other hand – this way separated regularization as well as limitations for the positions (e.g upper and lower limits for the radii) became possible.

3. The data

For testing the described point mass method refined Bouguer anomalies from the White Sands test area were used, where the topographic irregularities with respect to a smooth mean height surface are removed (Residual Terrain Model – reduction). This RTM – reduced data were made available by C.C. Tscherning in the framework of SSG 3.90. For detailed data description see: (SCHWARZ 1983); the RTM – reduction method was described in (FORSBERG and TSCHERNING 1981). To compute point mass models the RTM – reduced gravity anomalies covering the area bounded by $252.85^{\circ} < \lambda < 254.15^{\circ}$, $32.85^{\circ} < \varphi < 34.15^{\circ}$ were selected from the data set, which originally contains 3466 anomalies, resulting in 370 points. A second data set containing

102   RTM - reduced   (control) - anomalies,   bounded   by
$253^O < \lambda < 254^O$, $33^O < \varphi < 34^O$, and not included in the previous
set,   was   defined   to standardize the results of evaluating   the
prediction accuracies. Fig. 2 illustrates the distribution of the
data. The anomalies have a standard error of 2 mgal.

4. Results and Discussion

First   tests had shown that the full optimization of   point   mass
positions   in   all   directions   actually   results   in   a   good
approximation   accuracy with only a small number of masses   - but
with   an   unsatisfactory   prediction   accuracy.   This   does   not
surprise   if   one   considers that   the   algorithm   primarily   was
developed   having in mind the model approach to physical geodesy,
which implies continuous boundary values or, at the very least, a
discretization   as   dense as necessary.   The reason for   the   bad
prediction   accuracy   is   that   during   point   mass   position
improvement   we   did not prevent the possibility that   some   few
masses "slide" just under data holes, where on the other hand
prediction points exist. To avoid this, the point mass position
improvements   (steps   3.b   and 5.   of the   algorithm)   have   been
carried   out   in radial direction only,   but with   the   described
method of starting point determination. For the number of masses
which has to be improved commonly at each step a value of $N_\varepsilon = 6$
has   been proved sufficient,   and as initial value for the   depth
$D_O = 5$ km has been choosen.
Fig. 3   shows   the results. The numbers of masses for which   the
limits   of   approximation accuracy and   prediction   accuracy   are
reached   (N $\approx$ 70 $\rightarrow$ 80)   correspond   very   well.   The   result   of
1.8 mgal   for   the   limit of approximation accuracy   confirms   the
given data noise of 2 mgal. The prediction accuracy of 6.48 mgal
corresponds   exactly   to the best value reached with   collocation
(6.47 mgal) in the comparison of different techniques based upon
the standardized 102 control anomalies (but using indeed a larger
surrounding   area   of   3244   data   points);   see: (FORSBERG   and
TSCHERNING in: SCHWARZ 1983).
It   is remarkable and usefull for a better understanding that the
point   mass   method   is nothing else   than   collocation   (with   a
defined type of covariance function), if the number of masses and
the   number   of measurements are equal,   and if   the   masses   are

located below the observation points by defining the depth by a
Kelvin transformation at the Bjerhammar-sphere (see: FORSBERG
1984; HAUCK and LELGEMANN 1985; BARTHELMES 1986, pp.34).
Considering this connection it is understandable that the
described approximation procedure (optimizing the radii only in a
small range) will converge to least squares collocation with an
increasing number of masses. But contrary to collocation, where
additional information is nesseccary to determine the covariance
function, in this algorithm the base functions (the depths of the
masses) were determined automatically using only the information
contained in the data. Fig. 4 shows a classified distribution of
the point masses' depths.

5. Conclusion

As the test computations have shown, the investigated point mass
method is advantageously usable for local gravity field
approximation. The computation of such point mass models can be
rather expensive because of the iteratively setting up and
solving of systems of linear equations - but this expense can be
kept in reasonable limits by not improving all, but only the N_ε
selected masses at each step, and by the possibility (which was
not used here) of not using all data points, but only the
observations up to a fixed distance from the point masses which
should be improved at the actual step (see: BARTHELMES 1986).
Once the point mass model is determined, prediction values of
gravity anomalies (and, although not tested yet, on principle of
all quantities of the gravitational field) are computable with a
very high efficiency - in the present case the sums (8) and (9)
must be computed for N = 70 only. The valuation of the prediction
accuracy for deflections of the vertical and the computation of
height anomalies based on point masses are topics of further
investigations.
In addition to the economical aspect a uniform representation of
the gravitational field could be of importance - and for both,
local and global representation, probably no other method is
better suited than point masses (comp. the global application of
the point mass method by DIETRICH and GENDT 1988).

References

Barthelmes, F: Untersuchungen zur Approximation des äußeren
     Schwerefeldes der Erde durch Punktmassen mit optimierten
     Positionen.
     Veröff. Zentralinst. Physik der Erde Nr. 92, Potsdam 1986

Dietrich, R.; Gendt, G.: A gravity field model from Lageos based
     on point masses (POEM – L1).
     Paper presented at the 6th International Symposium "Geodesy
     and Physics of the Earth", GDR, Potsdam, August 22 – 27, 1988

Forsberg, R.:   Local   covariance   functions   and   density
     distributions.
     Dept. geod. Sci., Ohio State Univ., Columbus (1984), Rep. 356

Forsberg, R.; Tscherning, C.C.: The use of height data in gravity
     field approximation by collocation.
     J. geoph. Res., Washington 86 (1981) B9, pp. 7843 – 7854

Hauck, H., Lelgemann, D.: Regional gravity field approximation
     with buried masses using least – norm collocation.
     Manuscripta geodaetica, Sindelfingen 10 (1985), pp. 50 – 58

Kearsley, A.H.W.;   Sideris, M.G.;   Krynski, J.;   Forsberg, R.;
     Schwarz, K.P.:   White Sands revisited – A comparision of
     techniques to predict deflections of the vertical.
     Division of Surveying Engineering, The University of Calgary,
     Calgary (1985), Publ. 30007

Scales, L.E.: Introduction to non – linear optimization.
     MAC MILLAN PUBLISHERS LTD, London and Basingstoke (1985)

Schwarz, K.P. (ed.): Techniques to predict gravity anomalies and
     deflections of the vertical in mountainous areas (a joint
     report of members of the IAG SSG 4.70).
     Division of Surveying Engineering, The University of Calgary,
     Calgary (1983), Publ. 30004

Tscherning, C.C.: Evaluation of local gravity field determination
     methods.
     Report of IAG SSG 3.90 for the period 1983 – 1987, presented
     at the XIX General Assembly of the IUGG, Vancouver (1987)
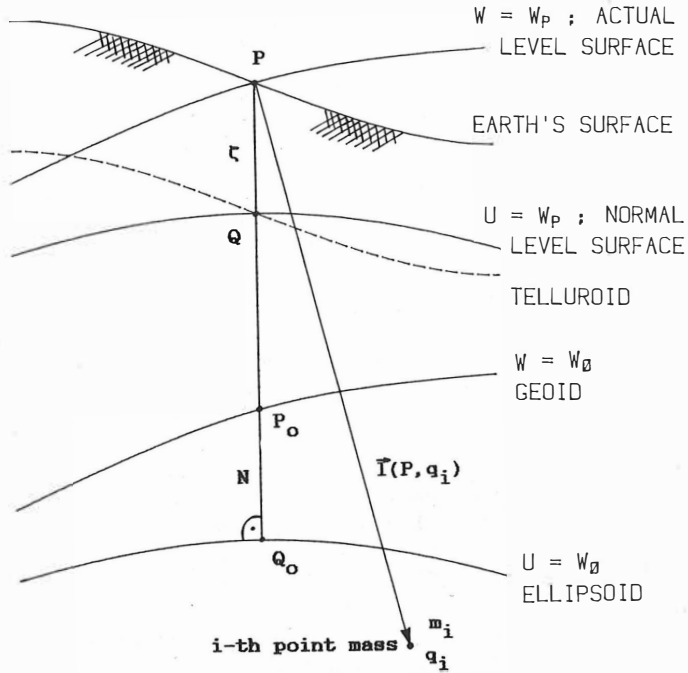
Figure 1: The basic geometry
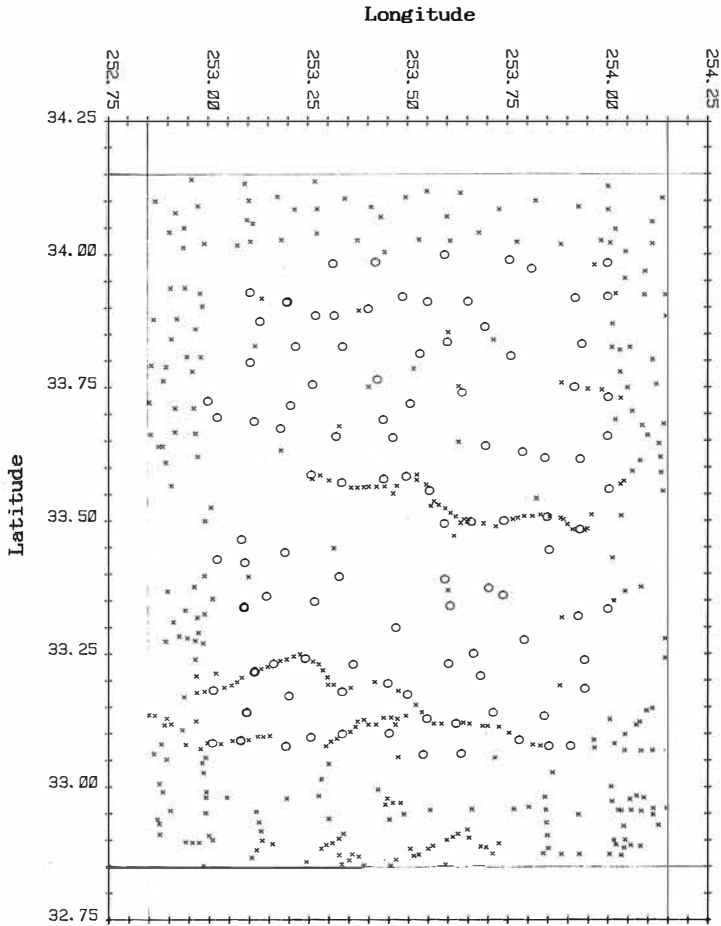
Figure 2: Distribution of used gravity anomalies: x
and prediction points: o

Figure 3: Approximation and prediction accuracy for various numbers N of point masses

$$\sqrt{\dfrac{\displaystyle\sum_{i=1}^{102} (predicted_i - control_i)^2}{102}}$$

$$\sqrt{\dfrac{\displaystyle\sum_{i=1}^{370} (computed_i - observed_i)^2}{370 - 2N}}$$

collocation accuracy
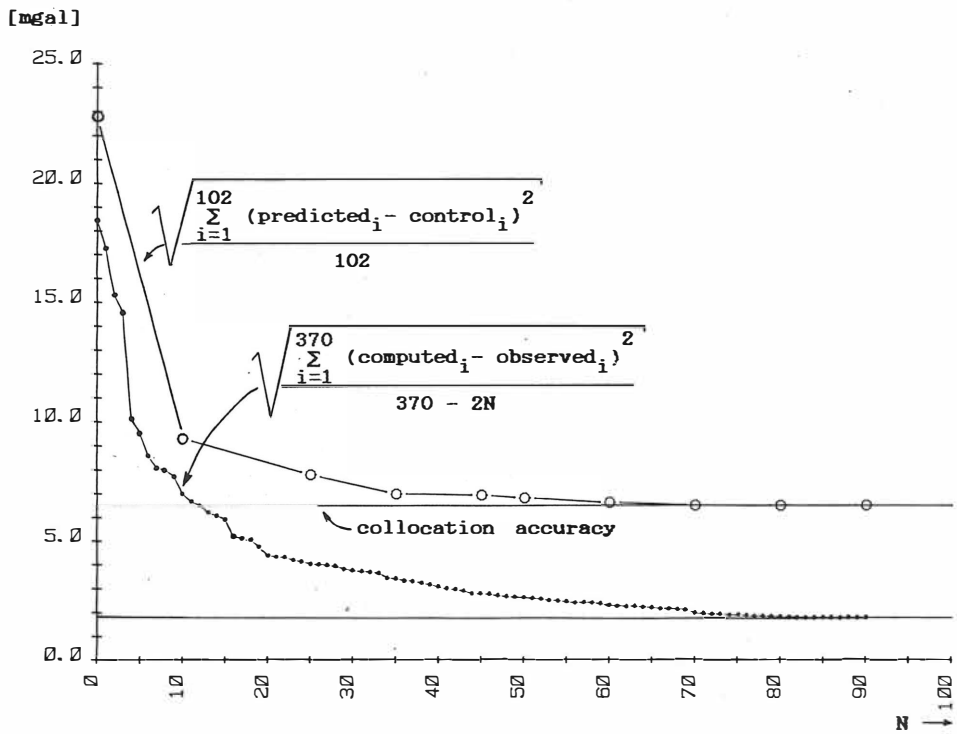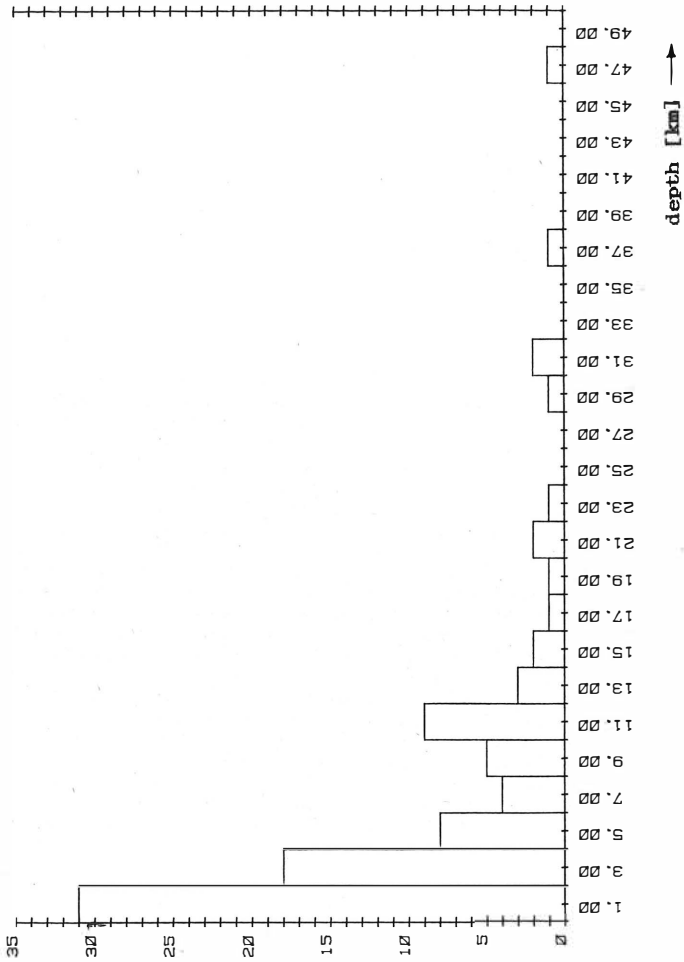
Figure 4: Histogram of point mass depth [km] for 90 point masses
(class intervall width: 2.0 km)

THE GEOID
AND THE MOHOROVIČIĆ DISCONTINUITY

**Krešimir Čolić, Nada Vučetić
and Svetozar Petrović**

Yugoslavia[4]

ABSTRACT:

In the prediction of the Mohorovičić discontinuity between the measured DSS profiles - besides geological information - terrain heights and/or Bouguer anomalies had been sometimes used for the interpolation. The authors of the present paper were the first to introduce also the application of the geoid - the most outstanding level surface of the earth's gravity field - for such purposes. At the beginning, the results were disappointing. However, in the course of investigation it came out that the geoid as such was not responsible for that, but the small area astrogeodetic geoid model for the considered region (Yugoslavia), which was available at that time. After the very same model has been reoriented - using our "method of maximal linear correlation coefficients", which resulted in the recent solution POTS88 - the absolute geoid undulations proved to be the best parameter for the above mentioned prediction of the Mohorovičić discontinuity. Using the geoid and the Bouguer gravity anomalies simultaneously gave the most acceptable result. In that way we succeeded to elaborate the enclosed map, as presently the best presentation of the Mohorovičić discontinuity for the Yugoslav territory.

----

[4] Address: Prof.Dr. Krešimir Čolić, Nada Vučetić, Svetozar Petrović,
Geodetic faculty, University of Zagreb, Kačićeva 26,
41000 Zagreb, Yugoslavia

ZUSAMMENFASSUNG:

*Für die Verlaufsvorhersage der Mohorovičić-Diskontinui-
tät zwischen den gemessenen TSS-Profilen benutzte man
früher – samt geologischen Informationen – bisweilen
die Geländehöhen und/oder die Bougueranomalien der
Schwere. Erst die Verfasser dieser Abhandlung führten
auch die Verwendung des Geoides, der ausgezeichneten
Niveaufläche des Erdschwerefeldes, für diese Zwecke
ein. Am Anfang brachte dies jedoch keine befriedigten
Ergebnisse, aber bald stellte sich heraus, dass sich
dabei gar nicht um die Unbrauchbarkeit des Geoides als
solches handelt, sondern dass die Ursache in dem damals
vorhandenen astrogeodätischen Geoidmodell für das kleine
betrachtete Gebiet (Jugoslawien) gelegen ist. Nach der
Verbesserung der Raumorientierung von demselben Geoid-
modell – mittels unserer "Methode der maximalen linearen
Korrelationskoeffizienten" entstand neulich die Lösung
POTS88 – war es festzustellen, dass die absoluten
Geoidundulationen sogar der beste Parameter für solch
eine Prognose der Mohorovičić-Diskontinuität sind.
Gleichzeitige Benutzung von Geoidhöhen und Bouguer-
anomalien liefert das annehmbarste Resultat. So konnte
die beiliegende Karte erstellt werden, als momentan die
beste Präsentation der Mohorovičić-Diskontinuität für
jugoslawisches Territorium.*

1. INTRODUCTION

It is well known that the depths of the Mohorovičić
discontinuity ("Moho") can be determined by aid of the
expensive deep seismic sounding (DSS) along chosen
profiles. In order to obtain an idea of the shape of
that boundary surface between such profiles, it is a
common practice to use Bouguer gravity anomalies and
terrain heights (in fact, in place of orthometric relief
heights, one should use the corresponding ellipsoidal
heights) on the whole considered region as prognostic
parameters. But, it is not hard to imagine that some
other quantities – for instance geoid undulations, as
in the present study – could be used for that purpose
as well. Moreover, it came out that the geoid is a
very significant – even the most important – parameter
for the prediction of the shape of the Mohorovičić
discontinuity, at least when the region in question
is the territory of Yugoslavia.

Four years ago, not far from the beginning of those
investigations of ours, we had presented a paper at
the previous symposium held under the same title as
the present one. Now we felt obliged to come again
with first completed results. Besides that, we consider
that the procedure for the prediction of the
Mohorovičić discontinuity relief between the existing

DSS-profiles, which is presented in this study, can be successfully applied also in other countries, respectively regions.

2. PREDICTING THE SHAPE OF THE MOHOROVIČIĆ DISCONTINUITY

2.1. Data files

For the computations we have used the following data files:
- a file containing the measured values M of the Mo-horovičić discontinuity depths along individual DSS profiles – in all 4 profiles with 173 points[3],
- a file of the mean values Δg of Bouguer anomalies, given in a 10'x15' grid, obtained by a manual digitizing of the Bouguer map 1:500000 for the whole Yugoslav territory – 716 points, see e.g. (Čolić et al. 1984),
- a file of mean relief heights H in a 10'x15' grid, see e.g. (Petrović et al. 1985), generated by means of a 2.5'x2.5' digital terrain model,
- a file of absolute geoid undulations N, also in a 10'x15' grid, obtained by the "method of maximal linear correlation coefficients". We will call that file POTS88, and all relevant details concerning it and the mentioned method are contained in the paper (Petrović et al. 1988), which is published in this same Proceedings.

In order to test the correctness of our approach, we added this time also:
- a file of geoid undulations n obtained by classical least squares fitting of a relatively oriented geoid model (Muminagić 1971) onto the spherical harmonic model GPM2 (Wenzel 1985), see (Čolić et al. 1987/1989).

Of course, a fitting to some other spherical harmonic model could have served for that purpose as well. Parallel usage of two representations of the absolutely oriented geoid for the Yugoslav territory is justified, because the first solution was achieved by the authors applying a rather unusual procedure – see (Čolić et al. 1986), or preferably (Petrović et al. 1988) – and the second solution was obtained in a more or less conventional way.

---

[3] From our considerations we have already earlier excluded the profile Cavtat-Loznica-Kanjiža (which is a part of the International profile III, respectively of the Geotraverse II), because it needed a geophysical reinterpretation, and the two profiles in Macedonia are too short, see e.g. (Čolić and Petrović 1983).

2.2. Correlation between the DSS data and the remaining parameters

In order to use any parameters for the prediction of some quantity, it is necessary to make an assumption regarding the nature of the really existing relation between them and the required quantity. To achieve that in the considered example, we computed first the linear correlation coefficients between the values M of the Mohorovičić discontinuity depths measured in the DSS points, and the corresponding values of each of the remaining three resp. four parameters. Generally high correlation coefficients (in the sense that their absolute values were close to 1) have been obtained, not only for individual profiles, but also when taking all their points together. Therefore,the *Table 1* displays only those last mentioned, more important values, together with the resulting interval estimations.

parameters	r	interval estimation
M and Δg	+0.86	+0.79<R<+0.91
M and H	-0.81	-0.72>R>-0.88
M and N	-0.89	-0.83>R>-0.93
M and n	-0.84	-0.75>R>-0.89

Table 1. The linear correlation coefficients r computed using the considered sample (173 points), and the interval estimations for the corresponding linear correlation coefficients R of the universal sets

We see that all linear correlation coefficients have absolute values close to 1, and conclude that the existent relations have strongly pronounced linear components! Further conclusion following from the table is that, in the considered region, the isostatic compensation takes place mostly inside the earth's crust, because the linear correlation coefficient between M and H amounts -0.81. However, when we consider the relation between the gravity anomalies Δg and the depths M, the absolute value of the coefficient becomes even larger (0.86). To tell the truth, the Bouguer anomalies are much more influenced by irregularities of the mases lying near under the surface, than are the geoid undulations. Therefore, the *largest absolute value has just the linear correlation coefficient between N and M (0.89)*, and the estimation

interval is of course the most narrow just in that
case. It should be probably added that the positive
sign of r in *Table 1* belongs to the case where one
surface is almost a stretched (in vertical direction)
image of the other one, while in other cases we have
a negative sign – one surface is close to a mirrored
and stretched image of the other.

2.3. Prediction of the depths M

In order to obtain the formulas for the prediction,
it is first necessary to choose their form. From the
facts described in the previous section, it is clear
that it makes sense to consider the linear expressions
of the form:

$$M(\Delta g, H, N) = \bar{M} + a(\Delta g - \overline{\Delta g}) + b(H - \bar{H}) + c(N - \bar{N}) \tag{1}$$

where $\bar{M}$ represents the mean value of the parameter
M for the considered region; $\overline{\Delta g}$, $\bar{H}$ and $\bar{N}$ being the
mean values of the parameters Δg, H and N; while a,
b and c are the required coefficients. In the case
when we wish a prediction with less than three
parameters, some of those three coefficients should
be in advance set to zero.

The coefficients a, b and c should be determined in
such a way that the values $M(\Delta g, H, N)$ of the Mohoro-
vičić discontinuity depths, computed by using the for-
mula (1), deviate as little as possible from the values
M measured along the DSS profiles, which can be achieved
by the method of least squares. In such a manner, we
obtained the following *relations for the prediction:*

$$M(\Delta g) = 37.9 - 0.186(\Delta g + 27.7)$$

$$M(H) = 37.9 + 0.0131(H - 580)$$

$$M(N) = 37.9 + 2.92(N - 44.28)$$

$$M(\Delta g, H) = 37.9 - 0.138(\Delta g + 27.7) + 0.0041(H - 580) \tag{2}$$

$$M(\Delta g, N) = 37.9 - 0.087(\Delta g + 27.7) + 1.83(N - 44.28)$$

$$M(H, N) = 37.9 + 0.0046(H - 580) + 2.16(N - 44.28)$$

$$M(\Delta g, H, N) = 37.9 - 0.075(\Delta g + 27.7) + 0.0014(H - 580) + 1.75(N - 44.28)$$

When we in place of the geoid undulations N, use the
geoid undulations n, then the expressions, which con-
tain the absolute geoid undulations as a prognostic
parameter, become:

$$M(n) = 37.9 + 4.42(n - 45.74)$$

$$M(\Delta g, n) = 37.9 - 0.118(\Delta g + 27.7) + 2.14(n - 45.74)$$

$$M(H, n) = 37.9 + 0.0067(H - 580) + 2.63(n - 45.74)$$

(3)

$$M(\Delta g, H, n) = 37.9 - 0.110(\Delta g + 27.7) + 0.0011(H - 580) + 2.02(n - 45.74)$$

Using all those formulas, we obtained *11 predictions (7 basic ones, and 4 for the control) for the shape of the Mohorovičić discontinuity under the whole Yugoslav territory*. For further treatment, we formed the data files of those predictions using the same 10'x15' grid, which had been used for the files of the prognostic parameters Δg, H, and N, respectively n.

2.4. Evaluation of the effected predictions

The quality of individual predictions can be estimated on the basis of their deviations from the measured DSS data, which can be seen from *Table 2*. Having in mind possible errors in the measured DSS data, neither the r.m.s. differences, nor the ranges of differences, should be considered as exaggerated, because they lie inside the limits of the measurement accuracy itself. Namely, according to the majority of authors, the uncertainty of the measured depths M amounts up to several kilometers, and the r.m.s. error has been estimated to approximately ±3km, see e.g. (Geiss 1987).

Of course, the best two predictions are those which use all three parameters each. However, out of those two triparametric predictions, better is the one which, besides Bouguer anomalies and relief heights, uses our model POTS88 of the absolutely oriented astrogeodetic geoid for the territory of Yugoslavia. Analogous statement holds for biparametric and uniparametric predictions: wherever the absolute geoid undulations occur, the r.m.s. differences and the ranges of differences have the smallest values, i.e. they deviate least from the measured DSS data. In other words, according to both accepted criteria, the best uniparametric prediction is M(N), the one which makes/ use of the geoid, and among the biparametric predictions it is M(Δg,N), which is based on Bouguer anomalies, and again on the geoid – moreover, that prediction is practically identical to the triparametric M(Δg,H,N).

It is visible as well, that also the model of the absolutely oriented geoid, obtained by the least squares fitting of the original Muminagić's model onto the geoid surface according to GPM2, represents a prognostic parameter which is surely better then relief heights, and almost equally as good as Bouguer anomalies!

predicted depths	measured depths M	
	r.m.s. diff.	range of diff.
M(Δg)	3.1	13.7
M(H)	3.5	19.9
M(N)	2.8	10.8
M(Δg,H)	3.0	15.4
M(Δg,N)	2.4	10.1
M(H,N)	2.6	10.5
M(Δg,H,N)	2.4	10.0
M(n)	3.3	15.0
M(Δg,n)	2.7	13.2
M(H,n)	3.0	15.4
M(Δg,H,n)	2.6	13.4

Table 2. The r.m.s. differences and the ranges of dif-
ferences between the DSS data and the pre-
dicted values for the Mohorovičić disconti-
nuity depths – for all 4 profiles taken to-
gether (173 points)

On the other hand, for the evaluation of the obtained
results one can also use the *r.m.s. differences be-
tween individual predictions* computed using points
uniformly distributed over the whole Yugoslav
territory. In place of listing all those differences,
we will comment only some most significant among them.
For instance, the amount of 4.8km for the r.m.s.
difference between the depths M(N) and M(Δg) seems to
be too large, but, when compared with the figures in
Table 2, it shows that *those two predictions mainly
deviate in opposite directions from the probable position
of the Mohorovičić discontinuity!* Therefore, it seems
to be profitable to use just their combination for
the prediction. On the contrary, the r.m.s. difference
of just 1.0km distinguishing the predictions M(Δg) and
M(Δg,H), as well as the 1.4km r.m.s. difference between
M(N) and M(H,N), speak that the relief heights make no
significant contribution to the improvement of the
prediction. It is especially stressed by the difference
of 4.9km, respectively 5.2km, between the predictions

M(H) and M(N), respectively M(n). However, it should be
mentioned as well, that the difference between the
predictions which use the N-values, respectively the
n-values, alone, is characterized by an amount of even
3.3km. But, to avoid eventual misunderstandings, it
should be emphasized that the corresponding pairs of
the predictions, obtained using the two considered
alternate geoid representations, are in principle much
more close, than any two predictions which are more
heterogeneous with respect to the applied parameters
- regardless whether uniparametric or biparametric
predictions are considered.

When we finally look at the relations between the
biparametric and the triparametric predictions, we are
led to conclude that the *inclusion of the relief as a
third prognostic parameter brings no such improvement,*
which would justify that step. Namely, the prediction
$M(\Delta g,H,N)$ resp. $M(\Delta g,H,n)$ is practically identical to the
prediction $M(\Delta g,N)$ resp. $M(\Delta g,n)$ - both considered r.m.s.
differences amounting only 0.3km. All that does not
mean that we completely exclude the relief heights as
a possible prognostic parameter. We only establish
that - at least on the considered territory - the
Bouguer gravity anomalies, and especially the absolute
geoid undulations, are significantly better for that
purpose.

2.5. The choice of the optimal prediction

On the basis of the just completed evaluation, we can
conclude that the consideration of biparametric
predictions of depths M really makes sense, which can
not be said for the triparametric ones. The conclusion
can be confirmed by considering the contribution of
every single parameter in biparametric and tripara-
metric predictions, which we did in a somewhat unusual
way. *Table 3* offers the *linear correlation coeffi-
cients between the predictions and the individual
parameters* which took part in them.

From the upper part of the table it is easily seen
that the *linear correlation coefficient associated with
the geoid undulations N is always the largest,*regard-
less whether in the prediction the N-values are com-
bined with Bouguer anomalies, with relief heights, or
with both those parameters simultaneously. Therefore,
it may be stated that - at least on the Yugoslav
territory - *the geoid undulations are the best
prognostic parameter for the determination of the shape
of the Mohorovičić discontinuity in the space between
the existing DSS profiles.* In accordance with the
expectations, the corresponding linear correlation
coefficients for the n-values are just somewhat
lower. Therefore, the prediction with the use of geoid

	Δg	H	N	n
M(Δg,H)	+0.98	−0.89	−	−
M(Δg,N)	+0.87	−	−0.96	−
M(H,N)	−	−0.81	−0.98	−
M(Δg,H,N)	+0.87	−0.80	−0.95	−
M(Δg,n)	+0.91	−	−	−0.88
M(H,n)	−	−0.85	−	−0.93
M(Δg,H,n)	+0.91	−0.81	−	−0.88

Table 3. The linear correlation coefficients as a measure of the contribution of individual parameters in miscellaneous predictions of the Mohorovičić discontinuity for the Yugoslav territory

undulations should be considered also when the geoid is represented by this other model, which has a slightly different absolute orientation and completely the same detailed forms.

On the basis of everything that has been laid out, it is obvious that *the final choice falls on the prediction* M(Δg,N), presented in *Figure 1*, which is the optimal solution in the considered case. One could almost use geoid undulations combined with relief heights as well, and even the geoid undulations alone. However, in the emergency case, the prediction based on Bouguer anomalies alone (Čolić et al. 1984) could be applied, or better in combination with relief heights (Petrović et al. 1985).

For the sake of completeness, let us emphasize that for the Mohorovičić discontinuity on the Yugoslav territory − besides our former predictions − there exists from the earlier times also a presentation given by geophysicists (Aljinović et al. 1985), which we examined in (Čolić et al. 1985) and used at a time as well. Although it was not obtained in a completely exact manner, that map coincides rather well with our solution M(Δg,N), presented here in *Figure 1*; it is, of course, also close to our former solution M(Δg), see (Čolić et al. 1984), respectively to M(Δg,H), (Petrović et al. 1985). Its r.m.s. deviation from the measured DSS values along the profiles amounts to 2.7km (after the *level difference of 2.5km* has been removed), the
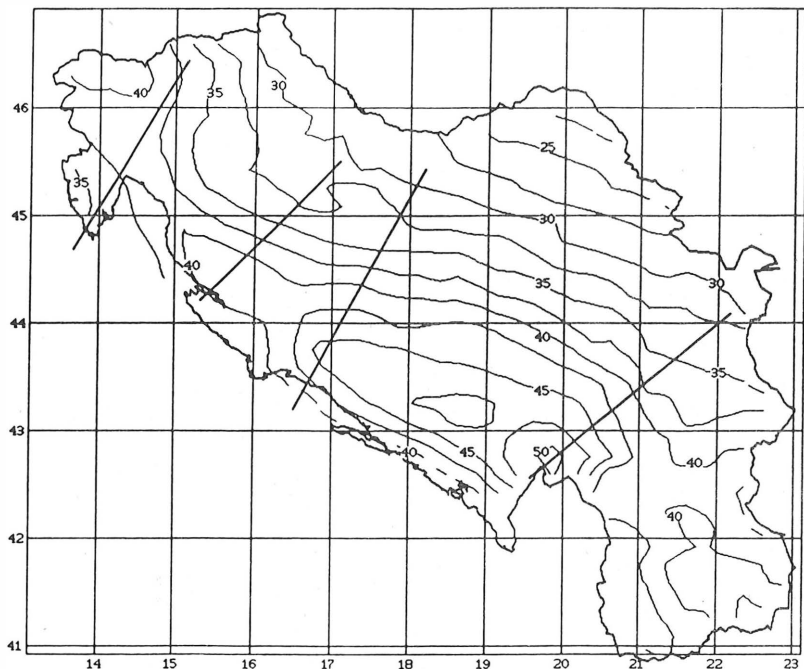
Figure 1. The map of the Mohorovičić discontinuity pre-
dicted by aid of absolute geoid undulations
and Bouguer anomalies; the positions of the
4 used DSS profiles are also presented

range of differences being 11.7km. *According to those
two criteria, our predictions - M(Δg,N), and even M(H,N)
- are not only produced in a more correct way, but are
also somewhat more accurate.*

3. CONCLUSIONS

This study completes our investigations of the relation
between the geoid and the Mohorovičić discontinuity.
The eventual objection that we "closed the circle" -
i.e. that we used the DSS profile data for the absolute
orientation of the astrogeodetic geoid model POTS88,
and then predicted again the Mohorovičić discontinuity
for the whole Yugoslav territory - is out of question.
Namely, for the absolute orientation of the geoid we
could use only the Bouguer anomalies and the relief

heights, or even the Bouguer anomalies alone, but it is obvious that it is better to use all the three parameters at the same time. Besides that, it came out that in place of the absolutely oriented geoid model POTS88, for the purpose of prediction could almost equally well serve the geoid model obtained by the least squares fitting of the astrogeodetic original onto the geoid surface according to GPM2, or onto some other recent (and kindred) spherical harmonic model.

As far as we know, we were first to introduce the use of absolute geoid undulations into the prediction of the Mohorovičić discontinuity shape in the regions between the existing DSS profiles. Now it came out that the *geoid is the best prognostic parameter*, and that the prediction of the shape of Mohorovičić discontinuity depths by combining the geoid and the Bouguer anomalies represents the most reliable solution. Therefore, our map – determined in an exact way – can surely replace the Aljinović's preliminary one, as the best presentation of the Mohorovičić discontinuity for the Yugoslav territory available at the moment.

REFERENCES

1. Aljinović, B., I.Blašković, E.Prelogović and D.Skoko (1985): Preliminary map of the Mohorovičić discontinuity within the area of the middle and southeastern part of Europe in correlation with the geological structure. *IAG-workshop "Density distribution of the lithosphere – Static and dynamic models"*, Zürich; abstract in: *ETH Bericht*, No.102, p.12.

2. Čolić, K., B.Aljinović and S.Petrović (1985): A comparison of the existing preliminary map of Mohorovičić discontinuity with the predicted values of the depths of that surface in the Dinaric-Pannonian region of Yugoslavia. *IAG-workshop "Density distribution of the lithosphere – Static and dynamic models"*, Zürich, 7 pp; abstract in: *ETH Bericht*, No.102, p.16.

3. Čolić, K. and S.Petrović (1983): Correlation between gravity anomalies, geoid heights and Mohorovičić discontinuity depths in the Dinaric-Pannonian region of Yugoslavia. *The XVIIIth General Assembly of IUGG*, Hamburg; published in: *Proceedings of the International association of geodesy (IAG) symposia*, Columbus (1984), pp.137–146.

4. Čolić, K., S.Petrović and B.Aljinović (1986): Testing the existing absolute geoid heights in Yugoslavia using information offered by the Mohorovičić discontinuity, the Bouguer gravity anomalies and

the relief heights. *International symposium on the definition of the geoid, Proceedings*, Florence, pp.29-38; also published in: *Bollettino di geodesia e scienze affini*, XLVI, No.4 (1987), pp.309-322.

5. Čolić, K., S.Petrović and T.Bašić (1984): A new about the correlation between Mohorovičić discontinuity depths, geoid undulations and Bouguer gravity anomalies in the Dinaric-Pannonian region of Yugoslavia. *5th International symposium "Geodesy and physics of the earth"*, Magdeburg; published in: *Akademie der Wissenschaften der DDR, Veröffentlichungen des Zentralinstituts für Physik der Erde*, No.81 (1985), Vol. I, pp.68-76.

6. Čolić, K., S.Petrović, and T.Bašić (1987/1989): What happens when using the method of least squares for the fitting of geoid model surfaces?. *INTERCOSMOS scientific conference "Use of artificial satellite observations for geodesy and geophysics"*, Szentendre; published in: *Observations of artificial satelites of the earth*, No.25 (1987), pp.173-181. A new, more complete version of the paper will be published in: *Bollettino di geodesia e szienze affini*, XLVIII, No.1 (1989), 15 pp.

7. Geiss, E. (1987): Die Lithosphäre im mediterranen Raum - Ein Beitrag zu Struktur, Schwerefeld und Deformation. *Deutsche Geodätische Komission*, Reihe C, No.332, 124 pp.

8. Muminagić, A. (1971): Investigation of real geoid in Yugoslavia. Separate publication presented at: *15th General Assembly of IUGG*, Moscow.

9. Petrović, S., K.Čolić, Z.Biljecki and T.Bašić (1985): The use of complex data for the prediction of Mohorovičić discontinuity depths in the Dinaric-Pannonian region of Yugoslavia. *IAG-workshop "Density distribution of the lithosphere - Static and dynamic models"*, Zürich, 10 pp; abstract in: *ETH Bericht*, No.102, p.29.

10. Petrović, S., N.Vučetić and K.Čolić (1988): Absolute orientation of the astrogeodetic geoid model for the Yugoslav territory achieved by the method of the maximal linear correlation coefficients. *6th International symposium "Geodesy and physics of the earth"*, Potsdam; published in this same Proceedings.

11. Wenzel, H.-G. (1985): Hochauflösende Kugelfunktionsmodelle für das Gravitationspotential der Erde. *Wissenschaftliche Arbeiten der Fachrichtung Vermessungswesen der Universität Hannover*, No.137.

A GRAVITY FIELD MODEL FROM LAGEOS BASED ON POINT MASSES (POEM-L1)

R. Dietrich and G. Gendt

Academy of Sciences of the GDR
Central Institute for Physics of the Earth
Potsdam, GDR, 1561

Summary: By using the capabilities of the POTSDAM-5 software complex and LAGEOS laser ranging data of 12 months a gravity field model of the earth based on point masses was derived. A 70-point-mass model computed by BARTHELMES(1986), which is an approximation of the GEM 10 model, served as initial one. The positions of the masses were fixed and their magnitudes were improved.
    The new POTSDAM EARTH MODEL POEM-L1 is tailored for LAGEOS; the orbital fit rms values for 5-, 15- and 30-days arc length (3rd generation laser devices) are 6, 8 and 10 centimeters. After transformation into spherical harmonics the nonzonal part of the field up to degree 5 was compared with other models. A rss value for geoid undulation differences between GEM-T1 and POEM-L1 of ±14 cm was obtained. This value illustrates the accuracy of the representation of the long-wavelength part of the geopotential in both models.

1. Introduction

    The determination of the geopotential is a fundamental aim of geodesy. The progress in this field of research during the last few years has been remarkable, and satellite geodesy has played an important role in this context. Satellite laser ranging (SLR) data can be used to improve a gravity field model – on the other hand the gravity field model used in the force part of orbit computation software is one limiting factor for the accuracy of all parameters determinable by SLR data analysis (e.g. station coordinates, earth rotation, plate tectonics, earth tides).
    In the present paper we have tried to determine a gravity field model tailored for the mostly used Laser Geodynamics Satellite LAGEOS. For this investigation we applied our own software and also an alternative parametrization of the gravity field. We adjusted a set of point masses, which contains – as we think – a quite independent estimate of the long-wavelength part of the geopotential.

2. Initial model and software

    The initial gravity field model used in the computation is a 70-point-mass model with optimized positions named PM2/70G and published by BARTHELMES (1986) together with a detailed description of the applied algorithm. It is an approximation of GEM 10 (LERCH et al. 1979). The horizontal positions of the masses are shown in Figure 1. In addition to the 70 point masses one point mass was placed in the geocenter. To approximate efficiently the zonal term C_{20} (and C_{30}) three masses (one in the geocenter, two at the z-axis, sum equal to zero) were computed and not improved. Thus the complete model contains 74

point masses.

The potential V of a point mass m at the position $\underline{p}$ inside the earth can be written as follows:

$$(1) \quad V(\underline{r}) = G \cdot m \cdot l^{-1}(\underline{p}, \underline{r})$$

Expressing the reciprocal distance l^{-1} between $\underline{p}$ and $\underline{r}$ in spherical harmonics one gets:

$$(2) \quad V(\underline{r}) = G \cdot m \frac{1}{R_r} \sum_{N=0}^{\infty} \left(\frac{R_p}{R_r}\right)^N \cdot P_N(\cos \psi_{\underline{p},\underline{r}})$$

If one inserts the spherical coordinates λ and ϑ of $\underline{p}$ and r to describe $\cos \psi$ finally eq. (1) can be rewritten (see BARTHELMES 1986, p.32):

$$(3) \quad V(\underline{r}) = G \cdot m \cdot \sum_{N=0}^{\infty} \frac{R_E^N}{R_r^{N+1}} \sum_{M=0}^{\infty} (C_{NM}\cos M\lambda_r + S_{NM}\sin M\lambda_r) \cdot P_{NM}(\cos\vartheta_r)$$

where the (fully normalized) coefficients C_{NM}, S_{NM} are functions of the position vector $\underline{p}$ of the point mass only. In this way the potential of a point mass model can be transformed into spherical harmonics.

The power spectra of the models PM2/70G - after transformation into spherical harmonics - and GEM 10 (Figure 2) clearly reflect the fact that with the limited number of point masses especially the lower degree harmonics of GEM 10 were fitted by PM2/70G, whereas with increasing degree N (beginning at N about 10) the power of PM2/70G falls more and more below that of GEM 10.

We estimated that the PM2/70G model could be advantageously matched to the gravity field information contained in LAGEOS laser ranging observations, because both the sensitivity of LAGEOS with respect to the gravity field (see e.g. LERCH et al. 1982) and the PM2/70G model are focussed on the long-wavelength part of the geopotential. This was one main reason for the decision to choose this approach in our investigations.

The gravity field model PM2/70G was implemented in the POTSDAM-5 orbital program system and replaced here the GEM-L2 model which has served as the standard up to now. All other software components were in accordance with the MERIT standards (MELBOURNE et al. 1983). This includes solid earth tides (WAHR model without permanent tide), ocean tides (SCHWIDERSKI model), solid earth tide effects on station coordinates and ocean loading site displacement, tidal variations of UT1, precession and nutation. Relativistic effects were not applied.

As the initial set for pole coordinates we used the values determined at our institute in the frame of MERIT and post MERIT activities, UT1 data were taken from IRIS-Earth Orientation Bulletin. For the station coordinates we introduced our own determination from MERIT named SSC(ZIPE)85L02. A comparison of this coordinate set with those of other analysis centers of MERIT Campaign by a similarity transformation showed rms values of the residuals of 2...3 centimeters.

The orbital fit rms value for the initial point mass model PM2/70G (monthly arcs for LAGEOS) was in the order of 40 centimeters, the same value for GEM 10 was within 20...30 centimeters.

The coefficients of the observation equations (partial derivations of the unknowns) were computed for all geometric parameters during the orbit integration, whereas those for

dynamical parameters were determined separately by integrating
variational equations. Later the observation equations and
finally the normal equations for each pass containing all
parameters of interest were constructed and stored. The parameter
estimation was performed in a separate program part named SOLVE,
which can select and combine the normal equations. Arc length,
solve-for parameters, station weigths etc. can be varied here in
a wide range.

3. Data

For the improvement of the gravity field model 12 months (30-
days intervals) of LAGEOS data in the time span of 1983-1985 were
introduced. The distribution of the data and the stations are
summarized in Table 1. No other data or information were added.

4. Estimation technique

The technique for parameter determination is least squares
adjustment. The following parameters were determined:
- magnitudes of the point masses
- orbital elements and empirical acceleration for 15-days
  intervals
- pole coordinates for 5-days intervals (No adjustment of LOD).
In test computations also station coordinates were adjusted, but
it turned out that this had practically no influence on the
magnitudes of the point masses. The adjusted station coordinates
agreed within 3 cm with the initial ones (rms after similarity
transformation), so that in the final computation the station
coordinates were fixed. As the introduced UT1 values from IRIS
are very accurate (and for strengthening of the solution) we
decided to exclude an adjustment of LOD.
Individual weights for the stations were applied. These weights
did not only depend on the precision of the laser devices. To
secure a balanced influence of the observations with respect to
the coverage of the orbit also the density of stations in a
certain region was taken into consideration.
The final normal equation matrix for the magnitudes of the
point masses showed - as expected for this typical improperly
posed problem - a bad numerical stability. TODD's condition
number k computed by an eigenvalue decomposition:

$$(4) \qquad k = \frac{\lambda_{MAX}}{\lambda_{MIN}}$$

was in the order of 10^{11}.
To improve the numerical stability of the normal equation
matrices in our software a special kind of congruence
transformation is applied as a standard, which normalizes the
normal equation matrix before inversion in such a way that all
diagonal elements are equal to one.
The application of this transformation is especially useful, if
the condition is affected by very different scales of the
unknowns. But also in the present case k could be slightly
improved by a factor of 10 (see Figure 3). Nevertheless the
problem is improperly posed and a numerical stabilization of the
normal equation matrix is necessary. We used TICHONOV's
regularization, known as a standard for solving improperly posed
problems (see MORITZ 1980, pp. 240), which leads to the

minimization of the following sum:

(5) $\underline{v}^T \underline{P} \underline{v} + \alpha \ \underline{x}^T \underline{x} \Longrightarrow$ Min

with: $\underline{v}$: residuals
$\underline{P}$: weight matrix of observations
$\underline{x}$: solution vector
α : regularization parameter

The choice of an optimum value of α needs further investigations (see SCHWARZ 1979), but also numerical experiments and experience are profitable. We decided to iterate in our computations. In a first step we determined an interim field. Here the second term in eq. (5) was in the order of 20% of the first one. In the final solution however α was fixed on a smaller value so that the size of this second summand was about 1% of the first one.
To realize the coincidence of the center of gravity and the origin the three corresponding condition equations were added to the normal equation system. It is interesting to note and gives an insight into the stability of the solution that without these conditions the deviations of the center of gravity from the origin were in the order of a few centimeters in X and Y and in the order of one decimeter for Z.

5. Results

The computed gravity field model named POEM-L1 (P̲O̲TSDAM E̲ARTH M̲ODEL for LAGEOS No.1̲) is presented in original form in Table 2 and , transformed into spherical harmonics up to degree and order 20, in Table 3. The model includes the permanent tide.
The sum of all point masses (relativ to GM) is m = -0.3355 10^{-8}.
The value of GM$_2$ introduced into the computations was GM$_\circ$ = 398600.440 km^3/s^2, the adjusted GM for POEM-L1 is therefore GM = GM$_\circ$ (1+m) = 398600.439 km^3/s^2.

6. Evaluation of the results

6.1. Orbital fit of LAGEOS and station coordinate comparisons

For the evaluation of the model four months of LAGEOS data, which are not included in the determination of POEM-L1, were selected (month 6,7,14 and 15 in the scheme of Table 1). For these four months the gravity field models GEM-L2 (LERCH et al. 1982), GRIM-3B (REIGBER et al. 1983), our model POEM-L1 and – just published – GEM-T1 (MARSH et al. 1988) were used for comparative investigations. Software, data and standards – excluding the gravity field model – were identical. The achieved orbital fits are shown in Table 4. POEM-L1 has nearly equivalent orbital fits as GEM-T1 and GEM-L2, but significantly better ones than GRIM-3B. One weak point for POEM-L1 should be mentioned: monthly arcs with adjusted empirical acceleration for the whole month gave orbital fits of about 15 cm, an indication, that the modelled along-track-component in monthly arcs differs slightly more from reality.

As already mentioned in the introduction also geometric unknowns in SLR data analysis are affected by the used gravity field model. We selected the station coordinates adjusted in these computations for some investigations. The rms value of station coordinate differences after a 7-parameter similarity

transformation served as a measure of the accuracy.

In Table 5 these values for all pairs of gravity field models used and for different arc lengths are shown. The agreement of coordinates derived by using POEM-L1 compared to those of GEM-T1 and GEM-L2 is by a factor of about 2 better than the agreement of these three solutions with the GRIM-3B solution. For the further evaluation of each model the coordinate sets from different arc lengths and from data subsets were analyzed in the same way (Table 6). The results show the consistency of the POEM-L1 solutions compared to the other ones. A more detailed interpretation can be left to the reader.

6.2. Spherical harmonics and geoid undulation differences

It is a good property of a point mass model that it can easily be expressed in spherical harmonics. In this way POEM-L1 can be compared to other geopotential models. In Table 3 we have presented POEM-L1 up to degree and order 20. It was clear before that only coefficients of lower degree could be determined with high accuracy. The presentation of higher order terms in Table 3 was performed mainly to facilitate possible tests of POEM-L1. With increasing degree the coefficients contain more and more the a priori information of the initial point mass model PM2/70G and, finally, of GEM 10 as the starting point of the PM2/70G determination - as far as the point masses could approximate them (see Sec. 2). This is emphasized by the fact that the power spectrum of POEM-L1 had the same quality as that of the initial model PM2/70G (cf. Figure 2).

By using only one satellite also larger inaccuracies for all zonal harmonics had to be expected in advance. This inaccuracy of the zonal terms is no severe problem because they are in principle much better known than the nonzonal ones.

If one takes all these facts into consideration, it is useful to analyze the long-wavelength part of our model. In Tabel 7 spherical harmonic coefficients up to degree and order 5 are compared. GEM-T1 is taken as a reference, and the differences of the C and S for different models containing LAGEOS information (GRIM3-L1 from REIGBER et al. 1985), additionally the initial point mass model PM2/70G and its source GEM 10 are presented.

A correct estimation of potential coefficient accuracies is a difficult question (see e.g. LERCH et al. 1985, MARSH et al. 1988, KLOKOČNIK 1985, SJÖBERG 1985). As far as published we have added in one column accuracy estimates of the authors of some geopotential models. At present we cannot offer serious accuracy estimates for our results. As POEM-L1 is a relatively independent estimation we therefore investigated the differences to other models. At first glance the deviations from GEM-T1 and GEM-L2 are quite satisfactory, except - as expected - the zonal terms.

To have a more detailed view we decided to compute rss values of the geoid undulation differences per degree (without zonal terms) using the relation:

$$(6) \quad rss_N = R_E \cdot \sqrt{\sum_{M=1}^{N} (\Delta c_{NM}^2 + \Delta s_{NM}^2)}$$

The results for POEM-L1 and GEM-T1 in comparison with the other models are shown in Figures 4 and 5. The following conclusion can be drawn: The initial point mass model was significantly improved up to degree 5. On the other hand an increasing relationship of POEM-L1 with the initial model PM2/70G for higher degrees is valid. In Table 8 the geoid undulation

differences up to degree 5 between all models under investigation
are summarized. One can state a value of 14 centimeters between
GEM-T1 and POEM-L1, which is behind GEM-T1/GEM-L2 (12
centimeters), but about a factor of 2 better than all other
combinations (except GEM 10 and PM2/70G, which are not
independent).

7. Conclusions

It could be demonstrated that the applied approach of using a
geopotential model described by point masses for gravity field
improvement using LAGEOS laser ranging data was convenient. The
derived model can be used either in its original form or after
tranformation into spherical harmonics.
The creation of the model POEM-L1 was our first attempt in
gravity field determination using SLR data. Taking this fact into
consideration one can be satisfied both with the achieved orbital
fit of LAGEOS and with the accuracy of the nonzonal harmonics up
to degree 5.
Further refinements and deeper investigations at different
stages of the applied procedure seem to be useful. An extended
data set should also contribute to a further improvement of POEM-
L1. Moreover one should consider an introduction of additional
information on the zonal harmonics from external sources.

References

Barthelmes, F.: Untersuchungen zur Approximation des äusseren
    Schwerefeldes der Erde durch Punktmassen mit optimierten Posi-
    tionen.
    Veröff. Zentralinst. Physik der Erde Nr. 92, Potsdam 1986

Klokočnik, J.: Further Comparisons of Earth Gravity Models by
    Means of Lumped Coefficients (part I and II).
    Bull. Astron. Inst. Czechosl. 36(1985), pp. 27-43 and
    37 (1986), pp. 26-42

Lerch, F.J.; Klosko, S.M.; Laubscher, R.E.; Wagner, C.A.: Gravity
    Model Inprovement using GEOS-3 (GEM 9 and 10)
    J. geoph. Res. 84(1979)88, pp. 3897-3915

Lerch, F.J.; Klosko, S.M.; Patel, G.B.: A Refined Gravity Model
    from LAGEOS (GEM-L2)
    NASA, G.S.F.C., Techn. Mem. 84986. - Greebelt 1983

Lerch, F.J.; Klosko, S.M.; Wagner, C.A.; Patel, G.B.: On the
     Accuracy of Recent Goddard Gravity Models
     J. geophys. Res. - 90(1985)B11. - pp. 9312-9334

Marsh, J.G.; Lerch, F.J., Putney, B.H.; Christodoulidis, D.C.;
     Smith, D.E.; Felsentreger, T.L.; Sanchez, B.V.; Klosko, S.M.;
     Pavlis, E.C.; Martin, T.V.; Robbins, J.W.; Williamson, R.G.;
     Colombo, O.L.; Rowlands, D.D.; Eddy, W.F.; Chandler, N.L.;
     Rachlin, K.E.; Patel, G.B.; Bhati, S.; Chinn, D.S.: A New
     Gravitational Model for the Earth from Satellite Tracking
     Data: GEM-T1
     J. geoph. Res. 93(1988)B6, pp. 6169-6215

Melbourne, W.; Anderle, R.; Feissel, M.; King, R.; McCarthy, D.;
     Smith, D.; Tapley, B.; Vicente, R.: Project MERIT standards
     U.S. Nav. Obs., Circ. No. 167, Washington 1983

Moritz, H.: Advanced Physical Geodesy
     Karlsruhe: Herbert Wichmann Verlag, Tunbridge Wells Kent;
     Abacus Press, 1980

Reigber, Ch.; Müller, H.; Rizos, Ch.; Bosch, W.; Balmino, G.;
     Moynot, B.: An Improved GRIM3 Earth Gravity Model (GRIM 3B)
     Paper XVIII. IUGG Gen. Assembly, IAG Symp. C, Hamburg 1983

Reigber, Ch.; Balmino, G.; Müller, H.; Bosch, W.; Moynot, B.:
     GRIM Gravity Model Improvement using LAGEOS (GRIM3-L1)
     J. geoph. Res. 90(1985)B11, pp. 9285-9299

Schwarz, K.P.: Geodetic Improperly Posed Problems and their
     Regularization.
     Boll. Geod. Sci. Aff. 38(1979)3, pp. 389-416

Sjöberg, L: The Estimation of the Power Spectrum and Reliabi-
     lity of Models of the Earth's Gravity Field by Intercompa-
     rison of Independent Models.
     Manuscr. geod. 12(1987), pp. 104-112

Table 1: Number of LAGEOS passes introduced into the computation.
"month" means 30-days interval after Aug. 30th 1983
(MJD =45576.5)

| Station | | months after Aug. 30th 1983 | | | | | | | | | | | SUM |
No.	Name	1	2	3	8	9	10	11	12	13	19	20	21	
7907	AREQU	40	43	41	24	37	34	43	50	48	8	12	34	414
7939	MATER	20	18	7	24	32	35	41	48	36	8	9	14	292
1181	POTSD	2	7	6	9	5	5	6	10	9	1	2	4	66
7834	WETTZ	5	20	23	24	29	21	24	32	21	2	7	8	216
7112	PLATT	10	14	11	27	9	20	6	10	9	.	.	.	116
7121	HUAHI	5	14	9	13	14	13	10	8	1	10	2	.	99
7109	QUINC	49	21	3	44	60	34	43	54	39	11	22	33	413
7210	MAUI	31	29	26	35	52	44	23	18	30	3	3	6	300
7838	SIMOS	3	23	23	10	14		9	22	21	3	7	33	168
7086	FTDAV	10	3	11	16	14	8	11	9	16	1	1	7	107
7839	GRAZ	6	23	14	11	8	11	19	9	13	2	9	9	134
7105	GREEN	16	27	20	13	41	15	11	17	23	29	24	25	261
7833	KOOTW	3	7	.	25	9	7	5	6	.	.	.	.	62
7122	MAZAT	4	21	16	.	.	11	.	10	11	23	14	25	135
7840	HERST	.	20	13	28	10	26	45	33	31	32	11	9	258
7110	MTPEA	.	32	11	28	24	47	25	41	43	25	47	39	362
7090	YARAG	.	.	22	12	35	36	21	14	36	42	55	62	335
7805	METSA	.	.	1	3	6	.	.	4	10	.	.	.	24
7835	GRASS	.	.	.	3	1	4	10	4	2	7	16	9	56
7400	SANTI	.	.	.	24	10	.	.	.	.	.	.	.	34
7401	CERRO	.	.	.	.	13	39	.	.	.	.	.	.	52
7810	ZIMME	.	.	.	.	1	2	9	13	6	.	.	.	31
7886	QUINC	.	.	.	.	.	.	4	30	14	.	.	.	48
7837	SHANG	.	.	.	.	.	1	.	2	15	.	.	.	18
SUM		204	322	257	373	424	413	365	444	434	207	241	317	4001

Table 2: Gravity field model POEM-L1 expressed in point masses. Coordinates in units of the earth radius R_E=6378144.11 m, masses in units of the earth mass $*$ 10^6 (GM=398600.440 km^3/s^2). The permanent tide is included in the model.

X	Y	Z	M
-0.03091647	-0.03825675	0.89905777	0.26434589
-0.21898278	0.40299749	0.76265564	-0.32476566
-0.30980759	-0.25507156	0.71042076	2.33680035
-0.41560249	0.19614976	0.67624113	1.22151567
0.20550109	-0.13979503	0.66115045	7.33392582
0.00936872	-0.34417242	0.65187833	-6.16029592
-0.49126417	-0.17465094	0.64175950	1.44445059
0.24783491	0.41934422	0.63367255	2.05814385
0.55239449	0.15660396	0.61379885	1.16886462
0.40308854	0.10222966	0.55883479	-5.32315917
0.31126292	0.45869962	0.55554780	-5.63284465
0.57540743	-0.38653651	0.53295342	0.78047103
-0.17701807	-0.46227166	0.49167781	11.51293153
-0.53652776	0.16288297	0.47113615	-2.63738593
-0.30127224	0.37721474	0.43669394	10.14133479
0.01971268	0.70251528	0.41419209	2.81541833
-0.04047954	0.45323646	0.37618863	-20.28210665
0.59784890	-0.28398710	0.36308728	-3.51153688
0.48764136	0.55212153	0.36055080	-3.76019485
0.59910600	0.32279645	0.35524931	-3.46347016
-0.67620645	0.48873893	0.33399041	0.23994832
0.37032208	0.41870726	0.33313859	24.37227259
-0.44219299	-0.42805147	0.33029770	9.80540128
0.80694390	-0.02503858	0.31909956	-0.45657080
-0.69742346	-0.19072962	0.29450892	2.15629539
-0.27095883	-0.35484992	0.28495467	-50.49571982
-0.09124126	-0.59744213	0.22146788	10.07119237
0.35746291	-0.23021395	0.21407169	40.26696792
0.39784295	0.68729004	0.21402384	-1.18441071
0.22881256	-0.44169185	0.13379864	-47.01573010
-0.42658979	0.71596998	0.12094230	1.33999674
0.16881973	-0.65768258	0.05001890	16.32363615
-0.06828015	0.78598216	0.04635578	3.26719620
0.09727218	0.69809454	0.04434223	-8.98452711
-0.52495482	-0.37770350	-0.00189175	9.93078353
0.60143125	0.63799155	-0.01516987	-0.66192887
-0.29370554	0.78917993	-0.03693428	1.58453336
0.77737580	0.30969505	-0.04046316	-1.69776441
0.06538622	-0.70980228	-0.09143593	-4.52768941
-0.44117995	0.37452632	-0.11134059	15.92841186
-0.21389846	-0.56571578	-0.13605268	5.10794735
0.85060805	0.03452125	-0.16314741	-0.76098315
0.60076664	0.18500108	-0.17642314	4.77736600
0.28077017	-0.79611061	-0.17793424	0.96099767
-0.45195217	-0.34783115	-0.18747316	-6.19858633
0.78933916	-0.34311120	-0.20290570	-0.52282395
0.64547409	0.49538389	-0.23072037	-1.02863262
-0.11475806	0.38618306	-0.23584466	-24.95947460

```
  0.29617572      0.72588646     -0.31551979      0.83534024
  0.34439496     -0.73929192     -0.31880287      0.85128530

 -0.67523563      0.07531701     -0.32460033      3.27337787
 -0.57753269      0.57576628     -0.37346717     -0.32013614
  0.77117329     -0.15990049     -0.40155640     -0.18908392
 -0.67673999      0.21932926     -0.43341767     -0.96231358
  0.03770777      0.42871341     -0.44505304      9.99645881
 -0.17171771      0.68152922     -0.46373011     -0.60699076
  0.21874576     -0.52358814     -0.48427753      3.77953017
  0.32870861     -0.34171071     -0.49563800     -7.84618829
 -0.43467166      0.54528630     -0.49844390     -0.85707527
  0.47632593     -0.13390025     -0.49976093      4.42485218

  0.62184335      0.01273509     -0.50065194     -1.61500429
  0.05076759     -0.67203700     -0.53900134     -0.46724169
  0.41014376      0.42596269     -0.64109066      0.56258590
  0.26090032     -0.32027211     -0.70808931      2.11506792
 -0.32122637     -0.24158864     -0.70957275      1.33252599
 -0.24253066     -0.16490348     -0.72971651     -2.12208208
 -0.46701659     -0.02820318     -0.74769976     -0.38115210
  0.09868695      0.16935682     -0.78628617      2.04588850
 -0.18731348      0.13814358     -0.82455419     -0.69503138
  0.03458882     -0.26183815     -0.84798774      0.34626674

  0.0             0.0             0.0            -1.12478271
  0.0             0.0             0.00232198947 -66755021.95
  0.0             0.0            -0.00466249241 -33244978.05
  0.0             0.0             0.0            100000000.00
```

Table 3: POEM-L1 normalized coefficients (unit of 10^{-6}), C_{20} includes permanent tide

N	M	C	S	N	M	C	S
2	0	-484.162270		3	0	0.9528	
4	0	0.5225		5	0	0.0488	
6	0	-0.1307		7	0	0.0945	
8	0	0.0437		9	0	0.0364	
10	0	0.0497		11	0	-0.0535	
12	0	0.0236		13	0	0.0507	
14	0	-0.0073		15	0	-0.0054	
16	0	0.0046		17	0	-0.0012	
18	0	0.0019		19	0	0.0150	
20	0	0.0031					
2	1	-0.0000	0.0021	2	2	2.4411	-1.3984
3	1	2.0333	0.2487	3	2	0.9052	-0.6159
3	3	0.7187	1.4135	4	1	-0.5394	-0.4733
4	2	0.3402	0.6555	4	3	0.9904	-0.2004
4	4	-0.1886	0.3096	5	1	-0.0678	-0.0967
5	2	0.6519	-0.3301	5	3	-0.4454	-0.2128
5	4	-0.2885	0.0434	5	5	0.1781	-0.6646
6	1	-0.0591	0.0219	6	2	0.0778	-0.3450

6	3	0.0645	0.0031	6	4	-0.0855	-0.4732
6	5	-0.2672	-0.5392	6	6	0.0079	-0.2366
7	1	0.2882	0.1134	7	2	0.3282	0.1164
7	3	0.2451	-0.2105	7	4	-0.2838	-0.1045
7	5	0.0273	0.0457	7	6	-0.3587	0.1521
7	7	0.0084	0.0217	8	1	-0.0136	0.0706
8	2	0.0680	0.0597	8	3	-0.0107	-0.0915
8	4	-0.2429	0.0714	8	5	-0.0151	0.1028
8	6	-0.0660	0.3130	8	7	0.0663	0.0795
8	8	-0.1232	0.1308	9	1	0.1563	0.0067
9	2	0.0077	-0.0362	9	3	-0.1719	-0.1111
9	4	-0.0222	-0.0045	9	5	-0.0283	-0.0547
9	6	0.0572	0.2395	9	7	-0.1046	-0.1024
9	8	0.2014	-0.0073	9	9	-0.0635	0.0775
10	1	0.1059	-0.1308	10	2	-0.0855	-0.0268
10	3	-0.0292	-0.1582	10	4	-0.0921	-0.0521
10	5	-0.0654	-0.0213	10	6	-0.0390	-0.0829
10	7	0.0232	0.0160	10	8	0.0257	-0.0587
10	9	0.1050	-0.0345	10	10	0.1205	-0.0240
11	1	0.0140	-0.0077	11	2	0.0346	-0.0892
11	3	-0.0483	-0.1231	11	4	-0.0451	-0.0704
11	5	0.0716	0.0541	11	6	-0.0042	0.0387
11	7	0.0173	-0.0692	11	8	0.0258	0.0045
11	9	-0.0267	0.0220	11	10	-0.0435	0.0142
11	11	0.0407	-0.0728	12	1	-0.0783	-0.0513
12	2	-0.0045	0.0042	12	3	0.0460	-0.0058
12	4	-0.0427	-0.0269	12	5	0.0528	0.0142
12	6	-0.0068	0.0358	12	7	-0.0242	0.0271
12	8	-0.0197	0.0005	12	9	0.0225	0.0120
12	10	-0.0040	0.0611	12	11	0.0099	-0.0066
12	12	-0.0119	-0.0038	13	1	-0.0466	0.0167
13	2	0.0253	-0.0462	13	3	-0.0082	0.0532
13	4	-0.0247	-0.0063	13	5	0.0377	0.0382
13	6	-0.0259	-0.0020	13	7	0.0103	-0.0143
13	8	-0.0216	0.0065	13	9	0.0131	0.0278
13	10	0.0097	-0.0130	13	11	-0.0077	-0.0119
13	12	-0.0026	0.0646	13	13	-0.0531	0.0540
14	1	-0.0093	0.0266	14	2	-0.0219	0.0133
14	3	0.0448	-0.0058	14	4	-0.0308	-0.0022
14	5	0.0222	-0.0026	14	6	-0.0017	-0.0193
14	7	0.0028	-0.0261	14	8	-0.0418	-0.0156
14	9	0.0238	0.0157	14	10	0.0305	0.0145
14	11	0.0203	-0.0201	14	12	0.0060	-0.0411
14	13	0.0142	0.0320	14	14	-0.0460	0.0058
15	1	0.0054	-0.0033	15	2	-0.0126	-0.0155
15	3	0.0053	0.0064	15	4	-0.0268	0.0053
15	5	-0.0114	0.0099	15	6	0.0094	-0.0393
15	7	0.0389	0.0224	15	8	-0.0301	0.0104
15	9	0.0043	0.0161	15	10	0.0044	-0.0033
15	11	-0.0023	0.0029	15	12	-0.0202	-0.0047
15	13	-0.0197	0.0069	15	14	-0.0040	-0.0114
15	15	0.0022	-0.0021	16	1	0.0092	0.0016
16	2	-0.0111	0.0295	16	3	0.0078	-0.0016
16	4	0.0391	0.0064	16	5	-0.0226	-0.0051

16	6	-0.0072	-0.0080	16	7	0.0018	-0.0054
16	8	-0.0020	-0.0034	16	9	-0.0071	-0.0227
16	10	-0.0094	0.0092	16	11	0.0134	-0.0014
16	12	0.0155	0.0049	16	13	0.0069	-0.0049
16	14	-0.0308	-0.0248	16	15	0.0024	-0.0097
16	16	-0.0136	0.0003	17	1	-0.0109	-0.0152
17	2	0.0068	0.0048	17	3	-0.0161	0.0109
17	4	0.C025	0.0176	17	5	-0.0106	0.0003
17	6	-0.0088	-0.0130	17	7	0.0090	0.0046
17	8	-0.0045	0.0092	17	9	-0.0068	-0.0149
17	10	0.0138	0.0007	17	11	-0.0115	-0.0035
17	12	0.0173	0.0113	17	13	0.0030	0.0261
17	14	-0.0198	0.0185	17	15	0.0023	0.0053
17	16	-0.0091	0.0039	17	17	-0.0247	-0.0028
18	1	-0.0058	-0.0152	18	2	0.0026	-0.0033
18	3	-0.0075	0.0002	18	4	0.0172	0.0049
18	5	0.0108	0.0188	18	6	0.0029	-0.0023
18	7	-0.0008	-0.0005	18	8	0.0168	-0.0052
18	9	-0.0133	0.0042	18	10	-0.0022	-0.0036
18	11	-0.0059	0.0153	18	12	-0.0243	-0.0162
18	13	-0.0051	-0.0126	18	14	-0.0174	0.0015
18	15	-0.0298	-0.0095	18	16	0.0035	-0.0018
18	17	0.0010	-0.0019	18	18	-0.0160	-0.0083
19	1	-0.0098	0.0024	19	2	0.0018	0.0025
19	3	-0.0107	-0.0091	19	4	-0.0063	-0.0041
19	5	-0.0076	-0.0108	19	6	-0.0062	0.0146
19	7	0.0019	0.0041	19	8	0.0086	0.0035
19	9	0.0014	0.0040	19	10	-0.0076	-0.0068
19	11	0.0084	0.0144	19	12	-0.0056	0.0030
19	13	-0.0112	-0.0201	19	14	0.0028	-0.0166
19	15	-0.0114	-0.0087	19	16	-0.0079	-0.0154
19	17	0.0100	0.0006	19	18	0.0158	0.0007
19	19	-0.0010	-0.0050	20	1	0.0037	-0.0030
20	2	0.0017	0.0035	20	3	0.0011	0.0099
20	4	0.0028	-0.0083	20	5	-0.0009	0.0045
20	6	0.0051	0.0013	20	7	-0.0071	-0.0009
20	8	-0.0023	0.0002	20	9	0.0008	0.0062
20	10	-0.0095	-0.0046	20	11	0.0029	-0.0130
20	12	-0.0048	0.0106	20	13	0.0022	0.0020
20	14	0.0025	-0.0113	20	15	-0.0006	0.0000
20	16	-0.0018	-0.0067	20	17	-0.0057	-0.0009
20	18	-0.0015	0.0071	20	19	0.0066	0.0007
20	20	0.0056	0.0009				

Table 4: Orbital fit rms values for 4 months LAGEOS data in
dependence of the gravity field model and the arc
length. First value: all stations, in brackets: only 3rd
generation stations.
Additionally adjusted: station coordinates, empirical
acceleration (15 days), pole coordinates and LOD
(5 days)

model	5-days arcs	15-days arcs	30-days arcs
POEM-L1	7.6 (6.0)	8.9 (7.7)	10.9 (9.9)
GEM-T1	7.4 (5.8)	8.5 (7.3)	10.6 (9.6)
GEM-L2	7.9 (6.5)	8.9 (7.8)	10.5 (9.6)
GRIM 3B	10.1 (9.0)	11.5 (10.7)	15.0 (14.3)

Table 5: Station coordinate comparisons between different
gravity field models from 4 months test data.
The rms value after a 7-parameter transformation is
shown (unit centimeters)

	arc length [days]	GEM-T1 arc length [days] 5 15 30			GEM-L2 arc length [days] 5 15 30			GRIM 3B arc length [days] 5 15 30		
POEM-L1	5 15 30	3.0	3.1	3.6	3.3	3.9	4.5	6.2	6.0	6.2
GEM-T1	5 15 30		———		2.2	2.5	2.4	5.9	5.7	6.1
GEM-L2	5 15 30		———			———		6.5	6.6	7.1

Table 6: Station coordinate comparisons from 4 months test data within different gravity field models. Coordinate sets obtained with different arc lengths (left side) and by further division of the data into two subsets (right side). The rms values after a 7-parameter transformation are shown (unit: centimeters).

Model	4 months data			months 6+14 versus months 7+15		
	5-days arcs versus 15-days arcs	5-days arcs versus 30-days arcs	15-days arcs versus 30-days arcs	arc length (days)		
				5	15	30
POEM-L1	1.9	3.2	2.1	6.4	6.3	7.3
GEM-T1	1.8	3.2	2.3	6.4	6.1	7.2
GEM-L2	1.9	3.9	2.6	6.3	6.6	8.4
GRIM 3B	2.2	3.7	3.1	7.7	7.4	8.7

Table 8: Undulation differences between different models up to degree 5 (without zonal terms). rss-values in centimeters.

	GEM-T1	GEM-L2	GRIM 3B	GRIM3-L1	PM2/70G	GEM 10
POEM-L1	14.1	16.5	36.6	33.1	33.8	31.7
GEM-T1	-	12.0	30.0	27.1	31.3	28.2
GEM-L2	-	-	31.6	30.2	31.3	26.9
GRIM 3B	-	-	-	26.6	47.4	44.3
GRIM3-L1	-	-	-	-	50.7	47.3
PM2/70G	-	-	-	-	-	16.0

Table 7: Comparisons of different gravity field models up to 5,5
with the most recent GEM-T1 model. Error estimations
σ for some models published by the authors of these
models are added. (Point mass models corrected for
permanent tide (k_2=0.29)). Units: 10^{-10}. Sign.:model
minus GEM-T1

N M	GEM-T1 C	S	σ T1	L2	GR3-L1	POEM-L1 ΔC	ΔS	GEM-L2 ΔC	ΔS	GRIM 3B ΔC	ΔS	GRIM3-L1 ΔC	ΔS	PM2/70G ΔC	ΔS	GEM 10 ΔC	ΔS
2 0	-4841650		0	3	10	+67		0		+21		+36		+73		-4	
3 0	9572		0	1	5	-44		+5		+ 9		0		-15		+12	
4 0	5387		10	10	10	-162		+26		+42		+72		+97		+24	
5 0	688		0	10	10	-200		+ 4		+28		+39		-37		-2	
2 1	0.0	0.0	0	10	–	0	+20	-1	+10	0	0	0	0	-35	-2	+10	-24
2 2	24389	-13998	0	10	10	+22	+14	-10	+ 7	+31	+4	+9	+9	-79	+4	-49	+8
3 1	20297	2496	10	30	60	+35	- 9	- 9	+ 1	-37	-20	+13	-17	+88	+12	-12	+24
3 2	9035	-6204	10	20	40	+16	+45	+ 5	+44	+117	+92	+85	-13	-90	-37	-108	-30
3 3	7210	14132	10	30	50	-22	+ 4	+22	+20	+ 91	+58	+135	+56	-196	-26	-207	-7
4 1	-5334	-4751	10	30	30	-59	+18	-18	+88	+ 17	+19	-26	-48	-139	+81	-18	+59
4 2	3470	6640	20	40	70	-68	-85	+76	-32	- 88	+75	-43	+17	+4	+38	+51	0
4 3	9910	-2006	10	20	40	- 6	+ 2	+23	-21	+ 72	-47	+44	-26	-25	-37	-25	-12
4 4	-1900	3085	10	20	30	+14	-11	-21	-14	+ 35	-30	+7	+4	-33	-36	-53	-96
5 1	-590	-955	30	40	100	-88	-11	+49	+ 4	+227	+121	+11	+92	+57	-9	+78	+17
5 2	6558	-3234	30	60	120	-39	-66	-48	-72	- 71	+140	-234	+161	+64	-39	-43	-43
5 3	-4482	-2151	20	50	100	+28	+23	-18	+23	+ 75	+215	-166	+21	-167	+106	-189	+121
5 4	-2948	524	20	40	90	+63	-90	+32	-28	-111	+42	-92	+114	+11	-23	+73	-25
5 5	1777	-6660	20	40	70	+ 3	+15	+ 2	+53	+ 49	-31	+66	-8	-289	+109	-216	+62
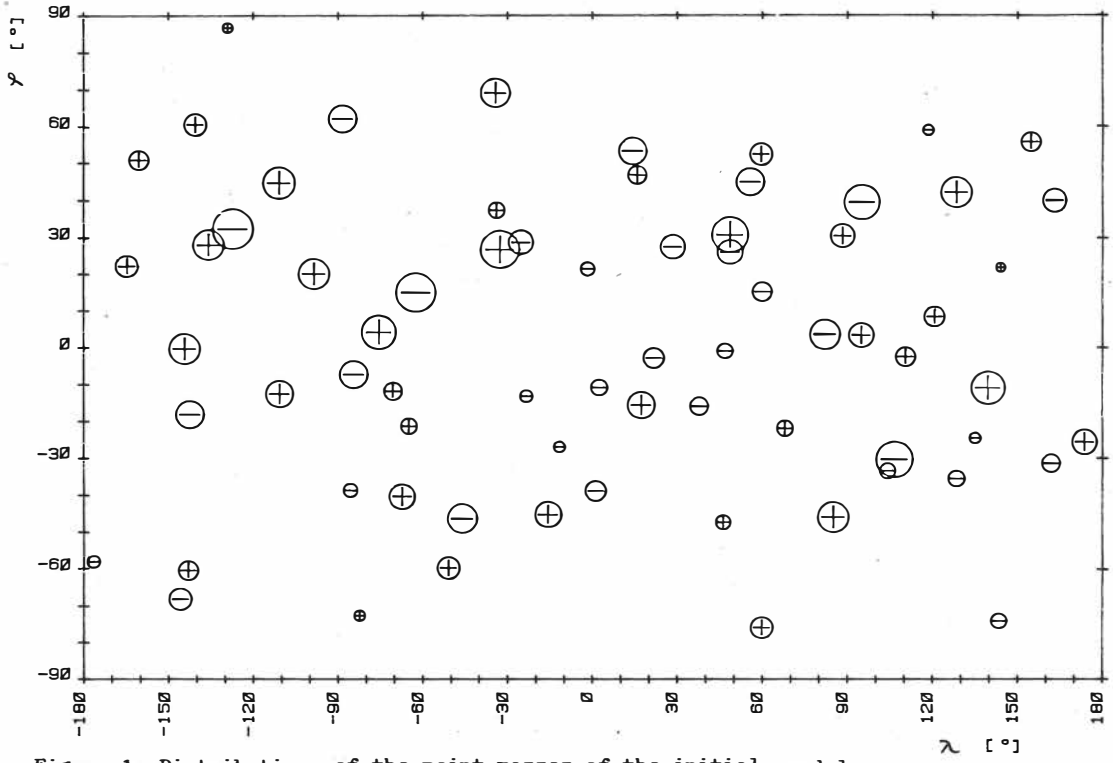
Figure 1: Distribution of the point masses of the initial model PM2/70G (from BARTHELMES 1986)

Figure 2: Power spectra of the models GEM 10 (o) and PM2/70G (●)

Figure 3: Spectrum of the eigenvalues of the normal equation matrix for point masses without (●) and with (o) normalization of the matrix
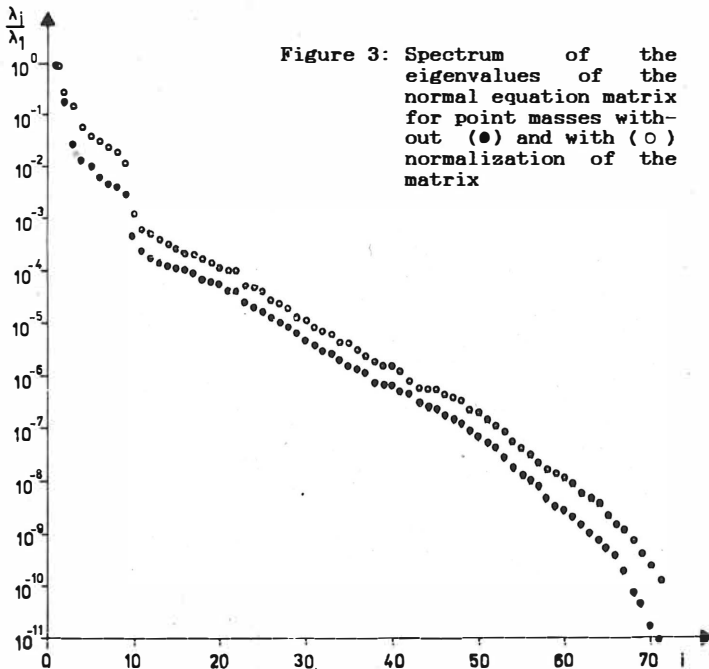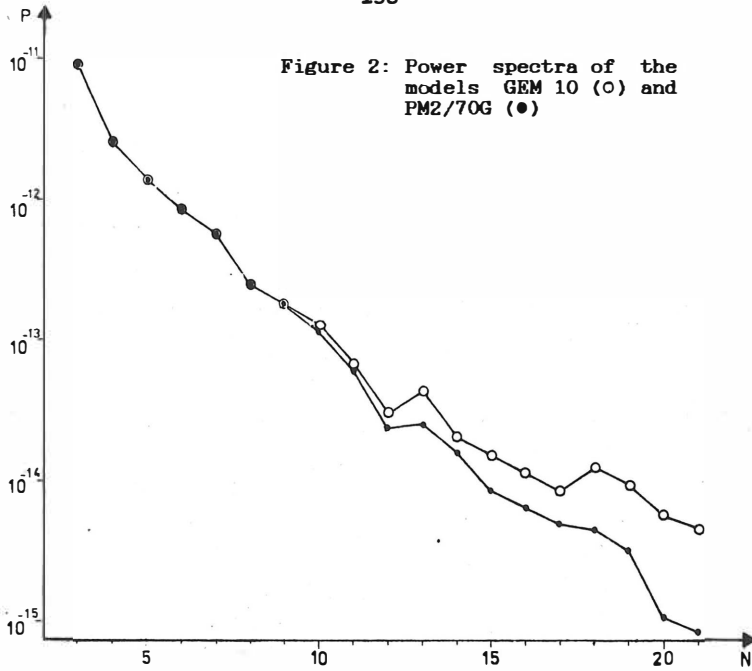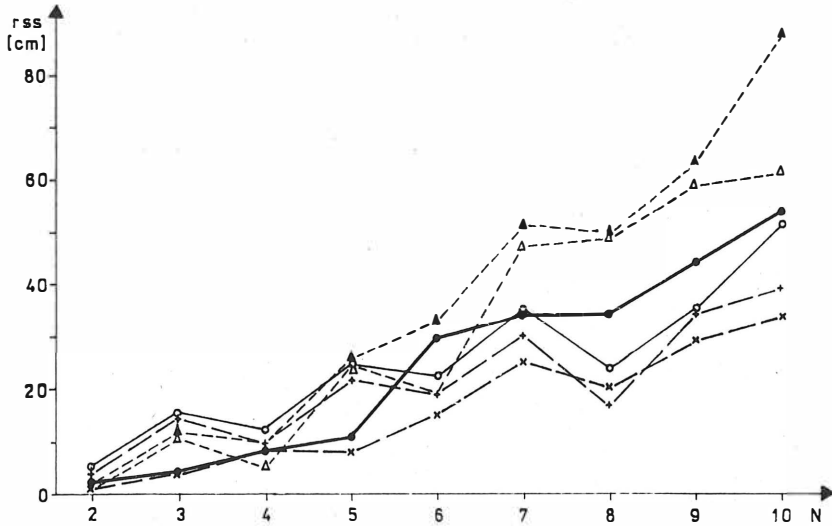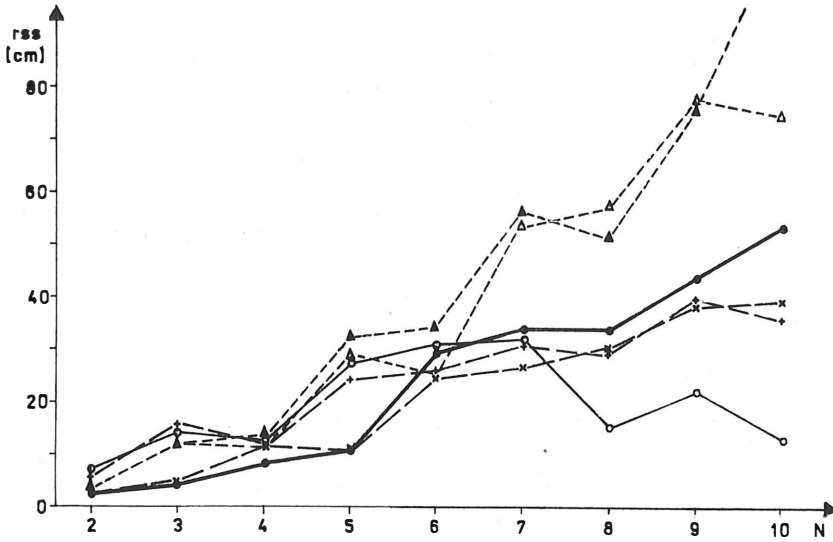
Figure 4 and Figure 5: Geoid undulation differences per degree N (without zonal part) between POEM-L1 (top) resp. GEM-T1 (bottom) and GEM-T1 resp. POEM-L1 (●), PM2/70G (o), GEM-L2 (×), GEM 10 (+), GRIM 3B (▲) and GRIM3-L1 (△)

APPLICATION OF FFT TO FREE AIR ANOMALIES WITH LITHOSPHERIC SIGNAL FOR MODELING THE DISTURBING GRAVITY POTENTIAL

M. Doufexopoulou[x] and J. Czompó[xx]

Summary

Free. air anomalies with lithospheric signal were used
to compute 2D power and amplitude spectra which were aver-
aged to receive isotropic (radial) ones, for the purpose
to estimate the effect of lithospheric sources in terms
of the harmonic expansion degree n. This estimation was
done assuming the simple anomaly degree variance model $A/_{n}x$.
The estimated parameter x (exponent) of the model, shows
dependence on the location of the data windows used for the
FFT. In the best case, this model can be applied until .
n=360, but the computed values of x are 3 times higher than
in the Tscherning-Rapp model (x=1). This result is compared
with the same modeling but through a local covariance func-
tion derived in the space domain. Both results agree con-
sidering the different data manipulation in each case. The
deviation from Tscherning-Rapp model is discussed. The
spectral information of the used data set is limited due to
the lithospheric sources at various depths and to the lim-
ited length data window, as it can be confirmed in the am-
plitude spectra where the noisy part starts at n=1000. The
results confirm previous investigations in the same area
and promote a mass modeling, instead of the use of a low
degree spherical harmonic model, to combine with local data
for the purpose to model the disturbing potential.

[x] Higher Geodesy Lab. of N.T.U. Athens, 9, H.Polytechniou,
157-73 Zographou, Greece

[xx] Geodetical and Geophysical Research Institute of the Hungarian
Academy of Sciences, H-9401 Sopron, P.O.B. 5, Hungary

Introduction

Modeling of the disturbing gravity potential is needed
in geodesy and geodynamics, mainly to assist at accurate
positioning. In the related models the assumption of a
stochastic mass distribution in the interior of the earth
is kept. The average gravity field spectra show an exponen-
tial form of decay when the frequency (or the degree of
expansion in terms of spherical harmonics) increases. The
global/local structure of the gravity field is represented
by the degree variances of the different gravity field
quantities. Degree variance modeling had been restricted
mainly to the low part of the spectrum of gr. field quan-
tities (e.g. Tscherning-Rapp 1974, Moritz 1976). The auto-
covariance of gravity anomalies had been used to fit the
rest of the spectrum for a predefined structure of the
degree variance model. The structure of degree variances
describes the speed of decrease of the spectrum for high
degrees of expansion in spherical harmonics. These degrees
represent the local structure of the gravity field.

The frequency domain methods for the analysis of
gravity field data are used in geodesy (e.g. Forsberg 1984,
Schwarz 1985) in spite their extended use in geophysics
with other potential fields (Spector and Grant 1970, Hahn,
Kind, Mishra 1976). These methods include the Fourier ex-
pansion for periodic data and the Fourier transform for
random data. The FFT (Fast Fourier Transform) technique is
suitable to analyse data belonging to the anomalous gr.
field because an evaluation of the information about the
local structure can be done. However the FFT technique is

mostly used for the high frequency part of the spectrum
mainly for two reasons:
- The best known and most influencing the signal, gravity
  field sources are located within the upper lithosphere.
- The increasing accuracy of instrumentation and of the
  space positioning techniques require the refined gr. field
  modeling at the high frequency part of its spectrum.

In the present work a set of about 6000 F.A anomalies
5'x5' in gridded form is used to compute 2-D (and average
radial) power and amplitude spectra. The radial spectra are
used to estimate the speed of decrease of the power when
the degree of expansion in spherical harmonics increases
for harmonics degree 70-350. This speed is expressed with
the power to which the harmonic degree is raised, in a
simple degree variance model. The (radial) amplitude spectra
can be used in order to estimate the depth difference of the
dominant sources which produce the local gr. field and to
receive an estimate of the harmonic degree, beyond which the
signal is due to noise. This data set belongs to East
Mediterranean part (Greece-Aegean), an area which is highly
oomplicated in the tectonic pattern. Within it, major tec-
tonic sources occur like:

The sinking lithospheric slab of African plate which
creates the Aegean trench with F.A anomalies at the level
of -200 mgal. The mean slab length is estimated to be
~ 250 km (Paparachos and Comninakis 1971).

The continuation of the Alpine fold to South-East
Europe which produces large Moho depths ($\sim$48 km) in the
continental North-middle part of the region (Makris 1977).
Various microplates and faults are also occuring in this
area.

The purpose of these numerical estimations is to re-
ceive a picture whether this tectonic background can have
an effect upon the analytic local gravity field modeling,

i.e. to investigate deviations from available degree vari-
ance models like e.g. Tscherning'-Rapp's (1974) and meaning-
ful results for degree variance decay can be received only
for degrees up to 360. Due to the limited extend of the area
(6^0), the F.T of Δg can give information beyond the degree
70 of a spherical harmonic expansion. However it is of inter-
est to mention some earlier investigations in the same area
concerning lower degrees than 1=70. The investigations were·
done in space domain.

A comparison among GEM10B, GRIM3B, GRM3L1 and OSU81 models
with the same set of local data in space domain showed that the
referencing of local data to any model increases the variabil-
ity of the residuals $\Delta g_r = \Delta g_{Model} - \Delta g_{F.A}$ in terms of in-
homogeneity of the Δg field. This increasing of variability
starts since 1=20 and achieves its highest value around n=45
(Doufexopoulou-Papafitsorou 1986). This result is confirmed
recently (Doufexopoulou-Paradissis 1988) with the use of ac-
curate doppler undulations and the OSU81 model, independently
of the grav. field data.
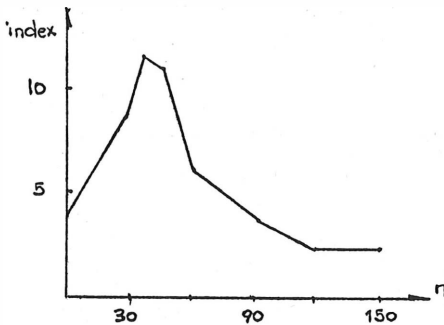
Fig. 1.

Planar approximation is used not only because the area
is small ($6^0 \times 6^0$) but also because the expedted signal is

much stronger than the corrections for a spherical earth
(Jordan 1978). Also, no gravity field model is subtracted
from the data as it is wished to keep the original informa-
tion. If any long wavelengths are present, they will not
affect the decrease of the power at higher (l > 70) degrees.
However, spectral leakage cannot be avoided due to this
treatment.

Frequency information of the gravity field

The degrees of a spherical harmonic expansion of
gr. field are related to the law, medium and high frequency
information as:

$$2 < l < 36 \quad \text{low}$$
$$37 < l < 360 \quad \text{medium}$$
$$361 < l < 3600 \quad \text{high}$$

(e.g. Schwarz 1985). The anomalous potential T and gravity
anomalies Δg have different behaviour in the corresponding
spectra, as it can be seen in the following table (derived
for the global behaviour of these functionals):

Table 1

Functional	low %	medium %
T (or N)	99.2	0.8
Δg	22.5	41.9

% information of the gr. field spectrum for low and medium part and
for the disturbing potential T and grav. anomalies Δg.

The high frequency part of Δg contains still 37 % of in-
formation. A frequency analysis of Δg to resolve informa-
tion about the medium and high part depends on the following
factors: data density, overall coverage, data accuracy.

Additionally, the "weighting" between the global and local
information for the gr. field modelling depends on how much
of the total spectral power of the grav. anomaly field is
contained in a solution of a sph. harmonic expansion (model)
and on how "good" is the approximation given by a specific
model of sph. harmonic coefficients.

The power spectrum of the gravity field. - Degree variances

The power spectrum of a potential field expressed in a
spherical harmonic expansion, is given by the (numerical)
coefficients of the expansion. For the disturbing potential
of the earth's gravity field, the spectral estimate for the
degree n of expansion is given:

$$\sigma_n^2 = \sum_{m=0}^{n} (\bar{C}_{nm}^2 + \bar{S}_{nm}^2) \tag{1}$$

where σ_n^2 is the degree variance of the disturbing poten-
tial and $\bar{C}_{nm}^2$, $\bar{S}_{nm}^2$ are the harmonic coefficients used as
orthogonal base functions, for the expansion. The plot of
the σ_n^2 from n = 2 gives the power spectrum of the disturb-
ing potential. The harmonic coefficients $\bar{C}_{nm}$, $\bar{S}_{nm}$ differ
between various spherical harmonic models. In addition, the
sph. harmonic models exist for degrees of expansion which
belong to the low and medium frequency in formation. However,
most of the currently used models are of degree 36 (e.g.
GEM10B) or of degree 180 (e.g. OSU81, GEM10C). Higher ex-
pansion models also exist. Therefore the computation of the
degree variances σ_n^2 is based mainly on the modelling of
the behaviour of the sph. harmonic coefficients. The first
attempt of this modelling is Kaula's rule (1966):

$$\sigma_n^2 = (2n+1) (10^{-5}/n^2)^2 \tag{2}$$

Other approach is of Tscherning-Rapp (1974) etc. For degrees
n > 60 this rule gives higher power than which the spherical
harmonic models give(Fig. 2). The corresponding degree
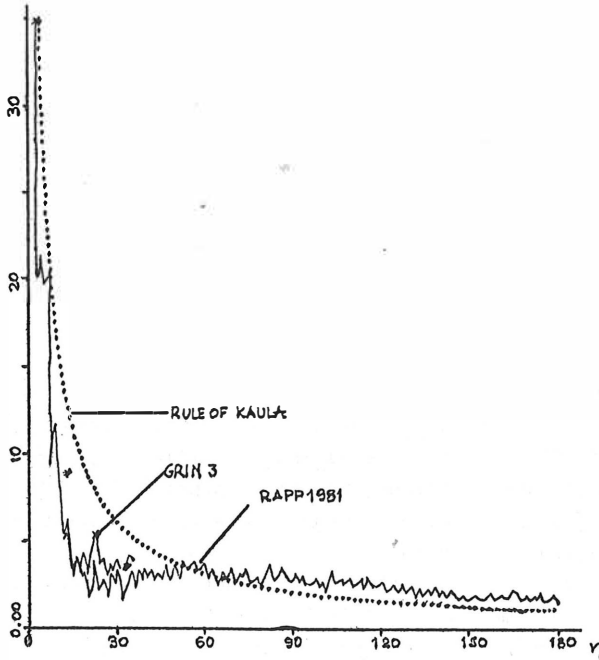
Fig. 2. Kaula's rule and degree variances 6_n^2 for Rapp 81 and GRIM3
models

variances for the gravity anomaly Δg, the anomaly degree
variances c_n^2, are related to 6_n^2 with (Meissl 1971):

$$c_n^2 = R^2(n-1)^2 \, 6_n^2 \qquad (3)$$

It is evident that since the more frequently used gravity

field quantity is the gravity anomaly, degree variance
modeling starts from the anomaly degree variances. For this
modeling, a basic assumption should be valid: The spherical
harmonic coefficients for the various degrees of expansion
are uncorrelated. The consequence of this assumption is
obvious: On the sphere the Δg or T quantities are inde-
pendent of the azimuth i.e. the operations:

$$ M \left\{ \Delta g \right\} \quad \text{or} \quad M \left\{ T \right\} \tag{4} $$

on the surface of the sphere, have meaning.

The spectrum of a quantity can be received with one
of two methods:
- As the Fourier transform of its covariance function.
- As the square of the functional quantity expressed in the
  frequency domain.

The covariance function of the disturbing potential T
can be received following its definition:

$$ K_{TT} = M \left\{ T(p), T(Q) \right\} \tag{5} $$

where T(P), T(Q) is the disturbing potential at the points
P, Q. The expansion of Eq. (5) in Legendre polyonyms is:

$$ K_{TT} = \sum_{n=2}^{\infty} \sigma_n^2 \, P_n(\cos\psi) \tag{6} $$

ψ is the spherical distance between points.

When the assumption Eq. (4) is valid, Eqs (6) and (1)
(for each n) form a Fourier pair. There is equivalence of
the Fourier transform pairs between the spherical and
planar case which is only formal.

Any change in the spectrum or in the covariance function
(isotropic) on the sphere is expressed through the change of

the degree variances.

Fourier transform and its meaning in grav. field modeling

The spectral analysis of a functional series of data in time or space domain is done with a) Fourier series expansion (for periodic data) and b) with the Fourier transform (for random data).

The direct Fourier transform (spectrum) of $\Delta g(x)$ is given:

$$S_{gg}(f) = \int_{-\infty}^{\infty} \Delta g(x)\, e^{-j2\pi fx}\, dx \qquad -\infty < f < \infty \qquad (7)$$

where $\Delta g(x)$ is a function (e.g. gravity anomaly) in space domain

      f is the frequency (cycles/unit of distance)

      $j = \sqrt{-1}$

$$e^{\pm 2\pi fx} = \cos(2\pi fx) \pm j\,\sin(2\pi fx) \qquad (8)$$

$S_{gg}(f)$ is the power spectrum of $\Delta g(x)$.

If $S_{gg}(f)$ is known, $\Delta g(x)$ can be expressed by the inverse Fourier transform:

$$\Delta g(x) = \int_{-\infty}^{\infty} S_{gg}(f)\, e^{j2\pi fx}\, df \qquad -\infty < x < \infty \qquad (9)$$

The sets Eqs (7) and (9) form a Fourier transform pair in the continuous case:

$$\Delta g(x) \longleftrightarrow S_{gg}(f) \qquad (10)$$

The spectrum of the disturbing potential can also be represented by a pair of the form (10):

$$T(\vartheta,\lambda) = \sum_{n=0}^{N} \sum_{m=0}^{n} (\bar{C}_{nm} \cos m\lambda + \bar{S}_{nm} \sin m\lambda) \, \bar{P}_{nm}(\cos\vartheta) \qquad (11)$$

$$T_{gg}(m,n) = \left\{ \begin{array}{c} C_{nm} \\ \bar{S}_{nm} \end{array} \right\} = \sum_{n=0}^{N-1} \sum_{m=0}^{2N-1} \bar{P}_{nm}(\cos\vartheta) \left\{ \begin{array}{c} \cos m\lambda \\ \sin m\lambda \end{array} \right\} T(\vartheta,\lambda) \, \Delta_{kl} \qquad (12)$$

where Δ_{kl} is the grid spacing (discrete function) of the $T(\vartheta,\lambda)$ values. The corresponding covariance function $T_{gg}(\psi)$ (ψ = radial distance) is also expressed in terms of the spectrum (6_n^2) (see Eq. (6)). Thus,

$$K_{gg}(\psi) \longleftrightarrow T_{gg}(\psi) = 6_n^2 \qquad (13)$$

For flat earth approximation, the circular frequencies ($\omega = 2\pi f$) of a radial (isotropic) spectrum are related to the degree n of a spherical harmonic expansion:

$$\omega = \frac{n + \frac{1}{2}}{R} \qquad (14)$$

where R is the mean earth radius (Forsberg 1984, Schwarz 1985). The degree variances of the disturbing potential 6_n^2 are related to those of the gravity anomaly through Eq. (3) (spherical approximation), through the degree n of the spherical harmonic expansion by a factor n^{-2}. But since the degree variances c_n^2 or 6_n^2 are the coefficients of the corresponding covariance function expanded in Legendre polynoms ((6) for the c.f. of disturbing potential) the knowledge of the spectrum of gravity anomalies, permits the estimation of the anomaly degree variances c_n^2 because:

$$C_{gg}(\psi) \longleftrightarrow S_{gg}(n) = c_n^2 \qquad (15)$$

The modeling of the anomaly degree variances can be done if it is adopted that they show a decrease when the degree n increases. This decrease is expressed as exponent of the degree n like e.g. in a model:

$$c_n^2 = \frac{A}{n^x} \qquad (16)$$

where A and x are parameters. This model has been used in Schwarz (1985). From these two parameters A is a scaling one, related to the variance of the field (and to the variance of the covariance function). The x (exponential) is more important because it is related to the speed with which the infinite series of type (6) converges to a closed analytical expression. Its physical meaning is related to the wavelengths which dominate in the field under investigation. Taking the logarithms of Eq. (16):

$$2 \ln c_n = \ln A - x \ln n \qquad (17)$$

For known n and c_n (derived by the spectrum), the parameters A, x are estimated with a simple regression adjustment.

From the model c_n^2 one can shift to the model for σ_n^2 by taking into consideration:

$$\sigma_n^2 \sim n^{-2} c_n^2 \sim n^{-2} \frac{A}{n^x} \sim \frac{1}{n^{x+2}} \qquad (18)$$

Relation (18) can give an approximate model of potential degree variances.

Application of the FFT to the local data set

The total data file consists of a matrix 84x72 mean Δg values (Fig. 3). From this set, four data windows were selected. These windows are full 64x64 matrices for a 2-D FFT.

Fig. 3. Area covered by the total data set 84x72 matrix of
F.A anomalies

The three have the same latitudes on the rows but from each ·
to ⼧he next, a shift of 10 columns ($\sim$ 85 km) is done, from
west to east. The fourth window is located in the longitude
of the second one, but there is a shift of 10 rows to the
north.

The 2-D amplitude and power spectra were averaged and
the isotropic (radial) corresponding spectra were evaluated
at the frequency (wavenumber) $(n+\frac{1}{2}/R)$. The amplitude spectra
were received in semilogarithmic form for further investiga-
tions and only marginally will be refered here.

The four isotropic power spectra were used to derive
the power x with which a model of type (16) for the anomaly
degree variances,decreases when the expansion degree n in-
creases. The part of the modeled power spectrum (degree
variances modeling) is between n=70 to, at maximum, n=350.
Numerical results are presented in the following table and
in Fig. 4.

Table 2. Results for the anomaly degree variance model (16)

Window	Modeled degrees n	Value of exponent x	RMS
GRW1A	n=70-210	5.91	0.7 (12%)
GRW2A	n=70-280	3.83	0.39 (7.6%)
GRW3A	n=70-350	3.20	0.80 (25%)
GRW5A	n=70-420	3.86	0.70 (18%)
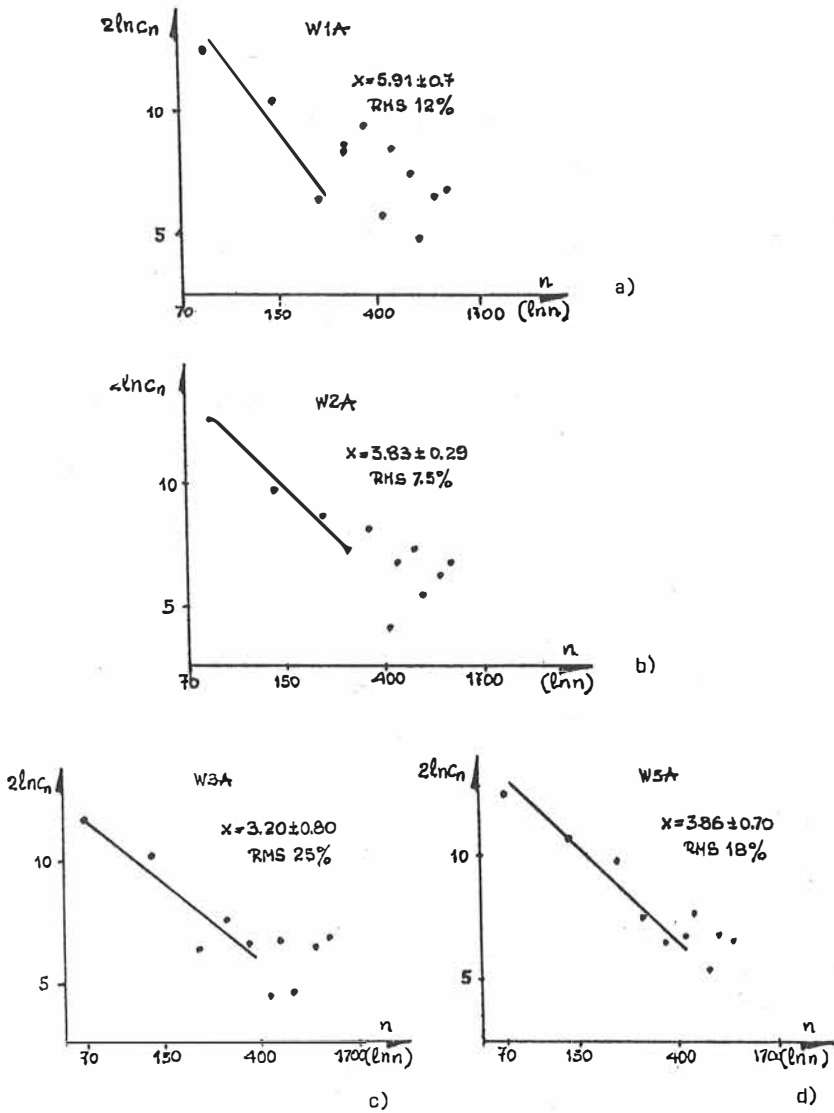
Fig. 4. Linear fit of anomaly degree variances to the power spectra of F.A Δg

From this table it can easily observed that the values of x
and the RMS of estimated x, vary considerably within one
part of the area to the nearest one. Thus, a common x value
for the total area <u>can't be adopted.</u>

The averaged amplitudes represent spectra (log A-f,
Fig. 5) which show straight line segments decreasing when
the frequency increases. In all the four amplitude spectra
these segments are two. Beyond this part, the noisy part of
the spectrum starts <u>at a degree n$\geq$ 1000 in a spherical</u>
<u>harmonic expansion.</u> This behaviour of the log. amplitude
spectrum occurs when sources at different depths exist. The
greater depth sources are stronger while the spectrum due
to the upper layer dips more gently. The layers at all
frequencies produce amplitudes as well as the noise does.
The waves with greater amplitude are undisturbed by smaller
waves but the smaller waves are hidden by the stronger ones
(Ciancara and Marcak 1976).

Comparison with the spectrum derived from a local covariance
flot earth model

In earlier investigations (1984) with the same data
set, a local covariance function was computed: The 5'x5'
mean F.A Δg's were averaged to 15'x15' mean values. Then
the file was referenced to the spherical harmonic model
GEM10B (n=36). The final data matrix was used to compute a
2-D local covariance function. The c.f. inspite the crude
low pass and high pass filtering (averaging and referencing
to GEM10B) was anisotropic (Fig. 6). This c.f. was made
isotropic (radial) by averaging the covariance values at
8 azimuths and for distances up to 2ξ where ξ is the
correlation distance parameter.

The final isotropic c.f. was fitted to Gauss, 2d order
Markov, Hirvonen and the simple exponential, local models.

AMPL. LOG 10 AVERAGE OF GRV1S ; FFT 2D OF GRV1 ; WINDOW ROW=9-72, COLUMN=1-64
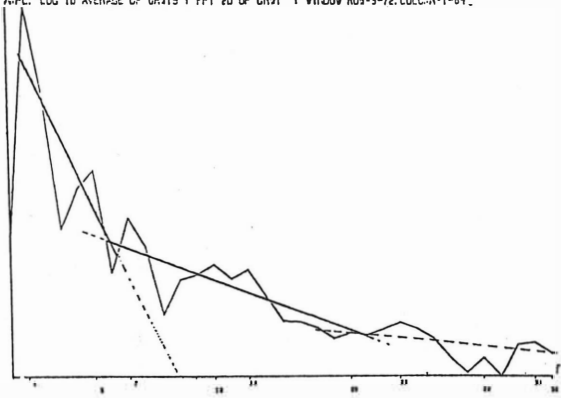
AMPL. LOG 10 AVERAGE OF GRV2S ; FFT 2D OF GRV2 ; WINDOW ROW=9-72, COLUMN=9-72
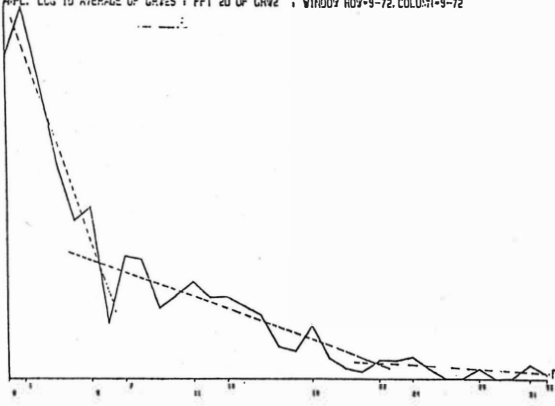
AMPL. LOG 10 AVERAGE OF GRV3S ; FFT 2D OF GRV3 ; WINDOW ROW=9-72, COLUMN=21-84
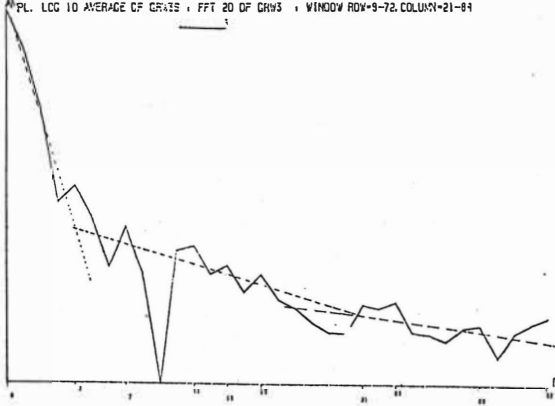
AMPL. LOG 10 AVERAGE OF GRVS : FFT 2D OF GRV9   : WINDOW ROW-1-32, COLUMN-27-58
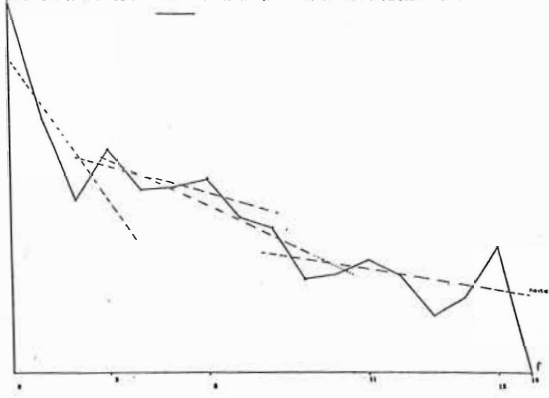
AMPL. LOG 10 AVERAGE OF GRVSS : FFT 2D OF GRVS   : WINDOW ROW-1-54, COLUMN-11-74
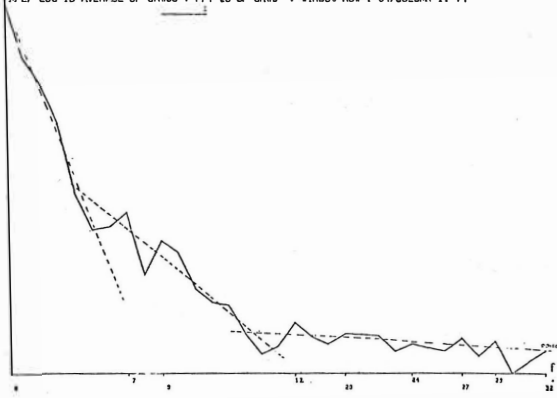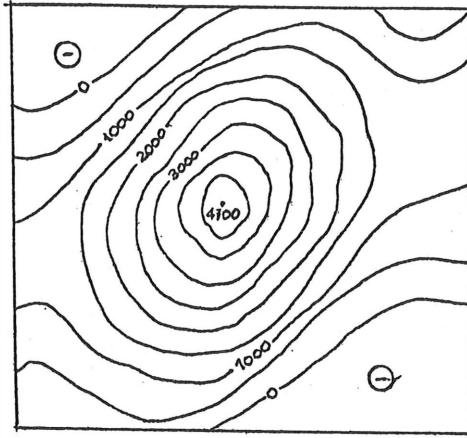
Fig. 6. 2-D covariance function in the study area. 5'x5' mean F.A anom-
alies used. Reference to FEM10B model. Estimated representation
of information in harm. degree n=36-720 (Doufexopoulou 1984)

The best fit (considering up to 1.5ξ distances for fit-
ting (e.g. Schwarz 1980)) was for the exponential model:

$$C(\psi) = 5080 \exp(-\psi/64.4) \tag{19}$$

The Fourier transform of this exponential function is
(Bäth 1974, p. 92):

$$e^{-ax} \longrightarrow \frac{2a^2}{(a^2+\omega^2)} \qquad \text{with } a = \frac{1}{64.4} \tag{20}$$

The spectrum $\frac{2a^2}{a^2+\omega^2}$ is a simple Markov process. The "model"
spectrum of (19) when (20) is considered and with the sub-
stitution $\omega = n+\frac{1}{2}/R$, becomes:

$$S_{gg}(n) \sim \frac{2R^2}{R^2+(n+1)^2\beta^2} \qquad \beta = a^{-1} \tag{21}$$

For spectrum (21) the anomaly degree variances c_n^2 for
n=70,140 ... 350 were computed, assuming again the simple
model (16). The value of the exponent x was found in the
straight line fit:

$$x = 2.60$$

Thus a local anomaly degree variance model up to n=350
behaves as

$$n^{-2.6}$$

when n increases.

Concluding remarks

The exponent values received via the FFT (radial)
power spectrum of gravity anomalies (Table xx) for n=350
are very big and vary after the location of the data
windows. The spectrum computed from the model covariance
gives also a big number (2.6) for the exponent of the same
anomaly degree variance model (relat. 16). The global
anomaly degree variance models of Kaula or Tscherning-Rapp
(1974) assume x=1.

The numbers in this work deviate largely also from
similar computations reported in Schwarz (1985) for the
Canadian area and for higher sph. harmonic degrees
n > 1000 (1.6±0.13 for flat areas and 1.16±0.23 for moun-
tainous areas). It can be stated that the area of applica-
tion shows an average exponent x=3.2 for the medium degrees
of sph. harmonic expansion n=70-360. This speed is very
fast and for potential degree variances can be more faster
(from relation (3)).

This result can be explained only when attention is
paid to the lithospheric structure of this area. In fact
in a limited area a variety of depth sources acts upon

the gravity anomaly field. The effect of shallower sources
is hidden due to the deeper ones in the corresponding
spectra, which practically give not detailed information
about the local grav. field structure in analytic form for
n > 360. The found (approximate) exponent 3.2 of the de-
creasing power in an anomaly degree variance model is 3
times bigger than in the model of Tscherning-Rapp. This
result is in accordance with the earlier result
(Doufexopoulou and Barbaroussi 1983) where local geoid
undulations referenced to GEM10B (n=36) model gave an RMS
of δN differences 3 times bigger than the RMS (δN) com-
puted with Kaula's and Tscherning-Rapp model.

The application of FFT to extract information on the
high frequency part of the gr. field spectrum (n > 360)
can be used only when the local data set is referenced to
a low degree model. For this purpose a mass model can be
more effective than existing sph. harmonic models. Finally
the careful consideration of the amplitude spectra can
support to the construction of the mass model.

References

Bäth,M. (1974): Spectral analysis in geophysics. Elsevier
  Co. New York.
Bracewell,R. (1965): The Fourier transform and its applica-
  tions. McGraw Hill, New York.
Ciancara,B., Marcak,H. (1976): Interpretation of gr. anomalies
  by means of local power spectra. Geoph. Prospecting, 24,
  273-286.
Doufexopoulou,M. (1984): Study of the local gravity field
  in Greece for the geoid approximation. Ph.Thesis, N.T.U.
  Athens (in Greek).
Doufexopoulou,M., Barbaroussi,V. (1983): Geophysical aspects
  of local gr. field data analysis. XVIII General Assembly

IUGG/IAG, Hamburg.

Doufexopoulou,M., Papafitsorou,A. (1986): Inversibility of
  geopotential model for local gravity field approximation.
  IAG Symposium "Figure and dynamics of the Earth, Moon and
  other planets", Prague, Czechoslovakia.

Doufexopoulou,M., Paradissis,D. (1988): Doppler undulations
  and local gravity field in Greece. Presented at the Int.
  Conference "Integrated Geodesy", Sopron, Hungary, May 1988.

Forsberg,R. (1984): Local covariance functions and density
  distributions. O.S.U. Report, No. 356, Department of Geo-
  detic Science, Columbus, Ohio.

Jordan,S.K.(1978): Fourier Physical Geodesy. Report No.
  AFGL-TR-78-0056, Reading, Massachussets TASC.

Hahn,A., Kind,E.G., Mishra,D.C. (1976): Depth calculation
  of magnetic sources by means of Fourier amplitude spectra.
  Geophysical Prospect, 24, 287-308.

Makris,I. (1977): Geophysical Investigations of the Hellenides.
  Ed. Hamburg University, 28-43.

Meissl,P. (1971): A study of covariance functions related
  to the Earths disturbing potential. Report No. 151.
  Department of Geodetic Science, O.S.U. Columbus, Ohio.

Papazachos,D., Comninakis, . (1971): J.G.R. Vol. 76, No. 35.

Spector,A., Grant,F.S. (1970): Statistical models for in-
  terpreting aeromagnetic data. Geophysics, 35, 293-302.

Schwarz,K.P. (1985): "Data types and their spectral properties"
  in Proceedings of Beijing intern. Summer School on "Local
  gravity field approximation", China.

Tscherning,C.C., Rapp,R.H. (1974): Closed covariance
  expressions for gravity anomalies geoid undulations and
  deflections of the vertical implied by anomaly degree
  variance models. O.S.U. Report No. 208.

ON THE THEORY OF THE GEOID DETERMINATION IN CONTINENTAL AREAS

P. Holota

Research Institute of Geodesy, Topography and Cartography
250 66 Zdiby 98, Praha-východ, Czechoslovakia

Summary

In the paper a free boundary value problem is formulated for the geoid
determination from surface initial data. On the geoid an additional boundary
condition is deduced by means of Green´s identity. The problem is linearized
in a sense of the Fréchet functional derivative. A boundary integral condi-
tion is deduced for the linear perturbation of an initial model of the grav-
ity potential which has to be met on the surface of the model of the geoid.

Резюме

В докладе приводится формулировка краевой задачи с свобод-
ной границей для определения геоида из поверхностных началь-
ных данных. На поверхности геоида выводится дополнительное
граничное условие с помощью тождества Грина. Задача линеаризи-
руется в смысле функциональной производной Фреше. Выводится
граничное условие интегрального типа для линейного возмущения
исходной модели потенциала силы тяжести, которое должно быть
выполнено на поверхности модели геоида.

1. Introduction

The geoid is represented in oceanic areas by the ("mean") see level,
in land regions one would have to regard as "geoid" surface the hypothetical
continuation of the sea level into land. The sea level represents an equipo-
tential surface of the gravity field, its continuation would therefore be
the continuation of the same equipotential surface on land. The principal
departure of the geoid from a spherical shape is due to the rotation of the
Earth around its axis. Moreover, an inspection shows that there is a slight
"pear"-shape present in the geoid.

Gravity, however, is essentially measured only on the surface of (or
above) the ground. If an equipotential surface is to be determined, it is
therefore first of all necessary to continue the gravity field downward to

the geoid surface. Inasmuch as the gravity field depends on the masses present, and the distribution of the latter is somewhat hypothetical, it is seen that the shape of the geoid depends on the model of the subsurface which one envisages.

Apart from the above drawback of the geoid, the traditional definition of the figure of the Earth as the figure of the geoid has not fully lost its importance up to the present time. It is only the principal difficulty of the geoid determination in continental areas which motivates the use of the notion of the quasi-geoid in a rigorous approach to the theory of the figure of the Earth, cf. (Pellinen, 1978, p. 6). The quasi-geoid is uniquely defined (apart from a space shift) through the astrogeodetic, gravimetric and levelling measurements made on the surface of the Earth, it coincides with the geoid on the seas and oceans and it is very close to the geoid in the continental areas.

Paradoxially the gravity field over the oceans has now become far better determined than over many continental regions of the Earth. In oceanographic research the investigation of the geoid, its height variations, steps and slopes, has a very important position. In comparison with the continental areas the shape of oceanic parts of the geoid is known with a relatively high accuracy, particularly due to satellite altimetry and recent developments of space technology. Obviously, there is a desire to extent this degree of accuracy globally and to increase it homogeneously. For that reason and others, new satellite projects have been conceived, e.g. satellite gravity gradiometer mission, to map the detailed gravity field of the Earth independently of whether it be over the oceans or continents.

In this connection one usually speaks about the geoid in terms of its planetary notion. The geoid is taken for a level surface of a potential function which is an extension of the Earth´s external gravity potential inside the Earth, especially inside those parts of the Earth´s body which are given by land topography. Under this extension the harmonic part of the Earth´s external gravity potential is analytically continued inside the Earth and, as a rule, it is expressed by means of a spherical harmonic expansion. Obviously, the gravitational effect of the masses situated between the geoid and the surface of the Earth is ignored in a global approach like this. A pertinent discussion may also be found in (Moritz, 1977).

The geoid is a surface of an important physical meaning and recently new stimulations appeared for a discussion on the materialization of its defini

tion in practice. A relevant reasoning may be found in the IUGG collection
of open problems in geodesy and other branches of geo-science, e.g. in the
contributions by (Grafarend, 1987), (Holota, 1987) and (Moritz, 1987).

Undoubtedly, the geoid has an important position in the geodetic and
geodynamical research, see (Anderson and Cazenave, 1986), (Pellinen, 1978) or
(Kakkuri, 1985). Moreover, the essence of its determination is not typical
for geodesy only. E.g. the investigation of the thermal field inside the lito-
sphere leads to a very similar problem, see (Matyska, 1986). Here an optimal
shape design method has been used to determine the geometry of the bottom of
a solution domain, provided that the temperature and the heat flow are measur-
ed on the Earth's surface and an additional boundary condition is known on the
bottom (and sides) of the solution domain. The analogy with the determination
of the geoid is quite obvious.

A feeling could appear that our aim is to discuss a renaissance of the
theory of the so-called non-regularized geoid. This theory was investigated
by several authors especially in the twenties and thirties, see (Moiseev,
1934), (Malkin, 1935), (Molodensky, 1936, 1945) or also (Neklyudova, 1950)
and (Moritz, 1961). A general review may be found in (Pick, Pícha and
Vyskočil, 1973, Chap. X).

Bearing in mind the reasoning above, we can conclude this somewhat long-
er introduction with a claim that the geoid is an important notion in geodesy,
geophysics and geodynamics and that the refinement of its theory still de-
serves some additional work. A contribution in the mentioned direction is
also the aim of this paper.

2. Initial Data and the Geoid Determination Problem

In our paper we will discuss the problem of the geoid determination
within a continent. We will assume that we know the shape of the surface of
the continent as well as the mass density distribution ρ of the uppermost
layers of the Earth's interior within the continent where the figure of the
geoid has to be determined.

In addition let us recall that at the surface of the continent gravimet-
ric measurements give the length $|G|$ of the gravity vector G and level-
ling combined with gravimetric measurements gives the differential of the
gravity potential W , and thus yields W apart from an additive constant.

We will also assume that the Earth is a rigid body and that our data are de-
purated from luni-solar tidal effects and other temporal variations, so that
our problem is independent of time.

Finally, we will assume that $W_o =$ const. is the given value of the
gravity potential on the surface of the geoid.

To determine the shape of the geoid's segment within a continental area
we have to reconstruct the internal gravity field of the Earth in a necessary
extent. It is obvious that the way which leads to this goal under the above
assumptions, means to solve an initial value problem for Poisson s
equation. However, it is well-known that the solution of the problem like this
does not continuously depend on the data, see an example in (Courant, 1964,
Chap. 2, §6.2). Indeed, we will also show that our study leads to a formula-
tion of a boundary integral condition.

Let D be the domain between the surface of the continent and the sur-
face Γ representing the part of the geoid under consideration. Let ∂D de-
note the boundary of D . Our aim is to determine the geometry of Γ so
that

$$\Delta w = -4\pi k\rho + 2\omega^2 \quad \text{in} \quad D \quad , \tag{2.1}$$

$$w = W \quad \text{on} \quad \partial D - \Gamma \quad , \tag{2.2}$$

$$|\text{grad } w| = |G| \quad \text{on} \quad \partial D - \Gamma \quad , \tag{2.3}$$

and

$$w = W_o \quad \text{on} \quad \Gamma \tag{2.4}$$

where w is the gravity potential, k is Newton's gravitational constant
and ω is the velocity of the Earth's rotation.

Let us note that there are two boundary conditions given on ∂D - Γ in
our formulation above. (2.2) is of the Dirichlet type. However, (2.3) is al-
ready less traditional. Obviously, it represents a non-linear boundary condi-
tion and its application is connected with a number of non-trivial and even
open problems. In general they concern the existence and uniqueness of the
solution of a particualar problem under consideration and also techniques
for its calculation, see (Backus, 1968) but also (Aleksidze, 1987).

Nevertheless, taking into consideration that (apart from the Earth's
rotation) grad w results from gravitational effects of all masses of the
Earth, we can easily verify the well-known fact that the direction of

grad w is very close to the geocentric radial direction. For this and also simplicity reasons we will substitute (2.3) by

$$\partial w/\partial r = - |G| \qquad \text{on} \qquad \partial D - \Gamma \tag{2.5}$$

where $\partial/\partial r$ means the derivative in the direction of the geocentric radius r .

We will suppose, in addition, that Γ may be parametrized by means of the usual spherical coordinates B, L, i.e. by the geocentric latitude and the geocentric longitude, respectively. Let σ be that part of the surface of the (geocentric) unit sphere which corresponds to Γ .

Generally our problem is to find a function $r = r(B,L)$, $B,L \in \sigma$, such that

$$\Delta w = - 4 \pi k \mu + 2 \omega^2 \qquad \text{in} \qquad D \quad , \tag{2.6}$$

$$w = W \qquad \text{on} \qquad \partial D - \Gamma \quad , \tag{2.7}$$

$$\partial w/\partial r = - |G| \qquad \text{on} \qquad \partial D - \Gamma \tag{2.8}$$

and

$$w[\ r(B,L),B,L\ ] = W_o \qquad \text{for} \qquad B,L \in \sigma \tag{2.9}$$

where μ represents a mass density distribution.

(2.6) - (2.9) is a kind of the free boundary value problem. In contrast to the usual situation there is only one boundary condition given on the free part of the boundary (i.e. on Γ) while the known part of the boundary is covered by two boundary conditions. Recall, however, that the problem above is actually a way how to reconstruct from the surface initial data the necessary part of the internal gravity field of the Earth so as to be able to determine the investigated segment of the geoid.

To use the data given in (2.6) - (2.9) for the determination of $r(B,L)$ we will start with Green's third identity. We easily deduce that

$$0 = 4 \pi k \int_D (1/l') \mu \, dD - 2 \omega^2 \int_D (1/l') dD - \int_\Gamma (1/l)\partial w/\partial n' \, dS -$$

$$- \int_{\partial D - \Gamma} [\ (1/l)|G|\cos(n,r) + (W - W_o)\partial(1/l)/\partial n\ ]dS \tag{2.10}$$

where $\underline{n}$ is the outer normal of D , $\underline{n}' = - \underline{n}$ and l (resp. l') is the

distance between the variable point and the computation point of integra-
tion. The latter (we will dentote it by P) belongs to Γ. Obviously,
(2.10) may be takem for a boundary condition for w given on Γ.

3. Linear Problem

We will confine our study of the problem (2.6) - (2.9) to an examina-
tion of the linear equations. Supposing that we have r, W, |G|, w, ∂w/∂r,
μ as above which are smooth and depend smoothly on a parameter t . Denoting
the derivatives with respect to t by a dot, we obtain from (2.6) - (2.10)
that

$$\dot{\Delta w} = - 4 \pi k \dot{\mu} \quad \text{in} \quad D \quad , \tag{3.1}$$

$$\dot{w} = \dot{W} \quad \text{on} \quad \partial D - \Gamma \quad , \tag{3.2}$$

$$\partial \dot{w}/\partial r = - |\dot{G}| \quad \text{on} \quad \partial D - \Gamma \quad , \tag{3.3}$$

$$\dot{w}[r(B,L),B,L] + \dot{r} \, \partial w[r(B,L),B,L]/\partial r = 0 \tag{3.4}$$

for B,L ∈ σ   and

$$0 = 4\pi k \int_D (1/l) \, \dot{\mu} \, dD - 4\pi k \int_\Gamma (\dot{r}/l) \, \mu \, Q^{-1} dS -$$

$$- 2\pi k(\dot{r_p}/r_p) \int_D [1/l + (r_p^2 - z^2)/l^3] \mu \, dD +$$

$$+ 2 \omega^2 \int_\Gamma (\dot{r}/l) \, Q^{-1} dS + \omega^2 (\dot{r_p}/r_p) \int_D [1/l + (r_p^2 - z^2)/l^3] dD -$$

$$- \int_{\partial D - \Gamma} [(1/l)|\dot{G}|\cos(n,r) + \dot{W}\partial(1/l)/\partial n] dS -$$

$$- \int_\Gamma (1/l)(\partial \dot{w}/\partial n') \, dS + (\dot{r_p}/2r_p) \int_\Gamma (1/l)(\partial w/\partial n') dS -$$

$$- (3/2) \int_\Gamma (1/l)(\partial w/\partial n')(\dot{r}/r) dS + F(\partial w/\partial n', r, \text{grad } r, \dot{r}, \text{grad } \dot{r}) \tag{3.5}$$

where the quantities with and without the subscript p are referred to the computation point and the variable point of integration, respectively; z is the length of the position vector of the variable point in the volume integral,

$$F = F(\partial w/\partial n\,',r,\text{grad } r,\dot{r},\text{grad } \dot{r}) =$$

$$= -\int_\Gamma (1/1)(\partial w/\partial n\,')(\dot{r}/r)|\text{grad } r|^2 Q^{-2} dS +$$

$$+ \int_\Gamma (1/1)(\partial w/\partial n\,') \langle \text{grad } r,\text{grad } \dot{r} \rangle Q^{-2} dS +$$

$$+ (1/2) \int_\Gamma (1/1^3)(\partial w/\partial n\,')(\dot{r}/r - \dot{r}_p/r_p)(r^2 - r_p^2) dS \qquad (3.6)$$

with $\langle,\rangle$ denoting the scalar product and

$$Q = (1 + |\text{grad } r|^2)^{1/2} . \qquad (3.7)$$

Obviously, the right hand side of (3.5) is nothing else but the Fréchet functional derivative of the right hand side of (2.10), cf. (Holota, 1976). In addition let us recall that $\dot{r}$ actually expresses a perturbation of the length of the radius vector of the equipotential surface $W_o = $ const. of an adopted model of the gravity field given by the potential w and $\dot{w}$ expresses the corresponding perturbation of w .

Equation (3.5) contains a number of quantities which should be adapted to an initial model adopted in the linearization of our problem. As an illustration we give the following example.

Example. Let us take for the model of w in D the analytical continuation of the external gravity potential of the Earth, provided that it exists. In consequence $W = 0$, $|G| = 0$ and also $\mu = 0$. In case that the mentioned analytical continuation is not possible we will use the Runge property of Laplace equation to approximate the harmonic part of w by a function with a greater domain of harmonicity, see (Bers, John and Schechter, 1964, p. 140). A more ample discussion on this problem may be found e.g. in (Moritz, 1978). Finally, let $\mu = \rho$. Now for the model specified above equation (3.5) attains the following form

$$0 = 4\pi k \int_D (1/\Gamma)\,\rho\,dD - \int_\Gamma (1/1)(\partial w/\partial n')\dot{}\,dS +$$

$$+ (\dot{r}_p/2r_p)\int_\Gamma (1/1)(\partial w/\partial n')dS - (3/2)\int_\Gamma (1/1)(\partial w/\partial n')(r/r)dS \qquad (3.8)$$

where F and the terms multiplied by ω^2 were neglected and

$$\dot{r} = - (\partial w/\partial r)^{-1}\,\dot{w} \qquad \text{on} \qquad \Gamma \qquad\qquad (3.9)$$

in view of (3.4). In addition

$$(\partial w/\partial n')\dot{} = \partial\dot{w}/\partial n' + \dot{r}\,\partial^2 w/\partial n'\partial r \qquad \text{on} \qquad \Gamma \quad, \qquad (3.10)$$

as may be easily verified. Denoting by M the total mass of the Earth and putting approximately

$$w \doteq kM/r \qquad \text{in} \qquad D \quad, \qquad\qquad (3.11)$$

we immediately obtain

$$\partial w/\partial n' \doteq \partial w/\partial r = kM/r^2 \quad, \qquad\qquad (3.12)$$

$$(\partial w/\partial n')\dot{} \doteq \partial\dot{w}/\partial n' + (2/r)\dot{w} \quad. \qquad\qquad (3.13)$$

The substitution in (3.8) yields

$$r_p\dot{w}_p \int_\Gamma (1/r^2 1)dS - 3\int_\Gamma (1/r1)\dot{w}dS + 2\int_\Gamma (1/1)\left[\,\partial\dot{w}/\partial n' + (2/r)\dot{w}\,\right]dS \doteq$$

$$\doteq 8\pi k \int_D (1/\Gamma)\,\rho\,dD \qquad\qquad (3.14)$$

i.e.

$$r_p\dot{w}_p \int_\Gamma (1/r^2 1)dS + \int_\Gamma (1/r1)\dot{w}dS + 2\int_\Gamma (1/1)(\partial\dot{w}/\partial n')dS \doteq$$

$$\doteq 8\pi k \int_D (1/\Gamma)\,\rho\,dD \quad, \qquad\qquad (3.15)$$

Equation (3.15) represents a boundary integral condition for $\dot{w}$ on Γ which together with

$$\dot{w} = 0 \qquad \text{on} \qquad \partial D - \Gamma \qquad\qquad (3.16)$$

and

$$\partial w/\partial r = 0 \quad \text{on} \quad \partial D - \Gamma \tag{3.17}$$

may be used to determine $\dot{w}$ in D so that

$$\dot{w} = - 4\pi k \rho \quad . \tag{3.18}$$

The corresponding $\dot{r}$ is given by (3.9). Obviously, we have a choice which one from the two boundary conditions (3.16) and (3.17) to use in combination with (3.15) for the determination of $\dot{w}$ in D. It is also possible that a common use of (3.16) and (3.17) will be of advantage for a stabilization of the solution in practice. The final reply, however, requires an analysis.

Remark. To have a comparison with literature we will suppose that Γ represents the whole surface of the model of the geoid and that, approximately,

$$r_p \doteq r \doteq R \quad . \tag{3.19}$$

In this case

$$\int_{\Gamma} (1/l)dS \doteq 4\pi R \tag{3.20}$$

and (3.14) turns into

$$\dot{w}_p - (3/4\pi R) \int_{\Gamma} (1/l)\dot{w}dS + (1/2\pi) \int_{\Gamma} (1/l)\left[\partial\dot{w}/\partial n' + (2/r)\dot{w} \right]dS \doteq$$

$$\doteq 2k \int_{D} (1/l') \rho \, dD \quad . \tag{3.21}$$

Formally (3.21) has a structure which is very close to eq. (X-32; 12) from (Pick, Pícha and Vyskočil, 1973) derived by Malkin:

$$T_p - (3/4\pi R) \int_{\Gamma} (1/l)TdS - (1/2\pi) \int_{\Gamma} (1/l) \Delta g_{Pr}dS =$$

$$= 2T_e = 2k \int_{D} (1/l') \rho \, dD \quad . \tag{3.22}$$

Here, in contrast to (3.21), T represents the usual disturbing potential and Δg_{Pr} is Prey´s anomaly which actually eliminates the normal derivative $\partial T/\partial n'$ from (3.22). Although (3.22) is an integral equation for the value of

T on the geoid, its use is not free from serious problems related to the determination of Δg_{Pr} . Equation (3.22) was derived within the theory of the non-regularized geoid which is essentially based on gravity reductions. The gravity reductions depend on the mass distribution which is somewhat hypothetical up to now. This problem has already been discussed many times in the past. In addition, in the computation of the reductions the shape of the geoid and also the gravity field inside the Earth are used prior to their determination. Clearly, without a sound modification having an iteration nature the computations result in a vicious circle.

References

Aleksidze, M.A. (1987) Approximation Methods of Solution of Direct and inverse Problems in Gravimetry. Nauka Publishers, Moscow (in Russian).

Anderson, A.J. and A. Cazenave (1986) Space Geodesy and Geodynamics. Academic Press Inc. (London).

Backus, G.E. (1968) Application of a Non-linear Boundary-Value Problem for Laplace's Equation to Gravity and Geomagnetic Intensity Surveys. Quart. Journ. Mech. and Applied Math., Vol. XXI, Pt. 2, pp. 196-221.

Bers, L.; John, F. and M. Schechter (1964) Partial Differential Equations. John Wiley and Sons, Inc., New York-London-Sydney.

Courant, R. (1964) Partial Differential Equations. Mir Publishers, Moscow (in Russian).

Grafarend, E.W. (1987) Geodesy - Six Problems. A Collection of Contributions to IUGG Symp. Ul - "Quo vadimus", XIXth Gen. Assembly of IUGG, Vancouver, 1987. Publ. Inst. of Theoretical Geodesy, Techn. Univ. Graz, pp. 46-49.

Holota, P. (1976) Determination of the Free Boundary in Potential Theory, the Boundary Problem of Physical Geodesy. Presented at the 3rd Int. Symp. Geodesy and Physics of the Earth, Weimar, 1976. Veröff. d. Zentr. Inst. f. Phys. d. Erde, Teil II, Nr. 52(1977), pp. 269-279.

Holota, P. (1987) Physical Geodesy - Three Problems. A Collection of Contributions to IUGG Symp. Ul -·"Quo vadimus", XIXth Gen. Assembly of IUGG, Vancouver, 1987. Publ. Inst. of Theoretical Geodesy, Techn. Univ. Graz, p. 50.

Kakkuri, J. (1985) Die Landhebung in Fenoskandien im Lichte der heutigen Wissenschaft. ZfV, 110, H. 2, pp. 51-59.

Malkin, N. (1935) Über die Bestimmung der Figur der Erde. Gerl. Beitr. Geoph., 45, p. 133.

Matyska, C. (1986) The Optimal Shape Design Method Applied to Modelling Thermal Thinning of the Oceanic Lithosphere Near Hot Spots. Studia geoph. et geod. 30, pp. 356-375.

Moiseev, N. (1934) Über die Bestimmung der Figur des Geoides der nicht regularisierten Erde. Gerl. Beitr. Geoph., 42, p. 279.

Molodensky, M.S. (1936) On the Reduction of the Gravity to the Sea Level for the Non-regularized Earth. Trudy-Reports of TsNIIGAiK, Vol. 17, Moscow (in Russian).

Molodensky, M.S. (1945) Fundamental Problems of Geodetic Gravimetry. Trudy-Reports of TsNIIGAiK, Vol. 42, Moscow (in Russian).

Moritz, H. (1961) Eine Integralgleichung des Geoids. Gerl. Beitr. Geoph., 70, pp. 373-379.

Moritz, H. (1977) Der Begriff der mathematischen Erdgestalt seit Gauss. AVN, 4, pp. 133-138.

Moritz, H. (1978) On the Convergence of the Spherical-Harmonic Expansion for the Geopotential at the Earth´s Surface. Anno XXXVII - Boll. di Geod. e Sci. Affini - N. 2-3, pp. 363-381.

Moritz, H. (1987) Geodesy - Seven Problems. A Collection of Contributions to IUGG Symp. U1 - "Quo vadimus", XIXth Gen. Assembly of IUGG, Vancouver, 1987. Publ. Inst. of Theoretical Geodesy, Techn. Univ. Graz, pp. 39-41.

Neklyudova, N.F. (1950) On a Method of the Earth´s Figure Determination. Bull. Inst. Theor. Astr., Vol. 4, No. 8(61), p. 408.

Pellinen, L.P. (1978) Higher Geodesy (Theoretical Geodesy). Nedra Publishers, Moscow (in Russian).

Pick, M.; Pícha, J. and V. Vyskočil (1973) Theory of the Earth´s Gravity Field. Elsevier, Amsterdam - Academia Prague.

An overdetermined boundary value problem for a nonspherical
boundary

by

Wolfgang Keller
Dresden University of Technology

Abstract:
Recently, in a number of publications overdetermined BVP are
discussed. In the most cases a spherical boundary surface is
used. This paper is an attempt to treat a overdetermined BVP
for an arbitrary surface. By an imbedding technique the non-
spherical problem is decomposed into a sequence of spherical
BVP. The spherical BVP are solved by an estimation procedure,
based on a Hilbert-space technique.

Zusammenfassung:
Gegenwärtig werden in einer Reihe von Veröffentlichungen
überbestimmte Randwertprobleme diskutiert. In den meisten
Fällen wird eine Kugel als Randfläche benutzt. Dieser Beitrag
ist ein Versuch, ein überbestimmtes Randwertproblem für eine
beliebige Randfläche zu behandeln. Durch eine Einbettungs-
technik wird das nichtsphärische Problem in eine Folge von
sphärischen Randwertproblemen zerlegt. Die sphärischen Rand-
wertprobleme werden durch ein Schätzverfahren gelöst, das
auf einer Hilbertraumtechnik beruht.

The claccical Molodensky problem is one to one. We have two
types of data: gravity and potential and two unknowns: the
gravitational potential outside the earth and the earth's sur-
face.

The progress in space technique, especially GPS, now provides
a good knowledge of the size and the shape of the earth's sur-
face. Consequently the number of unknowns reduces to one. On
the other hand, new kinds of data like gravity gradients or
gradiometer measurements became available. We are confronted
now with an overdetermined boundary value problem (BVP).
There are already a number of publications on this topic. Most
of them use, in the one or the other way, a spherical surface
in order to take advantage of the orthogonality of spherical
harmonics. The good knowledge of the geometry of the earth's
surface is frequently not fully exploited.

This paper is an attempt to discuss the overdetermined BVP for
a nonspherical surface. The problem will be decomposed into a
sequence of overdetermined BVP's for a spherical boundary.
Each of them can be solved by a least-square approach.

The paper consists of three parts. In the first part the
decomposition technique used by us will be illustrated for a
finite-dimensional example. In chapter two, the approach will
be generalized to the infinite-dimensional case. The appli-
cation of this infinite-dimensional approach to our overdeter-
mined BVP yields a sequence of overdetermined BVP's for the
sphere. For each of them the differential operator and the
boundary conditions are the same; only the boundary values
vary from step to step.

Consequently, all these overdetermined BVP's can be solved by
the same method. Here we will apply a least-square approach.
The least-square approach in terms of a Hilbert-space technique
will be given in chapter three.

1. Nonlinear adjustment in the finite-dimensional case

The overdetermined BVP for a nonspherical surface is a non-
linear adjustment problem in an infinite-dimensional space.
It will be treated by an imbedding procedure. In order to
demonstrate how this procedure works, a finite dimensional
anology should be considered before.
Let be

$$F, F_0 : D \subset \mathbb{R}^n \longrightarrow \mathbb{R}^m \quad, \quad m > n \tag{1}$$

$$D - \text{domain},$$

nonlinear mappings. Furthermore let be $y, y_0 \in \mathbb{R}^m$.
Let exist a $x_0 \in \mathbb{R}^n$ such that

$$y_0 = F(x_0) \tag{2}$$

holds. We suppose that a random vector ε

$$E\,\varepsilon = 0 \,, \quad E\varepsilon_i \varepsilon_j = \delta_{ij}\,\sigma_i^2 \,, \quad i,j = 1(1)m \tag{3}$$

exists such that

$$y = F(x) + \varepsilon \tag{4}$$

for a certain $x \in \mathbb{R}^n$ holds.
We are looking for an estimation $\hat{x}$ of x.
The situation can be described as follows: The problem (4)
is an overdetermined problem which we want to solve. In the
"neighbourhood" of (4) there exists a "trivial" problem (2)
with a well known solution x_0.
Now we want to construct an imbedding which gives a conti-
nuous transition from the "trivial" problem to the problem
under consideration. For this imbedding we have to make some
comparatively strong assumptions:

We assume that there exist:

- a stochastical vector field $\mathcal{E}(t)$, analytical on $[0,1]$ with

$$\mathcal{E}(0) = 0, \quad \mathcal{E}(1) = \mathcal{E} \tag{5}$$

- analytical curves $x(t)$, $y(t)$ with

$$x(0) = x_0, \; x(1) = x, \; y(0) = y_0, \; y(1) = y. \tag{6}$$

- a function $H(x, t)$ analytical with respect to x and t
  such that

$$H(x, 0) = F_0(x), \qquad H(x, 1) = F(x) \tag{7}$$

holds.
Finally, we assume that

$$y(t) = H(X(t), t) + \mathcal{E}(t), \qquad t \in [0,1] \tag{8}$$

is valid. We see that for $t = 0$ the problem (8) is identical
with the trivial problem (2) and for $t = 1$ to the problem (4).
We know the solution of (8) for $t = 0$, and what we have to do
is to continue this solution up to $t = 1$.
Please notice that a very simple possibility to construct an
imbedding H is the following:

$$H(x, t) = t F(x) + (1-t) F_0(x),$$
$$y(t) = ty + (1-t) y_0, \; \mathcal{E}(t) = t\mathcal{E}. \tag{8'}$$

But this simple possibility is not necessary the best.
Because all quantities are supposed to be analytical, the
equation (8), can be expanded into a power series with respect
to t:

$$\sum_{\nu=0}^{\infty} y^{(\nu)}(0)\frac{t^{\nu}}{\nu!} = \sum_{\nu=0}^{\infty} \frac{d^{\nu}}{dt^{\nu}}\left[H(x(t),t)\right]\Big|_{t=0} \cdot \frac{t^{\nu}}{\nu!} + \sum_{\nu=0}^{\infty} \mathcal{E}^{(\nu)}(0)\frac{t^{\nu}}{\nu!}. \tag{9}$$

If we compare the coefficients of corresponding powers of t,
we obtain the following equations:

$$\nu = 0 : y_0 = H(x(0),0) = F_0(x_0)$$

$$\nu = 1 : \dot{y} = \frac{\partial H}{\partial x}(x_0,0) \cdot \dot{x} + \frac{\partial H}{\partial t}(x_0,0) + \dot{\varepsilon} \tag{10}$$

$$\nu = 2 : \ddot{y} = \frac{\partial^2 H}{\partial x^2}(x_0,0) \cdot \dot{x}^2 + \frac{\partial H}{\partial x}(x_0,0) \cdot \ddot{x} + 2 \frac{\partial^2 H}{\partial x \partial t}(x_0,0) \cdot \dot{x}$$

$$+ \frac{\partial^2 H}{\partial t^2}(x_0,0) + \ddot{\varepsilon}$$

$$\nu = \dots$$

In the equations (10) and in the following the derivation
with respect to t is denoted by a dot.
As we can see, we have decomposed the nonlinear adjustment
problem (8) into a sequence of linear adjustment problems

$$\nu = 1 : \qquad (\dot{y} - \frac{\partial H}{\partial t}) = \frac{\partial H}{\partial x} \cdot \dot{x} + \dot{\varepsilon}$$

$$\nu = 2 : (\ddot{y} - \frac{\partial^2 H}{\partial x^2} \cdot \dot{x}^2 - 2 \frac{\partial^2 H}{\partial t \partial x} \cdot \dot{x} + \frac{\partial^2 H}{\partial t^2}) = \frac{\partial H}{\partial x} \cdot \ddot{x} + \ddot{\varepsilon} \tag{11}$$

$$\nu = \dots$$

Each of these linear adjustment problems has the same
design-matrix $\partial H / \partial x$, only the left-hand sides vary with ν .
The left-hand sides contain the results obtained in the
previous adjustment steps. Therefore, the linear adjustment
problems (11) can be solved subsequently for $\hat{x}$, $\hat{\ddot{x}}$... and
we obtain

$$x = x_0 + \hat{x} + \frac{1}{2} \hat{\ddot{x}} + \dots \tag{12}$$

We will close this chapter by considering a special case,
which adapts this common procedure to our overdetermined BVP.
Let be A a linear mapping from $\mathbb{R}^n$ to $\mathbb{R}^m$, depending on k
parameters $b_1, \ldots, b_k$. Furthermore, let be b(t) an analyti-
cal curve in $\mathbb{R}^k$ with

$$b\,(0) = b_0, \quad b\,(1) = b \quad . \tag{13}$$

Now let be

$$F_0\,(x) \; := \; (A \circ b_0)\,x, \tag{14}$$

$$F\,(x) \; := \; (A \circ b)\,x \tag{15}$$

and

$$H\,(x(t),\,t) := \; (A \circ b(t))\,x(t). \tag{16}$$

Hereby, the composition of two mappings is symbolized by a o:

$$f \circ g\,(x) \; := \; f\,(g(x)). \tag{17}$$

If we denote the derivation of A with respect to b by a
prime

$$A' \; := \; \frac{\partial A}{\partial b} \tag{18}$$

and the scalar product in $\mathbb{R}^k$ by $(\cdot\,,\cdot)$, we can write the equa-
tions (10) in the following form:

$$\nu = 0 : \quad y_0 = H(x_0,0) = (A \circ b_0)x_0 = F_0(x_0)$$

$$\nu = 1 : \quad \dot{y} = \frac{d}{dt} H(x(t),t)\Big|_{t=0} = \frac{d}{dt}\left[(A \circ b(t))\,x(t)\right]\Big|_{t=0}$$

$$= (A' \circ b_0, \dot{b})\,x_0 + (A \circ b_0)\,\dot{x} \tag{19}$$

$$\nu = 2 : \quad \ddot{y} = \frac{d^2}{dt^2} H(x(t),t)\Big|_{t=0} = \frac{d^2}{dt^2}\left[(A \circ b(t))\,x(t)\right]\Big|_{t=0}$$

$$= ((A'' \circ b_0, \dot{b}), \dot{b})\,x_0 + (A' \circ b_0, \ddot{b})\,x_0$$

$$+ 2\,(A' \circ b_0, \dot{b})\,\dot{x} + (A \circ b_0)\,\ddot{x}$$

In this form the equations are well suited for the application
to the overdetermined BVP.

2. An overdetermined BVP

We now want to adopt the procedure presented in chapter one to
an overdetermined BVP.

Let be

$$
S_o(\lambda,\vartheta) = \begin{bmatrix} R \cos\lambda \, \sin\vartheta \\ R \sin\lambda \, \sin\vartheta \\ R \cos\vartheta \end{bmatrix} \tag{20}
$$

a parameter representation of a sphere with the radius R, and

$$
S(\lambda,\vartheta) = \begin{bmatrix} r(\lambda,\vartheta) \cos\lambda \, \sin\vartheta \\ r(\lambda,\vartheta) \sin\lambda \, \sin\vartheta \\ r(\lambda,\vartheta) \cos\vartheta \end{bmatrix} \tag{21}
$$

a parameter representation of the earth's surface.
We assume that S is continuously covered with gravity data g
and vertical gravity gradients data Γ. The data are supposed
to be already corrected for gravitational and centrifugal
influences. We are looking now for a function V such, that

$$
\Delta V(r,\vartheta,\lambda) = 0 \quad , \quad r > r(\vartheta,\lambda) \quad ,
$$

$$
g(\lambda,\vartheta) = -\frac{\partial V}{\partial r} \circ S(\lambda,\vartheta) + \mathcal{E}_g(\lambda,\vartheta) ,
$$

$$
\Gamma(\lambda,\vartheta) = -\frac{\partial^2 V}{\partial r^2} \circ S(\lambda,\vartheta) + \mathcal{E}_\Gamma(\lambda,\vartheta) \tag{22}
$$

holds. Hereby ε_g and ε_Γ are modelling the measuring errors. Now, we are looking for an estimation $\hat{V}$ of V.

Beside this, we also consider a trivial problem in the "neighbourhood" of (22): Let be

$$g_0 (\lambda, \vartheta) = \mu R^{-2}, \tag{23}$$

μ — constant of gravity · mass of the earth

$$\Gamma_0 (\lambda, \vartheta) = 2 \mu R^{-3}. \tag{24}$$

We are looking for a function V_0 such that

$$\Delta V_0 (r, \vartheta, \lambda) = 0 , \quad r > R$$
$$g_0 = -\frac{\partial V_0}{\partial r} \circ S_0$$
$$\Gamma_0 = -\frac{\partial^2 V}{\partial r^2} \circ S_0 \tag{25}$$

holds. Of course, the solution of (25) is well known

$$V_0 = \mu r^{-1}. \tag{26}$$

Let us now relate these problems to the procedure, presented in chapter one. There is the following correspondence

$$x(t) \triangleq V(r, \lambda, \vartheta; t)$$
$$y(t) \triangleq (0, g(\lambda, \vartheta; t), \Gamma(\lambda, \vartheta; t))^T$$
$$\varepsilon(t) \triangleq (0, \varepsilon_g (\lambda, \vartheta; t), \varepsilon_\Gamma (\lambda, \vartheta; t))^T$$
$$A \triangleq (\Delta , -\frac{\partial}{\partial r} , -\frac{\partial^2}{\partial r^2})^T \tag{27}$$
$$b(t) \triangleq S(t)$$

Inserting these relations in the equations (19), we arrive at

$\nu=1$:

$$\begin{bmatrix} 0 \\ \dot{g} \\ \dot{\Gamma} \end{bmatrix} = \begin{bmatrix} \Delta\dot{V} \\ -\frac{\partial\dot{V}}{\partial r}\circ S_o + (\nabla(-\frac{\partial V_o}{\partial r})\circ S_o, \dot{S}) \\ -\frac{\partial^2\dot{V}}{\partial r^2}\circ S_o + (\nabla(-\frac{\partial^2 V_o}{\partial r^2})\circ S_o, \dot{S}) \end{bmatrix} + \begin{bmatrix} 0 \\ \dot{\varepsilon}_g \\ \dot{\varepsilon}_\Gamma \end{bmatrix} \quad , \quad (28)$$

$\nu=2$:

$$\begin{bmatrix} 0 \\ \ddot{g} \\ \ddot{\Gamma} \end{bmatrix} = \begin{bmatrix} \Delta\ddot{V} \\ -\frac{\partial\ddot{V}}{\partial r}\circ S_o + 2(\nabla(-\frac{\partial\dot{V}}{\partial r})\circ S_o, \dot{S}) + (\nabla(-\frac{\partial V_o}{\partial r})\circ S_o, \ddot{S}) \\ -\frac{\partial^2\ddot{V}}{\partial r^2}\circ S_o + 2(\nabla(-\frac{\partial^2\dot{V}}{\partial r^2})\circ S_o, \dot{S}) + (\nabla(-\frac{\partial^2 V_o}{\partial r^2})\circ S_o, \ddot{S}) \end{bmatrix}$$

$$(29)$$

$$+ \begin{bmatrix} 0 \\ ((\nabla^2(-\frac{\partial V_o}{\partial r})\circ S_o, \dot{S}), \dot{S}) \\ ((\nabla^2(-\frac{\partial^2 V_o}{\partial r^2})\circ S_o, \dot{S}), \dot{S}) \end{bmatrix} + \begin{bmatrix} 0 \\ \ddot{\varepsilon}_g \\ \ddot{\varepsilon}_\Gamma \end{bmatrix} \quad .$$

Obviously, we have

$$\nabla\frac{\partial V_o}{\partial r} = 2\mu \times r^{-4} \quad , \quad \nabla\frac{\partial^2 V_o}{\partial r^2} = 6\mu \times r^{-5}$$

$$(30)$$

$$\nabla^2\frac{\partial V_o}{\partial r} = -\frac{2\mu}{r^4}(I - 4\frac{xx^T}{r^2}) \quad , \quad \nabla^2\frac{\partial^2 V_o}{\partial r^2} = -\frac{6\mu}{r^5}(I - 5\frac{xx^T}{r^2})$$

Inserting (30) in (28), (29), we obtain

$\gamma = 1$:

$$\Delta \dot{V} = 0$$

$$\dot{g} + \frac{2\mu}{R^4}(x, \dot{S}) \quad = -\frac{\partial \dot{V}}{\partial r} \circ S_0 + \dot{\mathcal{E}}_g \, ,$$

$$\dot{\Gamma} + \frac{6\mu}{R^5}(x, \dot{S}) \quad = -\frac{\partial^2 \dot{V}}{\partial r^2} \circ S_0 + \dot{\mathcal{E}}_\Gamma \tag{31}$$

$\gamma = 2$:

$$\Delta \ddot{V} = 0$$

$$\ddot{g} + 2\left(\nabla \frac{\partial \dot{V}}{\partial r} \circ S_0 \, , \, \dot{S}\right) + \frac{2\mu}{R^4}\left(|\dot{S}|^2 - 4\frac{(x, \dot{S})^2}{R^2}\right) = -\frac{\partial \ddot{V}}{\partial r} \circ S_0 + \ddot{\mathcal{E}}_g \, ,$$

$$\ddot{\Gamma} + 2\left(\nabla \frac{\partial^2 \dot{V}}{\partial r^2} \circ S_0 \, , \, \dot{S}\right) + \frac{6\mu}{R^5}\left(|\dot{S}|^2 - 5\frac{(x, \dot{S})^2}{R^2}\right) = -\frac{\partial^2 \ddot{V}}{\partial r^2} \circ S_0 + \ddot{\mathcal{E}}_\Gamma \, . \tag{32}$$

We have a sequence of overdetermined BVP's for the sphere. They are of the following type

$$\Delta U = 0 \, , \quad |x| > R ,$$

$$f_1 = -\frac{\partial U}{\partial r} \circ S_0 + \mathcal{E}_1 \, ,$$

$$f_2 = -\frac{\partial^2 U}{\partial r^2} \circ S_0 + \mathcal{E}_2 \, . \tag{33}$$

In the next chapter we will discuss a procedure that gives an estimation $\hat{U}$ for U.
Before, we will consider an example, to illustrate how our imbedding procedure works.

<u>Example:</u>

Let be

$$r = r(\lambda,\vartheta) = R(1 + \alpha \sin\vartheta), \quad \alpha > 0 \qquad (34)$$

and

$$S = \begin{bmatrix} r(\lambda,\vartheta) \cos\lambda \sin\vartheta \\ r(\lambda,\vartheta) \sin\lambda \sin\vartheta \\ r(\lambda,\vartheta) \cos\vartheta \end{bmatrix} \qquad (35)$$

Obviously, we have taken an ellipsoid for our surface S.
Furthermore, we use a spherical gravitational field.

$$V = \mu r^{-1} \qquad (36)$$
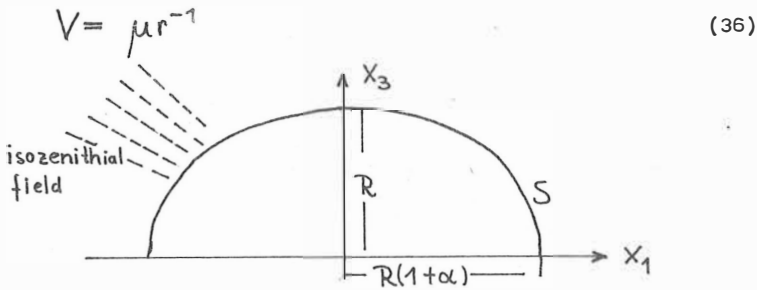
This field produces on S the following boundary values:

$$g(\lambda,\vartheta) = \frac{\mu}{R^2(1 + \alpha \sin\vartheta)^2},$$

$$\qquad (37)$$

$$\Gamma(\lambda,\vartheta) = \frac{2\mu}{R^3(1 + \alpha \sin\vartheta)^3}$$

We use

$$V_o = \mu r^{-1} = V \tag{38}$$

as reference field and construct the following imbedding:

$$g(\lambda,\vartheta;t) = \frac{\mu}{R^2(1+t\alpha \sin \vartheta)^2} \quad)$$

$$\Gamma(\lambda,\vartheta;t) = \frac{2\mu}{R^3(1+t\alpha \sin\vartheta)^3} \quad , \tag{39}$$

$$S(\lambda,\vartheta;t) = \begin{bmatrix} R(1+t\alpha\sin\vartheta) \sin\vartheta \cos\lambda \\ R(1+t\alpha \sin\vartheta) \sin\vartheta \sin\lambda \\ R(1+t\alpha \sin\vartheta) \cos\vartheta \end{bmatrix}$$

Now, we expand this imbedding into power series with respect to t:

$$g(\lambda,\vartheta;t) = g_o(1-2\alpha t \sin\vartheta + 3\alpha^2 t^2 \sin^2\vartheta....)$$

$$\Gamma(\lambda,\vartheta;t) = \Gamma_o(1 - 3\alpha t \sin\vartheta + 6\alpha^2 t^2 \sin^2\vartheta...) \tag{40}$$

$$S(\lambda,\vartheta;t) = S_o(1+t\alpha \sin\vartheta).$$

Herefrom, we can derive $\dot{g}$, $\ddot{g}$, $\dot{\Gamma}$, $\ddot{\Gamma}$, $\dot{S}$ and insert in (31), (32)

$$\nu = 1:$$

$$\Delta\dot{V} = 0 \quad, \quad r > R$$

$$-\frac{2\alpha\mu}{R^2}\sin\vartheta + \frac{2\alpha\mu}{R^2}\sin\vartheta = -\frac{\partial\dot{V}}{\partial r}\circ S_o + \dot{\epsilon}_g \quad, \tag{41}$$

$$-\frac{6\mu\alpha}{R^3}\sin\vartheta + \frac{6\mu\alpha}{R^3}\sin\vartheta = -\frac{\partial^2\dot{V}}{\partial r^2}\circ S_o + \dot{\epsilon}_\Gamma.$$

$\nu = 2:$

$\Delta \ddot{V} = 0 , \ r > R ,$

$$\frac{6\alpha^2 \mu}{R^2} \sin^2\vartheta + \frac{2\mu}{R^4}(R\alpha^2\sin^2\vartheta - 4R^2\alpha^2\sin^2\vartheta) = -\frac{\partial \ddot{V}}{\partial r} \circ S_0 + \ddot{\varepsilon}_\vartheta ,$$

$$\frac{12\alpha^2\sin^2\vartheta \cdot 2\mu}{R^3} + \frac{6\mu}{R^5}(R\alpha^2\sin^2\vartheta - 5R\alpha^2\sin^2\vartheta) = -\frac{\partial^2 \ddot{V}}{\partial r^2} \circ S_0 + \ddot{\varepsilon}_r . \qquad (42)$$

The estimations $\hat{V}$, $\overset{\wedge}{\dot{V}}$ are easily found from (41), (42):

$$\hat{V} = \overset{\wedge}{\dot{V}} = 0 \qquad (43)$$

and we obtain an estimation $\hat{V}$ of second order for V by

$$\hat{V} = V_0 + \overset{\wedge}{\dot{V}} + \frac{1}{2}\overset{\wedge}{\ddot{V}} = V. \qquad (44)$$

Due to the academical nature of our example the estimation
gives the exakt solution.

3. An estimation procedure for a linear overdetermined BVP

3.1. The Hilbert-space $L^2(S_o)$

Let be $L^2(S_o)$ the set of all functions u, defined on the sphere S_o, for which the condition

$$\frac{1}{2\pi R^2} \int_{S_o} u^2 ds < + \infty \tag{45}$$

is fulfilled. We introduce a scalar product $\langle \cdot , \cdot \rangle$ in $L^2(S_o)$ by

$$\langle u,v \rangle := \frac{1}{2\pi R^2} \int_{S_o} u \cdot v \, ds \quad . \tag{46}$$

It can be proved that $L^2(S_o)$ is a Hilbert space with respect to (46). We now construct a complete orthonormal system in $L^2(S_o)$. The functions

$$V_{nm} := \begin{cases} \overline{P}_n^{(m)}(\cos\vartheta) \cos m\lambda \sqrt{\frac{2}{1+\delta_{om}}} & , \ m = 0,1,...,n \\[2em] \overline{P}_n^{(-m)}(\cos\vartheta) \sin m\lambda & , \ m = -n,...,-1 \end{cases} \tag{47}$$

belong to $L^2(S_o)$ for every $n \in \mathbb{N} \cup \{0\}$, $m \in \{-n,...,n\}$.

Furthermore, we have

$$\langle V_{nm} , V_{pq} \rangle = \delta_{np} \delta_{mq} \tag{48}$$
$$n,p \in \mathbb{N} \cup \{0\} \ , \ m \in \{-n,...,n\} , q \in \{-p,...,p\}$$

Consequently, the functions V_{nm} form an orthonormal set in $L^2(S_o)$. It can be proved too, that this set is complete. Occasionally, the following property of the base functions V_{nm} will be used:

$$P_n(\cos\psi) = \frac{2}{2n+1}\sum_{m=-n}^{n} V_{nm}(\vartheta,\lambda) \, V_{nm}(\vartheta',\lambda')$$

(49)

$$\cos\psi = \cos\vartheta\cos\vartheta' + \sin\vartheta\sin\vartheta'\cos(\lambda-\lambda')$$

Each function $u \in L^2(S_o)$ can be developed into a series of these base functions

$$u = \sum_{n=0}^{\infty} \sum_{m=-n}^{n} u_{nm} V_{nm} \, , \quad u_{nm} = \langle u, V_{nm} \rangle$$

(50)

Consequently, for $u, v \in L^2(S_o)$ with

$$u = \sum_{n=0}^{\infty} \sum_{m=-n}^{n} u_{nm} V_{nm} \, , \quad v = \sum_{n=0}^{\infty} \sum_{m=-n}^{n} v_{nm} V_{nm}$$

(51)

the identity

$$\langle u, v \rangle = \sum_{n=0}^{\infty} \sum_{m=-n}^{n} u_{nm} v_{nm}$$

(52)

holds. Now we introduce an isotropic kernel function K

$$K : \begin{cases} S_o \times S_o \longrightarrow \mathbb{R}^1 \\ (\vartheta,\lambda;\vartheta',\lambda') \longmapsto \sum_{n=0}^{\infty} \sum_{m=-n}^{n} k_n \frac{2}{2n+1} V_{nm}(\vartheta,\lambda) V_{nm}(\vartheta',\lambda') \, . \\ k_n > 0 \end{cases}$$

(53)

The kernel K has the following properties

(1) $\quad K(\vartheta,\lambda,\cdot,\cdot) \in L^2(S_0)$

(2) $\quad K(\vartheta,\lambda,\vartheta',\lambda') = K(\vartheta',\lambda',\vartheta,\lambda)$ $\qquad\qquad$ (54)

(3) $\quad K(\vartheta,\lambda,\vartheta',\lambda') = \sum_{n=0}^{\infty} k_n P_n(\cos\psi)$

With the help of the kernel K, we construct a mapping $\bar{K}$ by

$$\bar{K} : \begin{cases} L^2(S_0) \longrightarrow L^2(S_0) \\ \\ u \longmapsto \langle K(\vartheta,\lambda,\cdot,\cdot), u \rangle \end{cases} \qquad (55)$$

Obviously, the mapping $\bar{K}$ is linear and bounded.
Explicitely, we have

$$\bar{K}u = \sum_{n=0}^{\infty} \sum_{m=-n}^{n} k_n u_{nm} \frac{2}{2n+1} V_{nm} \qquad (56)$$

3.2. An estimation procedure in $L^2(S_0)$

Let us now return to our overdetermined BVP.

$$\Delta U = 0 \; , \quad r > R \; ,$$

$$f_1 = -\frac{\partial U}{\partial r} \circ S_0 + \varepsilon_1 \; ,$$

$$f_2 = -\frac{\partial^2 U}{\partial r^2} \circ S_0 + \varepsilon_2 \; . \qquad (57)$$

The idea is the following. If U is harmonic outside the sphere S_o, its restriction u on S_o will belong to $L^2(S_o)$

$$\Delta U = 0, \ r > R \ \Rightarrow \ u := U \circ S_o \ \in \ L^2(S_o)$$

Hence it will be sufficient to get an estimation $\hat{u}$ for the restriction u. From this estimation $\hat{u}$ an estimation $\hat{U}$ can be obtained by Poison's formula.

We now introduce the isotropic kernels

$$L_i := \sum_{n=0}^{\infty} \ell_{i,n} P_n (\cos\psi) \quad , \ i = 1,2 \tag{58}$$

$$\ell_{1,n} = \frac{2n+1}{2R} (n+1) \ , \quad \ell_{2,n} = \frac{2n+1}{2R^2} (n+1)(n+2)$$

$$n \in \mathbb{N} \cup \{0\}.$$

Easily it can be seen, that for $u = U \circ S_o$

$$- \frac{\partial U}{\partial r} \circ S_o \ = \ \langle L_1, u \rangle$$

$$- \frac{\partial^2 U}{\partial r^2} \circ S_o \ = \ \langle L_2, u \rangle$$

holds. If we modell the observation errors ε_i, i = 1,2 by homogeneous isotropic stochastical processes with

$$E\varepsilon_i = 0 \ , \quad E\varepsilon_i \varepsilon_k = C_{ii} \delta_{i,k} \ ,$$

$$C_{ii} = \sum_{n=0}^{\infty} \sigma_{i,n} P_n \ , \quad \sigma_{i,n} > 0 , \ \sum_{n=0}^{\infty} \sigma_{i,n} < + \infty \ , \tag{59}$$

$$i,k = 1,2 \ , \quad n \in \mathbb{N} \cup \{0\} ,$$

we can reformulate our problem as follows:

For an arbitrary a $\in L^2(S_o)$ and for u according to

$$U \in L^2(S_o)$$

$$f_i = \langle L_i, u \rangle + \varepsilon_i \quad , \; i = 1,2 \tag{60}$$

find the best linear unbiased estimation (BLUE)
$\widehat{\langle a, u \rangle}$ for $\langle a, u \rangle$.

We make the following ansatz for $\widehat{\langle a, u \rangle}$:

$$\widehat{\langle a, u \rangle} = \sum_{i=1}^{2} \langle c_i, f_i \rangle \tag{61}$$

and try to determine the $c_i \in L^2(S_o)$, i = 1,2 according to
the BLUE principle.
First of all, we consider the condition of unbiasedness

$$\langle a,u \rangle = E \widehat{\langle a,u \rangle} = E \sum_{i=1}^{2} \langle c_i, f_i \rangle = \sum_{i=1}^{2} \langle c_i, E f_i \rangle$$

$$= \sum_{i=1}^{2} \langle c_i, \langle L_i, u \rangle \rangle \tag{62}$$

$$= \langle \sum_{i=1}^{2} \langle c_i, L_i \rangle, u \rangle.$$

Because this condition has to be fulfilled for every
u $\in L^2(S_o)$, we obtain

$$a = \sum_{i=1}^{2} \langle c_i, L_i \rangle \tag{63}$$

Next, we discuss the condition of minimum variance

$$E\left\{(\sum_{i=1}^{2}\langle c_i, f_i\rangle - E\sum_{i=1}^{2}\langle c_i, f_i\rangle)^2\right\} \longrightarrow \min \tag{64}$$

We have

$$E\left\{(\sum_{i=1}^{2}\langle c_i, f_i\rangle - E\sum_{i=1}^{2}\langle c_i, f_i\rangle)^2\right\}$$

$$= E\left\{(\sum_{i=1}^{2}\langle c_i, f_i - Ef_i\rangle)^2\right\} = E\left\{(\sum_{i=1}^{2}\langle c_i, \varepsilon_i\rangle)^2\right\}$$

$$= E\sum_{i,k=1}^{2}\langle c_i, \varepsilon_i\rangle\langle c_k, \varepsilon_k\rangle \tag{65}$$

$$= \sum_{i=1}^{2}\langle c_i, \langle c_i, C_{ii}\rangle\rangle.$$

Consequently, our minimum variance condition reads:

$$\sum_{i=1}^{2}\langle c_i, \langle c_i, C_{ii}\rangle\rangle \longrightarrow \min \tag{66}$$

The formulae (63) and (66) together lead to the following optimization problem

$$\min_{c_i \in L^2(S_0)} \left\{\sum_{i=1}^{2}\langle c_i, \langle c_i, C_{ii}\rangle\rangle \;\middle|\; \sum_{i=1}^{2}\langle c_i, L_i\rangle = a\right\} \tag{67}$$

We solve this problem by introducing a Lagrange function

$$\phi(c_1, c_2, \lambda) := \sum_{i=1}^{2}\langle c_i, \langle c_i, C_{ii}\rangle\rangle + 2\langle\lambda, \sum_{k=1}^{2}\langle c_k, L_k\rangle - a\rangle \tag{68}$$

Now we are looking for a saddle point. That means, we have to solve

$$0 = \frac{\partial \phi_i}{\partial c_i} = \langle c_i, C_{ii} \rangle + \langle \lambda, L_i \rangle \qquad , \quad i = 1, 2$$

$$0 = \frac{\partial \phi_i}{\partial \lambda} = \sum_{k=1}^{2} \langle c_k, L_k \rangle - a \qquad (69)$$

To solve the normal equations (69), we write them by components

$$\sum_{n=0}^{\infty} \sum_{m=-n}^{n} \left(\frac{2}{2n+1} \sigma_{i,n} C_{i,nm} V_{nm} + \frac{2}{2n+1} \ell_{i,n} \lambda_{nm} V_{nm} \right) = 0$$

$$\sum_{k=1}^{2} \sum_{n=0}^{\infty} \sum_{m=-n}^{n} \frac{2}{2n+1} \ell_{k,n} C_{k,nm} V_{nm} = \sum_{n=0}^{\infty} \sum_{m=-n}^{n} a_{nm} V_{nm} \qquad (70)$$

$$i = 1, 2$$

First, we solve the equations (70) for $c_{i,nm}$

$$C_{i,nm} = - \frac{\ell_{i,n} \lambda_{nm}}{\sigma_{i,n}}$$

$$i = 1, 2 \ , \quad n \in \mathbb{N} \cup \{0\} \ , \quad m \in \{-n, ..., n\}. \qquad (71)$$

Inserting (71) in (70), we obtain

$$\lambda_{nm} = - \frac{2}{2n+1} \frac{a_{nm}}{\sum_{k=1}^{2} \ell_{k,n}^{2} / \sigma_{k,n}} \qquad (72)$$

$$n \in \mathbb{N} \cup \{0\}, \quad m \in \{-n, ..., n\}.$$

and finally

$$c_{i,nm} = - \frac{2n+1}{2} \frac{l_{i,n}}{\sigma_{i,n}} \frac{a_{nm}}{\sum\limits_{k=1}^{2} l_{k,n} / \sigma_{k,n}} \qquad (73)$$

$$i = 1,2 \ , \ n \in \mathbb{N} \cup \{0\} \ , \quad m = \{-n,\dots,n\}$$

Introducing the abbreviations

$$p_{1,n} := \sigma_{2,n} \ , \quad p_{2,n} := \sigma_{1,n} \ , \ n \in \mathbb{N} \cup \{0\}, \quad (74)$$

we can compress (73) to

$$c_{i,nm} = - \frac{2n+1}{2} \ a_{nm} \frac{p_{i,n} \ l_{i,n}}{\sum\limits_{k=1}^{2} p_{k,n} \ l_{k,n}^{2}} \qquad (75)$$

$$i = 1,2 \ , \ n \in \mathbb{N} \cup \{0\} \ , \quad m = \{-n,\dots,n\}$$

This is our final result. We obtained the coefficients $c_{i,nm}$ of the functions c_i, which give the best linear unbiased estimation $\widehat{\langle a, u \rangle}$ for $\langle a, u \rangle$.

A further discussion is possible only for special choices of a. Expecially interesting is the choice

$$a_{nm} = \delta_{nn_o} \ \delta_{mm_o} \qquad n \in \mathbb{N} \cup \{0\} \ , \quad m = \{-n,\dots,n\}$$

$$(76)$$

In this case

$$\langle a, u \rangle = u_{n_o m_o} \tag{77}$$

holds and formula (75) gives the estimation $\hat{u}_{n_o m_o}$ for the coefficient $u_{n_o m_o}$:

$$\hat{u}_{n_o,m_o} = -\frac{\dfrac{P_{1,n_o}(n_o+1)}{R} f_{1,n_o m_o} + \dfrac{P_{2,n_o}(n_o+1)(n_o+2)}{R^2} f_{2,n_o m_o}}{\dfrac{P_{1,n_o}(n_o+1)^2}{R^2} + \dfrac{P_{2,n_o}(n_o+1)^2(n_o+2)^2}{R^4}} \tag{78}$$

To verify this result, at the moment we assume that no measuring error occurs

$$\varepsilon_1 = \varepsilon_2 = 0, \quad p_{1,i} = p_{2,i} = 1$$

$$f_{1,nm} = \frac{(n+1)}{R} u_{nm}, \quad f_{2,nm} = \frac{(n+1)(n+2)}{R^2} u_{nm} \tag{79}$$

$$i = 1,2, \quad n \in INV\{0\}, \quad m = \{-n, \dots, n\}.$$

This leads to

$$\hat{u}_{nm} = \frac{\dfrac{(n+1)^2}{R^2} u_{nm} + \dfrac{(n+1)^2(n+2)^2}{R^4} u_{nm}}{\dfrac{(n+1)^2}{R^2} + \dfrac{(n+1)^2(n+2)^2}{R^4}} = u_{nm} \tag{80}$$

In the case of missing measuring errors the estimation procedure gives the exakt values.

Finally, we want to consider the extreme cases of very good gravity data and very bad gravity gradients and vice versa very bad gravity data and very good gravity gradients. We introduce

$$q_n = \sigma_{1,n} / R^2 \sigma_{2,n} \quad , n \in \mathbb{N} \cup \{0\} \tag{81}$$

and obtain the estimation formulae

$$
\hat{u}_{nm} = \frac{R(n+1)}{(n+1)^2 + q_n(n+1)^2(n+2)^2} \, f_{1,nm}
$$
$$
+ \frac{q_n \, R^2(n+1)(n+2)}{(n+1)^2 + q_n(n+1)^2(n+2)^2} \, f_{2,nm} \tag{82}
$$

$n \in \mathbb{N} \cup \{0\}, \quad m = \{-n, \ldots, n\}$

case 1: $\sigma_{1,n} \gg R^2 \sigma_{2,n}$ (bad gravity data)

$q_n \longrightarrow \infty$

$$
\boxed{
\begin{array}{l}
\hat{u}_{nm} \longrightarrow \dfrac{R^2}{(n+1)^2(n+2)^2} \, f_{2,nm} \\[2mm]
n \in \mathbb{N} \cup \{0\}, \quad m = \{-n, \ldots, n\}
\end{array}
} \tag{83}
$$

case 2: $\sigma_{1,n} \ll R^2 \sigma_{2,n}$ (bad gravity gradients)

$$
\boxed{
\begin{array}{l}
u_{nm} \longrightarrow \dfrac{R}{n+1} \, f_{1,nm} \\[2mm]
n \in \mathbb{N} \cup \{0\}, \quad m = \{-n, \ldots, n\}
\end{array}
} \tag{84}
$$

Formula (84) is basically the well known Hotine-rormula.

Up to now we have an approach to solve an overdetermined
BVP of type (57). Our original problem was of type (22).
In chapter 2 we have decomposed (22) into a sequence of
problems of type (57). If we apply our estimation
procedure on each of these problems we obtain

$$\hat{V}_{nm} = \frac{R(n+1)\left\langle g + \frac{2\mu(x,\dot{S})}{R^4} , V_{nm}\right\rangle}{(n+1)^2 + q_{\frac{}{n}}(n+1)^2(n+2)^2}$$

$$+ \frac{q_n \ddot{R}^2(n+1)(n+2)\left\langle \dot{\Gamma} + \frac{6\mu(x,\dot{S})}{R^4} , V_{nm}\right\rangle}{(n+1)^2 + q_{\frac{}{n}}(n+1)^2(n+2)^2} \qquad (85)$$

$$n \in \{0\} \cup \mathbb{N} , \quad m = -n,\ldots,n$$

$$\hat{\dot{V}}_{nm} = \frac{R(n+1)\left\langle \ddot{g} + 2(\nabla\frac{\partial \hat{V}}{\partial r} \circ S_0, \dot{S}) + \frac{2\mu}{R^4}(|\dot{S}|^2 - \frac{4(x,\dot{S})}{R^2}) , V_{nm}\right\rangle}{(n+1)^2 + q_{\frac{}{n}}(n+1)^2(n+2)^2}$$

$$\qquad (86)$$

$$+ \frac{q_n R^2(n+1)(n+2)\left\langle \ddot{\Gamma} + 2(\nabla\frac{\partial^2 V}{\partial r^2} \circ S_0, \dot{S}) + \frac{6\mu}{R^5}(|\dot{S}|^2 - \frac{5(x,\dot{S})}{R^2}) , V_{nm}\right\rangle}{(n+1)^2 + q_{\frac{}{n}}(n+1)^2(n+2)^2}$$

$$n \in \{0\} \cup \mathbb{N} , \quad m = -n,\ldots,n.$$

4. Conclusions

We have decomposed our overdetermined BVP for an arbitrary
boundary into a sequence of overdetermined BVP's for the
sphere. Each of these spherical BVP's has the same mathemati-
cal structure only the boundary values vary from step to step.
We developed a procedure which gives the best linear unbiased
estimation for the solution of our spherical overdetermined
BVP. Because the solution of the nonspherical overdetermined
BVP is a superposition of the solutions of the spherical over-
determined BVP's, we estimate the solution of the nonspherical
problem by a superposition of the estimates for the solutions
of the spherical problems.
Further investigations should concern the statistical property
of the estimations and the transformation of the estimation
procedure in an integral formula form.
The applied decomposition method works under the above mentio-
ned severe assumptions. If we do not suppose anything, the
implicite function theorem ensures the convergence of the
decomposition for t sufficiently small. For the interesting
case t = 1 about convergence nothing can be said get.

5. References

/1/   Grafarend, E. W.; Schaffrin, B.:
       The overdetermined Geodetic Boundary Value Problem
       In: P. Holota (ed.) Proc. of the Int. Symp. Figure and
       Dynamics of the Earth, Moon and Planets.
       Prague 1986. Monograph Series VUGTK, Research Institute of
       Geodesy, Topography and Cartography, Prague 1987, 185 - 193

/2/   Rummel, R.; Teunissen, P.:
       Geodetic Boundary Value Problem and Linear Inference
       In: Holota (ed.) Proc. of the Int. Symp. Figure and
       Dynamics of the Earth, Moon and Planets.
       Prague 1986. Monograph Series VUGTK, Research Institute of
       Geodesy, Topography and Cartography, Prague 1987, 227 - 264

/3/   Sacerdote, F.; Sanso', F.:
       Overdetermined boundary value problems in physical geo-
       desy. Man. Geod., $\underline{10}$(1985), 195 - 207

/4/   Sacerdote, F., Sanso', F.:
       On the Overdetermined Gravimetry-Gradiometry Problem in
       Physical Geodesy
       In: P. Holota (ed.) Proc. of the Int. Symp. Figure and
       Dynamics of the Earth, Moon and Planets.
       Prague 1986. Monograph Series VUGTK, Research Institute
       of Geodesy, Topography and Cartography, Prague 1987,
       265 - 276

О КАМЕРНОЙ ГРАВИМЕТРИИ

А.В.Копаев, Е.А.Монахов, М.У.Сагитов
Московский Государственный Университет,
Государственный Астрономический институт
им. П.К.Штернберга (ГАИШ МГУ),
отдел гравитационных измерений,
II9899 Москва, Университетский просп., I3

Разработаны теоретические, экспериментальные и вычислительные методы для учёта влияния неоднородности локального гравитационного поля фундаментальных гравиметрических лабораторий на результаты прецизионных гравитационных измерений.

ABOUT THE CHAMBER GRAVIMETRY

A.V.Kopayev, E.A.Monakhov, M.U.Sagitov
Moscow State University,
P.K.Sternberg State Astronomical Institute,
Department of Gravitational Measurements,
119899, Moscow, USSR, University prosp., 13

The theoretical, experimental and calculational methods have been developed for taking into account for the influence of the local gravitational field inhomogeneity of the fundamental gravimetric laboratories on the results of the precise gravitational measurements.

При определении силы тяжести баллистическими и маятниковыми гравиметрами, а также при редукции полученных результатов необходимо тщательно учитывать влияние неоднородности гравитационного поля фундаментальных гравиметрических лабораторий / 6 /. Это является основной задачей камерной гравиметрии - молодой науки, возникшей на стыке гравиметрии с метрологией / 5 /.

Для коррекции и редукции результатов измерений силы тяжести в соответствие с / 2, 5 / необходимо знать приращения силы тяжести относительно марки в некотором объёме пространства над постаментом, а также некоторые вторые производные гравитационного потенциала / 4 / в этом же объёме. Для этого мы разработали специальную методику измерений статическими гравиметрами и вариометрами по пространственной сети точек с использованием методов оптимального планирования / 3 /. Для обработки в качестве аппроксимирующих функций используются гармонические полиномы в комбинации со специальными "параллелепипедальными"функциями /I /. Использование метода наименьших квадратов позволяет сглаживать

шумы измерений и комбинировать гравиметрические данные с варио-
метрическими / 4 /. Создан специальный диалоговый комплекс про-
грамм. Выполнены и обработаны пространственные съёмки в несколь-
ких фундаментальных гравиметрических лабораториях, в том числе
в лаборатории "Лёдово" в окрестности марки № 5035 Международной
опорной гравиметрической сети. Проведенные исследования выявили
значительную неоднородность гравитационного поля над постамента-
ми, а также временные вариации вертикального градиента силы тя-
жести различной периодичности (во всех лабораториях).

Рис. I
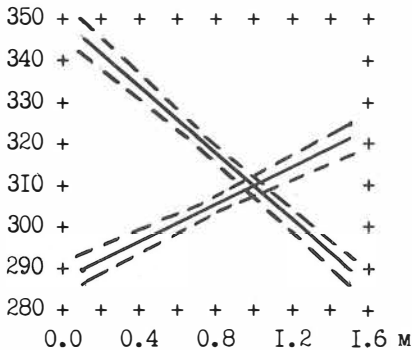
Зависимости вертикального гра-
диента силы тяжести от высоты
для двух пунктов на постамен-
тах лаборатории "Лёдово", раз-
несённых на 2 м. Использованы
только гравиметрические данные.
По вертикали – мкГал/м. Пунк-
тирные линии – 95 %-ные довери-
тельные интервалы.
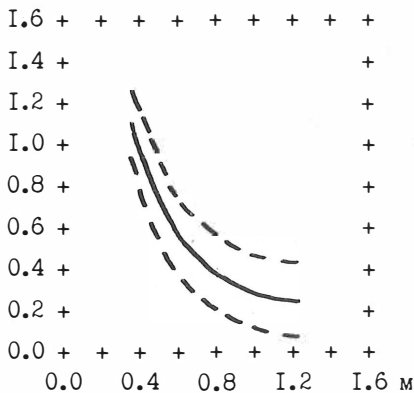
Рис. 2

Детальн. зависимость второго
вертикального градиента силы
тяжести от высоты над маркой
№ 5035 Международной опорной
гравиметрической сети в Лёдово.
Использованы только вариометри-
ческие данные. По вертикали –
Этвеш/см. Пунктирные линии –
95 %-ные доверительные интер-
валы.

Совместная компьютерная обработка пространственных гравимет-
рических и вариометрических съёмок по нашей методике приводит к
построению оптимальной модели гравитационного поля в виде набора
коэффициентов для каждой фундаментальной гравиметрической лабора-

тории. Эта методика уже применяется на пунктах Государственной гравиметрической сети СССР. Нам представляется перспективным предложить использовать её и при создании Международной абсолютной опорной гравиметрической сети.
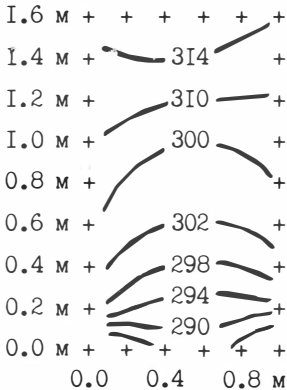
Рис. 3

Вертикальное сечение поля вертикального градиента силы тяжести над основным постаментом лаборатории "Лёдово", проходящее через марку № 5035 Международной опорной гравиметрической сети. Использована комбинация гразиметрических данных с вариометрическими. Изолинии проведены через 4 мкГал/м.

Список литературы:

1. Копаев А.В. Принципы оптимального планирования гравиметрических и вариометрических съёмок над постаментами // Повторные гравиметрические наблюдения.-М.: изд. МГК, 1986.-С. 39-43.

2. Копаев А.В. О влиянии неоднородности гравитационного поля на маятниковые измерения силы тяжести // Геодезия и картография.- 1987.-№ 10.-С. 30-32.

3. Копаев А.В., Штейман М.Б., Леонтьев И.А. О редукции абсолютного значения силы тяжести // Геодезия и картография.-1987.- № 4.-С. 13-15.

4. Монахов Е.А., Харитонов С.В. Результаты измерения второго вертикального градиента силы тяжести с помощью гравитационного вариометра // Повторные гравиметрические наблюдения.-М.: изд. МГК, 1986.-С. 31-38.

5. Сагитов М.У. Влияние неоднородности гравитационного поля помещений на результаты гравитационных экспериментов // Изв. АН СССР, Физика Земли.-1984.-№ 4.-С. 46-59.

6. Сагитов М.У., Копаев А.В., Харитонов С.В. Пространственные редукции при измерении абсолютного значения силы тяжести // Повторные гравиметрические наблюдения.-М.: изд. МГК, 1986.- С. 19-30.

TESTING THE COMPATIBILITY
OF DIFFERENT SETS OF GEOPOTENTIAL COEFFICIENTS

B. Middel & B. Schaffrin
Geodetic Institute, Stuttgart University,
Keplerstr. 11, D-7000 Stuttgart 1,
Federal Republic of Germany

Abstract

The spherical harmonic coefficients of earth's high degree gravity models are
usually determined by a combination of global gravity data (*i.e.* gravity
anomalies and geoid undulations) and the lower coefficients of a satellite
derived model. In this contribution the method of *"robust collocation"* is
applied where spherical harmonics derived from terrestrial observations are
merged with the coefficients of a satellite model. In this solution *incon-
sistencies* between these two data groups can be detected and taken into
account by a special weighting procedure. By comparing the result with the
traditional collocation solution, based on the appropriate *statistical test*,
a sure judgement of the solution becomes possible at a chosen significance
level.

1. Introduction

In the early eighties the permanent improvement of spherical harmonics' ex-
pansions for the Earth's gravity field finally led to high resolution models
such as GEM-10C, OSU 81, GPM-2 or OSU 86F; see, e.g., *F.J. Lerch et al. (1981),
R.H. Rapp (1981), H.G. Wenzel (1985)* and *R.H. Rapp/J.Y. Cruz (1986a,b)*. On
the other hand, the lower degree terms could be derived most accurately from
Satellite Laser Ranging (SLR), thus arriving at models like GEM-L2 or
GRIM-3L1 which *in this part* further improve GEM-10C and GRIM-3/GRIM-3B,
respectively; we particularly refer to *F.J. Lerch et al. (1982; 1985)* and
Ch. Reigber et al. (1985).

In this situation measures are required which enable us to discriminate between the different sets of coefficients with respect to their *quality* and/or *reliability*, thereby allowing us to judge more realistically upon the respective data sources, too. For this purpose, one method had tentatively been introduced by *B. Middel/B. Schaffrin (1987)* proving useful under certain circumstances. In the following we generalize this concept, simultaneously extending it beyond the reasoning of *L.E. Sjöberg (1987)*.

2. Data and Prior Information

Beside the (supposedly most reliable) GEM-L2 coefficients up to degree and order 20 which are described together with their variances in *F.J. Lerch et al. (1982; 1985)* we consider two different data sets for either single or joint combination: namely, 35008 *gravity anomalies* as terrestrial data, and 34380 *geoid heights* derived from SEASAT-1 altimeter data together with their respective standard deviations, both types being mean values in a $1° \times 1°$ grid. In order to get an uniform parametrization we first calculate the corresponding spherical harmonic coefficients up to degree and order $\ell_{max} = 36$ by a simple least-squares adjustment within a *Gauß-Markov Model* of type

$$E\{y_i\} = A_i \xi \quad , \quad D\{y_i\} = \sigma^2 Q_i^{-1} \ . \tag{2.1}$$

Here $i \in \{1,2\}$ denotes the index of the data set which is collected in the observation vector y_i, with the Jacobian matrix A of size $n_i \times m$, n_i being the number of observations ($n_1 = 35008$, $n_2 = 34380$) and m the number of coefficients in the parameter vector ξ ($m = (\ell_{max} + 1)^2 - 4 = 1365$); σ^2 is the variance of unit weight, Q_i the $n_i \times n_i$ a-priori weight matrix while E denotes "expectation" and D "dispersion".
Then we obtain the respective solutions ($i = 1,2$)

$$\hat{\xi}_i = (A_i^T Q_i A_i)^{-1} A_i^T Q_i y_i =: \kappa_i \tag{2.2a}$$

with the *estimated* variance-covariance matrix

$$\hat{D}\{\hat{\xi}_i\} = \hat{\sigma}_i^2 (A_i^T Q_i A_i)^{-1} =: P_i^{-1} \tag{2.2b}$$

where we introduced the estimated variance component

$$\hat{\sigma}_i^2 = (n_i - m)^{-1} (y_i - A_i \hat{\xi}_i)^T Q_i (y_i - A_i \hat{\xi}_i) \ . \tag{2.2c}$$

In addition, we confer the index i = 3 to the *combined solution*

$$\hat{\xi}_3 = (A_1^T Q_1 A_1 + A_2^T Q_2 A_2)^{-1} (A_1^T Q_1 y_1 + A_2^T Q_2 y_2) =: \kappa_3 \tag{2.3a}$$

with the *estimated* variance-covariance matrix

$$\hat{D}\{\hat{\xi}_3\} = \hat{\sigma}_3^2 (A_1^T Q_1 A_1 + A_2^T Q_2 A_2)^{-1} =: P_3^{-1} \tag{2.3b}$$

and the estimated variance component

$$\hat{\sigma}_3^2 = (n_1 + n_2 - m)^{-1} [(n_1 - m)\hat{\sigma}_1^2 + (n_2 - m)\hat{\sigma}_2^2] \tag{2.3c}$$

which nicely follows from the *"addition theorem"* for normal equations.

In order to compare these estimated coefficients with those coming from the GEM-L2 model, we introduce the latter in the form of an *expanded vector* $z := [z_I^T, z_{II}^T]^T$ with the corresponding *error vector* $e := [e_I^T, e_{II}^T]^T$ being distributed as

$$\begin{bmatrix} e_I \\ e_{II} \end{bmatrix} \sim \left(\begin{bmatrix} 0 \\ 0 \end{bmatrix}, \begin{bmatrix} P_\ell & 0 \\ 0 & \lim_{\varepsilon \to 0} \varepsilon I \end{bmatrix}^{-1} \right), \quad \hat{\sigma}_0^2 = 1, \tag{2.4}$$

where the $\ell \times 1$ vector z_I contains the GEM-L2 coefficients up to $\ell_{max} = 20$, *i.e.* $\ell = 437$; P_e denotes the appropriate $\ell \times \ell$ *diagonal* weight matrix whereas the second part of the vector z, namely z_{II}, can be chosen *arbitrarily* due to its vanishing weight matrix. Now we are in a position to define a suitable *Mixed Model* in which the adjustment can be performed in a *robust* way thereby taking care of any errors in the vectors κ_i (i = 1,2,3).

3. Combining Different Sets of Coefficients

The computations for combining the different vectors of coefficients, κ_i and z, are carried out in a *Mixed Linear Model* (i = 1,2,3) given by

$$z = x + e = (\kappa_i + e_i) + e,$$

$$E\{x\} = \kappa_i \text{ given}, \quad e_i \sim (0, P_i^{-1}), \quad C\{e_i, e\} = 0, \tag{3.1}$$

$$e \sim (0, P_0^{-1}), \quad P_0 := \begin{bmatrix} P_\ell & 0 \\ 0 & \lim_{\varepsilon \to 0} \varepsilon I \end{bmatrix}$$

In this rather flexible form x denotes the m × 1 *random vector* containing the coefficients to be predicted, z and κ_i contain the sets of coefficients which are combined, e and e_i are the error vectors of z and x, respectively, and P_o, P_i are the corresponding weight matrices. The vector z is treated in this model as an *observation vector* and κ_i as *prior information* of the parameter vector x. The character of a "mixed model" is given by the assignment of e_i with the weight matrix P_i as defined in (2.2b) or (2.3b) to one of the vectors κ_i (i = 1,2,3), nevertheless resulting in the vector $x = \kappa_i + e_i$ independent of the index i!

Of course the question about a convenient assignment of the coefficient sets arises. In the case of the traditional "geodetic collocation" according to *H. Moritz (1973)*, which turns out to be the *Best inhomogeneously Linear Prediction (inhom-BLIP)* of x, we get the solution as a weighted mean of the two sets

$$\tilde{x}_i = (P_o + P_i)^{-1} [P_o z + P_i \kappa_i] \, , \quad i \in \{1,2,3\} .. \tag{3.2}$$

The corresponding "matrix of mean square prediction errors" is given by

$$MSPE\{\tilde{x}_i\} = D\{\tilde{x}_i - x\} = (P_o + P_i)^{-1} \, , \quad i \in \{1,2,3\} . \tag{3.3}$$

The situation changes considerably with the transition to "robust collocation" which is according to B. Schaffrin (1985; 1986) the *Best homogeneously Linear (weak) Unbiased Prediction (hom-BLUP)*. In this procedure the vector κ_i containing the prior information is compared with and fitted to the observation vector z. Of course, with this treatment the assignment of the coefficient sets becomes of particular importance. For each least-squares solution $\hat{\xi}_i = \kappa_i$ we have two alternatives, *either* to handle the GEM-L2 coefficients in $\kappa_o := z$ as prior information and to fit them to the coefficients $\hat{\xi}_i$ *or* to take the satellite solution superior for the longer wavelengths and to fit $\kappa_i = \hat{\xi}_i$ to the vector z.

The possible solutions are given by

$$\tilde{\tilde{x}}_{ij} = (P_o + P_i)^{-1} [a_{oj} P_o \kappa_o + a_{ij} P_i \kappa_i] \, , \tag{3.4}$$

$$i \in \{1,2,3\} \, ; \, j \in \{1,2\} .$$

The new index j describes the chosen character of the two combined coefficient sets.

In the case $j = 1$ a formal replacement is done in the following way:

$$z \rightarrow \hat{\xi}_i \text{ with } P_i$$
$$\kappa_i \rightarrow \kappa_o \text{ with } P_o \qquad i \in \{1,2,3\} \qquad (3.5)$$

while for $j = 2$ we still have

$$\kappa_o \rightarrow z \text{ with } P_o$$
$$\hat{\xi}_i \rightarrow \kappa_i \text{ with } P_i \qquad i \in \{1,2,3\} \ . \qquad (3.6)$$

The factors $a_{kj} = a_{kj}(i)$ appearing in (3.4), which are responsible for the fitting of κ_o to $\hat{\xi}_i$ or κ_i to z, can be taken from the following table:

a_{kj}	$k = 0$	$k = i$	
$j = 1$	$\alpha_{o1} \kappa_o^T P_o (P_o + P_i)^{-1} P_i \kappa_i$	1	(3.7)
$j = 2$	1	$\alpha_{i2} \kappa_i^T P_i (P_o + P_i)^{-1} P_o \kappa_o$	

with the factors $\alpha_{kj} = \alpha_{kj}(i)$ being computed from the table:

α_{kj}	$k = 0$	$k = i$	
$j = 1$	$[\kappa_o^T P_o (P_o + P_i)^{-1} P_i \kappa_o]^{-1}$	0	(3.8)
$j = 2$	0	$[\kappa_i^T P_i (P_o + P_i)^{-1} P_o \kappa_i]^{-1}$	

Corresponding to (3.3) we can also give a formula for the "matrix of mean square prediction errors"

$$\text{MSPE}\{\tilde{\tilde{x}}_{ij}\} = D\{\tilde{\tilde{x}}_{ij} - x\} = (P_o + P_i)^{-1} +$$
$$+ \alpha_{oj}(P_o + P_i)^{-1} P_o \kappa_o \kappa_o^T P_o (P_o + P_i)^{-1} + \qquad (3.9)$$
$$+ \alpha_{ij}(P_o + P_i)^{-1} P_i \kappa_i \kappa_i^T P_i (P_o + P_i)^{-1} \ ,$$
$$i \in \{1,2,3\} \ , \ j \in \{1,2\} \ .$$

Obviously $\text{MSPE}\{\tilde{\tilde{x}}_{ij}\}$ has slightly increased in comparison with (3.3) by a rank-1 modification.

4. Statistical tests

In order to compare the *three* different solutions which are possible for each set of coefficients κ_i, we present in the following a *test strategy* in three steps.

At first we want to examine whether the two hom-BLUP results *coincide* with the result from inhom-BLIP. Obviously different solutions are caused by a deviation of a_{kj} from 1 in (3.4). Therefore our *first test* considers the null hypothesis

$$H_0 : a_{kj} \sim N(1, \sigma_k^2 \alpha_{kj}) \quad , \quad j \in \{1,2\} \quad , \quad k \in \{0,i\} . \tag{4.1}$$

The proper test criterion is given by

$$T(a_{kj}) = \frac{(1-a_{kj})^2}{\sigma_k^2 \, \alpha_{kj}} \sim \chi^2(1) \quad , \quad j \in \{1,2\} \quad , \quad k \in \{0,i\} . \tag{4.2}$$

Of course, we can also check the *compatibility* between the two used datasets which is done in a *second test* regarding the null hypothesis

$$H_0 : x \sim N(\kappa_k, P_k^{-1}) \quad , \quad k \in \{0,i\} . \tag{4.3}$$

In the case of "geodetic collocation" the proper test statistic is distributed as

$$T_i(k) := \frac{R_i}{\ell \hat{\sigma}_k^2} \sim \begin{cases} F(\ell, d) & \text{for } k = 0 \quad (\text{if } j = 2) \\ F(\ell, n_i - m) & \text{for } k = i \quad (\text{if } j = 1) \end{cases} \tag{4.4}$$

with

$$R_i := (\kappa_0 - \tilde{x}_i)^T P_0 (\kappa_0 - \tilde{x}_i) + (\kappa_i - \tilde{x}_i)^T P_i (\kappa_i - \tilde{x}_i) \quad , \quad i \in \{1,2,3\} . \tag{4.5}$$

d is the degree of freedom in the original GEM-L2 solution, namely d = 442428.

If the "robust collocation" is applied we get a different test statistic being distributed as

$$T_{ij}(k) := \frac{R_{ij}}{(\ell - 1) \hat{\sigma}_k^2} \sim \begin{cases} F(\ell - 1, d) & \text{for } k = 0 \ (\text{if } j = 2) \\ F(\ell - 1, n_i - m) & \text{for } k = i \ (\text{if } j = 1) \end{cases} \tag{4.6}$$

with

$$R_{ij} := (a_{oj}\kappa_o - \tilde{\tilde{x}}_{ij})^T P_o (a_{oj}\kappa_o - \tilde{\tilde{x}}_{ij}) +$$
$$+ (a_{ij}\kappa_i - \tilde{\tilde{x}}_{ij})^T P_i (a_{ij}\kappa_i - \tilde{\tilde{x}}_{ij}) , \qquad (4.7)$$
$$i \in \{1,2,3\} , \quad j \in \{1,2\} .$$

Note that for the application of the test statistics (4.4) and (4.6) we assumed the estimated variance factor of the original GEM-L2 solution to be $\hat{\sigma}_o^2 = 1$; the same choice $\sigma_k^2 = 1$ has been made in (4.1).

Finally we want to check whether the use of the prior information - even if the second test has failed - leads to an improvement of the prediction. For this purpose, in a *third step*, we test the hypothesis

$$H_o : MSPE\{\tilde{x}_i\} \leq MSE\{\kappa_k\} , \quad k \in \{0,i\} , \qquad (4.8a)$$

for the "geodetic collocation" and

$$H_o : MSPE\{\tilde{\tilde{x}}_{ij}\} \leq MSE\{\kappa_k\}, \quad k \in \{0,i\} , \qquad (4.8b)$$

when the "robust collocation" is applied. Under these null hypotheses our test statistics (4.4) and (4.6), respectively, are distributed as

$$T_i(k) \sim \begin{cases} F'(\ell,d; \vartheta \leq \frac{1}{2}) & \text{for } k = 0 \text{ (if } j = 2) \\ F'(\ell,n_i-m; \vartheta \leq \frac{1}{2}) & \text{for } k = i \text{ (if } j = 1) \end{cases} \qquad (4.9a)$$

$$T_{ij}(k) \sim \begin{cases} F'(\ell-1,d; \vartheta \leq \frac{1}{2}) & \text{for } k = 0 \text{ (if } j = 2) \\ F'(\ell-1,n_i-m; \vartheta \leq \frac{1}{2}) & \text{for } k = i \text{ (if } j = 1) \end{cases} \qquad (4.9b)$$

ϑ being the appropriate *non-centrality parameter*.

A weaker form of this test is based on the null hypothesis

$$H_o : tr(W \cdot MSPE\{\tilde{x}_i\}) \leq tr(W \cdot MSE\{\kappa_k\}) \qquad (4.10a)$$

or

$$H_o : tr(W \cdot MSPE\{\tilde{\tilde{x}}_{ij}\}) \leq tr(W \cdot MSE\{\kappa_k\}) \qquad (4.10b)$$

with

$$W := P_o(P_o + P_i)^{-1}P_i = (P_o^{-1} + P_i^{-1})^{-1} . \qquad (4.11)$$

Then our test statistics obey the following distributions

$$T_i(k) \sim \begin{bmatrix} F'(\ell,d; \; \vartheta \leq \frac{\ell}{2}) & \text{for } k=0 \text{ (if } j=2) \\ F'(\ell,n_i-m; \; \vartheta \leq \frac{\ell}{2}) & \text{for } k=i \text{ (if } j=1) \end{bmatrix} \qquad (4.12a)$$

$$T_{ij}(k) \sim \begin{bmatrix} F'(\ell-1,d; \; \vartheta \leq \frac{\ell-1}{2}) & \text{for } k=0 \text{ (if } j=2) \\ F'(\ell-1,n_i-m; \; \vartheta \leq \frac{\ell-1}{2}) & \text{for } k=i \text{ (if } j=1) \end{bmatrix} \qquad (4.12b)$$

under the null hypotheses. More details about the theoretical background of these test procedures can be found in B. Schaffrin (1987; 1988); we only mention the relation

$$\hat{\sigma}_k^2[T_{ij}(k) - T_i(k)] = \frac{1}{\ell} [T_{ij}(k) - \sigma_k^2 T(a_{kj})] \qquad (4.13)$$

for i,j,k as above which seems to be of particular importance for numerical calculations.

5. Results

After describing the mathematical approach we are now presenting the test results, which are given in tables (5.1) and (5.2). Table (5.1) contains the results we obtained for j=2, where the GEM-L2 coefficients are used as observation data and the coefficient sets κ_i as prior information.

The test statistics $T_i(k=0)$ obtained by the "geodetic collocation" indicate only for the coefficient set κ_2 containing the coefficients derived from geoid heights a good compatibility with the GEM-L2 coefficients in vector κ_o. The criteria for the other two data sets are higher than the proper fractiles and therefore these tests have to be rejected.

Following the test strategy described in chapter 4 we can interpret the results in table (5.1) for the "robust collocation". The test criteria $T(a_{12})$ and $T(a_{32})$ show that the solutions are significantly different from the traditional collocation solution while $T(a_{22})$ indicates nearly identical solutions. Therefore it is not necessary to test the compatibility between κ_o and κ_2 since the test statistic T_{22} must lead to the same decision as T_2 (k=0) whereas the compatibility of κ_1 and κ_3 with κ_o is to be tested

separately. *Both test statistics indicate that the used data sets are not compatible, and hence the used prior information will not improve the prediction results.*

Table 5.1: Test results for j=2

	i = 1	i = 2	i = 3
$T_i(k=0)$	(2.85417)	0.23626	(2.50668)
a_{i2}	0.74559	0.99415	0.96807
$T(a_{i2})$	(328.586)	0.93787	(37.7244)
$T_{i2}(k=0)$	(2.10594)	0.23452	(2.42459)

Fractiles:

	significance level		
	0.95	0.99	0.999
$F(\ell,d)$	1.11388	1.16417	1.22230
$F'(\ell,d; \frac{1}{2})$	1.11516	1.16550	1.22369
$F'(\ell,d; \frac{\ell}{2})$	1.66086	1.73165	1.81333
$F(\ell-1,d)$	1.11401	1.16437	1.22257
$F'(\ell-1,d; \frac{1}{2})$	1.11529	1.16570	1.22397
$F'(\ell-1,d; \frac{\ell-1}{2})$	1.66105	1.73193	1.81371
$x^2(1)$	3.84190	6.63722	10.80858

It has to be mentioned that all test statistics $T_{i2}(k=0)$ are automatically lower than the corresponding $T_i(k=0)$ which points out that, with this choice of prior information and observation data, any tests based on the "robust collocation" are less sensitive and thus more realistic (in a way) than those based on the "geodetic collocation".

Table 5.2: Test results for $j=1$

	$i = 1$	$i = 2$	$i = 3$
$T_i(k=i)$	(2.86276)	0.22938	(2.55263)
a_{o1}	1.01184	1.00210	1.00241
$T(a_{o1})$	0.52414	0.12005	0.20740
$T_{i1}(k=i)$	(2.86657)	0.22950	(2.55662)

Fractiles for significance level 0.95:

	$i = 1$	$i = 2$	$i = 3$
$F(\ell,n_i-m)$	1.11467	1.11469	1.11424
$F'(\ell,n_i-m; \frac{1}{2})$	1.11595	1.11596	1.11551
$F'(\ell,n_i-m; \frac{\ell}{2})$	1.66211	1.66213	1.66143
$F(\ell-1,n_i-m)$	1.11480	1.11482	1.11437
$F'(\ell-1,n_i-m; \frac{1}{2})$	1.11608	1.11610	1.11565
$F'(\ell-1,n_i-m; \frac{\ell-1}{2})$	1.66228	1.66232	1.66161

$\chi^2(1) = 3.84190$

Remark: Brackets indicate values above the respective fractiles, and therefore the corresponding null hypotheses are to be rejected.

In table (5.2) we present the results of case j=1 where the GEM-L2 coefficients are used as prior information. Here the test statistics T_i (k=i) lead to the same decisions as those in case j=2; again only κ_2 is accepted to be compatible with κ_o. The test criteria $T(a_{o1})$ indicate for all three data sets κ_i that the robust solution is not significantly different from the solution obtained by geodetic collocation. This is confirmed by the numbers T_{i1} (k=i) which are in fact nearly the same as the corresponding T_i (k=i), thereby leading to the same decisions.

As a common result if regarding both T_{22} (k=0) and T_{22} (k=i), we may well conclude that the coefficient set κ_2 obtained by a least-squares-adjustment from 34380 1° x 1° mean geoid heights is indeed *completely compatible* with the GEM-L2 coefficients up to degree and order ℓ_{max} = 20 in vector κ_o. In view of the large differences between the two (non-homogenized) coefficient sets this is a very surprising result; but as soon as we homogenize the coefficient vectors with respect to the weight matrices we get, in fact, nearly identical vectors. This behaviour has to be explored in further investigations.

6. Conclusions

In this study the new method of "robust collocation" is exploited for the combination of different sets of geopotential coefficients, together with a *test strategy* to judge the obtained results.

We point out that it is of essential importance how these coefficient sets are combined. When using the robust method with the GEM-L2 coefficients as prior information of the coefficients to be predicted and with coefficients derived by gravity anomalies and/or geoid heights as observation data, we obtain nearly the same results as with the application of the "geodetic collocation".

However, by interchanging the character of the two data sets to be combined, the "robust collocation" yields a completely different solution with a clear tendency to be superior to the solution of the "geodetic collocation" as confirmed by the corresponding tests. Nevertheless, inconsistencies between the respective data sets are easily detected and can thus be taken into account.

All these results prove that robust alternatives to "geodetic collocation" can indeed help to improve the merging of terrestrial and satellite derived data in order to estimate geopotential coefficients most reliably.

7. References

Lerch, F.J., B.H. Putney, C.A. Wagner and S.M. Klosko (1981): Goddard Earth models for oceanographic applications (GEM-10B and GEM-10C), Marine Geodesy 5 (1981), 145-187.

Lerch, F.J., S.M. Klosko and G.B. Patel (1982): A refined gravity model from LAGEOS (GEM-L2), Geophys. Res. Letters 9 (1982), 1263-1266.

Lerch, F.J., S.M. Klosko, C.P. Wagner and G.B. Patel (1985): On the accuracy of recent Goddard gravity models, J. Geophys. Res. B-90 (1985), 9312-9334.

Middel, B. and B. Schaffrin (1987): Robust determination of the Earth's gravity potential coefficients, Proc. of the IAG Intersection Symp. "Advances in Gravity Field Modelling", XIX. IUGG General Assembly, Vancouver (Canada), August 1987.

Moritz, H. (1973): Least squares collocation, Publ. Deutsche Geodät. Komm. A-75, München 1973.

Rapp, R.H. (1981): The Earth's gravity field to degree and order 180 using SEASAT altimeter data, terrestrial gravity data, and other data, OSU-Report No. 322, Columbus/Ohio 1981.

Rapp, R.H. and J.Y. Cruz (1986a): The representation of the Earth's gravitational potential in a spherical harmonic expansion to degree 250, OSU-Report No. 372, Columbus/Ohio 1986.

Rapp, R.H. and J.Y. Cruz (1986b): Spherical harmonic expansions of the Earth's gravitational potential to degree 360 using 30' mean anomalies, OSU-Report No. 376, Columbus/Ohio 1986.

Reigber, Ch., G. Balmino, H. Müller, W. Bosch and B. Moynot (1985): GRIM gravity model improvement using LAGEOS (GRIM-3L1), J. Geophys. Res. B-90 (1985), 9285-9299.

Schaffrin, B. (1985): Das geodätische Datum mit stochastischer Vorinformation, Deutsche Geodät. Komm. C-313, München 1985.

Schaffrin, B. (1986): On robust collocation, Proc. of the 1st. Hotine-Marussi Symp. on Math. Geodesy (Roma 1985), Milano 1986, pp. 343.361.

Schaffrin, B. (1987): Less sensitive tests by introducing stochastic linear hypothesis; in: T. Pukkila/S.Puntanen (eds.), Proc. of the 2nd. Int. Tampere Conf. on Statistics, Univ. of Tampere Press, Tampere (Finland) 1987, 647-664.

Schaffrin, B. (1988): Tests of random effects based on homogeneously linear
    predictors, Int. Workshop on Theory and Practice in Data Analysis,
    Berlin (East), August 1988.

Sjöberg, L.E. (1987): The estimation of the power spectrum and reliability
    of models of the Earth's gravity field by intercomparison of independent
    models, manus. geodaet. $\underline{12}$ (1987), 104-112.

Wenzel, H.G. (1985): Hochauflösende Kugelfunktionsmodelle für das Gravitations-
    potential der Erde, Wiss. Arb. der FR Vermessungswesen der Univ. Hannover
    Nr. $\underline{187,}$ Hannover (FRG) 1985.

ABSOLUTE ORIENTATION OF THE ASTROGEODETIC GEOID MODEL FOR THE YUGOSLAV TERRITORY ACHIEVED BY THE METHOD OF THE MAXIMAL LINEAR CORRELATION COEFFICIENTS

SVETOZAR PETROVIĆ, NADA VUČETIĆ AND KREŠIMIR ČOLIĆ
YUGOSLAVIA [1]

ABSTRACT
*The paper critically considers possibilities for a geometrical
interpretation of the linear correlation coefficient in the
investigation of the correlative relationship between such data
which can be represented by surfaces. It is shown that this
coefficient between two surfaces is the consequence of two
components of their actual relationship: the relation between
their shapes, and their mutual position in space. A new
procedure is offered which enables the separation of those two
components, and which is the basis for the "method of maximal
linear correlation coefficients". By that method, the absolute
orientation of a geoid model can be effected using measured
DSS-data, Bouguer's gravity anomalies and terrain heights. We
have already used the method earlier in order to improve the
absolute orientation of solutions obtained by the least squares
fitting of the relatively oriented original astrogeodetic geoid
model for Yugoslavia onto spherical harmonic geoid models. Now
we have offered the improved solution POTS88 obtained by our
method, and also we have demonstrated that the result does not
depend on the used intermediary solution. Therefore, the method
can be applied for the direct absolute orientation in space of
relatively oriented geoid models as well.*

ZUSAMMENFASSUNG
*In der Abhandlung werden die Möglichkeiten für eine geometrische
Interpretation des linearen Korrelationskoeffizienten zur
Untersuchung der korrelativen Beziehung zwischen verschiedenen,
durch die Flächen darstellbaren Daten kritisch betrachtet. Es
zeigt sich, dass dieser Koeffizient eine Folge zweier
Komponenten ihres aktuellen Verhältnisses ist: erstens der
Beziehung zwischen ihren Formen und zweitens ihrer gegenseitigen
Raumlage. Ein neues Verfahren wird angeboten, das die Trennung
dieser zwei Komponenten ermöglicht, und die Basis für die*

[1]Address: Svetozar Petrović, Nada Vučetić, Prof. Dr. Krešimir
Čolić, Geodetic faculty, University of Zagreb,
Kačićeva 26, 41000 Zagreb, Yugoslavia

"Methode der maximalen linearen Korrelationskoeffizienten" ist.
Mit dieser Methode kann die absolute Raumorientierung eines
Geoidmodells mittels gemessenen TSS-Daten, Bougueranomalien der
Schwere und Geländehöhen vollgebracht werden. Vorher benutzten
wir die Methode um absolute Orientierung der Lösungen zu
verbessern, die durch die nach kleinsten Quadraten erzielten
Anpassung des relativ orientierten ursprünglichen astrogeo-
dätischen Geoidmodells an einer der Kugelfunktionsmodelle
gewonnen wurde. Nun bieten wir die verbesserte, mittels unserer
Methode gewonnene Lösung POTS88 an, und zugleich beweisen, dass
das Ergebnis unabhängig von der verwendeten Zwischenlösung ist.
Daher kann die Methode auch für unmittelbare absolute
Raumlagerung von relativorientierten Geoidmodellen eingesetzt
werden.

1. MOTIVATION

In (Čolić et al. 1986) we have reported about the first
successful application of *the method of the maximal linear*
correlation coefficients, and have given a short
presentation of it. Later on, in the paper (Petrović et al.
1987) – published in Croato-Serbian language – we explained the
way of thinking which was the base for the method, and gave the
formulas for practical computations. In the meantime, we
formulated in a more strict and general manner that same method
in the study (Petrović et al. 1988). Being sure that our new
approach to the interpretation of the linear correlation
coefficient makes sense in a lot of cases, when one wishes to
investigate correlative relations between data which result out
of measurements effected in individual points in space – i.e.
when the data manifest surface-like or curve-like behavior – we
give here, before the description of the subject application of
the method, also a theoretical basis together with the
application hints.

When studying the existing relations between the geoid model
surface, the Mohorovičić discontinuity ("Moho"), the relief of
the earth's physical surface and the Bouguer anomalies, we
wanted to investigate *to what extent* is the shape of each of
them reflected in the shapes of the remaining three. In order to
achieve that, we computed the linear correlation coefficients
between the geoid undulations, the Mohorovičić discontinuity
depths, the values of Bouguer anomalies and the relief heights
on the Yugoslav territory. The results were published in
succession in (Čolić, Petrović 1983), (Čolić et al. 1984),
(Petrović et al. 1985), (Čolić et al. 1985), (Čolić et al.
1986), (Čolić et al. 1988). The computations itselves have been
done in usual way, and as samples representing the considered
surfaces we chose an appropriate number n (finitely many) of
points, distributed over the whole, or over a part of the region
of interest.

Now, there emerges the question of the interpretation of the
obtained results. When the linear correlation coefficient is

almost +1 (respectively close to -1), the really existing relation between the considered two parameters has a strong linear component. In the discussed case - when the parameters are representable by surfaces - it can be interpreted as expressively similar (respectively similar, but mirrored) look of the two surfaces. Such a geometric interpretation is completely correct.

On the other hand, when the linear correlation coefficient is close to zero, the stochastic relation between the parameters does not contain a pronounced linear component. If we remember that really the aim was to investigate the relationship between the shapes of the respective surfaces, the lack of linear component should be interpreted geometrically. In accordance with the interpretations common up to now - a conclusion offers itself naturally: the relationship between the forms of the two surfaces is not simple, it is, there is no visible similarity between their shapes.
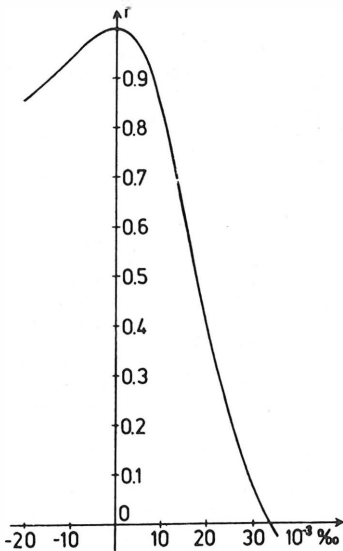
Figure 1. The change of the linear correlation coefficient with the inclination of one among two surfaces which have identical shapes

Alas, this last conclusion is erroneous. Namely, when the linear correlation coefficient is close to zero, it may, but it is not necessarily the consequence of essential differences between the forms of the two surfaces. Moreover, even in the case when the surfaces have completely identical shapes, the linear correlation coefficient can however be close to zero, or just zero. It is nicely illustrated by the example taken from (Vučetić 1986, pp. 27-28), where the linear correlation between two surfaces of the completely identical shape has been considered. The first surface was the geoid model for Yugoslavia with the absolute orientation in space which was originally given in (Čolić 1978), and the second one was that same geoid model, but with modified positions in space, obtained by tilting it continuously around the chosen horizontal axis. The sample used for computations consisted of 716 points evenly distributed over the whole territory (in a grid with sides $\Delta B=10'$ and $\Delta L=15'$). At first sight, the obtained result seems very curious: in spite of the fact that the two surfaces had identical shapes, even slight inclinations resulted in considerable changes of the linear correlation coefficient! For instance, an inclination of only 0.034 ‰

around the chosen axis changed the linear correlation coefficient even to zero! The linear correlation coefficient as the function of the tilt is represented in *Figure 1*. Any surface (with exception of the horizontal plane), regardless whether it has some physical meaning, or not – for instance a randomly generated surface – could serve as example as well. The result would be completely analogous – the only difference would be that the linear correlation coefficient would change with inclination somewhat more rapidly or slowly.

It means, in every case when the linear correlation coefficient is computed in order to compare two phenomena which can geometrically be represented as two surfaces, one should be very cautious in the geometrical explanation of the obtained results, it is when deriving *quantitative conclusions* regarding the relationship between the shapes of those surfaces.

2. NEW APPROACH TO THE PROBLEM

It is clear from the previous section that we are here dealing only with such phenomena which can be regarded as surfaces, and the calculation of the linear correlation coefficient between them is performed in order to make geometrical conclusions. From everything that has been said, it becomes obvious that the computed linear correlation coefficient is the consequence of *two components* of the relationship between the two surfaces: the relation between their **shapes**, and the relation between their positions in space. Our aim is *to separate those two components*, more precisely their influences upon the linear correlation coefficient.

First of all, we have to formulate more precisely what kind of relationship between the shapes of two surfaces are we investigating. In the previous section we have used intuitively terms like "the shape of one surface is reflected in the shape of the other one", "similar look of two surfaces", and alike. In fact, it can be demonstrated that *the linear correlation coefficient between two surfaces is +1 or –1 if and only if there exists a transformation which uniformly stretches one of the surfaces in some direction (eventually with an additional translation) so that it becomes identical with the other one. When the linear correlation coefficient is different both from +1 and –1, such a transformation does not exist, and that coefficient becomes a measure how close is the relation between two surfaces to the situation when one is a stretched image of the other*, see (Petrović et al. 1988). Therefore, all references to the geometrical relation between two surfaces made in the present paper, should be understood in that, just explained sense.

It is now clear that the mutual position alone, of two surfaces in space, may be responsible for the low absolute value of the linear correlation coefficient. Namely, the forms of the surfaces may differ just slightly, or even not at all, but when the surfaces are inclined one with respect to another, it is not

a wonder that no uniform stretching composed with a translation can transform one surface to something which is close to the other one.

Therefore, to make geometrical statements about the relationship between the forms of two surfaces based on the linear correlation coefficient, one should eliminate the influence of the position in space. We will imagine that one of the surfaces is kept fixed, and that the other one assumes all possible positions in space. In the case when there exists such a position for which the absolute value of the linear correlation coefficient is the largest possible, we will call it *the optimal position* and the corresponding value of the linear correlation coefficient will be called *the maximal linear correlation coefficient*. That value is, of course, the required measure for the investigated geometrical relation between the surfaces, which is independent of the mutual position. There exist some synthetic examples for which the optimal position does not exist, but in practical cases, where the surfaces are not defined analytically, but contain some stochastic behavior, that is almost impossible to happen - at least we could not up to now encounter such a practical situation. It should be added that, when solving a practical problem, one has to clear up whether the resulting difference between the original and the optimal position has some physical (or other) reasons and interpretation.

Every change of the position in space can be separated into a translation and a rotation. It can be easily demonstrated, and it is probably already clear from the above definition of the linear correlation coefficient by means of the stretching and the translation, that *no translation changes its value*. Therefore, in order to find the optimal position, *we have to consider only rotations*. Taking into account the physical nature of the mentioned surfaces which we want to investigate, and the possibility to find some reasonable interpretation of the obtained results, we can restrict ourselves only to rotations through very small angles. Moreover, such a rotation will have a component around the vertical axis which will be negligible from the point of view of the used data files (e.g. in the geoid file, the dimensions of the grid mesh were 10'x15', while the resolution of the third coordinate - the geoid undulation - was incomparably better, amounting in the worst case 1-2 decimeters). Therefore, we have to consider only rotations around horizontal axes.

Let us denote the considered phenomena (surfaces) with x and y, and let the sample representing them consists of n points. It means that for each of those n points, the corresponding values of x and y are known. The linear correlation coefficient can be then written in the form

$$r(x,y) = \frac{n \, \Sigma xy - \Sigma x \, \Sigma y}{\sqrt{n \, \Sigma x^2 - (\Sigma x)^2} \, \sqrt{n \, \Sigma y^2 - (\Sigma y)^2}}. \qquad (1)$$

Having in mind that translations do not change the linear correlation coefficient, we denote

$$X = x - \frac{\Sigma x}{n} , \qquad\qquad Y = y - \frac{\Sigma y}{n} . \qquad (2)$$

Therefore we have $\Sigma X = \Sigma Y = 0$, and (1) becomes

$$r(x,y) = r(X,Y) = \frac{\Sigma XY}{\sqrt{\Sigma X^2 \ \Sigma Y^2}} . \qquad (3)$$

Hence, we first replace the known values x and y by the values X and Y according to (2). Let the position of each considered point, in which we know those values, be described by two coordinates, let us denote them δ and ℓ. They can for instance be the geodetic latitude and longitude, as in our case. Again, we denote

$$B = \delta - \frac{\Sigma \delta}{n} , \qquad\qquad L = \ell - \frac{\Sigma \ell}{n} , \qquad (4)$$

with the consequence $\Sigma B = \Sigma L = 0$.

Because we are considering only very slight rotations, we can replace the rotation of the surface Y by the linear transformation

$$Y' = Y + bB + cL, \qquad (5)$$

where b and c are coefficients that describe the effected slight tilt. In that way we are solving a less complicated problem. But what is more important, it is easily seen that the rotations, whose amount is small enough to be physically explainable, can be approximated by transformations of the type (5) so well, that the difference between that approximation and the exact solution is many orders of magnitude beneath the resolution of the given data.

Replacing Y in the numerator of (3) by Y' from (5) gives

$$\Sigma XY' = \Sigma XY + (\Sigma BX)b + (\Sigma LX)c.$$

Analogously,

$$\Sigma Y'^2 = \Sigma(Y+bB+cL)^2 = \Sigma Y^2 + (\Sigma B^2)b^2 + (\Sigma L^2)c^2 + 2(\Sigma BY)b + 2(\Sigma LY)c + 2(\Sigma BL)bc.$$

We denote

$$F = \Sigma XY, \qquad G = \Sigma BX, \qquad H = \Sigma LX ; \qquad (6)$$

$$k_1 = \Sigma Y^2, \ k_2 = \Sigma B^2, \ k_3 = \Sigma L^2, \ k_4 = \Sigma BY, \ k_5 = \Sigma LY, \ k_6 = \Sigma BL; \qquad (7)$$

$$V = \sqrt{\Sigma X^2} , \qquad W = \sqrt{k_1 + k_2 b^2 + k_3 c^2 + 2k_4 b + 2k_5 c + 2k_6 bc} ; \qquad (8)$$

and finally, in place of (1), we have

$$r(X,Y') = \frac{F + Gb + Hc}{VW} . \qquad (9)$$

We are looking for such values of the parameters b and c, i.e. for such a transformation of the type (5), for which the absolute value of the linear correlation coefficient assumes the largest possible value. The quantities F, G, H and V being constants, and W a function of b and c, the relation (9) expresses the linear correlation coefficient as a function of b and c. Hence, the necessary condition for the extrema reads:

$$r_b = \frac{\partial r}{\partial b} = \frac{GVW - (F+Gb+Hc)VW_b}{V^2W^2} = 0$$

$$r_c = \frac{\partial r}{\partial c} = \frac{HVW - (F+Gb+Hc)VW_c}{V^2W^2} = 0.$$

(10)

By differentiating W from (9), we obtain after a little rearranging:

$$W_b = \frac{k_2 b + k_4 + k_6 c}{W}, \qquad W_c = \frac{k_3 c + k_5 + k_6 b}{W},$$

and in that way (10) becomes

$$\frac{GW^2 - (F+Gb+Hc)(k_2 b + k_4 + k_6 c)}{VW^3} = 0$$

$$\frac{HW^2 - (F+Gb+Hc)(k_3 c + k_5 + k_6 b)}{VW^3} = 0,$$

which gives the equations

$$(F+Gb+Hc)(k_2 b + k_4 + k_6 c) = GW^2$$

$$(F+Gb+Hc)(k_3 c + k_5 + k_6 b) = HW^2.$$

(11)

This is a nonlinear equations system with two unknowns: b and c. However, it can be solved exactly. Dividing the first equation by the second one yields

$$\frac{k_2 b + k_4 + k_6 c}{k_3 c + k_5 + k_6 b} = \frac{G}{H}.$$

From this equation we can express b:

$$b = \frac{k_3 G - k_6 H}{k_2 H - k_6 G} c + \frac{k_5 G - k_4 H}{k_2 H - k_6 G}.$$

Finally, we denote

$$b_1 = \frac{k_3 G - k_6 H}{k_2 H - k_6 G}, \qquad b_2 = \frac{k_5 G - k_4 H}{k_2 H - k_6 G},$$

(12)

and then, we have

$$b = b_1 c + b_2.$$

(13)

Substituting (8) and (13) into (11), leads to

$$(-Gk_6 b_1 + Hk_2 b_1 + Hk_6 - Gk_3) c^2$$
$$+ (Fk_2 b_1 + Fk_6 - Gk_4 b_1 - Gk_6 b_2 + Hk_2 b_2 + Hk_4 - 2Gk_5) c \qquad (14)$$
$$+ Fk_2 b_2 + Fk_4 - Gk_1 - Gk_4 b_2 = 0 .$$

From (12) we can easily derive

$$-Gk_6 b_1 + Hk_2 b_1 + Hk_6 - Gk_3 = 0$$

and

$$-Gk_6 b_2 + Hk_2 b_2 + Hk_4 - Gk_5 = 0 ,$$

which reduces (14) to

$$(Fk_2 b_1 + Fk_6 - Gk_4 b_1 - Gk_5) c + Fk_2 b_2 + Fk_4 - Gk_1 - Gk_4 b_2 = 0 ,$$

it means

$$c = \frac{-Fk_2 b_2 - Fk_4 + Gk_1 + Gk_4 b_2}{Fk_2 b_1 + Fk_6 - Gk_4 b_1 - Gk_5} . \qquad (15)$$

When we have this expression for c, the relation (13) gives the other needed parameter: b. The obtained solution for b and c satisfies the necessary condition for extrema (10). Now, one should check whether it is really the maximum, which in every individual practical case can be done rather easily.

Obviously, the angle between the horizontal axis around which the tilt was made, and the axis B, is given by

$$\alpha = \arctan(-b/c) . \qquad (16)$$

The amount of that tilt ν is:

$$\nu = b(\sin\alpha) - c(\cos\alpha) , \qquad (17)$$

and is expressed in units which are the ratio of the units which served for Y, and the units for both coordinates B and L.

We must admit that the derivation was rather complicated. Therefore, we make now a short recapitulation of the procedure for practical computations.

For n points $T_1, T_2, \ldots, T_n$, whose positions are described by the coordinate pairs $(\delta_1, \ell_1), (\delta_2, \ell_2), \ldots, (\delta_n, \ell_n)$, we know the values of two parameters $\varkappa$ and y, i.e. $\varkappa_1, \varkappa_2, \ldots, \varkappa_n$, and $y_1, y_2, \ldots, y_n$.

We calculate:

- from (2) and (4): X_i, Y_i and B_i, L_i (i=1,...,n)
- from (6) and (7): F,G,H and $k_1, k_2, k_3, k_4, k_5, k_6$
- from (12) : b_1, b_2

- from (15) : c
- from (13) : b
- from (16) and (17): α and ν
- finally, (5) gives the transformation of the surface Y into the surface Y', and (8) with (9) offer the required maximal linear correlation coefficient.

Naturally, the result makes sense only when the starting assumption is fulfilled, it is, when the tilt between the original and the newly obtained surface is small. In that case, the required maximal linear correlation coefficient r(X,Y') may be computed as well.

Of course, all considerations in the present section can be done for the two-dimensional case, i.e. when we in place of surfaces, investigate relations between curves. That case was included in (Petrović et al. 1987), and was dealt with in detail in the study (Petrović et al. 1988).

3. APPLICATION OF OUR METHOD IN THE ABSOLUTE ORIENTATION OF THE ASTROGEODETIC GEOID MODEL FOR YUGOSLAVIA

3.1 Some words about the model FIR86

An absolutely oriented geoid model for the Yugoslav territory had for the first time been obtained by the least squares fitting of the Muminagić's astrogeodetic original - which had been computed referring to the eccentric Bessel's reference ellipsoid (Muminagić 1971) - onto GEM10 (at that time the most recent and the best among the smooth long-wave satellite-terrestrial models), which was in detail described in (Čolić 1978). In the investigation of the linear correlation between that geoid surface model and the Mohorovičić discontinuity, the Bouguer anomalies, respectively the relief heights (what we have done using the values in 716 grid points distributed evenly over the whole territory of Yugoslavia), the resultant absolute values of the linear correlation coefficient were unexpectedly low.

Already from the beginning, due to the small area of the Yugoslav territory, and to the very smooth flow of the used long-wave geoid model GEM10, there existed some doubt whether the mentioned geoid model obtained by fitting is really well absolutely oriented in space. On the other hand - on the Yugoslav territory - the linear correlation coefficients between each pair, formed out of Bouguer anomalies, relief heights and Mohorovičić discontinuity depths, had high absolute values. The idea emerged - to improve the spatial position of that geoid model in such a way, so that it comes in the position for which the three linear correlation coefficients (in fact, their

absolute values!) between the geoid and the remaining parameters assume the largest possible values.

Using the procedure described in this paper, we have already on an earlier occasion computed the tilt, which should be applied to the existing geoid model, in order to make the absolute value of the linear correlation coefficient between it and the Mohorovičić discontinuity maximal. Analogous computations have been effected also for the relations between it and the Bouguer anomalies, respectively the relief heights. All the three obtained results being mutually rather similar, and leading to an immense increase of the absolute values of the respective linear correlation coefficients, we took some "mean value" of the three mentioned tiltings and obtained a new geoid model "FIR86" for Yugoslavia – *which had the same detailed forms as the original one, but an improved absolute orientation*, see (Čolić et al. 1986).

3.2 The improvements made for the geoid model POTS88

Now the need emerged to repeat the practical procedure again. Namely, we have made considerable essential improvements, which – to tell the truth – did not change a lot the existing results.

As a starting model, whose spatial position had to be improved, served again the Muminagić's geoid model, but this time digitized in a finer grid (10'x15') and fitted again onto GEM10.

While – when making the model FIR86 – we had used a Mohorovičić discontinuity map for Yugoslavia, which had been produced by the geophysicists, now we came back to the application of the DSS profile data, as original measured values.

The fact that we wish to orient absolutely the astrogeodetic geoid model on the basis of its relations towards three parameters (the Mohorovičić discontinuity, the Bouguer anomalies and the relief heights), means that we are looking for such a position in space, in which the absolute values of the three respective linear correlation coefficients assume the largest possible values. Of course, they do not assume the maximal values for the same position of the geoid; therefore the sum of their squares, respectively the sum of their absolute values, has to be maximized. In place of taking some mean value of the three solutions for the absolute orientation (as it was done when making the model FIR86), we used this time numerical methods to perform the maximization of the mentioned sums. It came out that both criteria (the sum of squares and the sum of absolute values) give almost perfectly the same result. That resultant new solution POTS88 for the absolutely oriented astrogeodetic geoid model on the whole Yugoslav territory, is given in *Figure 2*. It differs just a little from our former model FIR86. However, *the model POTS88 should be regarded as a new, improved solution*.
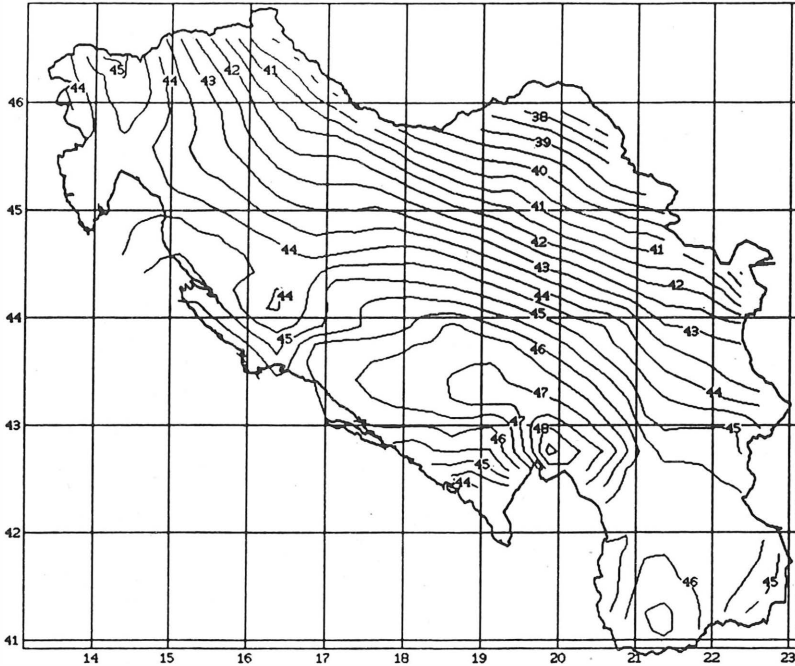
Figure 2. The astrogeodetic geoid model POTS88 for the Yugoslav
territory, absolutely oriented by the "method of
maximal linear correlation coefficients"

4. THE SCOPE OF THE APPLIED METHOD

4.1 Comparison with solutions obtained by the least squares fitting

Our new and unusual manner of making the absolute orientation of
a geoid model (of the astrogeodetic or some other origin) by
bringing it into accordance with the three mentioned physical
parameters, has already seemed unacceptable at first sight to
some people, or at least less acceptable than the old good least
squares fitting. Therefore, such a fitting has been done once
more, this time not onto the old GEM10, but onto the most recent
satellite-terrestrial models OSU81 (Rapp 1981), GPM2 (Wenzel
1985), OSU86 (Rapp and Cruz 1986) and IFE87 (Bašić 1988), see
(Čolić et al. 1987/1989). The *Figure 3* presents the result of

fitting the Muminagić's original onto the GPM2 (something similar gives the fitting onto OSU81, respectively OSU86 or IFE87).
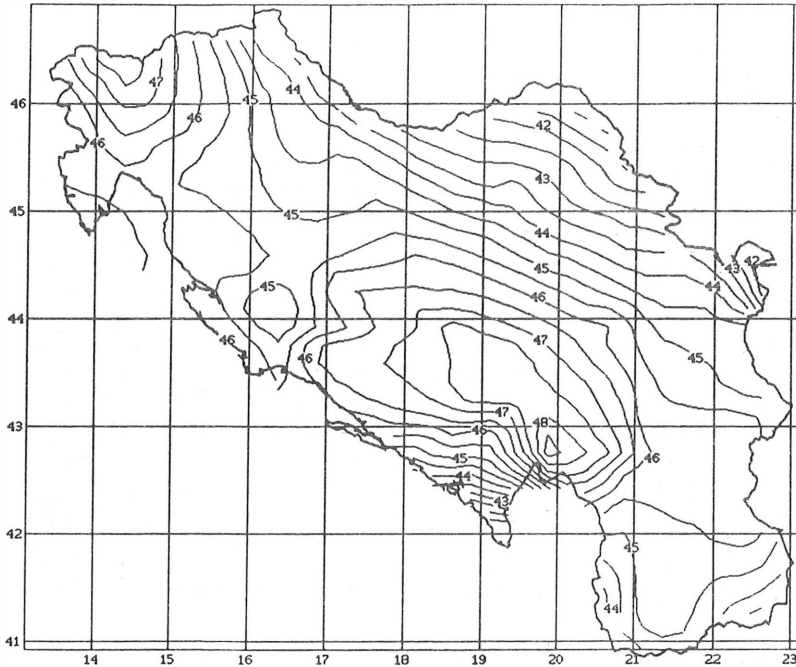
Figure 3. Astrogeodetic geoid model for the territory of Yugoslavia with absolute orientation obtained by fitting the geoid model according to Muminagić onto the corresponding part of the new geopotential model GPM2

In the *Figures 2* and *3* one can see a rather good agreement of the solution obtained by fitting with our solution POTS88. This is a certain confirmation of the correctness of our approach, although our solution is probably much better than any solution obtained by fitting onto existing spherical harmonic geoid models. Namely, we had also made a little investigation what happens when using the method of least squares for the fitting of parts of various geoid models. We had established that the results obtained in that way should be accepted with precaution, because they may contain some undesirable uncertainties, see (Čolić et al. 1987/1989).

4.2 Stability of the method

The next question is whether we would really obtain the same
result, if we - as the intermediary step by the absolute
orientation of the astrogeodetic geoid model, i.e. as a starting
point for the application of our method - in place of the model
obtained by fitting onto GEM10, have used the fitting onto some
other spherical harmonic model. To accomplish also a practical
test of the answer to that question, we chose to start from the
model for Yugoslavia obtained by fitting onto GPM2. In
accordance with the expectations, the resulting reoriented geoid
model was (up to slight numerical differences) identical with
the geoid model POTS88 (*Figure 2*)! The only real difference was
in level, in the given case it amounted 1.34m. It was, of
course, equal to the level difference between the two models
which served as starting points for the application of our
method. There is nothing curious about that, because, in fact,
the suggested method uses only the mean level from those
intermediary solutions. Therefore, by defining that level in
some other way, for instance by aid of GPS measurements, one
could completely leave out the fitting as an intermediary step.
It means that the "method of maximal linear correlation
coefficients" could be applied not only for the correction
(reorientation) of the solutions preliminary oriented by
fitting, but for the direct absolute orientation of relative
geoid models in space as well.

5. CONCLUSIONS

It is now obvious that even when investigating the simplest
possible relation between two phenomena - the linear relation -
there exist traps which require cautiousness. When we wish to
derive *geometrical conclusions* regarding the relation between
the forms of two surfaces on the basis of the linear correlation
coefficient, then its usual interpretation, which neglects the
fact that in such a case to every point - besides the two
considered parameters - also a position is assigned, may lead to
erroneous conclusions - in the existing literature one can
easily find such examples. Instead, one should apply the
procedure described in this study, *the procedure which separates
the influence of the relation between the shapes of two
surfaces, from the influence of their mutual position in space.*
It is clear without proving that there are no doubt a lot of
examples for the successful application of this procedure, not
only in the field of geodesy or earth sciences in general, but
also in the broad field of technology and elsewhere. Therefore,
we believe that such, until now unusual approach to the solution
of the considered problem, is very important and profitable, not
only from the theoretical, but also from the practical point of
view.

Regarding the possibility of achieving the absolute orientation
of a geoid model, our "method of maximal linear correlation

coefficients" proved to be independent of the used intermediary
solution (obtained by the least squares fitting onto some
spherical harmonic model), from which it takes over only the
corresponding level. Therefore, the method can be applied
directly for the orientation in space of a relative geoid model,
supposing that the absolute level is defined in some other
suitable way, for instance by means of GPS measurements.

REFERENCES

1. Bašić, T. (1988): *Untersuchungen zur regionalen Geoid-bestimmung mit "dm"-Genauigkeit.* Doctoral thesis, University of Hannover, in preparation.

2. Čolić, K. (1978): An investigation of the astrogeodetic geoid of Yugoslavia using gravimetric data. *Proceedings of the International symposium on the geoid in Europe and Mediterranean area*, Ancona-Numana, pp. 99-112.

3. Čolić, K., B.Aljinović and S.Petrović (1985): A comparison of the existing preliminary map of Mohorovičić discontinuity with the predicted values of the depths of that surface in the Dinaric-Pannonian region of Yugoslavia. *IAG-workshop "Density distribution of the lithosphere - Static and dynamic models"*, Zürich, 7 pp; abstract in: *ETH Bericht*, No.102, p.16.

4. Čolić, K. and S.Petrović (1983): Correlation between gravity anomalies, geoid heights and Mohorovičić discontinuity depths in the Dinaric-Pannonian region of Yugoslavia. *The XVIIIth General Assembly of IUGG*, Hamburg; published in: *Proceedings of the International association of geodesy (IAG) symposia*, Columbus (1984), pp. 137-146.

5. Čolić, K., S.Petrović and B.Aljinović (1986): Testing the existing absolute geoid heights in Yugoslavia using information offered by the Mohorovičić discontinuity, the Bouguer gravity anomalies and the relief heights. *International symposium on the definition of the geoid, Proceedings*, Florence, pp.29-38; also published in: *Bollettino di geodesia e scienze affini*, XLVI, No.4 (1987), pp. 309-322.

6. Čolić, K., S.Petrović and T.Bašić (1984): Anew about the correlation between Mohorovičić discontinuity depths, geoid undulations and Bouguer gravity anomalies in the Dinaric-Pannonian region of Yugoslavia. *5th International symposium "Geodesy and physics of the earth"*, Magdeburg; published in: *Akademie der Wissenschaften der DDR, Veröffentlichungen des Zentralinstituts für Physik der Erde*, No.81 (1985), Vol. I, pp. 68-76.

7. Čolić, K., S.Petrović and T.Bašić (1987/1989): What happens when using the method of least squares for the fitting of geoid model surfaces?. *INTERCOSMOS scientific conference "Use of artificial satellite observations for geodesy and geophysics"*, Szentendre; published in: *Observations of artificial satellites of the earth*, No.25 (1987), pp.173-181. A new, more complete version of the paper will be published in: *Bollettino di geodesia e scienze affini*, XLVIII, No.1 (1989), 15 pp.

8. Čolić, K., N. Vučetić and S. Petrović (1988): The geoid and the Mohorovičić discontinuity. *6th International symposium "Geodesy and physics of the earth"*, Potsdam; published in this same Proceedings.

9. Muminagić, A. (1971): Investigation of real geoid in Yugoslavia. Separate publication presented at: *15th General Assembly of IUGG*, Moscow.

10. Petrović, S., K.Čolić, Z.Biljecki and T.Bašić (1985): The use of complex data for the prediction of Mohorovičić discontinuity depths in the Dinaric-Pannonian region of Yugoslavia. *IAG-workshop "Density distribution of the lithosphere - Static and dynamic models"*, Zürich, 10 pp; abstract in: *ETH Bericht*, No.102, p.29.

11. Petrović, S., M. Lapaine and N. Vučetić (1988): Some new interpretations of the linear correlation coefficient. *6th Seminary in the applied mathematics*, Tara (Yugoslavia), 6 pp.

12. Petrović, S., N. Vučetić and K. Čolić (1987): Jedna nova interpretacija koeficijenta linearne korelacije pri obradi podataka mjerenja (A new interpretation of the linear correlation coefficient in the treatment of measurement data - Croato-Serbian). *Geodetski list*, 41, No.10-12, pp. 281-295.

13. Rapp, R.H. (1981): The earth's gravity field to degree and order 180 using SEASAT altimeter data, terrestrial gravity data, and other data. *OSU Report*, No.322.

14. Rapp, R.H. and J.Y.Cruz (1986): Spherical harmonic expansions of the earth's gravitational potential to degree 360 using 30' mean anomalies. *OSU Report*, No.376.

15. Vučetić, N. (1986): *Apsolutna orijentacija astro-geodetskog modela geoida za teritorij SFRJ pomoću Mohorovičićevog diskontinuiteta (Absolute orientation of the astrogeodetic geoid model for the territory of Yugoslavia by means of the Mohorovičić discontinuity*, Croato-Serbian). Student's paper submitted to the University of Zagreb and awarded a prize on the occasion of the Workers' day (1st May), Zagreb, 55 pp.

16. Wenzel, H.-G. (1985): Hochauflösende Kugelfunktionsmodelle für das Gravitationspotential der Erde. *Wissenschaftliche Arbeiten der Fachrichtung Vermessungswesen der Universität Hannover*, No.137.

METHOD OF COMPACT REPRESENTATION OF THE GEOPOTENTIAL MODELS

M.S. Petrovskaya, M.V. Belikov, K.V. Pischukhina

The Institute for Theoretical Astronomy of the Academy

of Sciences of the USSR, Leningrad, USSR

Abstract. A method of generalized Chebyshev economization has been elaborated allowing to contract partial sums of the spherical harmonic series representing the external potentials of gravitating bodies. The method has been approbated with respect to the zonal parts of the latest Earth's potential models, as well as the expansions of the potentials of some axial symmetric bodies.

МЕТОД КОМПАКТНОГО ПРЕДСТАВЛЕНИЯ МОДЕЛЕЙ ГЕОПОТЕНЦИАЛА

М.С. Петровская, М.В. Беликов, К.В. Пищухина

Резюме. Разработан метод обобщенной чебышевской экономизации, позволяющий сжимать частные суммы разложений внешних потенциалов гравитирующих тел в ряды сферических функций. Проведено численное исследование эффективности этого метода в применении к зональным частям современных моделей геопотенциала, а также к потенциалам простых тел вращения.

The generally accepted form of reprezentating the Earth's gravitatonal field is the spherical harmonic series. This is the simpliest presentation, most suitable for both analytical and numerical applications. The spherical harmonic models of the geopotential are of interest for a variety of geodetic purposes, as well as for solving problems of satellite dynamics, geophysics, oceanography, etc.

The current Earth's models become more and more cumbersome.

The latest ones contain harmonics up to 360 degree and order (the models : OSU 86 E, OSU 86 F, GPM 2 - E 2). In " long " models the number of terms attains hundreds thousands and in the nearest future there will be millions of them. The construction and application of such models entails great practical difficulties and, besides, the larger are degrees and orders of harmonics, the more significant become the errors of their determination. From this follows that " economical " geopotential models, whose coefficients provide more information about the geopotential than the conventional ones, are very desirable. More optimal Earth's potential models would furnish higher accuracy approximation for a fixed number of terms or, on the other hand, they would provide higher precision for a given " length " of a model. Such optimal approximations should exist in principal, at least theoretically, for the following reason. As a matter of fact, the conventional models represent the best mean square approximants, in the space L_2. At the same time there exist polynomials of the best uniform approximations over the sphere Σ , in Chebyshev metric C : ($//./\!/ = /./$), for the same basis of spherical functions. The latter polynomials, by definition, involve less uniform errors as compared to the uniform errors of the best L_2 - approximations.

On this ground the method of Chebyshev economization (CE - - method) of spherical harmonic approximation for the geopotential was developed (Petrovskaya, 1986, a, b; 1987). The results were presented at the Symposium on Mathematical Geodesy (Petrovskaya and Pischukhina, 1986). The method is based

on an alternative expansion for the geopotential whose terms decrease (approximately) $\sqrt{n}$ times rapidly than the ones of the conventional spherical harmonic series. Then the partial sums of the new series are expressed in terms of the spherical functions. As a consequence, additional numerical factors $\alpha_n^{(N)}$ emerge in the harmonic coefficients (factors of economization) which depend on the highest degree N of the terms in a model, as well as the degree n of a specific harmonic. The factors do not depend on the second index of the spherical function, that is of its order. In particular, for a model of 360 degree the number of factors is 360.

The present investigation extends CE – method to a generalized Chebyshev economization procedure (GCE – method). The generalization has been performed in several aspects. The CE – – version implyed only the Earth's case, corresponding to a certain rule of decreasing the harmonic coefficients (empirical Kaula's rule). Now, GCE – procedure is applicable to the potential of any volume body, with arbitrary behaviour of the coefficients of the series, as well as to various transformants of the potential. Besides, this method provides the possibility of strengthening the effect of economization, by means of double or multiple procedures, which is simply done by raising the factors of economization to the corresponding power. Subsequent (additional) economization can be attained when going from the global approximation (corresponding to the whole sphere) to a local one (relevant to a part of it).

As numerical experiments show, the most effective economization is attained at the sphere of convergence Σ , passing

through the singularities nearest to the origin of the referen-
ce set. For the Earth this is the enveloping sphere or, in pra-
ctice, the mean Earth's sphere. But it is namely on this sphere
that the convergence of the series is weakest and therefore the
economization is most desirable. The GCE - method can be modi-
fied to provide more optimal approximation for satellites, i.e.
at a specific elevation above the sphere of convergence. This
is supposed to be done in the future.

The GCE - method has been approbated numerically, at the
first stage, with respect to some homogeneous bodies with axial
symmetry : the oblate and prolate ellipsoids, the cone, the cy-
linder and the hemisphere. The closed expression for the poten-
tial, in terms of elementary functions, is known only for the
ellipsoids. In these cases it is possible to evaluate strict-
ly the uniform errors over Σ for the partial sums of the cor-
responding expansion of the potential. As to the other bodies
under consideration, no such expression for the potential is
known. But in each case the analytical expression for the gene-
ral term can be used (as many terms being taken into account
as necessary) to evaluate the potential with a given accuracy.
Basing on this, the corresponding uniform errors of the partial
sums of the series can be found (they have lesser number of
terms than those used for the potential evaluation). For all
the simple bodies, the real efficiency of GCE - method has been
established : either economization of terms is attained for a
fixed accuracy, or the accuracy is increased for a given number
of terms.

As far as the Earth's gravitational potential is concerned,

neither closed expression for the potential, nor analytical re-
presentation of the general term of the series is known. Instead,
only approximate numerical values of the harmonic coefficients
are available, derived from the observational data. Taking it
into account, a special test of efficiency of the economization
procedure is introduced (for similar cases) which implies the
comparison of the rate of inner convergence for both the initial
and new series. Practically, the inner convergence test is based
on comparing the maximum absolute values (over a chosen domain
of approximation) of differences between the partial sums rele-
vant to each series. The sums are taken at a certain interval
(e.g. 5,10 or 20 terms) and the above differences between them
are treated as the " errors " of approximation at such kind of
test. These " inner convergence errors " were compared with the
strict uniform errors mentioned above, for all simple bodies
under consideration. As a result, the similarity of both kinds
of testing the economization procedure was established. This
conclusion allowed to utilize the described inner convergence
test for the numerical approbation of GCE – method with respect
to the zonal parts of the geopotential models.

In the process of testing the GCE – method, in the case of
simple bodies, it turns out that the effect of economization
does not exist in the vicinity of the singularities of their
potentials (at the equator or at the axis of symmetry). Eli-
mination of these regions results in a rather strong effect of
economization over the remaining domain, which is conveyed
either in reducing the number of terms or in deminishing the
error of approximation. More stronger effect is attained, in

some cases, by double or multiple economization. It has been
also established that the lesser is the domain of approximation,
the more stronger becomes the effect of economization.

On Fig. 1 the results of testing the GCE – method are presen-
ted for the case of an oblate ellipsoid at the sphere of conver-
gence passing through its focuses.

Similar numerical experiments were carried out for the zonal
parts of the latest " long " models of the geopotential :
OSU 81 (Rapp, 1981), OSU 86 F (Rapp and Cruz, 1986),
GPM (Wenzel, 1985), GEM 10 C (Lerch et al., 1981). These
models contain harmonics up to 180, 360, 200 and 180 degrees
and orders, respectively. Absolute errors of approximation (by
inner convergence criterion) were calculated for the latitudes
$-\pi/2 \leqslant \varphi \leqslant \pi/2$, with the interval of 1° . For all the models the
effect of economization has been revealed and common characte-
ristics have been discovered. It is essential to note that,
contrary to the above simple bodies, the effect of economization
takes place over the whole Earth's mean sphere. This is due to
the fact that for the simple bodies the largest absolute errors
of approximation occur just at the singularities. As to the
Earth, at the latitudes where no economization effect appears,
the corresponding absolute errors of approximation are not es-
sential, as compared to the other parts of the sphere, and,
therefore, they do not influence the maximal errors of approxi-
mation. Thus the geopotential singularities do not " spoil "
the approximation of both the Earth's potential and its first
derivatives (no numerical experiments were performed yet for
the second order derivatives), and the GCE – procedure can be

used not only for conducting the economization but also for detecting the locations of the geopontial sinqularities, by revealing the places of poor economization effect. It appears that one of such regions corresponds to the latitude of Tibet.

On Fig. 2 and 3 the results relevant to the model OSU 86 F (as the " longest " one) are presented. It is of interest to note, as can be clearly seen from the pictures, that the worse are the analytical characteristics of a transformant of the potential (up to derivatives of certain order), the stronger is the economization effect.

The underlying table demonstrates the results of application of the GCE - method to the potential expansion of an oblate elipsoid, as well as the geopotential model GPM 2. In both cases the number of terms is N=200. The effect of multiple and local economizations are explicitely demonstrated. For the Earth, the local economization was accomplished in a region free of continents (between Africa and Antarctica).

The authors intend to proceed with numerical experiments for the geopotential models, taking also into consideration the tesseral parts (if the total models are available).

REFERENCES

Petrovskaya M. S. (1986a) Improving the convergence of the pla-
        netary potential expansion. General principles. Astronomical
        Journal, vol. 63, No. 2, pp. 356-365 (in Russian).

Petrovskaya M. S. (1986b) Improving the convergence of the pla-
        netary potential expansion. Utilization   of   the   series   of
        Chebyshev polynomials. Astronomical Journal, vol. 63, No. 4,
        pp. 791-799 (in Russian).

Petrovskaya M. S. (1987) Improving the convergence of the pla-
        netary potential expansion. Radial derivative of the poten-
        tial and the gravity anomaly. Astronomical Journal, vol. 64,
        No. 2, pp. 410-416 (in Russian).

Lerch F. J., Puthey F., Klosko S., Wagner C.(1981) Earth models
        for oceanographyc application (GEM 10 B and GEM 10 C),
        Marine Geodesy, vol. 5, pp. 145-187.

Petrovskaya M. S., Pishchukhina K. V. (1986) Methods of impro-
        ving the convergence of the Earth's potential expansion.
        Proc. of the 1 Hotine-Marussi Symp. on Math. Geod. (Roma,
        3-6 June, 1985), vol. 2, pp. 617-651.

Rapp R. H. (1981) The Earth's gravity field to degree and order
        180 using SEASAT altimeter data, terrestrial gravity data
        and other data. Report No. 322, Dept. of Geodetic Science
        and Surveying. The Ohio State University, Columbus.

Rapp R. H., Cruz J. Y. (1986) Spherical harmonic expansions of
        the Earth's gravitational potential to degree 360 using 30'
        mean anomalies. Report No. 376, Dept. of Geodetic Science
        and Surveying. The Ohio State University, Columbus.

Wenzel H. G. (1985) Hochaufloesende Kugelkenktionsmodelle fuer
        das Gravitationspotential der Erde, Wiss., Arb. Fachrich-
        ting Vermessungswesen der Universitaet Hannover.

Effectiveness of the economization

Approximated function	Region of approximation	Approximating function	Number of terms for fixed accuracy	(Init./ New)Err. for fixed number of terms (N=200)
Potential of ellipsoid	$\varphi > 3°$ $\varphi < -3°$	init. polyn. single econ. double econ.	200 140 112	1 4 13
	$\varphi > 20°$ $\varphi < -20°$	init. polyn. single econ. seven-time econ.	200 82 46	1 9 5600
Zonal part of geopoten- tial model GPM 2 $\quad$ T	mean Earth's sphere	init. model single econ. triple econ.	200 110 70	1 3 4
	$57.4° < \varphi < 61.6°$	init. model single econ. four-time econ.	200 60 60	1 3 9
$\dfrac{\partial T}{\partial r}$	mean Earth's sphere	init. model single econ. triple econ.	200 25 25	1 4 13

Fig. 1. Oblate ellipsoid. Uniform errors before and after economization ($20° \leq \varphi \leq 90°$).
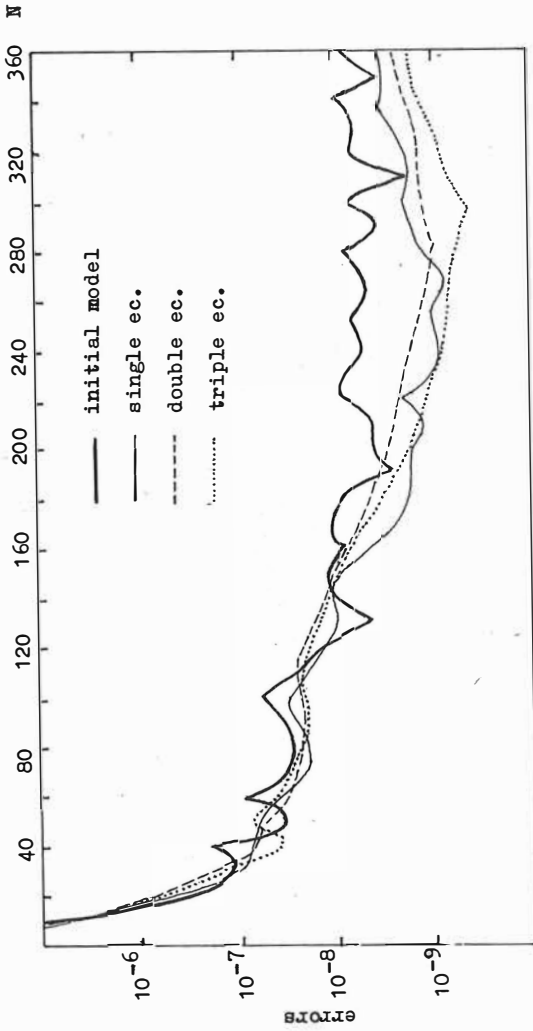
Fig. 2. Model OSU 86F. Disturbing potential. Uniform errors before and after economization $(-\frac{\pi}{2} \leqslant \varphi \leqslant \frac{\pi}{2})$.
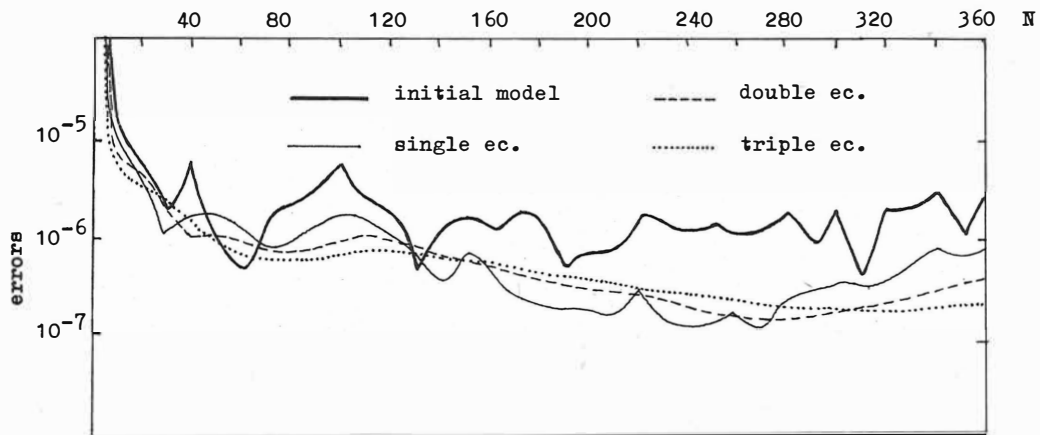
Fig. 3. Model OSU 86F. Gravity anomaly. Uniform errors before and after economization ($-\frac{\pi}{2} \leq \varphi \leq \frac{\pi}{2}$).

Results of the NAVGRAV-project, a gravimetric experiment on the North Sea [+)]

G.L. Strang van Hees, Technological University, Delft,
The Netherlands

Abstract

The NAVGRAV-project, a combined NAVigation and GRAVimetric experiment, was carried out successfully in the period April 23 - May 13, 1986. The objectives of the project were:

- to establish the perspectives of the Global Positioning System (GPS) for positioning at sea;
- to investigate the quality of terrestrial navigation systems in the North Sea region;
- to establish the achievable resolution and (internal and external) accuracy of the gravity field characteristics, derived from sea gravimetry, in comparison with results obtained from satellite altimetry.

A dense grid of gravity survey lines are measured. On board the ship two gravimeters were installed, the Bodensee GSS-30 system of the Geophysical Institute of the University of Hamburg and the KSS-5 gravimeter of the Technological University Delft, The Netherlands. The two gravimeters could be compared to determine the internal precision of the gravity meters. On the cross points of the network the external accuracy is determined. The results are also compared with previous gravity measurements in the same area.

DEVELOPMENT

OF PRECISE TERRESTRIAL AND SPACE TECHNIQUES

OF GEODETIC MEASURING

FUTURE SATELLITE SYSTEMS FOR EARTH SCIENCES

Ivan I. Mueller
Dept. of Geodetic Science and Surveying, Ohio State University
Columbus, Ohio 43210-1247 USA

ABSTRACT

As the Chairman of the Space Science Board of the U.S. National Academy of Sciences, T.M. Donahue, described in detail in an article published in *Physics Today* (May 1988), the space research programs of the USSR, Western Europe and Japan are flourishing. Their scientists are busy analyzing the results of recent successes in solar system exploration and in astrophysics. They are also busy constructing new projects, some of which are joint international ventures. International cooperation is the mode of operation in Western Europe and the USSR.

In contrast, the American space research program, due to the inability to launch spacecraft built during the past five years, is restricted to several productive orbiting remnants of the once prominent space program. It is also keeping a rich collection of scientific spacecraft in storage and continues to build more, most of them sophisticated and complex. Elaborate plans are also being developed projecting the future of space research for the next 30 years or more. If these spacecraft get launched successfully, the US will be restored to parity, and more, with the rest of the world.

One can thus anticipate a time of incomparable richness in the space sciences, which, ironically, will be due partly to the collapse of the U.S. launch system that took place.

In these exhilarating times it is a sobering thought for earth scientists that much of this "golden age" technology will belong to astronomers and astrophysicists. In fact, the only major Earth-oriented program appears to be the joint NASA/ESA/Japan Earth Observation System (EOS). The paper analyzes what this program may do for geodesy and geodynamics and suggests some ways and means of how earth scientists could play a more aggressive future role in "selling" Earth-oriented space research programs.

A POSSIBLE APPLICATION OF THE SPACE VLBI OBSERVATIONS FOR ESTABLISHMENT OF A NEW CONNECTION OF REFERENCE FRAMES[*]

József Ádám
Institute of Geodesy, Cartography and Remote Sensing;
Satellite Geodetic Observatory
H-1373 Budapest, Pf. 546.
Hungary

SUMMARY: Three dedicated space VLBI projects are currently in preparation to launch one or more VLBI radio telescopes in orbits between 1992-1996. One in the Soviet Union called RADIOASTRON which is already an approved mission. The second one is a Western European mission called QUASAT with potential international participation. A consortium in Japan is studying an orbiting VLBI mission called VSOP. Therefore, it is to be expected that space VLBI will be a reality in the next decade. However, the main goals of all three current space VLBI projects are astrophysical purposes.

In this paper it will be pointed out that a space VLBI system offers a good opportunity to connect two types of Conventional Inertial System (CIS): a direct tie between reference frames of the so-called Radio Source-CIS and Dynamic (Satellite Orbit)-CIS inherent in the space VLBI system can be established. On the basis of the ground-based VLBI network coordinates adopted in the Conventional Terrestrial System (CTS), and related to the mass center of the Earth by the space VLBI system itself, the relationship between frames of the CTS and the two above-mentioned CIS can also be established. Therefore, a space VLBI system may make a considerable contribution to geodynamics as well.

A fundamental element of the space VLBI observation geometry is illustrated. Some characteristics of the space VLBI network with respect to the different types of satellite geodetic networks will be emphasized from the viewpoint of theoretical geodesy. Some problems involved in space VLBI network design are discussed. Results from a preliminary estimability (rank defect) analysis of simultaneous space VLBI observations are also reviewed.

Aktuelle Probleme des Präzisionsnivellements
Actual Problems of the Precise Levelling

F. Deumlich

Zusammenfassung

Fortschritte bei der wirtschaftlichen Höhenbestimmung ergaben
sich durch die operative satellitengestützte Ortung sowie das
trigonometrische Nivellement. Ihre Genauigkeit steht aber
gegenwärtig derjenigen des geometrischen Präzisionsnivellements
nach. Daher ist dessen Weiterentwicklung eine aktuelle Aufgabe.
An Hand der Arbeitsgänge werden die Möglichkeiten und Gegeben-
heiten der Automatisierung des Präzisionsnivellements sowie
der weitgehenden Elimination der Einflüsse der Hauptfehler-
quellen diskutiert.

Summary

A progress in the economical determination of heights is
obtained by measuring with the operative positioning with
satellites (like GPS) and the trigonometric levelling. Today
there isn't obtained the accuracy of the geometric precise
levelling. Consequently it is an actual problem to continue
the development of the geometric precise levelling.
By means of the phases of the levelling the possibilities and
the situation of the automation of the precise levels and the
far extending elimination of the main sources of errors are
discussed.

Prof. Dr. sc. techn. Dr. h. c. F. Deumlich
Technische Universität Dresden
Sektion Geodäsie und Kartographie

Bei der Bestimmung der Lage von Punkten wurden in den letzten
Jahrzehnten erhebliche Fortschritte erzielt. Unter dem Einfluß
der Entwicklung der Mikroelektronik wurden Funktionen der
Strecken- und Winkelmeßinstrumente automatisiert. Die Entwick-
lung in der Satellitengeodäsie führte mit der operativen
satellitengestützten Ortung zum Eindringen neuer Wirkprinzipien
und einer beträchtlichen Steigerung der Arbeitsproduktivität.
Die Epoche der klassischen Geodäsie mit der Triangulation wurde
damit beendet.

Während aber die Genauigkeit der Lagebestimmung bei der opera-
tiven satellitengestützten Ortung derjenigen mit terrestrischen
Verfahren gleicht oder sogar besser ist, wurde bei der satelli-
tengeodätischen Höhenbestimmung bisher noch nicht die Genauig-
keit des geometrischen Präzisionsnivellements erreicht. Die
Genauigkeit ellipsoidischer Höhen in einem GPS-Zug wird mit
2 cm/10 km angegeben.

Die trigonometrische Höhenbestimmung erlangte in Verbindung mit
der Erhöhung ihrer Wirtschaftlichkeit und Automatisierung mit
durchgängigem Datenfluß durch das motorisierte trigonometrische
Nivellement mit Hilfe elektronischer Tachymeter größere Bedeu-
tung. Die Probleme der Refraktion lassen aber bisher eine dem
geometrischen Präzisionsnivellement ähnliche Genauigkeit nur
mit sehr großem, in der Praxis kaum vertretbarem Aufwand errei-
chen. Es bleibt abzuwarten, ob weitere gegenwärtige Versuche,
die Genauigkeit des geometrischen Präzisionsnivellements zu
erreichen, in nächster Zeit zum Erfolg führen.

So bleibt die Weiterentwicklung des geometrischen Präzisions-
nivellements mit einer Genauigkeit besser als $\pm$ 0,5 mm/km eine
aktuelle Aufgabe.

Während Instrumente zur Strecken- und Winkelmessung weitgehend
automatisiert wurden, weisen Nivelliere in dieser Hinsicht nur
geringe Ansätze auf. Die Realisierung der Möglichkeiten ihrer

Automatisierung seien an Hand der bekannten Darstellung der
einzelnen Arbeitsgänge beim Nivellement (Bild 1) untersucht /4,5/.
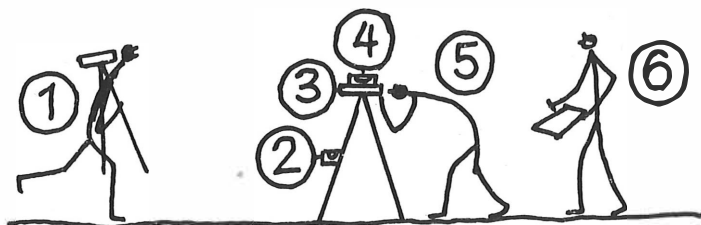
Bild 1

		Ungefährer Zeitanteil in %
1	Transport des Instrumentes und der Latten von Punkt zu Punkt	50
2	Aufstellen des Stativs, Grobhorizon- tieren der Ziellinie	13
3	Anzielen der Nivellierlatte	12
4	Feinhorizontieren der Ziellinie	13
5	Ablesen an der Nivellierlatte	12
6	Protokollieren (gleichzeitig mit 5 durch besondere Person)	

Der 1. Arbeitsgang mit dem größten Zeitaufwand ist kaum automa-
tisierbar. Eine bedeutende Steigerung der Wirtschaftlichkeit ergab
sich durch den in der DDR unter Leitung von Peschel /16/ ent-
wickelten beschleunigten Instrumenten- und Lattentransport mit
Hilfe von Kraftfahrzeugen ("motorisiertes Präzisionsnivellement")
unter Verwendung des dafür besonders geeigneten Präzisionskompen-
satornivelliers NI 002 A des VEB Carl Zeiss JENA und einigen
konstruktiven Maßnahmen zum schnellen Aufstellen von Instrument
und Latten sowie zum Einstellen der Zielweite.

Inzwischen wurden damit in der DDR 15 000 km Wiederholungs-
nivellement gemessen und mittlere km-Fehler von ± 0,9 mm
erhalten /9/. Der Anteil lebendiger Arbeit wurde um 1/3 ver-
mindert, der Meßprozeß um 100 % beschleunigt.

Beim Grobhorizontieren (2. Arbeitsgang) führen Kugelkopf-
stative und ähnliche zu Zeiteinsparungen. Sie werden auch
beim "motorisierten"Präzisionsnivellement" verwendet /16/.
Andere Lösungen sind nicht bekannt und kaum denkbar.

Das Anzielen der Latte (3. Arbeitsgang) wird z. B. mit Ro-
tationslasernivellieren automatisiert. Diese Möglichkeit
wurde von Schlemmer [14] und Wüller [15] in Verbindung mit
einer fotoelektrischen Nivellierlatte genutzt. Auf diese Wei-
se konnten die Arbeitsgänge 3,5 und 6 (außerdem auch 4) auto-
matisiert werden. Wüllmer erreichte ± 1,5 mm/km. Beide sehen
Möglichkeiten zur Verwendung der Prinzipien beim Präzisions-
nivellement, doch bedarf diese noch einiger Anstrengungen.

Das Feinhorizontieren der Ziellinie (4. Arbeitsgang) wurde
mit den Kompensatornivellieren automatisiert. Zwar gibt es
und gab es von einigen Fachleuten Bedenken gegen die Verwen-
dung von Kompensatornivellieren beim Präzisionsnivellement
im Hinblick auf den Einfluß systematischer Fehler, doch werden
andererseits gute Ergebnisse z. B. mit dem NI 002 A des VEB
Carl Zeiss JENA erhalten. Die vor einigen Jahren diskutier-
ten magnetischen Einflüsse auf Kompensatoren spielen bei die-
sem Nivellier. keine Rolle.- Noack /12/ stellte fest, daß Ein-
flüsse elektrischer und magnetischer Felder auf Kompensator-
nivelliere wesentlich geringer als die der Refraktion sind.

Gegenwärtig sind zahlreiche Versuche zur Automatisierung des
Ablesens an der Nivellierlatte und des Registrierens dieser
Ablesung (Arbeitsgänge 5, 6) zu bemerken. Gegenüber der auto-
matischen Ablesung bzw. Abtastung in elektronischen Theodo-
liten und Tachymetern besteht der Unterschied, daß Sender und
Empfänger um die Zielweite, d. h. bis 50 m, voneinander ent-
fernt sind, somit sich auch der Bildmaßstab ändert.

Eine Lösung gaben Caspary, Heister und Kurz /2/ mit einer
fernbedienten Latte an, die den Meßwert automatisch abliest
und weiterverarbeitet. Über eine industrielle Verwertung ist
nichts bekannt. - Die Lösung von Schlemmer /14/ mit einem
Rotationslasernivellier und einer digitalen Latte, die Foto-
empfänger (in einer senkrechten Reihe angeordnet und abschnitts-
weise zu einer Matrix geschaltet) und Auswerteeinheit enthält,
mit technischer Genauigkeit wurde bereits erwähnt.
Der Vorschlag für ein Präzisionsnivellier wurde noch nicht
erprobt.
Erwähnt wurde auch die Entwicklung einer fotoeleletrischen
Latte (mit Differentialfotodiode, die mit einer Präzisions-
spindel rertikal verschoben wird) von Wüller /15/. Auch seine
Vorschläge für Präzisionsnivelliere wurden noch nicht erprobt.
Interessant ist die von ihm angegebene Korrektion wegen Re-
fraktion aus Laufzeitmessungen von Ultraschallimpulsen.

 Auf dem Markt befindet sich seit 1987 das registrierende
Präzisionskompemsatornivellier RENI 002A des VEB Carl Zeiss
JENA mit teilautomatisierter Meßwerterfassung und geräte-
internen Datenfluß, -berechnung und -speicherung /8/. An der
Latte ist nur noch (bzw. : noch) der Grobwert. Mit diesem
Instrument wird die Wirtschaftlichkeit, vor allem beim "moto-
risierten Präzisionsnivellement" weiter erhöht.

Zur Bedeutung des Refraktionseinflusses gibt es unterschied-
liche Meinungen. Ließe sich die automatische Berücksichtigung
ermöglichen, wäre da sicher von Vorteil. Grundlagen hierfür
wurden in jüngster Zeit in den Dissertationen von Becek /1/
über computergestützte Refraktionsuntersuchungen und von
Moroz /11/ geliefert. Moroz ermittelte den Refraktionsein-
fluß allein aus dem Bildflimmern (an Hand des Zusammenhanges
zwischen der Amplitude des Bildflimmern und dem Temperatur-
gradienten), so daß meteorologische Meßwerte nicht zu erfas-
sen sind und der Zeitraum der Messung erweitert werden kann.

Ihde und Steinberg /9/ stellten als erheblich größeren Ein-

fluß als die Refraktion den des Einsinkens der Lattenunter-
sätze (bis 0,5 mm/km!) fest. Durch Lattenuntersätze mit ge-
eigneten Fußformen und Verwenden eines speziellen Meßsystems
können nach Ihde, Steinberg und Wunderlich $\underline{/10/}$ derartige
Fehlereinflüsse weitgehend eliminiert werden.

Als hauptsächliche Fehlerquellen der Nivelierlatte erwiesen
sich Maßstabsfehler wegen ihres systematischen Chrakters
(bis 30.10^{-6}).Teilungsfehler sind nach Elmiger $\underline{/6/}$ praktisch
vernachlässigbar, da sie im Bereich der zufälligen Meßfehler
liegen. Die Bestimmung der Verbesserungen aller Teilstriche
- wie sie heute mit modernen Kompensatoren mit einem Laser-
interferometer als Längennormal praktiziert wird $\underline{/7, 13/}$ -
und ihre Berücksichtigung beim Auswerten von Präzisionsnivel-
lements ist ohnehin kaum vertretbar. Interferometrisch geteil-
te Latten $\underline{/13/}$ erwiesen sich zum andernen von hervorragender
Qualität, sowohl hinsichtlich der Teilungsfehlwr als auch der
Randschärfe der Striche.

Zweckmäßig erscheint auch die Verwendung eines anderen Werk-
stoffes als Teilungsträger mit einem gegenüber Invar (1 bis
$2 \times 10^{-6}/K$) niedrigerem Längenausdehungskoeffizienten, z. B.
Kohlenstoff. Auch dann bleibt die automatische Bestimmung und
Berücksichtigung der Lattentemperatur ein noch zu lösendes
Problem.

Insgesamt ist festzustellen, daß weitere Fortschritte bei der
Automatisie ung des geometsichen Präzisionsnivellements zu
verzeichnen und zu erwarten sind.

Literatur

$\underline{/1/}$ Bęcek, K.: Computerunterstützte Refraktionsuntersuchungen.
Dissertation, TU Dresden 1987

$\underline{/2/}$ Caspary, W., Heister, H., Kurz, B.,: Ein Beitrag zur

Automatisierung des geometrischen Nivellements.- Z. Ver-
messungswesen, Stuttgart 111 (1986) 8, S. 361 - 366

/3/ Deumlich, F.: Aktuelle Probleme geodätischer Höhenmeß-
instrumente. Vermessungstechnik, Berlin 24 (76) 4, S. 139
bis 142

/4/ Deumlich, F.: Beitrag zum Präzisionsnivellement. XVII.
FIG-Kongreß, Sofia 1983, Kommission 5

/5/ Deumlich, F.: Die Entwicklung geodätischer Instrumente -
Entwicklung eines Teilgebiets der Technik. Allgem. Ver-
messungs-Nachr., Karlsruhe 92 (1985) 11 - 12, S. 397 - 402

/6/ Elmiger, A., Meyer, U., Olsch, H.: Untersuchungen an
Präzisions-Nivellierlatten. In: Ingenieurvermessung 84.
Bonn: Dümmler 1984, Band 1, A 7, S. 1 - 5

/7/ Gottwald, R.: Das Aachener Komparator-System zur Kali-
brierung von Invarband-Nivellierlatten. In: Festschrift
E. Heletor. Veröfftl. Geod. Inst. RWTH Aachen, Nr. 40.
1986. 8.1 - 8.10

/8/ Hüther, G.: RENI 002A und NI 002A - zwei neue Präzisions-
kompensatornivelliere des Kombinates VEB Carl Zeiss JENA.
Vermessungstechnik, Berlin 36 (1988) 2, S. 53 - 55

/9/ Ihde, J., Steinberg, J.: Leistungsfähigkeit und Reserven
des geometrischen Präzisionsnivellements. Vermessungs-
technik, Berlin 33 (1985)9, S. 301 - 303; 10, S. 332 - 334

/10/ Ihde, J., Steinberg, J., Wunderlich, M.: Einsinkverhalten
von Nivellieruntersätzen und Instrumentenstativen beim
Präzisionsnivellement, Vermessungstechnik,Berlin,33 (1985)5,
S. 163 - 166

/11/ Moroz, A. I.: Untersuchung der nivellitischen Refraktion
in der bodennahen Luftschicht an Hand des Bildflimmerns.
Vermessungstechnik, Berlin 36 (1988)4, S. 124

/12/ Noack, G.: Einflüsse elektrischer und magnetischer Felder
auf das Präzisionsnivellement. Vermessungstechnik, Berlin
36 (1988)1, S. 22 - 25

/13/ Schlemmer, H.: Nivelliere und Nivellierlatten - der Stand
der Technik bei Justierung und Kalibrierung. In: Ingenieur-
vermessung 84. Band 1. Bonn: Dümmler 1984. A 6, S. 1 - 13

/14/ Schlemmer, H!: Zur digitalen Ablesung an Nivellierlatten.
DGK, Reihe C, Nr. 326. München

/15/ Wüller, H.: Entwicklung und Untersuchung eines Rotations-
nivellierinstrumentes und einer photoelektrischen
Nivellierlatte zur Automatisierung des geometrischen
Nivellements. Veröfftl. Geod. Inst. RWTH Aachen, Nr. 41
Aachen 1988

/16/ Peschel, H.: Das Motorisierte Präzisionsnivellement.
Vermessungstechnik, Berlin 22 (1974)2, S. 57 - 64

GEOMETRIC METHOD TO DETERMINE GEOCENTRIC COORDINATES OF THE GROUND STATIONS ON THE REFERENCE FRAME OF A VLBI COMPLEX

V.S. Gubanov, E.V. Brumberg and N.I. Solina

Institute of Applied Astronomy
USSR Academy of Sciences
197042 Leningrad, USSR

ABSTRACT. The paper deals with the problem of determining geo-
centric coordinates of the ground stations in vicinity of a
VLBI complex by using VLBI observations of the navigation
satellites NAVSTAR GPS. It is shown that the problem has a
reliable solution providing the clock of the station in
question are sufficiently accurate synchronized with the time
scale of the VLBI complex. The accuracy estimates and the
correlation matrices for the station coordinates are given.

At present, the most widespread technique of determine the
ground station coordinates is the dynamical method of satellite
geodesy realized on the USA global navigation systems TRANSIT
and GPS. In this method the ground station coordinates are
determined by user from Doppler observations of navigation
satellites in the reference system specified by the forecasting
elements of satellite orbits and the board scales of frequency

(TRANSIT) and time (GPS) standards. In turn, these standards
should be permanently improved using observations of these
satellites made by the special global set of the reference
stations with the known (adopted) coordinates in the Inter-
national terrestrial system of 1984. The coordinates of these
reference stations have been determined and are still in progress
of improving on the basis of Doppler observations of the same
navigation satellites with addition of laser observations of
LAGEOS and VLBI observations.

From this it follows that the reference frame inherent to the
dynamical method of satellite geodesy and fixed with respect to
the Earth body by the locations of the reference stations is
transmitted to the determined station not directly but by means
of the intermediate system of the forecasting positions of the
navigation satellites. The transmission is performed by Doppler
measurements being at present not the most accurate ones. Among
the radiotechnical tools of navigation satellite observations
the maximal precision is gained by the VLBI technique enabling
to measure at the radiointerferometric station the relative
delay of the noise broadband signal from the board of NAVSTAR
GPS satellite with the precision of 0.1 ns (Umarbaeva, N.D.,
Fridman, P.A.: 1984). There:fore , the question is wether it
is possible to transmit the Earth fixed reference frame to the
determined station in a direct manner avoiding the intermediate
system of satellite epheremis and using the VLBI technique as
the most accurate observation method. The aim of the present
paper is to show that the problem may be reliably solved by
means of the synchronization of the determined station clock
with the time scale of the VLBI complex.

Let X_i, Y_i, Z_i be the coordinates of the reference stations
$A_i(X_i, Y_i, Z_i)$ (i=1, 2, ..., n) of a VLBI complex. This complex
may represent a regional or global set stations performing VLBI
observations of navigation satellites NAVSTAR of the USA global
navigation system GPS. Let us assume that these observations as
well as any others (laser ranging of LAGEOS, Doppler observations
of TRANSIT or NAVSTAR, etc.) enabled by means of the dynamical
method of satellite geodesy to determine the geocentric coordi-
nates of all stations of the complex with sufficient accuracy.
Assume also that the time scales of these stations are synchro-
nized at the level of the maximal attainable accuracy of VLBI
observations, i.e. within the error of ± 0.1 ns. Such synchroni-
zation may be achieved by VLBI observations of the extragalactic
radiosources at the stations of the complex A (Counselman III,
C.C., Shapiro, I.I., Rodgers A.E.E.: 1977) or by the autonomous
synchronization technique with the use of the satellite communi-
cation channels (Imal, M., Okazawa, H., Sato, T. et al.: 1983,
Gubanov, V.S., Kaidanovsky, M.N., Umarbaeva, N.D., Zimovsky, V.F.:
1988, Saburi, Y.: 1976). The problem is to determine the geo-
centric coordinates X_0, Y_0, Z_0 of an arbitrary station A_0 in the
vicinity of the complex A_i using VLBI observations of the
navigation satellites NAVSTAR. The coordinates of the satellites
are considered as unknown quantities.
Admitting, as stated above, $\Delta X_i = \Delta Y_i = \Delta Z_i = 0$ (i=1,2,...,n) it is
easy to show (see Fig.1) that the VLBI measurable linear delay
$l_i = \Delta R_0 - \Delta R_i = \Delta \rho_i = c\Delta \hat{\tau}_i$ at the base $A_0 A_i$ for the moment t_j (j=1,2,...,n)
of observation of k-satellite $S_k(X_k, Y_k, Z_k)$ has the form
(omitting, for brevity, index j):

$$l_i = -a_{10} \Delta x_0 - a_{20} \Delta y_0 - a_{30} \Delta z_0 + b_{1i} \Delta x_k + b_{2i} \Delta y_k + b_{3i} \Delta z_k^+ \quad (1)$$
$$+ \Delta p + \Delta q t$$

$\Delta p, \Delta q$ being parameters of synchronization of clock of the station A_0 with the time scale of the VLBI complex

$$a_{10} = \frac{x_k - x_0}{R_0} \qquad a_{20} = \frac{y_k - y_0}{R_0} \qquad a_{30} = \frac{z_k - z_0}{R_0}$$

$$b_{1i} = a_{10} - \frac{x_k - x_i}{R_i} \qquad b_{2i} = a_{20} - \frac{y_k - y_i}{R_i} \qquad b_{3i} = a_{30} - \frac{z_k - z_i}{R_i} \qquad (2)$$

VLBI observations of the specific satellite at the station A_0, A_l being synchronized it is possible with the total number of the complex stations n =4 to exclude from Egs. (1) related to one and the same moment t_j all theres satellite coordinates ΔX_k, ΔY_k, ΔZ_k. This results in n-3 equations with 5 unknown parameters of the type

$$l_v = c_{v_1} \Delta x_0 + c_{v2} \Delta y_0 + c_{v3} \Delta z_0 + d_{v1} \Delta p + d_{v2} \Delta q$$
$$v = 1, 2, \cdots (n-3) \qquad (3)$$

Coefficients of the right-hand members of Egs. (3) and their free terms are expressed in terms of the coefficients (2) of Egs. (1) and their free terms l_i directly in alternate eliminating corrections $\Delta X_k, \Delta Y_k, \Delta Z_k$. There expressions are not listed here for brevity.

Introducing instead of the cartesian coordinates of the station A_0 the spherical ones and splitting out the vector of unknown corrections into two parts

$$u = (\Delta z_0, \Delta y_0 z_0, \Delta \lambda_0 z_0); \quad v = (\Delta p, \Delta q) \qquad (4)$$

Egs. (3) may be represented in the matrix form $\ell_{jk} = C_{jk}\, u + D_{jk}\, v + \mathcal{E}_{jk}$
with the weight matrix P_{jk} (4), $j=1,2,\ldots m_k$ is the index of the
moment of observations, $k=1,2,\ldots,N$ is the number of the observed
satellite, $\mathcal{E}_{jk}$-is the vector of the random errors of observations.
Combining Egs. (4) for all possible j and k one gets the system
of equations in the block matrix form as follows

$$\ell = C\, u + D\, v + \mathcal{E} \qquad , \text{ with the weight matrix } P, \qquad (5)$$

$$\ell = (\ell_{jk}), \mathcal{E} = (\mathcal{E}_{jk}), \quad \text{and } C = [C_{jk}], D = [D_{jk}], \ P = [P_{jk}]$$

being the block vectors and matrices respectively.
The system of equations (5) may be solved by the classical least
squares method or by the generalized parametric method (Klenitzkij,
B.M.: 1982) provided that the ad hoc covariation matrices of the
required parameters Q_u and Q_v are known.
The results of numerical simulation of the described observation
procedure and the estimates of errors of parameters determined by
the least squares technique are listed below. As the model of the
VLBI complex the following set of stations A_i (φ_i, λ_i) were
adopted: $A_1 = A_1(60^\circ, \ 30^\circ)$-Leningrad, $A_2 = A_2(50^\circ, \ 30^\circ)$-Kiev,
$A_3 = A_3(44^\circ, \ 42^\circ)$-North Caucasus, $A_4 = A_4(56^\circ, 44^\circ)$-Gorky, $A_5 = A_5(38^\circ,$
$58^\circ)$-Ashkhabad, $A_6 = A_6(52^\circ, 103^\circ)$-Irkutsk. The observed satellites
were simulated by 18 NAVSTAR satellites with orbital height
20200 km, excentricity e=0, argument of the perigee w=0, orbital
inclination to the equatorial plane i=55°. The longitudes of the
ascending node Ω and the mean anomalies for the epoch 0^h GST for
all satellites are tabulated in Table 1.

Table 1. Orbital elements of NAVSTAR satellites

Sat.N	Ω	M_o	Sat.N	Ω	M_o	Sat.N	Ω	M_o	Sat.N	Ω	M_o	Sat.N	Ω	M_o	Sat.N	Ω	M_o
1	0	240	4	60	280	7	120	200	10	180	240	13	240	280	16	300	200
2	0	0	5	60	40	8	120	320	11	180	0	14	240	40	17	300	320
3	0	120	6	60	160	9	120	80	12	180	120	15	240	160	18	300	80

The observation program has been constructed in the following way. For all NAVSTAR satellites one found the Greenwich time intervals ΔS_k for which the satellite $N_o k$ could be seen from all stations A_o, A_i (i=1,2,...,n). Then all the intervals ΔS_k for all satellites were added yielding the mean observation interval for each satellite

$$\Delta T = \sum_{k=1}^{N} \Delta S'_k / \Delta S \qquad (6)$$

ΔS being the actual interval between two consecutive observations (ΔS=15 min. was adopted in calculations). Therefore, the diurnal cycle of observations results in 1440/ΔS=96 groups of equations of the type (3). With n=6 system (5) consists of 96(n-3)=288 equations with 5 unknowns. The quantity ΔT calculated by (6) may slightly change herewith in dependence of the A_o location with respect to the stations of the complex A .
The diurnal cycle of observations started with 0^h GPS. For this moment as well as for all succeeding moments of time separated by the interval ΔS one has calculated the coordinates of the stations A_i in the non-rotating system X,Y,Z the coordinates of all satellites on the basis of their orbital elements and the coordinates of the mobile station $A_o(X_o, Y_o, Z_o)$. The latitude and the longitude of this station serve as the free parameters

of simulation. These data enabled to compute the coefficients of Egs. (1) and then the coefficients of Egs.(3) after eliminating the coordinates of satellites. The system of Egs (5) has been accumulated for all moments of observation of the specific satellite with the interval ΔT along the position of its orbit simultaneously visible from all stations A_o, A_i. This was done for all 18 satellites NAVSTAR intersecting the common domain of visibility during 24 hours. The solution of this system was simulated in two versions, namely, for all unknown parameters or without synchronization parameters. The latter version corresponds to the reduced form

$$\ell = C \, \mathcal{U} + \mathcal{E} \tag{7}$$

The error of the single measurement of the linear delay $\Delta \varsigma$, i.e. the error of the free terms of all Egs. (1), was admitted to be the same and equal $\delta_\rho = c\delta_\varsigma = \pm 3$ sm.

The errors of the free terms of Egs. (5) were computed together with their coefficients in eliminating the satellite coordinates. The data obtained by numerical simulation enable to draw the following conclusions:

1. Version 1. The problem to determine all the unknowns for the system (5) does not admit a reliable solution due to the occurence of strong correlations (see Table 2).

Table 2. Correlations for the unknowns of the system (5)

for $\varphi_o = 45°$, $\lambda_o = 60°$.

Unknowns	$\frac{\partial^2 q}{\partial \varphi_o z_o}$	$\frac{\partial^2 q}{\partial \lambda_o z_o}$	$\frac{\partial^2 q}{\partial p}$	$\frac{\partial^2 q}{\partial q}$	$\frac{\partial \varphi_o z_o}{\partial \lambda_o z_o}$	$\frac{\partial \varphi_o z_o}{\partial p}$	$\frac{\partial \varphi_o z_o}{\partial q}$	$\frac{\partial \lambda_o z_o}{\partial p}$	$\frac{\partial \lambda_o z_o}{\partial q}$	$\frac{\partial p}{\partial q}$
Correlations	0.9	0.1	0.9	0.1	0.1	1.0	0.0	0.2	-0.2	-0.2

The correlations indicated in Table 2 are very stable being
only slightly dependent on the coordinates of the station A .
That is why they are listed only for $\varphi = 45^{\circ}$, $\lambda_o = 60^{\circ}$. As will be
seen from the version 2 the strong correlation between $\Delta \tau_o$ and
$\Delta \varphi \tau_o$ is indyced by the actual correlations between $\Delta \varphi$ and $\Delta \tau_o$
or $\Delta \varphi \tau_o$.

    2. Version 2. The problem to determine all three geocentric
coordinates of the mobile station A_o may be solved quite reliably
for the large domain in the vicinity of the complex provided
that the A clock are synchronized with the time scale of the
VLBI complex A within the accepted accuracy $\delta_\tau = 0.1$ ns. The cor-
relation matrices and the estimates of the errors of the coor-
dinates of the station $A_o(r_o, \varphi_o, \lambda_o)$ are represented in Tables 3
and 4.

In conclusion, let us note once more that the problem of high
precision and operational determination of the geocentrio coor-
dinates of any point in the large vicinity of the VLBI complex
is of great scientific and practical importance. These coordinates
should be directly refered to the stable reference frame speci-
fied by the coordinates of the stations of the VLBI complex and
its atomic time scale. The solution of the stated problem
depends on our ablility to find a sufficiently precise, simple
and operational way of independent clock comparison. Speaking
otherwise, in VLBI measurement procedure the reference frame
of the VLBI complex may be directly extended by geometric
method to cover the surrounding domain with the maximal precision
only if it is possible to extend into this domain the atomic
time scale of this complex with the same accuracy as well.

Table 3. Correlations for the unknowns of the system (7).

	$0°$	$20°$	$40°$	$60°$	$80°$	$100°$	$120°$	$140°$	$160°$	$180°$	
$65°$	-.1	.0	.0	.0	.0	.0	.0	-.1	-.2	-.1	$\Delta z_0/\Delta\varphi_0 z_0$
	.0	.0	.0	.0	.0	.0	.0	-.1	.0	.1	$\Delta z_0/\Delta\lambda_0 z_0$
	.0	.0	.0	.0	.0	.0	.0	-.1	-.1	.1	$\Delta\varphi_0 z_0/\Delta\lambda_0 z_0$
$55°$	-.2	-.1	-.1	-.1	-.1	-.1	-.1	-.2	-.2	-.2	$\Delta z_0/\Delta\varphi_0 z_0$
	.2	.0	.0	.0	.0	.0	-.1	.0	.1	-.1	$\Delta z_0/\Delta\lambda_0 z_0$
	.0	.0	.0	.0	.0	.0	-.1	-.1	.1	.0	$\Delta\varphi_0 z_0/\Delta\lambda_0 z_0$
$45°$	-.2	-.2	-.2	-.2	-.2	-.2	-.2	-.3	-.3	-.3	$\Delta z_0/\Delta\varphi_0 z_0$
	.1	.0	.0	.0	.0	-.1	.0	.1	.0	-.2	$\Delta z_0/\Delta\lambda_0 z_0$
	.0	.0	.0	.0	.0	.0	-.1	.0	.0	.0	$\Delta\varphi_0 z_0/\Delta\lambda_0 z_0$
$35°$	-.3	-.2	-.3	-.3	-.3	-.2	-.2	-.4	-.3	-.5	$\Delta z_0/\Delta\varphi_0 z_0$
	.1	.1	.0	.0	.0	.0	.1	.0	.0	.2	$\Delta z_0/\Delta\lambda_0 z_0$
	-.1	.0	.0	.0	.0	-.1	-.1	.1	-.2	.0	$\Delta\varphi_0 z_0/\Delta\lambda_0 z_0$
$25°$	-.3	-.3	-.3	-.3	-.3	-.2	-.2	-.4	-.3	-.2	$\Delta z_0/\Delta\varphi_0 z_0$
	.2	.1	.0	.0	-.1	.0	.1	.0	-.1	.8	$\Delta z_0/\Delta\lambda_0 z_0$
	-.1	.0	.1	.0	.0	.0	-.1	-.1	.0	.5	$\Delta\varphi_0 z_0/\Delta\lambda_0 z_0$

Table 4. Mean square errors for the unknowns of the system (7) in sm.

	$0°$	$20°$	$40°$	$60°$	$80°$	$100°$	$120°$	$140°$	$160°$	$180°$	
$65°$	0.5	0.2	0.1	0.2	0.2	0.1	0.2	0.5	0.9	1.2	Δz_0
	0.5	0.2	0.1	0.2	0.2	0.1	0.3	0.6	0.9	1.4	$\Delta\varphi_0 z_0$
	1.3	0.5	0.3	0.5	0.5	0.3	0.6	1.4	2.2	3.1	$\Delta\lambda_0 z_0$
$55°$	0.7	0.2	0.1	0.2	0.2	0.1	0.3	0.8	1.2	1.6	Δz_0
	0.7	0.2	0.1	0.3	0.1	0.3	0.3	0.8	1.3	1.8	$\Delta\varphi_0 z_0$
	1.2	0.5	0.2	0.5	0.5	0.2	0.6	1.3	2.3	3.4	$\Delta\lambda_0 z_0$
$45°$	1.0	0.4	0.1	0.2	0.2	0.1	0.5	1.1	1.6	2.4	Δz_0
	0.9	0.4	0.1	0.2	0.2	0.1	0.5	1.0	1.7	2.1	$\Delta\varphi_0 z_0$
	1.5	0.6	0.1	0.3	0.3	0.2	0.8	1.6	2.5	3.4	$\Delta\lambda_0 z_0$
$35°$	1.4	0.8	0.3	0.2	0.2	0.4	0.9	1.6	2.2	5.1	Δz_0
	1.2	0.7	0.3	0.2	0.2	0.4	0.7	1.4	1.9	2.4	$\Delta\varphi_0 z_0$
	1.9	1.0	0.4	0.3	0.3	0.5	1.1	1.9	3.2	3.6	$\Delta\lambda_0 z_0$
$25°$	2.0	1.4	0.8	0.5	0.5	0.8	1.4	2.4	3.3	9.4	Δz_0
	1.6	1.0	0.6	0.4	0.4	0.6	1.0	1.7	2.2	3.3	$\Delta\varphi_0 z_0$
	2.6	1.4	0.9	0.6	0.6	0.9	1.6	2.2	3.8	8.6	$\Delta\lambda_0 z_0$

REFERNCES:

Gubanov, V.S., Kaidanowsky, M.N., Umarbaeva, N.D., Zimovsky, V.F.:
    1988. Preprint of Special Astroph. Obs. of USSR Ac. Sci.,
    No.57L, p. 1-17 (in Russian).

Imal, M., Okazawa, H., Sato, T. et al.: 1983. IEEE Trans.
    Instrum. Meas., IM-32, No.1, p. 199-203

Counselman III, C.C., Shapiro, I.I., Rogers, A.E.E.: 1977.
    Proc. IEEE, 65. N11, p. 1622-1623

Klenitzkij, B.M.: 1982. Sci.Inf., Astron. Coun. of USSR Acad.
    Sci., N55, p.98-126 (in Russian).

Umarbeeva, N.D., Fridman, P.A.: 1984, Obs. of Art. Sat., Astron.
    Coun. of USSR Acad. Sci., No.21, pt.2, p 661-668 (in Russian).

Saburi, Y.: 1976, J. Radio Research Laboratories, 23, No. 112,
    p. 255-265.
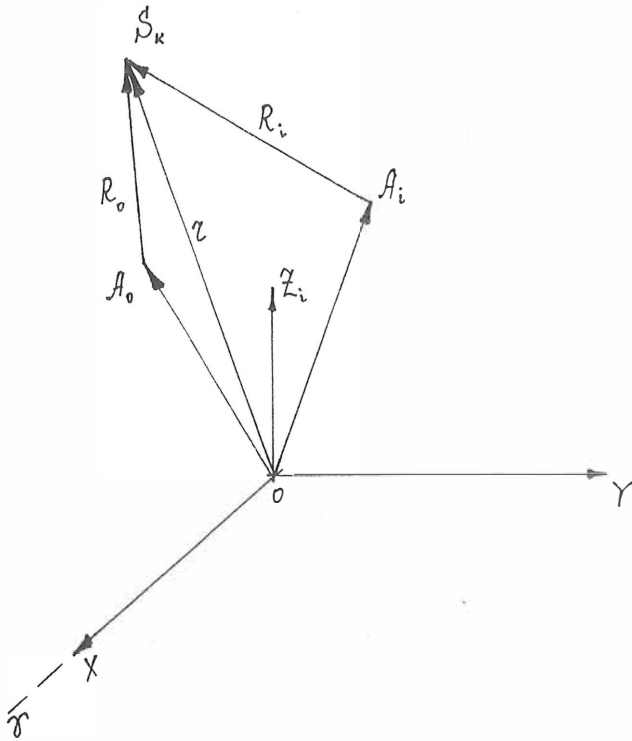
Fig. 1. Geometrical diagram of VLBI observations of Earth
        satellites

OXYZ is the non-rotating equatorial coordinate system
$S_k(X_k, Y_k, Z_k)$ are the satellite positions for the moment t_j.
$A_i(X_i, Y_i, Z_i)$ are the ground stations of the VLBI complex.
$A_o(X_o, Y_o, Z_o)$ is the mobile station supplied with the
        VLBI apparatuses for navigation satellite
        observations.

ERS-1 AND THE PRARE-SYSTEM

Christoph Reigber, Wolfgang Lechner, Herbert Wilmes

Deutsches Geodätisches Forschungsinstitut, (DGFI), Abt. I,
München, Federal Republic of Germany

ABSTRACT: In mid 1990, ERS-1, the first ESA Remote Sensing Satellite will be launched
with an expected lifetime of two to three years. One of the payloads is the Precise Range and
Range Rate Equipment PRARE, a spaceborne two-way two-frequency microwave tracking
system. The paper describes the scientific objectives as well as the technical features of the
PRARE system components and presents an actual survey of the project.

1. Introduction to ERS-1 Mission

In 1990 the European Space Agency ESA will launch the first European Remote Sensing Sa-
tellite ERS-1 from the Kourou site. The Spacecraft sensors will primarily support ocean and
sea-ice investigations and as a secondary goal also land applications. The core payload con-
sists of the following active and passive sensors:

- Active Microwave Instrument (AMI) operating as SAR or as wind and wave scatterom-
  eter

- Radar Altimeter (RA)

- Along Track Scanning Radiometer (ATSR)

- Laser retroreflector array

- Precise Range and Range Rate Equipment (PRARE)

Due to the high resolution of the Radar Altimeter the determination of precise orbit parame-
ters becomes an unalterable necessity. These computations will be performed in one of the
off-line components of the ERS-1 ground segment (s.fig. 2) the German Processing and Ar-
chiving Facility (D-PAF).

2. Products of the D-PAF

The German PAF is located in Oberpfaffenhofen and is just now being built up by a cooperat-
ing team of scientists from the Deutsche Forschungs- und Versuchsanstalt für Luft- und
Raumfahrt (DFVLR) and DGFI.

It will be the primary product center for:

- SAR-Processing

- High accuracy orbit restitution making use of PRARE, Laser Ranging and Radar Altimeter data

- High precision altimeter geophysical products requiring high accuracy orbits and gravity fields

The results of the processing are well defined so called "ESA Standard Products" or "Regular PAF Products". For the Radar Altimeter and Tracking system these are:

- Preliminary orbits

- Orbit predictions

- Precise orbits

- ERS-1 gravity field models

- Sea surface height models

- Oceanic geoid

- Large scale sea surface topography

In addition to this the PRARE Master Station will be integrated into the PAF activities.

3. PRARE - Principle, Objective, Capability

The new microwave tracking system PRARE is presently developed by the Institut für Navigation (INS), Universität Stuttgart in cooperation with DGFI/Abt. I and the industrial contractor Kayser Threde, München and will be a payload element of the ERS-1 mission. This spaceborne selfcontained autonomous tracking system with all-weather capability will allow precise two-way, two-frequency range and range rate measurements to transponder ground stations for the support of the Radar Altimeter as well as other sensors by precise and rapidly available orbit ephemeris information. In addition to this, corrective information such as Total Electron Content (TEC, ionospheric refraction) and meteorological data from the ground station sites (atmospheric refraction) will be available for all microwave measurements (s.fig. 3).

The PRARE system consists of three components, the space segment with minimum interface to the spacecraft (s.fig. 4), the control segment with the master ground station for control operations (s.fig. 5), data transfer and preprocessing of the tracking data and the ground segment with the network of ground tracking stations (s.fig. 6). The measurement principle of PRARE is explained in fig. 7.

Two signals are sent to earth form the space segment (one of which is in the S-band (2.2 GHz), the other in the X-band (8.5 GHz). Both signals are modulated with a PN code (pseudo random noise) for the distance measurement containing data signals ("broadcast information")

for the ground station operation (prediction of visibility etc.). The time delay in the reception of the two simultaneously emitted signals is measured in the ground station and retransmitted to the onboard memory for the later ionospheric correction of data. In the ground station the received X-band signal is transposed to 7.2 GHz, coherently modulated with the regenerated PN code (or with one of three orthogonal copies for code multiplexing) and retransmitted to the space segment where the PN code is fed into a correlator to determine on board the two-way signal delay which is a measure for the two-way slant range between ERS-1 and the ground station. In addition, the received carrier frequency is evaluated in a doppler counter to derive the relative velocity of the spacecraft in respect to the ground station. Four independent correlators and four doppler counters in the space segment allow simultaneous measurements with four ground stations in a code multiplex mode.

Due to these basic principles the objectives of the PRARE experiment on board ERS-1 are to

- prove that PRARE is an autonomous and almost automatically working tracking system for near real time orbit determination

- attain precise orbit determination for ERS-1 using PRARE measurements together with Laser data for
  - Radar Altimetry data reduction
  - gravity modelling
  - positioning improvements
  - other sensors on board ERS-1

- perform short-term orbit prediction for ERS-1 as support for
  - Laser tracking systems
  - the PRARE ground stations
  - other sensors on board ERS-1

- determine precise baseline lengths between PRARE tracking stations

- determine absolute (geocentric) coordinates of tracking stations.

To estimate the PRARE measurement precision it is necessary to examine the hardware limitations on the one hand and the model uncertainties on the other hand. What concerns the hardware it can be said that there will be noise values of

$$\pm 1.7 \text{ cm for X-band ranging}$$
$$\pm 30 \text{ cm for S-band ranging}$$
$$\pm 0.1 \text{ mm/s for X-band doppler}$$

(1 measurement per second for ranging; integration interval of 30 seconds for doppler; 90^0 elevation, one-way distances and velocities)

and, after calibration, some remaining bias values of

$$< 1 \text{ cm for the X-band ranging}$$
$$< 3 \text{ cm for the S-band ranging}$$

The model uncertainties can be specified with

322

<div align="center">

tropospheric error (vertical) $\delta R_T \approx 2 - 7cm$
ionospheric error (vertical) $\delta R_I < 1cm$
thermal noise and calibration errors $\delta R_C \approx 2 - 3cm$
antenna phase uncertainty $\delta R_A \approx 1cm$

</div>

so that the total error after correction can be estimated as a RSS value

$$\delta R = \sqrt{\delta R_T^2 + \delta R_I^2 + \delta R_C^2 + \delta R_A^2}$$

$$3 \; cm < \delta R < 7cm$$

This shows that the range error will be definitely smaller than 10cm for one measurement. With these measurement errors it has been verified by simulations in the dynamic and geometric mode that short arcs of a few thousand kilometer lengths can be recovered with radial position errors of less than 10 cm, and baselines for distances of less than 1000 km with a few centimeter precision.

4. Further Plans and Future Missions

For the next two years there will be the priority to complete the system development. After the hardware of the space segment has been delivered for integration, the master station with timing unit and connection to the D-PAF and the individual tracking stations are the primary issues to be finalized. Furtheron the PRARE calibration campaign must be prepared for the ERS-1 mission and the coordination of the PRARE tracking network with worldwide coverage and/or emphasis in specific areas will be another focal point of activities.
Besides this there are some proposals to use the PRARE system on several different missions for earth observation, navigation, manned missions, space probes, comet probes etc.
So it will be a high probability that the PRARE system will be in use at minimum up to the end of the century.

Literature:

[1] Hartl, Ph., Schäfer, W., Reigber, Ch., Wilmes, H.: PRARE System Description, Proceedings of an ESA Special Workshop on 'Solid Earth Science & Application Mission for Europe', SESAME, Chiemsee, F.R. Germany, 4-6 March 1986. (ESA SP 1080)

[2] Wilmes, H., Reigber, Ch.: Precise Range and Range Rate Equipment, PRARE, on board ERS-1 - Orbitography in Support to Radar Altimetry and Tool for Precise Geodetic Positioning, XIX IUGG General Assembly, Vancouver, Canada, 9-22 August 1987.

Characteristics of ERS-1

Orbit:

* Mean altitude 778 km
* Excentricity 0.001
* Inclination 98.5^0
* Sun-synchronous repetitive orbit (repeat cycle 3 to 35 days)

Scheduling:

* Planned launch date mid 1990
* Expected lifetime 2 to 3 years

Sensors:

* Active Microwave Instrument (AMI) operating as Synthetic Aperture Radar (SAR) or as wind and wave scatterometer,
* **Radar Altimeter (RA)**
* Along Track Scanning Radiometer (ATSR)
* **Laser retroreflector array**
* **Precise Range and Range Rate Equipment (PRARE)**

Fig. 1: Characteristics of ERS-1

Measurement Principle

* Two-way X-band PN-coded ranging (S/C → ground station → S/C; downlink: 8.5 GHz, uplink: 7.2 GHz)
* Two-way X-band doppler measurement
* One-way two-frequency X-versus S-band range difference measurement (S/C → ground station) 8.5 GHz, 2.2 GHz
* Measurement of meteorological ground data
* Simultaneous tracking of up to 4 ground stations
* Independency of other telemetry links

 − Storage of measurement data in the space segment
 − Dump of tracking data to the master station for centralized processing
 − Distribution of broadcast data with the measurement signal

Fig. 3: Principle of the PRARE System

Fig. 2: Off-Line Components of the ERS-1 Ground Segment